

Distribution Agreement

In presenting this dissertation as a partial fulfillment of the requirements for an advanced degree from Emory University, I hereby grant to Emory University and its agents the non-exclusive license to archive, make accessible, and display my dissertation in whole or in part in all forms of media, now or hereafter known, including display on the world wide web. I understand that I may select some access restrictions as part of the online submission of this dissertation. I retain all ownership rights to the copyright of the dissertation. I also retain the right to use in future works (such as articles or books) all or part of this dissertation.

Signature:

Erika M. Milczek

Date

Investigation of C-H Bond Oxidation Reactions:

I. Asymmetric Amination of C-H Bonds Using Ruthenium(II) Catalysts

II. Investigation of Structural Determinants of Monoamine Oxidase B

By

Erika M. Milczek
Doctor of Philosophy

Chemistry

Dale E. Edmondson, Ph.D.
Advisor

Dennis C. Liotta, Ph.D.
Committee Member

Simon B. Blakey, Ph.D.
Committee Member

Accepted:

Lisa A. Tedesco, Ph.D.
Dean of the James T. Laney School of Graduate Studies

Date

Investigation of C-H Bond Oxidation Reactions:

I. Asymmetric Amination of C-H Bonds Using Ruthenium(II) Catalysts

II. Investigation of Structural Determinants of Monoamine Oxidase B

By

Erika M. Milczek

B.S., University of Tennessee at Chattanooga, 2005

Advisor: Dale E. Edmondson, Ph.D.

An Abstract of

A dissertation submitted to the Faculty of the

James T. Laney School of Graduate Studies of Emory University

in partial fulfillment of the requirements for the degree of

Doctor of Philosophy

In Chemistry

2010

ABSTRACT

Investigation of C-H Bond Oxidation Reactions:
I. Asymmetric Amination of C-H Bonds Using Ruthenium(II) Catalysts
II. Investigation of Structural Determinants of Monoamine Oxidase B
By Erika M. Milczek

This dissertation focuses on exploiting catalytic processes for the oxidation of C-H bonds. Part I of this dissertation describes the development of an efficient asymmetric intramolecular C-H amination protocol. A series of chiral Ru(II)-pyridine bisoxazoline (pybox) complexes were synthesized, and their catalytic properties were investigated. These Ru(II)-pybox complexes catalyze the cyclization of a variety of aryl- and aliphatic-sulfamate ester ($R-(CH_2)_3OSO_2NH_2$) in the presence of hypervalent iodide oxidants. The cyclized sulfamidates were formed in up to 94% conversion and up to 92% ee.

Part II of this dissertation focuses on amine oxidation by the flavoprotein, monoamine oxidase (MAO). MAO exists in two isoforms, MAO A and MAO B, which differ greatly in substrate specificity and tissue distribution although they demonstrate similar catalytic function. The investigations detailed in this dissertation focus on two goals: 1. understanding the structural features unique to MAO B; and 2. exploiting these properties for the design of MAO B specific inhibitors.

The major structural difference in MAO A and MAO B is that MAO A has a monopartite substrate cavity of 550 \AA^3 and MAO B is dipartite with a 290 \AA^3 entrance cavity and a 400 \AA^3 substrate cavity. Ile199 and Tyr326 function to separate these two cavities. To probe the function of these gating residues, Ile199Ala and Ile199Ala-Tyr326Ala mutant forms of MAO B were constructed, expressed in *Pichia pastoris*, and purified. Both mutants exhibit catalytic activities that are altered with increased K_m values. These insights are applied to understand the molecular mode of inhibition of three distinct classes of MAO B specific inhibitors: 1. Mechanism based inhibition of MAO B by mofegiline; 2. Selective and reversible inhibition of MAO B by styrylisatin analogues; and 3. Allosteric mechanism of inhibition through imidazoline binding to the entrance cavity of MAO B.

This dissertation is dedicated to my advisor, Dr. Dale Edmondson.

Without his support, encouragement, and mentorship, I would not be here today.

Investigation of C-H Bond Oxidation Reactions:

I. Asymmetric Amination of C-H Bonds Using Ruthenium(II) Catalysts

II. Investigation of Structural Determinants of Monoamine Oxidase B

By

Erika M. Milczek

B.S., University of Tennessee at Chattanooga, 2005

Advisor: Dale E. Edmondson, Ph.D.

A dissertation submitted to the Faculty of the James T. Laney
School of Graduate Studies of Emory University in partial fulfillment
of the requirements for the degree of
Doctor of Philosophy
in Chemistry

2010

ACKNOWLEDGEMENTS

I would like to express my gratitude to my advisor, Dr. Dale Edmondson, for his constant support throughout my graduate career. As I develop new ideas, he is the first person that I seek out for scientific discussion. I will always admire his perspective and thorough approach to answering scientific problems, and I will always strive to achieve the level of excellence that he has achieved as a scientist. I am truly grateful that I had the opportunity to work with him, and I am proud to say that I came from the Edmondson lab.

I would also like to thank my committee members, Dr. Simon Blakey and Dr. Dennis Liotta for their useful advice and guidance over the past five years. I would also like to thank Dr. Stefan Lutz for always having an open door when I am seeking advisement.

I would like to thank my fellow lab members for their continual support over the last three years. I would like to extend a special thanks to Jin Wang and Milagros Aldeco who have always found time to teach me new techniques and protocols. Jin and Milagros have been extraordinary mentors and friends over the past three years. I would also like to extend my gratitude to Mrs. Joanie Edmondson for her friendship and advice.

I would also like to recognize Andrea Mattevi, Claudia Binda, and Daniele Bonivento for their collaboration. I am especially indebted to Andrea and Claudia for their lively scientific discussions that I have learned so much from over the past three years.

I have been blessed to have wonderful friends that made my graduate experience unforgettable: Ana Alcaraz, Uliana Danilenko, Brad Balthaser, Shana Topp, Jennifer Sorrells, and Annette Neuman. I would like to extend a special thanks to Valarie Truax for being the best roommate and writing companion that I could ask for throughout this process.

I would like to thank my family for their unconditional love and support throughout my graduate career: my mother and father for always believing in me; my big brother, Jason Milczek, for always coming to the rescue whenever I need him; and Mary Anne Flowers, Suzanne Wyche, and Laura Palmiero for their constant support.

Most importantly, I would like to thank my fiancé, Jeremy Olson, for his extraordinary support and love. Even during the toughest times he keeps me laughing and never lets me take myself too seriously. Thank you.

Table of Contents

Chapter 1 Introduction to C-H Bond Cleavage Reactions	1
References	4
Chapter 2 Asymmetric Amination of C-H Bonds Using Cationic Ruthenium(II)-pybox Catalysts.....	5
2.1 Background and Significance	5
2.1.1 Porphyrin Catalysts	7
2.1.2 Dirhodium(II) Tetracarboxylate Catalysts	8
2.2 Project Objectives.....	10
2.3 Results and Discussion	11
2.3.1 Catalyst Design	11
2.3.2 Surveying the reactivity of Catalyst 8 and Reaction Development.....	12
2.3.3 Novel Metal Complexes	18
2.4 Conclusions	23
2.5 Materials and Methods	24
2.6 References	38
Chapter 3 Monoamine Oxidase: Laboratory to Clinical	43
3.1 MAO as a Genetic Control for Behavior	45

3.2 Pharmacological Importance of MAO B	46
3.3 Pharmacological Importance of MAO A	48
3.4 Clinical Use of MAOIs	49
3.5 Understanding the Differences in MAO A and MAO B: A Molecular Look	50
3.6 Crystallographic Studies of MAO.....	51
3.7 Probing the Oligomeric States of MAO.....	54
3.8 Comparison of MAO A and MAO B Active Site Cavities	55
3.9 Inhibitor Design and Inhibitor Binding to MAO.....	58
3.10 Reactions Catalyzed by MAO.....	60
3.11 Mechanism of Amine Oxidation	63
3.11.1 Hydride Transfer Mechanism	64
3.11.2 Radical Mechanism	65
3.11.3. Deprotonation Mechanisms	66
3.11.3.1. Aminium Cation Radical Mechanism	66
3.11.3.2. Polar Nucleophilic Mechanism.....	69
3.11.4. Mechanism for Oxidation of Flavin by O ₂	70

3.12 Dissertation Objectives	71
3.12.1 Elucidating the Role of Ile199 and Tyr326	71
3.12.2 Investigation of the Molecular Mechanisms of MAO B Specific Inhibitors.....	72
3.12.2.1 Exploiting Substrate Reactivity Unique to MAO B	72
3.12.2.2 Rational Design of Inhibitors that Bridge the Entrance and Substrate cavities of MAO B.....	73
3.12.2.3 Targeting the Entrance Cavity of MAO B.....	74
3.13 References	75
Chapter 4 Development of MAO B Specific Inhibitors: From Investigation to Design.....	91
4.1 Mechanistic Studies of the Mechanism Based Inhibitor Mofegiline	91
4.1.1 Development of Mofegiline as an Inhibitor of MAO B	91
4.1.2 Results and Discussion.....	95
4.1.2.1 Inhibition of MAO B with Mofegiline	95
4.1.2.2 Structure of Mofegiline Inhibited MAO B.....	100
4.1.2.3 Mofegiline Interactions with Purified MAO A.....	102
4.1.2.4 Differential Inhibition Motifs with MAO A and MAO B	103

4.1.3 Conclusions.....	107
4.1.4 Materials and Methods.....	108
4.1.5 References.....	110
4.2 Development of Inhibitors that Bridge Both Active Site Cavities	115
4.2.1 Inhibitors that Bridge Both Cavities of MAO B	115
4.2.2 Results and Discussion.....	117
4.2.2.1 Design of Inhibitor Compounds	117
4.2.2.2 Biological Evaluation of Styrylisatin Analogues	119
4.2.2.3 Importance of Planarity in Designing MAO B Inhibitors.....	123
4.2.2.4 Differential Inhibition Motifs with MAO A and MAO B	123
4.2.3 Conclusions.....	125
4.2.4 Materials and Methods.....	125
4.2.5 References.....	126
4.3 Targeting the Entrance Cavity of MAO B as a Novel Site for Inhibition: Elucidation of the Imidazoline Binding Site.....	129
4.3.1 History of Imidazoline Ligands and MAO	129
4.3.1.1 Classification of IBS.....	130
4.3.1.2 Elucidation of the I ₂ -IBS.....	130

4.3.1.3 Evidence for MAO B as I ₂ -IBS	132
4.3.1.4 Tranylcypromine Potentiation	133
4.3.2 Results	136
4.3.2.1 Crystallization of MAO with 2-BFI	136
4.3.2.2 Competition Experiments with 2-BFI	140
4.3.2.3 Competition Experiments using Farnesylamine	144
4.3.2.4 Fluorescence Binding Assay	146
4.3.2.5 Thermal Denaturation Experiments	147
4.3.3 Discussion	149
4.3.4 Conclusions	152
4.3.5 Materials and Methods	153
4.3.6 References	160

Chapter 5 Elucidating the Role of the ‘Gating’ Residues of Human

Monoamine Oxidase B	168
5.1 Background and Significance	168
5.1.1 Identification of the ‘Gating’ Functions of Ile199	169
5.1.2 Role of the Tyr326	171
5.1.3 Point Mutation of the Ile199 to Phe	172

5.1.4 Abolishing the 'Gating' Mechanism of MAO B	173
5.1.5 Creating a Monopartite Active Site in MAO B	174
5.2 Inhibition Studies	174
5.2.1 Nonspecific Inhibitors	175
5.2.2 MAO B Specific Inhibitors	175
5.2.3 MAO A Specific Inhibitors	176
5.2.4 Mechanism Based Inhibitors	177
5.2.5 Aminoindans: Small Reversible Inhibitors	178
5.3 Discussion	179
5.3.1 Binding Properties of the Ile199Ala Mutant	179
5.3.2 Binding Properties of the Ile199Ala-Tyr326Ala Mutant	180
5.4 Structural Studies	180
5.4.1 Ile199Ala Mutant Structural Studies	181
5.4.2 Ile199Ala-Tyr326Ala Mutant Structural Studies	182
5.5 Activity Studies of the Ile199Ala Mutant	183
5.6 Activity Studies of the Ile199Ala-Tyr326Ala Mutant	185
5.7 pH Studies	186

5.8 Mechanistic Studies.....	191
5.8.1 QSAR Effects: Ile199Ala Mutant.....	195
5.8.2 QSAR Effects: Ile199Ala-Tyr326Ala Mutant	197
5.9 Conclusions	200
5.10 Materials and Methods	201
5.11 References	204

List of Figures

Figure 1.1. Easily deprotonated C-H bonds.	2
Figure 2.1. C-H functionalization via inner-sphere mechanism.....	5
Figure 2.2. C-H functionalization via outer-sphere mechanism	6
Figure 2.3. First transition metal catalyzed nitrene insertion into a C-H bond	7
Figure 2.4. Che's asymmetric C-H amination reaction.	8
Figure 2.5. Stereospecific nitrene insertion	9
Figure 2.6. Fruit's asymmetric C-H amination reaction.....	10
Figure 2.7. Davies' asymmetric C-H amination reaction.....	10
Figure 2.8. Ruthenium(II)-pybox complexes	11
Figure 2.9. Ru(II)ip-pybox as an active catalyst for C-H amination	19
Figure 3.1. Structure of flavin-adenine-dinucleotide (FAD).	44
Figure 3.2. Pathway for MAO B generated oxidative damage	48
Figure 3.3. FDA approved MAOIs	50
Figure 3.4. X-ray crystal structures of human MAO A, human MAO B, and rat MAO A	53
Figure 3.5. DEER measurements.....	55
Figure 3.6. Comparisons of the human MAO A and MAO B active site	56

Figure 3.7. MAO B specific reversible inhibitors	59
Figure 3.8. Reversible aliphatic MAO B inhibitors	59
Figure 3.9. Common mechanism based inhibitor flavin adducts	59
Figure 3.10. MAO A specific inhibitors	60
Figure 3.11. Comparison of the relative shapes of the MAO A and MAO B active sites	72
Figure 3.12. Structure of mofegiline.	73
Figure 3.13. Development of styrylisatin analogous.	74
Figure 3.14. Structure of 2-(2-benzofuranyl)-2-imidazoline (2-BFI).	74
Figure 4.1.1. Structure of mofegiline	92
Figure 4.1.2. Mofegiline inhibition of human MAO-B.	95
Figure 4.1.3. Titration of MAO B with substoichiometric levels of Mofegiline	96
Figure 4.1.4. The UV/Vis spectra of flavin N(5) and flavin C(4a) adducts of MAO B	97
Figure 4.1.5. Circular dichroism spectra of human MAO B	98
Figure 4.1.6. The UV/Vis spectra of anaerobic inhibition of MAO B	98
Figure 4.1.8. Structure of human MAO B in complex with the Mofegiline	100
Figure 4.1.7. Absorption spectra of reduced MAO B-Mofegiline adduct.	100

Figure 4.1.9. The binding mode of Mofegiline to the MAO B active site.....	101
Figure 4.1.10. Mofegiline inhibition of human MAO A	102
Figure 4.1.11. UV/Vis spectrum of human MAO A on anaerobic addition of Mofegiline	103
Figure 4.1.12. Absorption spectral properties of MAO B flavin adducts	106
Figure 4.1.13. Comparison of the inhibitory properties of Mofegiline	107
Figure 4.2.1. MAO B inhibitors that bridge the entrance and substrate cavities..	115
Figure 4.2.2. Structures and numbering system for caffeine, CSC, and isatin.	116
Figure 4.2.3. X-ray crystal structure of human MAO B in complex with isatin ...	116
Figure 4.2.4. Binding modes determined of isatin and Styrylisatins	118
Figure 4.2.5. The docking solutions for the binding of Styrylisatins to MAO A. .	119
Figure 4.2.6. Structures of the styrylisatin analogues.....	120
Figure 4.2.7. Lineweaver-Burk plots of (E)-5-styrylisatin and MAO.....	122
Figure 4.2.8. Lineweaver-Burk plots of (E)-5-(3-chlorostyryl)isatin and MAO ..	122
Figure 4.2.9. Lineweaver-Burk plots of (E)-5-(3-fluorostyryl)isatin and MAO ...	122
Figure 4.2.10. Lineweaver-Burk plots of (E)-6-Styrylisatin and MAO	122
Figure 4.2.11. Energy-minimized structures of Styrylisatins.....	124
Figure 4.3.1. The structures of common imidazoline ligands	129

Figure 4.3.2. Structures of I ₂ specific ligands.	132
Figure 4.3.3. Xray structure for TCP-inhibited human WT MAO B.....	135
Figure 4.3.4. TCP-WT MAO B in complex with 2-BFI.	137
Figure 4.3.5. Entrance cavity of MAO B when 2-BFI is bound	139
Figure 4.3.6. TCP-inhibited Ile199Ala MAO B co-crystallized with 2-BFI.	140
Figure 4.3.7. Lineweaver-Burk of human MAO B and 2-BFI	143
Figure 4.3.8. Dixon Plots of 2-BFI inhibition of human MAO B.....	143
Figure 4.3.9. Lineweaver-Burk plots of human MAO A and rat MAO B/2-BFI..	143
Figure 4.3.10. Lineweaver-Burk plots of Ile199Ala-Tyr326Ala and Ile199Ala ..	144
Figure 4.3.11. X-ray crystal structure the human MAO B-farnesol complex	144
Figure 4.3.12. The structures of farnesol and farnesylamine.	145
Figure 4.3.13. Lineweaver-Burk plots of human MAO B and rat MAO B	145
Figure 4.3.14. Fluorescence quenching assay of native MAO B and 2-BFI.....	147
Figure 4.3.15. Fluorescence quenching assay of TCP-MAO B and 2-BFI.....	147
Figure 4.3.16. X-ray crystal structure of TCP-inhibited human MAO B	150
Figure 4.3.17. T _m curves for WT MAO B and 2-BFI.	158
Figure 4.3.18. T _m curves for TCP-inhibited WT MAO B and 2-BFI.....	158

Figure 4.3.19. T_m curves for WT MAO B and R-MAI	159
Figure 4.3.20. T_m curves for Deprenyl-inhibited WT MAO B	159
Figure 4.3.21. T_m curves for WT MAO B and isatin.....	159
Figure 4.3.22. T_m curve for WT MAO B and safinamide.....	160
Figure 5.1. Cartoon of the human MAO B active site	168
Figure 5.2. Demonstration of the gating mechanism of human MAO B	170
Figure 5.3. Human MAO B in complex with rasagiline	171
Figure 5.4. Human MAO A co-crystalized with harmine.....	172
Figure 5.5. Inhibition of MAO B Ile199Phe Mutant	173
Figure 5.6. Comparison of the active site structures of MAO A and MAO B ...	174
Figure 5.7. Kinetic studies of nonspecific MAO inhibitors.....	175
Figure 5.8. Kinetic studies of MAO B specific inhibitors	176
Figure 5.9. Kinetic studies of MAO A specific inhibitors	177
Figure 5.10. Kinetic studies of mechanism based inhibitors.....	178
Figure 5.11. Kinetic studies of rasagiline metabolites	178
Figure 5.12. X-ray crystal structure of MAO B Ile199Ala mutant.....	181
Figure 5.13. X-ray crystal structure of MAO B Ile199Ala-Tyr326Ala mutant. ...	182

Figure 5.14. pH dependence of k_{cat} using benzylamine as a substrate.	187
Figure 5.15. pH dependence of V/K using benzylamine as a substrate	189
Figure 5.16. pH dependence of V/K using pCF ₃ -benzylamine as a substrate.	190
Figure 5.17. pH dependence of k_{cat} using pCF ₃ -benzylamine as a substrate	191
Figure 5.18. Effects of para-substitutions on the rates of reaction of MAO oxidation of benzylamine	193
Figure 5.19. Effects of para-substituent on the rate of oxidation	194
Figure 5.20. Out of plane interactions of para-substituted benzylamine analogues.	195
Figure 5.21. Dependence of k_{cat} on the electronic properties of the para- substituent.	197
Figure 5.22. Dependence of k_{cat} on the electronic properties of the para- substituent.	199

List of Schemes

Scheme 1.1. Oxidation of benzylamine by monoamine oxidase.	3
Scheme 3.1. MAO catalyzed oxidation of dopamine.	45
Scheme 3.2. MAO B bioactivation of MPTP.	46
Scheme 3.3. The catalytic reaction pathway of MAO.	60
Scheme 3.4. Reaction pathway presented by Dunn and colleagues.	61
Scheme 3.5. Proposed hydride transfer mechanism for C-H bond cleavage.	65
Scheme 3.6. Hydrogen atom abstraction.	65
Scheme 3.7. Aminium cation radical mechanism.	67
Scheme 3.8. Mechanism for C-H bond proposed by Ramsay and coworkers.	68
Scheme 3.9. Reaction of Rimoldi's amine with MAO B.	69
Scheme 3.10. Polar nucleophilic mechanism for C-H bond cleavage.	70
Scheme 3.11. Mechanism of reoxidation of flavin by molecular oxygen.	71
Scheme 4.1.1. The mechanism for allylamine inhibition of MAO.	92
Scheme 4.1.2. Development of allylamine analogues.	93
Scheme 4.1.3. Mechanism for inhibition of MAO B by Mofegiline.	104
Scheme 4.3.1. Description of modes of inhibition.	141

List of Tables

Table 2.1. Reactivity and solvent analysis.....	13
Table 2.2. Evaluation of silver salt additives.....	14
Table 2.3. Evaluation of base additives.....	15
Table 2.4. Temperature and rate analysis.....	16
Table 2.5. Effects of reagent stoichiometry on product formation.....	17
Table 2.6. Reduction in enantiometric excess over time.....	17
Table 2.7. Further investigation of reaction solvent.....	18
Table 2.8. Ru(II)indenyl-pybox 10 catalyzed cyclization.....	20
Table 2.9. Temperature and oxidant analysis using catalyst 13.....	21
Table 2.10. Substrate scope of C-H amination methodology.....	22
Table 2.11. Tolerance for olefin.....	23
Table 4.2.1. Inhibitory properties of isatin and styrylisatin analogues.....	121
Table 4.3.1. Competition experiments for 2-BFI inhibition of MAO.....	142
Table 4.3.2. Binding of 2-BFI to MAO B: fluorescences quenching assay.....	146
Table 4.3.3. Thermal denaturation experiments.....	148

Table 5.1. Substrate specificity of the Ile199Ala mutant form	183
Table 5.2. SAR study of benzylic amines.	184
Table 5.3. Substrate investigation	186
Table 5.4. Kinetic properties of the Ile199Ala mutant using benzylamine analogues.	195
Table 5.5. Kinetic isotope effects for the oxidation benzylamine analogs with the Ile199Ala mutant.	196
Table 5.6. K_d of the substrate for the Ile199Ala mutant	196
Table 5.7. Kinetic properties of the Ile199Ala-Tyr326Ala mutant using benzylamine analogues.	198
Table 5.8. Kinetic isotope effects for the oxidation benzylamine analogs with the Ile199Ala-Tyr326Ala mutant.	198
Table 5.9. K_d of the substrate for the Ile199Ala-Tyr326Ala mutant	199

Chapter 1

C-H Bond Cleavage: *From Nature to the Laboratory*

C-H bonds are ubiquitous in nature and are regularly used as a site of chemical modification in biological systems. The cleavage of C-H bonds can be synthetically challenging due to the relatively high bond dissociation energy (~75-115 kcal/mol) and their abundance in nature giving rise to a need for bond selectivity.¹ Nature overcomes these high energy transition barriers through activation of the C-H of interest thereby lowering the transition state energy for the transformation. Synthetic methods have been limited to insertion of highly activated complexes, or neighboring group assistance in order to obtain any degree of selectivity. The study of both biological and synthetic methods for the activation and functionalization of C-H bond is an area of tremendous interest in the chemical community.

Pathways for C-H bond cleavage include deprotonation (H^+), hydrogen atom abstraction (H^\bullet), hydride transfer (H^-), and insertion of a reactive chemical group into an activated C-H bond. Hydrogen atom abstraction and hydride transfer are far less common in synthetic chemistry; although, the utility of both H^\bullet and H^- chemistry has been demonstrated in a number of biological systems. Homolytic C-H bond cleavage produces radical products which are highly reactive chemical species resulting in poor chemoselectivity. For this reason, radical processes are less favorable for development of synthetic strategies. Similarly, the use of hydride transfer has limited utility in synthetic chemistry due

to the costly nature of organic hydride delivery agents (examples include nicotinamide adenine dinucleotide (NAD) and 1,4-cyclohexadiene). Generally these reagents are driven by aromatization of the product which imposes the requirement for in high energy, and therefore less stable, reagents.

The most common of pathway for C-H bond cleavage is deprotonation (H^+) of the C-H bond. This can be accomplished in variety of ways in both biological and synthetic systems. C-H bonds α to carbonyls, nitro groups, phosphines, nitriles, sulfones, and imines are all readily deprotonated using a variety of bases (Figure 1.1). These are common activating groups that result in the reduction of the pK_a of the C-H bond to pK_a values of ~ 10 -30. These transformations generally proceed smoothly with high selectivity both in natural and synthetic system.

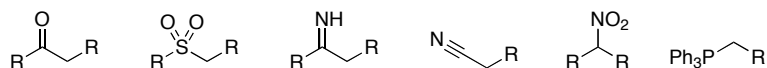
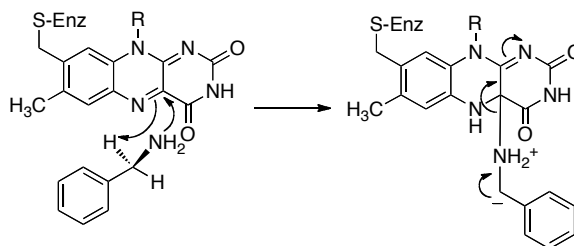


Figure 1.1. Easily deprotonated C-H bonds.

Chapters 3-5 highlight amine oxidation by the flavoprotein, monoamine oxidase (MAO), where deprotonation of a C-H bond proceeds with exceptional catalytic efficiency in the absence of an activating group. It is proposed that covalent adduct formation between the amine and flavin cofactor sufficiently activates the C-H bond for deprotonation (Scheme 1.1).



Scheme 1.1. Oxidation of benzylamine by monoamine oxidase.

To understand how nature deprotonates unactivated C-H bonds, an understanding of the substrate binding site of the protein is required. Chapter 4 details one method that can be utilized to aid in understanding the subtleties of the substrate binding site, which is inhibitor-active site binding interactions. These studies have provided great insights into understanding how binding interactions of the inhibitor-enzyme complex can result in extraordinary stabilization energy (up to -3.9 kcal/mol increase in free energy).

Chapter 5 explores the roles of amino acid residues as structural determinants for selective oxidation of substrates that are specific to MAO. This is a highly provocative investigation given the abundance of amines in nature and therefore the challenges that can be associated with substrate selectivity and recognition. These investigations provide a greater understanding of how nature circumvents the requirement for activating groups in achieving exceptional selectivity and reactivity in C-H bond cleavage reactions.

While deprotonation chemistry is a highly developed area in synthetic chemistry, insertion into seemingly unactivated C-H bonds is a field that is still in its infancy. The cytochrome P450 class of enzymes are perhaps the most widely known for C-H insertion reactions in a biological system. In this system C-H

bonds are hydroxylated by an oxo-ferryl heme. Oxygen atom transfer to the substrate completes the catalytic cycle. These processes are utilized by nature with a high degree of chemo- and enantioselectivity.

Inspired by the reactivity and selectivity of the cytochrome P450 enzymes, synthetic chemists have attempted to mimic the reactions of the P450 enzymes. These endeavors are generally focused on the development of transition metal complexes that can serve as catalysts. Chapter 2 highlights one approach for the development of C-H functionalization technology where cationic-Ru(II) complexes are employed for the asymmetric amination of C-H bonds. These reactions occur with high chemoselectivity for C-H insertion reactions over aziridination reactions, unlike existing technologies which favor aziridination. This methodology is also promising for the development of unactivated C-H bonds through the amination of aliphatic C-H bonds, which is an area of great pursuit that continues to challenge the synthetic community.

The selective cleavage of C-H bonds is a process that continues to be explored in both synthetic and biological systems. Through the study of enzymatic reaction pathways, and the development of new synthetic methodologies, selective functionalization of unactivated C-H bonds is becoming a viable solution to a complex problem.

References

1. CRC handbook of chemistry and physics. In CRC Press: Cleveland, Ohio, 1977; p v.

Chapter 2

Asymmetric Amination of C-H Bonds Using Cationic Ruthenium(II)-pybox Catalysts

2.1 Background and Significance

Functionalization of sp^3 C-H bonds is a topic of interest to many chemists due to their abundance and therefore, potential utility as a functional group. Recent work has showcased the conversion of C-H bonds to C-N, C-B, C-X (where X=halogen), C-C, and C-O bonds and has been the topic of many reviews.¹⁻⁴ These transformations are thought to proceed through one of two different mechanisms, 'inner-sphere' or 'outer-sphere'.

The inner-sphere mechanism involves the functionalization of an unactivated C-H bond through the formation of a discrete organometallic intermediate *via* transition metal mediated cleavage of the C-H bond. This is then followed by functionalization of the metal-alkyl species (Figure 2.1). These transformations typically proceed with high regioselectivity for the least sterically hindered C-H bonds.

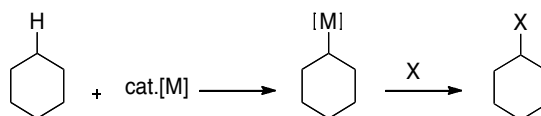


Figure 2.1. Transition metal mediated C-H functionalization via inner-sphere mechanism

The focus of this project is in transformations that proceed through the outer-sphere mechanism. These transformations occur by the formation of a metal oxo, carbene, or nitrene ligand that inserts into an activated C-H bond (Figure 2.2). Unlike the inner-sphere mechanism, the C-H bond does not react

directly with the metal. These transformations occur with high regioselectivity for weaker C-H bonds, which include benzylic, allylic and 3° C-H bonds, as well as C-H bonds α to heteroatoms. In contrast to C-H activation methods, C-H insertion can serve to functionalize sterically hindered C-H bonds. Current functionalization of C-H bonds via the outer-sphere mechanism includes C-O, C-C, and C-N bond formation.

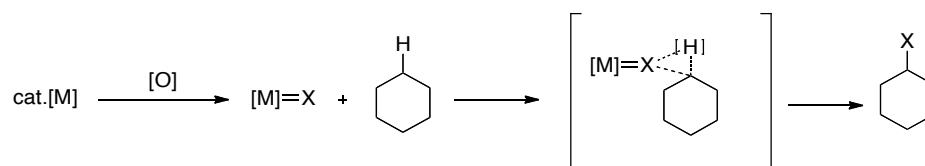
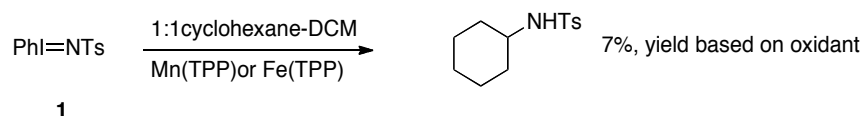


Figure 2.2. Transition metal mediated C-H functionalization via outer-sphere mechanism

Some of the most synthetically useful advances made in C-H insertion chemistry are those of C-H amination. C-H amination is an attractive way of introducing nitrogen functionality in the later stages of synthesis. Transition metal catalyzed nitrene insertion was pioneered by Breslow and Gellman in the early 1980s.⁵ Seminal studies provided a method for the intermolecular amination of cyclohexane by using both Fe and Mn porphyrins in conjunction with (tosyliminoiodo)-benzene **1** acting as both a stoichiometric oxidant as well as a nitrogen source (Figure 2.3A). The transformation proceeded in low yield and required an excess of substrate relative to oxidant. These limitations were addressed in further studies that lead to the development of intramolecular nitrene insertion of sulfonamide **2**. In these studies, $\text{Rh}_2(\text{OAc})_4$ was found to be superior to porphyrin catalysts (Figure 2.3B).⁶ These two systems paved the way

for further exploration of C-H amination methodology using both porphyrin and rhodium(II) catalysts.

A



B

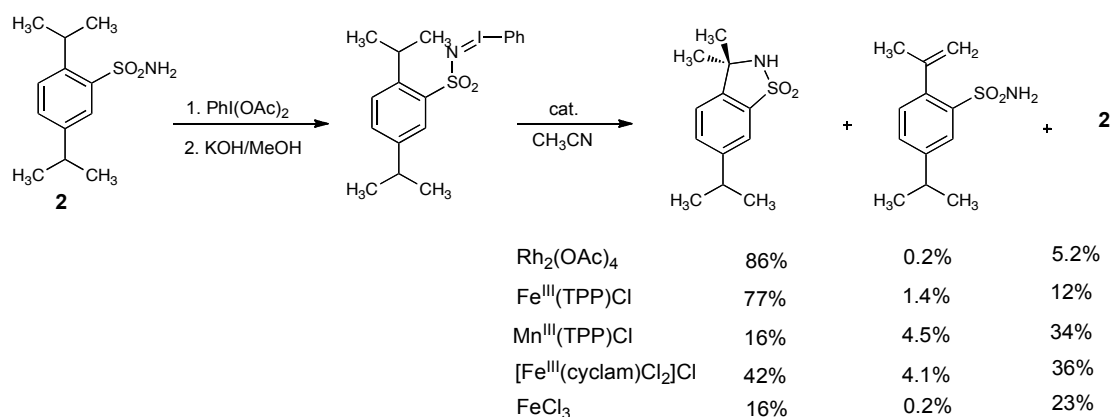


Figure 2.3. First transition metal catalyzed nitrene insertion into a C-H bond. A. Intermolecular C-H amination using cyclohexane and pre-oxidized amine. B. Intramolecular C-H amination using phenyl sulfamate ester condensed with iodobenzene.

2.1.1 Porphyrin Catalysts

Inspired by the finding of Breslow and Gellman, Che and coworkers have studied a variety of porphyrin catalysts for intermolecular and intramolecular amination of C-H bonds.⁷⁻¹⁵ While there are few reported studies in the asymmetric amination of C-H bonds, recent work by Che has shown ruthenium porphyrin catalyst **3** to assist in such transformations giving products with modest ee and yield (Figure 2.4)^{9, 11}.

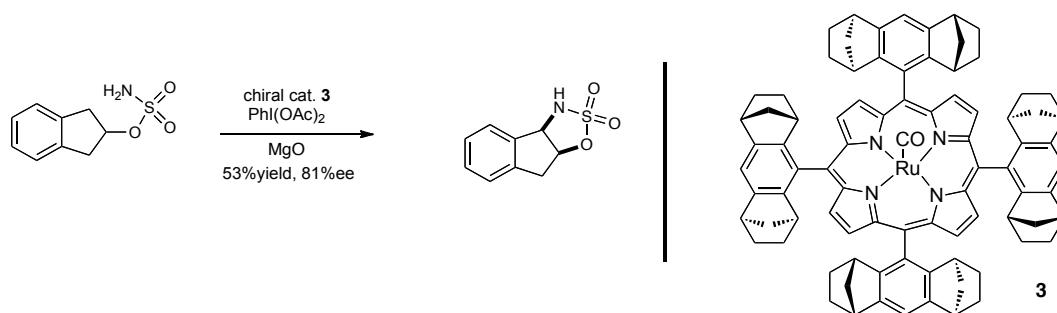


Figure 2.4. Che's asymmetric C-H amination reaction.

After extensive mechanistic studies, Che proposed that the Ruthenium(II) must be oxidized to Ruthenium(VI) for the nitrene to be activated sufficiently for C-H amination to occur.¹⁶ Che further proposed a stepwise hydrogen abstraction process followed by scavenging of the carboradical by the amido-metal complex to form the aminated product rather than a concerted insertion mechanism. However, further investigation is required for a conclusive mechanistic description.

2.1.2 Dirhodium(II) Tetracarboxalate Catalysts

Dirhodium(II) tetracarboxylates have shown extraordinary promise in intramolecular C-H amination. These catalysts are highly efficient and in some cases reach turnovers on the order of 600.¹⁷ The efficiency of these catalysts is attributed to the Rh-Rh bond. It has been suggested that only one metal interacts with the substrate while the other metal acts as an electron sink.¹⁸ The electron sink provides a more electrophilic nitrene species and therefore promotes insertion into a C-H bond. The increased reactivity of these catalysts allows for more challenging substrates to be explored. Dimeric rhodium catalysts

have been shown to cyclize not only sulfamate esters but also the more challenging carbamate substrates.^{17, 19, 20}

Early studies by Du Bois and coworkers demonstrated that the rhodium(II) catalyzed cyclization of carbamates selectively affords five member ring products.¹⁷ In these studies full retention of the stereochemistry of enantiomerically pure carbamate **4** was observed in the oxazolidinone product **5** (Figure 2.5). The full retention of stereochemistry suggests that the dirhodium(II) tetracarboxylates operate *via* a direct insertion mechanism, unlike the ruthenium porphyrins.

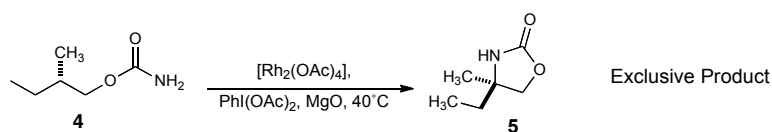


Figure 2. 5. Stereospecific nitrene insertion to form an enantiomerically pure **5** membered ring as the sole product

There are few reports of asymmetric amination using dirhodium(II) tetracarboxylates. Fruit has shown chiral dirhodium(II) tetracarboxylate **6** to assist in the cyclization of sulfamate esters with modest yield and enantioselectivity (Figure 2.6).²¹ More recently, Davies reported a slightly improved complex, **7**, catalyzing the asymmetric cyclization of pre-oxidized carbamates (Figure 2.7).²⁰ An inherent limitation of the dirhodium(II) tetracarboxylates system is that the site of diversification is removed from the active site of the catalyst. Because the source of asymmetry is removed from the

active site of the catalyst, the enantiomeric excess of the product is modest.

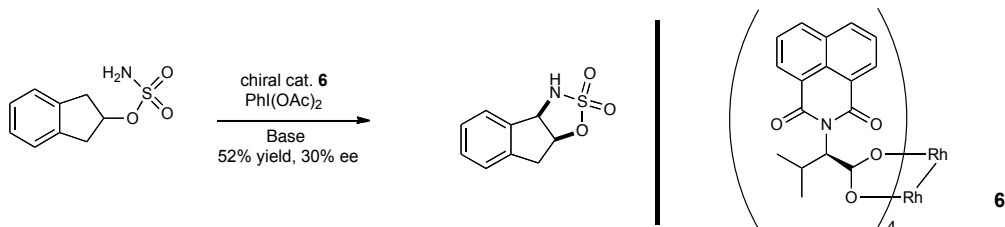


Figure 2.6. Fruit's asymmetric C-H amination reaction

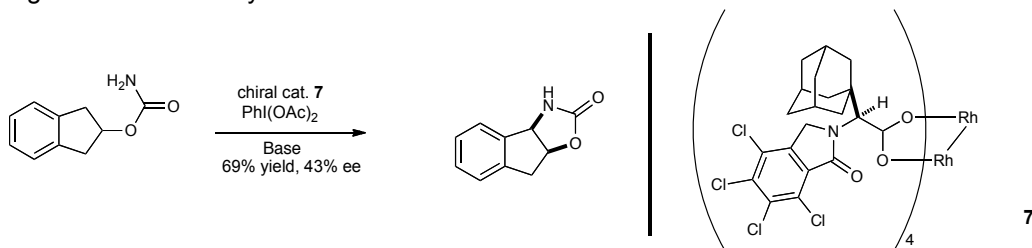


Figure 2.7. Davies' asymmetric C-H amination reaction.

In addition to suffering from modest enantioselectivities, current asymmetric C-H amination systems involve chiral porphyrin catalysts and chiral dirhodium(II) tetracarboxylates that are not commercially available. The expense of preparing these catalysts makes the methodology unattractive.

2.2 Project Objective

It was our goal to design a system for asymmetric intramolecular C-H amination that is a synthetically viable route to generate diverse 1,2- and 1,3-amino alcohols. We also hope to gain greater mechanistic understanding of C-H insertion chemistry to make this methodology more attractive to the synthetic community. This mechanistic insight will allow us to extend this methodology for intermolecular amination, C-C bond formation and C-O bond formation. We aim to accomplish this by utilizing readily available metal salts and ligands that can be made with few manipulations from commercial materials.

2.3 Results and Discussion

2.3.1 Catalyst Design

Two important features must be addressed to design a successful asymmetric C-H amination catalyst. The first is reactivity, and the second is selectivity. The catalyst must demonstrate reactivity that parallels that of the Rh-Rh bond of the dirhodium(II) tetracarboxylates. To accommodate this requirement we focused on aromatic ligands that can aid in stabilizing charge on the metal. To address the concern of selectivity, the source of chirality must be as close as possible to the reactive site of the catalyst. This would overcome the low asymmetric transfer associated with the chiral dirhodium(II) tetracarboxylates. Satisfying these two features resulted in the investigation of Ru(II) pyridine-bis-oxazoline (pybox) complexes (Figure 2.8). The modular nature of pybox in combination with having three open coordination sites on the ruthenium metal affords level of versatility in catalyst design not shared by the dirhodium tetracarboxylates or porphyrin based catalysts. Following literature procedures, phenyl, isopropyl and indenyl-substituted pybox ligands were metallated with ruthenium(II)chloride *p*-cymene to give catalysts **8**, **9**, and **10** (Figure 2.8).²²⁻²⁴

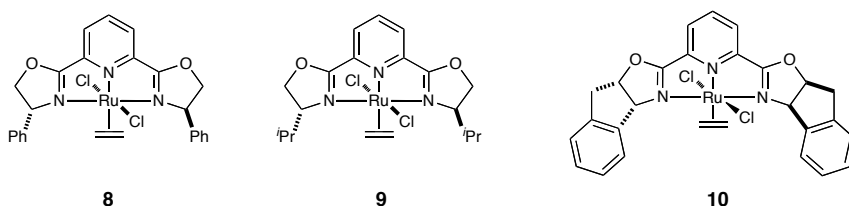


Figure 2.8. Ruthenium(II)-pybox complexes **8-10**.

2.3.2 *Surveying the Reactivity of Catalyst **8** and Reaction Development*

Using conditions adapted from the Du Bois laboratory²⁵, a preliminary assessment of the reactivity of Ru(II)-pybox complexes was carried out using **8** as a model complex in a variety of common organic solvents (Table 2.1). Surprisingly, catalyst **8** catalyzed the intramolecular C-H amination of sulfamate ester **11** to the cyclized product **12** in up to 59% yield (entry 2). This was contrary to the literature precedence for [Ru(pybox-ip)Cl₂(ethylene)] which suggested that these complexes were not active catalysts for C-H amination.⁹ Varying the reaction solvent played an important role in both enantioselectivity and conversion to product. Reactions performed in dichloromethane (DCM) and benzene gave high conversion to product, while reactivity was slightly reduced in diethyl ether. Enantiomeric excess was greatest in diethylether (~40% ee, entry 3), while enantioselectivities for DCM and benzene were comparable (~25% ee, entry 1 and 2). Using acetonitrile, hexanes and THF failed to produce any of the desired product. The intermolecular amination of tetrahydrofuran appears to be competitive with the intramolecular amination of the substrate, leading to only trace amounts of the desired product. With these encouraging results, investigations of C-H amination conditions using dichloromethane, diethyl ether and benzene as solvents were explored.

Table 2.1. Reactivity and solvent analysis

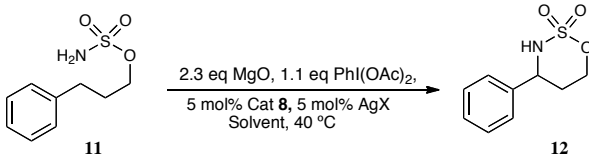
c1ccc(cc1)CCCS(=O)(=O)O $\xrightarrow[5 \text{ mol\% Cat } \mathbf{8}, \text{ Solvent}, 40 \text{ }^\circ\text{C}]{2.3 \text{ eq MgO}, 1.1 \text{ eq PhI(OAc)}_2}$ c1ccc(cc1)CCCS(=O)(=O)O

entry	catalyst	solvent	% conversion	% ee
1	8	DCM	50	24
2	8	Ph-H	59	26
3	8	Ether	47	43
4	8	MeCN	0	-
5	8	Hexanes	0	-
6	8	THF	Trace	-

Further efforts to optimize the system involved the addition of silver salts to dehalogenate the metal complex. With the knowledge that Rh catalyzed C-H insertion processes are driven by the electrophilicity of the metallonitrene, a cationic metal complex was explored to produce a more electrophilic, and therefore more reactive, metal-nitrene intermediate. To our delight, dehalogenation gave a significant boost in enantioselectivity and in some cases raised conversion as well (Table 2.2). The nature of the counterion played a very important role in this process with loosely coordinating and non-coordinating counter ions (^-OTf , $^-BF_4$, $^-SbF_6$, $^-PF_6$) affording higher enantioselectivities (entries 1-12). The acetate ion and trifluoroacetate ion were both very poor additives presumably due to the coordinating nature of the ions (entries 13-18). When examining sodium additives, like sodium tetrphenylborate, the results mirrored those found with no additive suggesting no dehalogenated of the ruthenium catalyst had occurred (entries 19-21). Again, the general trend of the solvent effects are that DCM and benzene gave the highest conversions, while the highest enantioselectivities were observed in diethyl ether. Interestingly, use of ruthenium(II)chloride *p*-cymene in the absence of pybox resulted in < 5% product

formation in diethylether and ~50 % product formation in DCM. Furthermore, AgOTf in the absence of catalyst **8** does not yield product. These results highlight the importance of the ligand system in stabilizing the metallonitrene intermediate, and they demonstrate that the silver salt alone is not capable of oxidizing the sulfamate esters.

Table 2.2. Evaluation of silver salt additives



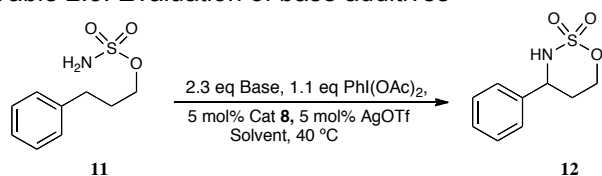
entry	Solvent	Additive	% conversion	% ee ^a
1	DCM	AgOTf	61	53
2	Ether	AgOTf	52	77
3	Ph-H	AgOTf	47	70
4	DCM	AgOAc	55	37
5	Ether	AgOAc	14	46
6	Ph-H	AgOAc	53	44
7	DCM	AgBF ₄	67	54
8	Ether	AgBF ₄	41	73
9	Ph-H	AgBF ₄	58	56
10	DCM	AgSbF ₆	63	48
11	Ether	AgSbF ₆	32	74
12	Ph-H	AgSbF ₆	81	66
13	DCM	AgPF ₆	61	48
14	Ether	AgPF ₆	36	72
15	Ph-H	AgPF ₆	69	64
16	DCM	AgCO ₂ CF ₃	78	33
17	Ether	AgCO ₂ CF ₃	14	55
18	Ph-H	AgCO ₂ CF ₃	53	38
19	DCM	NaBPh ₄	24	15
20	Ether	NaBPh ₄	19	33
21	Ph-H	NaBPh ₄	36	33

a. Enantiomeric excess and conversion determined using chiral HPLC.

After identifying the importance of the counter ions of the silver salts, our efforts focused on examining the role of the base (Table 2.3). Both conversion and enantioenrichment were higher when using the insoluble inorganic bases, MgO and Al₂O₃ (entries 1-6). Use of zinc oxide resulted in lower conversion and comparable enantioenrichment to MgO (entries 10-12). Stronger bases, like

potassium carbonate and dichloropyridine, were very poor additives resulting in much lower turnovers presumably due to coordination to the catalyst (entries 7-9 and 13-15). Surprisingly, the reaction proceeded in the absence of base (entries 16-18), although the reactions with MgO were still the most efficient.

Table 2.3. Evaluation of base additives

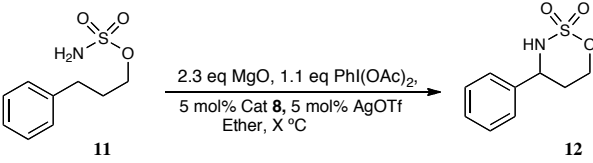


entry	Solvent	Base	% conversion	% ee
1	DCM	MgO	64	53
2	Ether	MgO	67	73
3	Ph-H	MgO	50	65
4	DCM	Al ₂ O ₃	41	49
5	Ether	Al ₂ O ₃	50	71
6	Ph-H	Al ₂ O ₃	55	51
7	DCM	K ₂ CO ₃	34	23
8	Ether	K ₂ CO ₃	20	52
9	Ph-H	K ₂ CO ₃	50	21
10	DCM	ZnO	30	43
11	Ether	ZnO	17	72
12	Ph-H	ZnO	64	52
13	DCM	2,6-chloropyridine	51	43
14	Ether	2,6-chloropyridine	50	65
15	Ph-H	2,6-chloropyridine	67	53
16	DCM	No Base	75	49
17	Ether	No Base	46	70
18	Ph-H	No Base	47	55

To further tune the reaction, we performed a collection of experiments to help us identify the causes of the incomplete conversion and lower enantioenrichment (Table 2.4). In side-by-side experiments, four identical reactions were set up. Two reactions were monitored at 40 °C, and two reactions were monitored at room temperature. At elevated temperatures, the reaction stalled after one hour giving 50% conversion (entries 1-4); however, at room temperature the reaction progressed steadily over an eight hour period but only

went to 41% conversion (entries 6-9). During the course of the analysis the two controls were held at the two temperatures, untouched, to evaluate the integrity of the experiment (entries 5 and 10). These experiments demonstrated that limited exposure to atmospheric conditions was not affecting the outcome of the reaction.

Table 2.4. Temperature and rate analysis

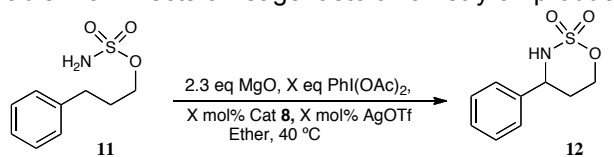


entry	Temp (°C)	Time (h)	% conversion	% ee
1	25	1	3	13
2	25	2	6	75
3	25	4.5	22	75
4 ^a	25	8	41	72
5	40	1	58	72
6	40	2	59	75
7	40	4.5	55	74
8 ^a	40	8	54	73

a. Standard ran side-by-side without extracting aliquots.

In an effort to identify the source of catalytic arrest, reactions were performed with double the amount of oxidant, catalyst and silver salt, individually (Table 2.5). No change in reactivity or enantioenrichment was observed when the stoichiometry of these reagents was changed. To evaluate the moisture sensitivity of this system, controlled amounts of water were added to the reactions. When as little as 1 equivalent of water was added (data not shown), no reaction was observed demonstrating that strictly anhydrous conditions are required.

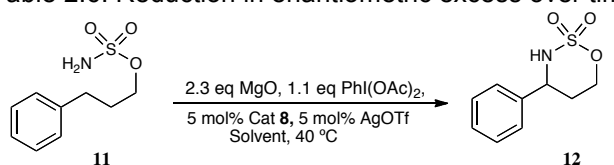
Table 2.5. Effects of reagent stoichiometry on product formation



entry	eq oxidant	eq cat	eq AgOTf	% conversion	% ee
1	2.2	0.05	0.05	48	77
2	1.1	0.10	0.10	43	70
3	1.1	0.05	0.10	53	71

During the course of our studies, we observed that the product of the reaction was susceptible to a reduction in % ee, particularly in benzene (Table 2.6). The cause of the reduction in enantiomeric excess could be due to either racemization or side reactions due to catalyst decomposition. This highlights the requirement for mild reaction conditions (weak base and mild temperature) in the development of an asymmetric C-H amination protocol.

Table 2.6. Reduction in enantiomeric excess over time

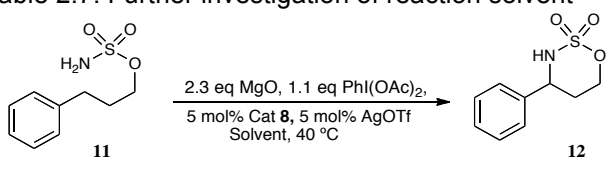


entry	Solvent	Time (h)	% ee
1	DCM	18	53
2	DCM	48	51
3	Ether	18	73
4 ^a	Ether	48	67
5	Ph-H	18	65
6	Ph-H	48	28

Optimization of the reaction conditions led to the reexamination of the reaction solvent. Because diethylether afforded the highest enantioselectivities, dimethylether (DME) and ^tbutylmethylether were explored (Table 2.7, entry 2 and 4). ^tButylmethylether provided good conversion (70%) with enantioselectivity (68% ee) rivaling diethyl ether (entry 4). However, DME produced moderate

enantioselectivities (56% ee) and only 58% conversion (entry 2). Similarly, benzene produce high levels of conversion with modest ee; therefore, toluene was explored (entry 3). Use of toluene as a solvent resulted in poor conversion to product (38%) and only modest enantioselectivity (63% ee). While anhydrous alcoholic solvents were explored, no conversions to product was observed (entry 1).

Table 2.7. Further investigation of reaction solvent



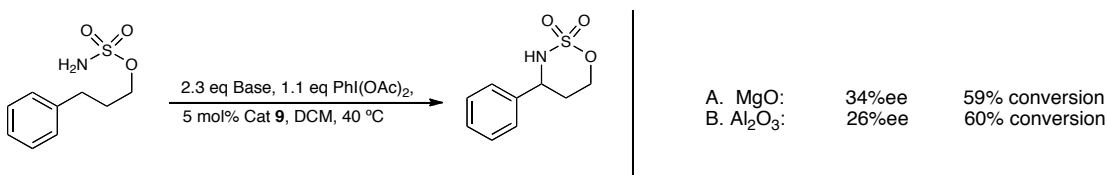
entry	Solvent	% conversion	% ee
1	MeOH	0	NA
2	DME	58	56
3	Ph-Me	38	63
4	^t BuOMe	70	68

2.3.3 Novel Metal Complexes: Survey of Pybox Ligands

After extensive optimization of the Ru(II)phenylpybox system, we focused our attention on additional pybox ligands. In particular we predicted that larger 'R' groups on the pybox would lead to improved enantioselectivities. Attempts to metallate ^tbutyl-pybox met with failure. Ruthenium(II) is too large to fit into the ligand pocket.²⁴ Therefore, metallation of *iso*propyl-pybox²⁴ **9** and indenyl-pybox **10** with ruthenium(II)chloride *p*-cymene was carried out, and these complexes were explored in the reaction conditions described above. Initial reports by Che suggested that Ru(II)ip-pybox **9** was a poor catalyst for C-H amination.⁹ We hypothesized that the tertiary C-H bond in the catalyst was aminated under the reaction conditions, and we set out to demonstrate this. To our surprise, Ru(II)ip-pybox **9** proved to be an adequate catalyst, yielding 60% conversion with modest

ee in our hands (Figure 2.9A). When treated with a silver salt, catalyst **9** was competitive with the phenyl pybox **8** as an enantioselective C-H amination catalyst (Figure 2.9B). These results provoked further optimization experiments analogous to those already described for the phenyl-pybox. The results of the experiments followed the trends previously mentioned in this section.

A



B

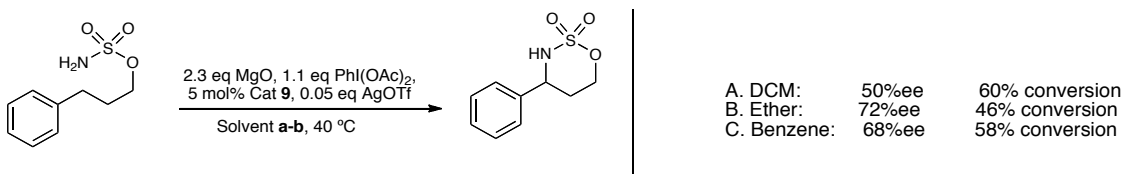
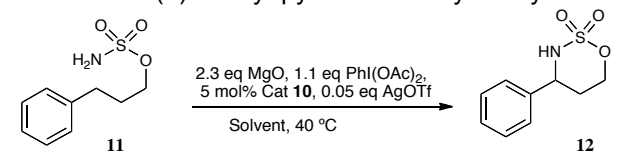


Figure 2.9. Ru(II)ip-pybox **9** as an active catalyst for C-H amination

The Ru(II)indenyl-pybox catalyst **10** proved to be superior to all other catalysts examined (Table 2.8). Reaction in dichloromethane was exceptionally efficient giving product with 94% conversion and 69%ee (the highest %ee observed in this solvent) (entry 1, Table 2.8). Diethylether and benzene provided very good enantioselectivities (84%ee, entries 2 and 3), although conversions were modest (40% and 45%, respectively). A strong counterion effect was observed in trifluorotoluene with silver hexafluoroantimonate giving significantly improved results compared with silver triflate (entries 5). These results provide

an excellent platform to further optimize this C-H amination protocol and to generate an asymmetric C-H amination protocol.

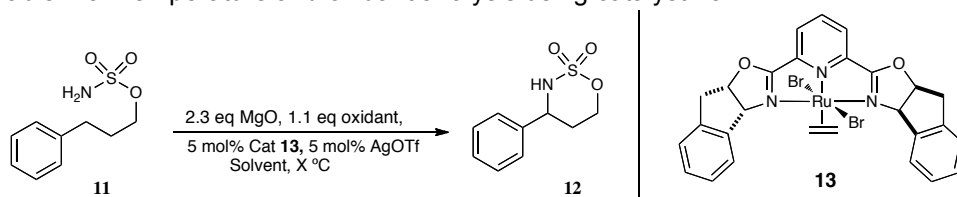
Table 2.8. Ru(II)indenyl-pybox 10 catalyzed cyclization



entry	Solvent	% conversion	% ee
1	DCM	94	69
2	Ether	40	84
3	Ph-H	45	84
4	^t BuOMe	48	72
5 ^a	CF ₃ Ph	55	57

^a. Reaction was run using AgSbF₆ in place of AgOTf.

Replacing the chloride ligands with the larger bromide ligands, **13**, was carried out to tighten the transition state imido complex through steric interactions with the hopes of increasing enantioselectivity. To our delight this change improved enantioselectivities and also resulted in an increase in the reactivity of the catalyst allowing the temperature to be reduced to 22 °C. Further optimization occurred when the acetate leaving groups of PhI(OAc)₂ were replaced with ^tbutyl groups increasing the solubility of the oxidant, which facilitated lower temperature reactions without a loss in reactivity (Table 2.9, entry 2 and 6). The lower temperatures also resulted in higher enantioselectivity in benzene (entry 5 and 6).

Table 2.9. Temperature and oxidant analysis using catalyst **13**

entry	solvent	temperature (°C)	oxidant	% conversion	% ee
1	DCM	40	PhI(OAc) ₂	92	72
2	DCM	rt	PhI(O ₂ C ^t Bu) ₂	88	63
3	Ether	40	PhI(OAc) ₂	34	87
4	Ether	rt	PhI(O ₂ C ^t Bu) ₂	-	-
5	Ph-H	40	PhI(OAc) ₂	34	69
6	Ph-H	rt	PhI(O ₂ C ^t Bu) ₂	79	79

Using catalyst **13** we decided to probe the utility of the reaction by evaluating the substrate scope (Table 2.10). The reaction was tested using a variety of functionalized aryl substrates. *Ortho*-methylated substrates **14** are not recommended for the reaction due to competition between nine membered ring **15** and six membered ring formation **16** (entry 1 and 2). Electron rich aromatics **17** and **18** (entry 3 and 5) are efficiently converted to product even in the presence of sterically hindered *ortho*-groups (entry 3). Electron poor aromatics **19** and **20** (entry 4 and 6) are also tolerated with slightly lower efficiency. Interestingly, unactivated alkyl chains **21** (entry 8) can be aminated using catalyst **13**, although with much lower efficiency.

Table 2.10. Substrate scope of C-H amination methodology

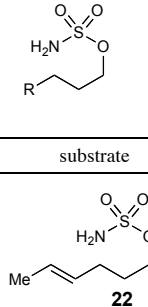
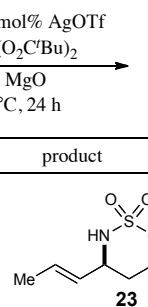
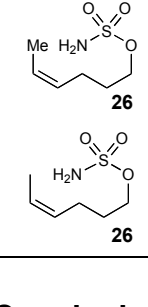
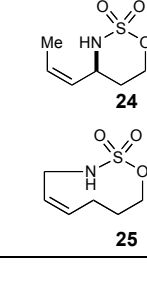
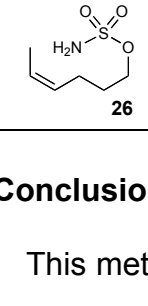
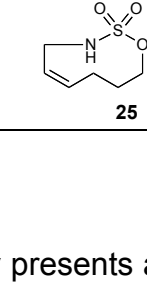
entry	substrate	product	% yield ^a	% ee
1			20	n.d.
2			23	-
3			71	88
4			60	88 ^b
5			68	90
6			58	92
7			42	75
8			14	n.d.

^a: isolated yield. ^b: absolute configuration determined by x-ray crystallography; all other configurations are assigned by analogy. Not determined (n.d.).

Existing catalysts for the amination of C-H bonds rapidly form aziridination products in the presence of olefins. To further probe the utility of this catalyst, we

subjected alkene containing sulfamate esters to the reactions conditions in the presence of catalyst **13** (Table 2.11). To our delight, no aziridination products were detected. *Trans*-alkenes **22** are converted to the corresponding six membered ring products **23** in modest yield and good ee (entry 1). Both six **24** and nine **25** member ring formation is observed for the (*Z*)-hex-4-enyl sulfamate **26** (entry 2 and 3). Moreover, **26** does not isomerizes in the presence of catalyst as would be expected if the reaction occurred through a radical process as first described by Che.¹⁶

Table 2.11. Tolerance for olefin

entry	substrate	product	% yield	% ee
1	 22	 23	60	89
2	 26	 24	42	50
3	 26	 25	16	-

2.4 Conclusions

This methodology presents an efficient route for the asymmetric amination of benzylic and allylic C-H bonds. The utility of the reaction is further highlighted by the modular nature of the catalyst, which can be tuned through the choice of pybox ligand or through ligand substitution of the three open coordination sites. Given the high selectivity of this catalyst for C-H bond functionalization over

aziridination, this methodology complements the existing C-H amination methodology that has been developed by Du Bois and Che.

2.5 Materials and Methods

General. All reagents were obtained commercially unless otherwise stated. Magnesium oxide was flame dried under reduced pressure prior to use. Bis(*tert*-butylcarbonyloxy)-iodobenzene was dried on the high vacuum for 12 hours prior to use. Silver triflate was used as received from Aldrich. All reactions were performed using oven dried glassware under an atmosphere of argon. Dichloromethane and diethyl ether were purified by passage through activated Alumina using the method of Grubbs, with a *Glass Contours* solvent purification system. Anhydrous α,α,α -trifluorotoluene, *t*-butylmethyldiethyl ether, and benzene were purchased from *Aldrich Chemical Company* and used without further purification. Pyridine was purified by distillation from calcium hydride. Benzene was dried over activated 4 Å molecular sieves and degassed by argon sparge prior to use. The dibromo(benzene)ruthenium(II) dimer was prepared by previously reported methods from commercial ruthenium(III) bromide hydrate.²⁶ Dichloro(benzene)ruthenium(II) dimer and di- μ -chlorobis[(*p*-cymene)chlororuthenium(II)] were purchased from Strem chemical company and used as received. Indenyl pybox and phenyl pybox were purchased from Strem chemical company and used as received. Sulfamate esters were prepared using a protocol previously outlined by Du Bois and coworkers.²⁵ Sulfamate esters 2-(2,3-dihydro-1H-inden-2-yl)ethyl sulfamate **27**, 3-phenylpropyl sulfamate **11**, and *tert*-butyl 3-(3-(sulfamoyloxy)propyl)-1H-indole-1-carboxylate **20** were prepared

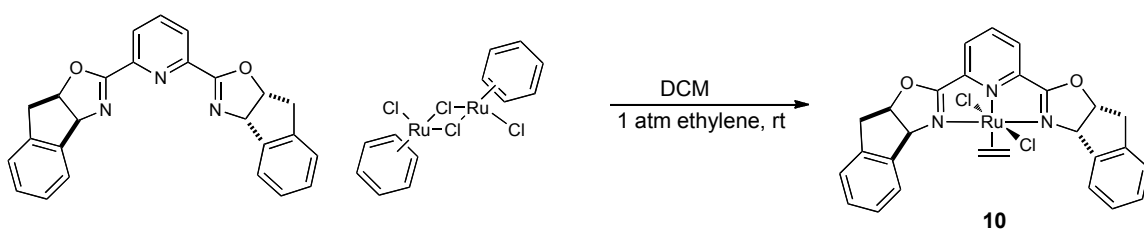
by previously reported methods.²⁵ 3-(2-Methoxyphenyl)propyl sulfamate **17** and 3-(4-methoxyphenyl)propyl sulfamate **18** were prepared by protocols outlined by Che and coworkers.⁹ Purification of reaction products was carried out by flash chromatography using Geduran silica gel 60 (40-63 μm). Analytical thin layer chromatography (TLC) was performed on EMD 0.25 mm silica gel 60 plates. Visualization was accomplished with UV light, ethanolic anisaldehyde, aqueous potassium permanganate, or aqueous ceric ammonium molybdate (CAM) solution followed by heating.

Proton and carbon magnetic resonance spectra (^1H NMR and ^{13}C NMR) were recorded using Varian 400 MHz NMR (^1H NMR at 400 MHz and ^{13}C NMR at 100 MHz) with solvent resonance as the internal standard. ^1H NMR data are reported as follows: chemical shift (δ , ppm), multiplicity (s = singlet, br s = broad singlet, d = doublet, br d = broad doublet, t = triplet, q = quartet, m = multiplet, dd = doublet of doublets, qd = quartet of doublets, td = triplet of doublets), integration, coupling constants (J, Hz). Data for ^{13}C NMR are reported in terms of chemical shift (δ , ppm). Gas chromatography analysis was performed using an Agilent 6850 Network GC system equipped with a CHIRASIL-DEX CB column (25 m x 0.250 mm, pressure = 17.02 psi, column flow = 2.0 mL/min, detector = FID, 225 $^\circ\text{C}$). High performance liquid chromatography (HPLC) was carried out on an Agilent 1100 series HPLC equipped with a Chiralpak AD-H or Chiracel OH-D column (UV detection at 210 nm). Infrared (IR) spectra were recorded using Nicolet 300 FT-IR spectrometer. High-resolution mass spectra were obtained using the Mass Spectrometry Facility, Emory University. We acknowledge the

use of shared instrumentation provided by grants from the NIH and the NSF. We gratefully acknowledge the contributions of Dr. Kenneth Hardcastle for the collection of all X-ray crystallography data.

Preparation of Pybox-Ru(II) complexes

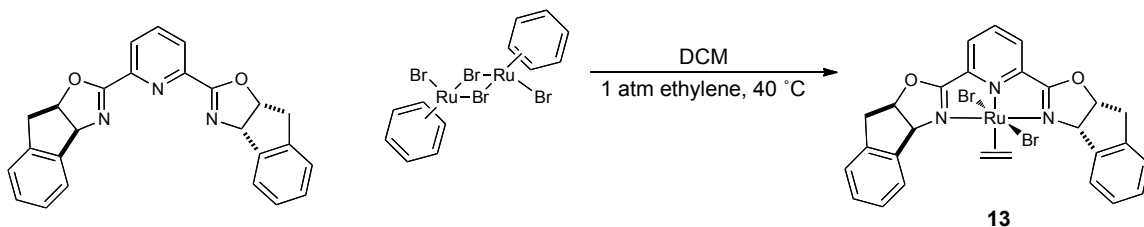
Phenyl-pybox-dichlororuthenium(II) **8** and isopropyl-pybox-dichlororuthenium(II) **9** were prepared by literature methods from commercially available pybox ligand and Di- μ -chlorobis[(*p*-cymene)chlororuthenium(II)].^{24,27}



Indenyl-pybox ruthenium(II) chloride ethylene complex 10

Indenyl-pybox (0.2 g, 0.50 mmol) and di- μ -chlorobis[(benzene)chlororuthenium(II)] (0.15 g, 0.25 mmol) in DCM (8 mL) was stirred at room temperature under an atmosphere of ethylene for 3 h. An opaque red solution can be observed after 10 min. The reaction mixture was then concentrated and recrystallized from DCM and hexanes. The solid was then isolated by filtration and washed with a solution of hexanes/ether (2:1, 10 mL) to remove excess *p*-cymene. The crystals were isolated as the dichloromethane adduct. Drying under vacuum for 24 h removes excess DCM to afford the dark red indenyl-pyboxRu(II)chloride ethylene complex (0.24 g, 80%). **¹H NMR** (CDCl₃, 400 MHz) δ 7.79-7.75 (m, 4H), 7.30-7.23 (m, 7H), 6.00 (t, 2H, J = 5.7 Hz), 5.82 (d, 2H, J = 6.4 Hz), 5.30 (s, 1H, DCM adduct), 5.67-5.64 (m, 2H), 5.40-5.38 (m, 2H), 3.67-3.52 (m, 4H) ppm; **¹³C NMR** (CDCl₃, 100 MHz) δ 165.5, 146.6,

139.4, 137.7, 133.8, 129.7, 128.3, 128.2, 125.0, 123.6, 91.6, 74.9, 74.6, 37.6 ppm; **HRMS** calcd for $C_{27}H_{23}N_3O_2Cl_2Ru$ 593.0213, found 593.02059; **IR** (thin film, cm^{-1}) ν 3068, 2333, 2320, 2145, 1965, 1650, 1556, 1393, 1005, 956, 756.



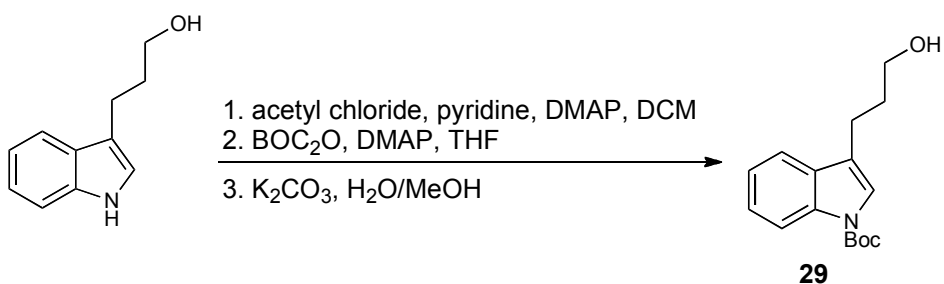
Indenyl-pybox ruthenium(II) bromide ethylene complex 13

Indenyl-pybox (0.15 g, 0.38 mmol) and di- μ -chlorobis[(p-cymene)chlororuthenium(II)] (0.14 g, 0.21 mmol) in DCM (15 mL) were stirred at 40 °C under an atmosphere of ethylene for 24 h. The reaction was then transferred to the glovebox and filtered over celite. The filter cake was washed with DCM until the filtrate ran clear (about 50 mL), and the filtrate was concentrated. The red powder was dissolved in minimal DCM and recrystallized by layering of hexanes/ether (1:1 v/v, 2.0 mL) then hexanes (2.0 mL). The solid was then isolated by filtration and washed with a solution of hexanes/ether (1:1, 20 mL) to remove any excess benzene. The dark burgundy crystals were dried under vacuum for 24 h (0.21 g, 79%). X-ray quality crystals were obtained by the slow diffusion of petroleum ether into chloroform. **1H NMR** ($CDCl_3$, 400 MHz) δ 7.86 (d, 2H, $J = 7.3$ Hz), 7.80 (s, 3H), 7.32-27 (m, 6H), 5.98 (t, 2H, $J = 6.4$ Hz), 5.83-5.77 (m, 4H), 5.55-5.52 (m, 2H), 3.67-3.51 (m, 4H) ppm; **^{13}C NMR** ($CDCl_3$, 100 MHz) δ 165.5, 146.6, 139.5, 137.4, 133.7, 129.7, 128.6, 128.2, 125.0, 123.7, 91.8, 74.7, 73.2, 37.5 ppm; **HRMS** calcd for $C_{27}H_{23}N_3O_2Br_2Ru$ 680.9201, found

695.9129; IR (thin film, cm^{-1}) ν 3497, 3060, 3003, 2966, 1605, 1581, 1556, 1475, 1393, 1291, 1242, 1001, 960, 817, 743, 723.

Preparation of aryl alcohols

3-(4-Bromophenyl)propan-1-ol **28** was prepared by $\text{BH}_3\text{-SMe}_2$ reduction of the commercially available carboxylic acid using a procedure outlined by Hartwig and coworkers.²⁸ 3-(1H-Indol-3yl)propan-1-ol was prepared by the Fisher indole reaction of phenylhydrazine-HCl with dihydrofuran in the presence of 4% sulfuric acid as outlined by Campos and coworkers.²⁹



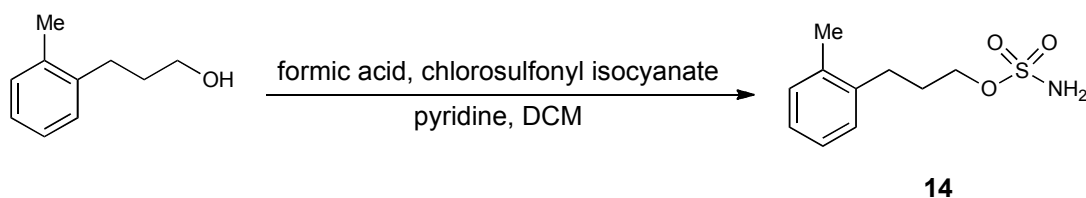
3-(1Boc-Indol-3yl)propan-1-ol (**29**)

To a solution of 3-(1H-indol-3yl)propan-1-ol (1.68 g, 9.6 mmol), pyridine (0.82 mL, 10 mmol) and DMAP (0.06 g, 0.48 mmol) in DCM (70 mL) was added acetyl chloride (0.72 mL, 10 mmol) dropwise. The resulting solution was stirred at room temperature until all of the starting material was consumed, as judged by TLC. The reaction was quenched by the careful addition of 1M HCl (60 mL). The organic layer was separated and washed with saturated sodium bicarbonate (60 mL) and brine (60 mL). The organic layer was dried over magnesium sulfate and concentrated to yield a white solid. The 3-(1H-indol-3yl)propan-1-ol acetate product was dissolved in DCM (3 mL) and to this solution was added DMAP

(0.008 g, 0.07 mmol) and Boc anhydride (0.82 g, 3.8 mmol). The reaction was stirred at room temperature until all of the starting material was consumed, as judged by TLC. The reaction was quenched by the addition of 1M HCl (3 mL). The organic layer was separated and washed with brine (60 mL), dried over magnesium sulfate and concentrated to yield yellow solid. The solid was dissolved in methanol/H₂O (1:1, 30 mL) and to this was added potassium carbonate (4.8 g, 34.5 mmol). The suspension was stirred at room temperature for 4 h and was then poured into a separatory funnel charged with H₂O (50 mL) and DCM (60 mL). The aqueous layer was extracted with DCM (20 mL). The combined organic extracts were washed with brine (50 mL), dried over magnesium sulfate and concentrated to yield 1.9 g, 72% overall yield. The 3-(1Boc-indol-3yl)propan-1-ol product was of sufficient purity for synthetic purposes: **¹H NMR** (CDCl₃, 400 MHz) δ 8.11 (br s, 1H), 7.54 (d, 1H, *J* = 7.9 Hz), 7.38 (br s, 1H), 7.31 (td, 1H, *J* = 7.3, 1.3 Hz), 7.24 (td, 1H, *J* = 6.4, 1.0 Hz), 3.75 (t, 2H, *J* = 6.4 Hz), 2.79 (t, 2H, *J* = 8.3 Hz), 2.02-1.95 (m, 2H), 1.67 (s, 9H) ppm; **¹³C NMR** (CDCl₃, 100 MHz) δ 124.5, 122.6, 122.5, 120.7, 119.2, 115.5, 62.6, 32.3, 28.4, 21.3 ppm; **HRMS** calcd for C₁₆H₂₁NO₃ 275.1522, found 276.15942; **IR** (thin film, cm⁻¹) ν 3334, 2974, 2925, 2868, 1720, 1442, 1364, 1148, 1078, 1050, 743, ; **TLC** R_f = 0.45 (3:1 hexane/EtOAc).

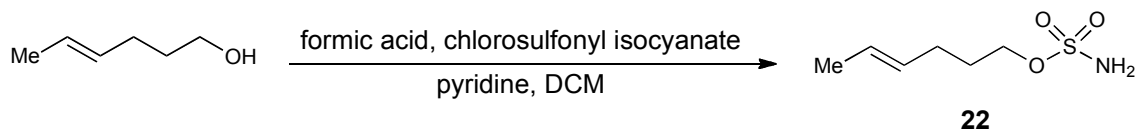
General procedure for preparation of sulfamate esters

These compounds were prepared from the respective alcohols according to a protocol reported by Du Bois and coworkers.¹



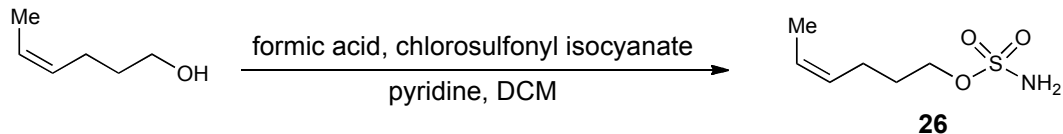
3-o-Tolylpropyl sulfamate (14)

Purified by chromatography on silica gel (3:1 hexanes/EtOAc); white solid (75%); **¹H NMR** (CDCl₃, 400 MHz) δ 7.16-7.13 (m, 4H), 4.87 (br s, 2H), 4.25 (t, 2H, *J* = 6.3 Hz), 2.75 (t, 2H, *J* = 7.5 Hz), 2.32 (s, 3H), 2.07-2.01 (m, 2H) ppm; **¹³C NMR** (CDCl₃, 100 MHz) δ 138.8, 136.2, 130.6, 129.1, 126.6, 126.3, 71.0, 29.2, 29.2, 19.5 ppm; **HRMS** calcd for C₁₀H₁₅NO₃S 229.08, found 228.06868; **IR** (thin film, cm⁻¹) ν 3379, 3281, 2950, 1356, 1168, 919, 739, 551; **TLC** R_f = 0.5 (2:1 hexane/EtOAc).



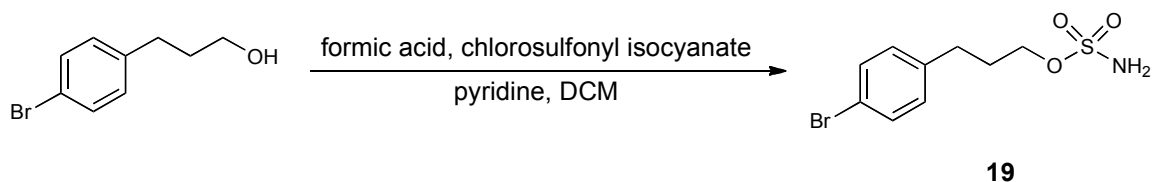
(*E*)-Hex-4-enyl sulfamate (22)

Purified by chromatography on silica gel (2:1 hexanes/EtOAc); colorless viscous oil (78%); **¹H NMR** (CDCl₃, 400 MHz) δ 5.52-5.34 (m, 2H), 4.9 (br s, 2H), 4.20 (t, 1H, *J* = 6.7 Hz), 2.18-1.83 (m, 2H), 1.81-1.76 (m, 2H), 1.65 (d, 3H, *J* = 6.3 Hz) ppm; **¹³C NMR** (CDCl₃, 100 MHz) δ 129.4, 126.8, 71.1, 28.7, 28.5, 18.1 ppm; **HRMS** calcd for C₆H₁₃NO₃S 179.06, found 178.05423; **IR** (thin film, cm⁻¹) ν 3375, 3285, 2934, 2382, 1360, 1172, 931, 813; **TLC** R_f = 0.3 (DCM).



(Z)-Hex-4-enyl sulfamate (26)

Purified by chromatography on silica gel (4:1 hexanes/EtOAc); colorless viscous oil (72%); $^1\text{H NMR}$ (CDCl_3 , 400 MHz) δ 5.56-5.48 (m, 1H), 5.38-5.31 (m, 1H), 5.02 (br s, 2H), 4.20 (t, 1H, $J = 6.7$ Hz), 2.16 (q, 2H, $J = 14.9$ Hz), 1.84-1.77 (m, 2H), 1.62 (d, 3H, $J = 7.0$ Hz) ppm; $^{13}\text{C NMR}$ (CDCl_3 , 100 MHz) δ 128.5, 125.8, 71.1, 28.7, 22.8, 13.0 ppm; **HRMS** calcd for $\text{C}_6\text{H}_{13}\text{NO}_3\text{S}$ 179.06, found 178.05379; **IR** (thin film, cm^{-1}) ν 3371, 3277, 3011, 2938, 2852, 1556, 1348, 1172, 927, 821, 543; **TLC** $R_f = 0.2$ (DCM).



3-(4-Bromophenyl)propyl sulfamate (19)

Purified by chromatography on silica gel (2:1 hexanes/EtOAc); white solid (83%); $^1\text{H NMR}$ (CDCl_3 , 400 MHz) δ 7.43 (d, 2H, $J = 8.2$ Hz), 7.08 (d, 2H, $J = 8.2$ Hz), 4.81 (br s, 2H), 4.20 (t, 2H, $J = 6.3$ Hz), 2.71 (t, 2H, $J = 7.4$ Hz), 2.04 (m, 2H) ppm; $^{13}\text{C NMR}$ (CDCl_3 , 100 MHz) δ 139.6, 131.8, 130.4, 120.3, 70.5, 31.2, 30.4 ppm; **HRMS** calcd for $\text{C}_{10}\text{H}_{15}\text{NO}_3\text{S}$ 290.99, found 291.96481; **IR** (thin film, cm^{-1}) ν 3354, 3260, 2966, 1483, 1352, 1164, 931; **TLC** $R_f = 0.4$ (2:1 hexane/EtOAc).

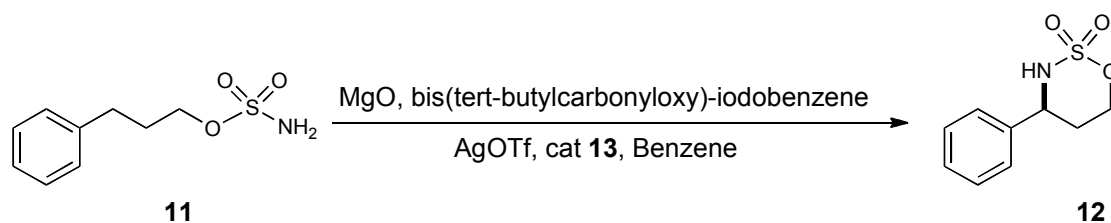
General procedure for cyclization of sulfamate esters

Procedure A

A 25 mL round bottom flask was charged with substrate (0.42 mmol), bis(tert-butylcarbonyloxy)-iodobenzene (0.206 g, 0.506 mmol), magnesium oxide (0.043 g, 1.07 mmol), catalyst (0.016 g, 0.023 mmol), and silver triflate (0.006 g, 0.023 mmol) and cooled to 4 °C under an atmosphere of Argon. Benzene (3 mL) was added, and the resulting suspension was stirred at 4 °C for 24 h. The reaction was then quenched at 4 °C by the addition of methanol (2.0 mL) and filtered over celite. The filter cake was washed with ethyl acetate (3 x 15 mL) and DCM (2 x 15 mL). The filtrate was concentrated under reduced pressure, and the crude oil was purified by chromatography on silica gel. The conversion of the reaction and enantiomeric excess of the product was analyzed by HPLC.

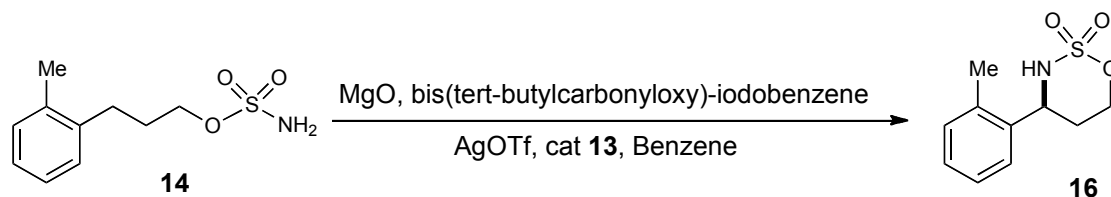
Procedure B

A 25 mL round bottom flask was charged with substrate (0.42 mmol), bis(tert-butylcarbonyloxy)-iodobenzene (0.206 g, 0.506 mmol), magnesium oxide (0.043 g, 1.07 mmol), catalyst (0.016 g, 0.023 mmol), and silver triflate (0.006 g, 0.023 mmol) at room temperature under an atmosphere of Argon. Benzene (3 mL) was added, and the resulting suspension was stirred at room temperature for 24-36 h. The reaction was then quenched by the addition of methanol (2.0 mL) and filtered over celite. The filter cake was washed with ethyl acetate (3 x 15 mL) and DCM (2 x 15 mL). The filtrate was concentrated under reduced pressure. The crude oil was purified by chromatography on silica gel. The conversion of the reaction and enantiomeric excess of the product was analyzed by HPLC.



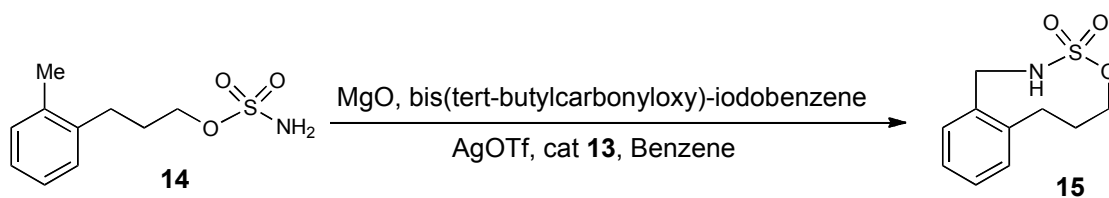
Phenyl-oxathiazinane (12)

Procedure A. Purified by chromatography on silica gel (4:1 hexanes/EtOAc); white solid (57%); $^1\text{H NMR}$ (CDCl_3 , 400 MHz) δ 7.43-7.34 (m, 5H), 4.86 (t, 2H, J = 11.7 Hz), 4.66 (ddd, 1H, J = 11.3, 4.7, 1.2 Hz), 4.51 (d, 1H, J = 9.4 Hz), 2.25 (qd, 1H, J = 14.5, 4.7 Hz), 2.00 (dq, 1H, J = 14.5, 2.4 Hz) ppm; **TLC** R_f = 0.9 (2:3 DCM/diethyl ether).



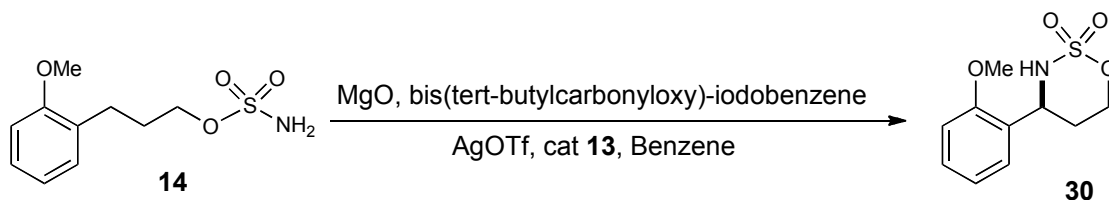
o-Me-oxathiazinane 6 membered ring (16)

Procedure B. Purified by chromatography on silica gel (3:1 hexanes/EtOAc); white solid (20%); $^1\text{H NMR}$ (CDCl_3 , 400 MHz) δ 7.34-7.22 (m, 4H), 5.04 (m, 1H), 4.87 (td, 1H, J = 11.7, 2.0 Hz), 4.67 (ddd, 1H, J = 11.7, 5.1, 1.6 Hz), 4.12 (br d, 1H, J = 9.8 Hz), 2.44 (s, 3H), 2.42-2.34 (m, 1H), 1.90 (dq, 1H, J = 14.5, 1.9 Hz) ppm; $^{13}\text{C NMR}$ (CDCl_3 , 100 MHz) δ 137.0, 135.8, 131.5, 129.1, 126.8, 124.9, 72.1, 55.7, 29.1, 19.2 ppm; **HRMS** calcd for $\text{C}_{10}\text{H}_{13}\text{NO}_3\text{S}$ 227.0617, found 228.06863; **IR** (thin film, cm^{-1}) ν 3265, 2954, 2921, 2852, 2357, 1712, 1462, 1409, 1356, 1176, 1017, 919, 784; **TLC** R_f = 0.9 (5% MeOH in DCM).



o-Me-oxathiazinane 9 membered ring (15)

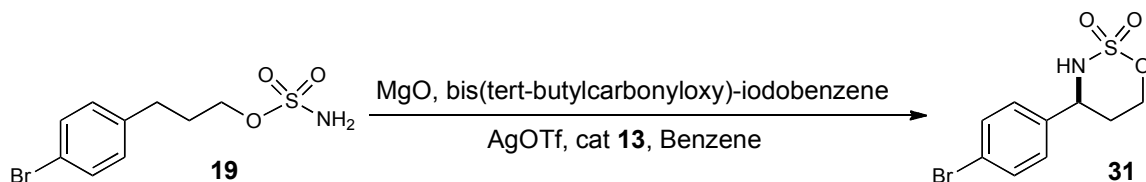
Procedure B. Purified by chromatography on silica gel (3:1 hexanes/EtOAc); white solid (23%); $^1\text{H NMR}$ (CDCl_3 , 400 MHz) δ 7.37 (t, 1H, $J = 7.9$ Hz), 7.30-7.28 (m, 2H), 7.20 (d, 1H, $J = 7.3$ Hz), 4.75 (br s, 1H), 4.34 (d, 2H, $J = 5.1$ Hz), 4.01 (t, 1H, $J = 5.4$ Hz), 2.99 (br s, 1H), 2.99 (d, 1H, $J = 12.1$ Hz), 2.09-2.03 (m, 2H) ppm; $^{13}\text{C NMR}$ (CDCl_3 , 100 MHz) δ 137.0, 136.4, 131.5, 130.6, 129.6, 127.6, 67.9, 45.0, 30.7, 27.6 ppm; **HRMS** calcd for $\text{C}_{10}\text{H}_{13}\text{NO}_3\text{S}$ 227.0617, found 228.06801; **IR** (thin film, cm^{-1}) ν 3293, 2966, 2913, 2615, 2357, 2169, 2043, 1344, 1168, 1066, 1001, 939, 837, 780, 739; **TLC** $R_f = 0.7$ (5% MeOH in DCM).



o-OMe-oxathiazinane (30)

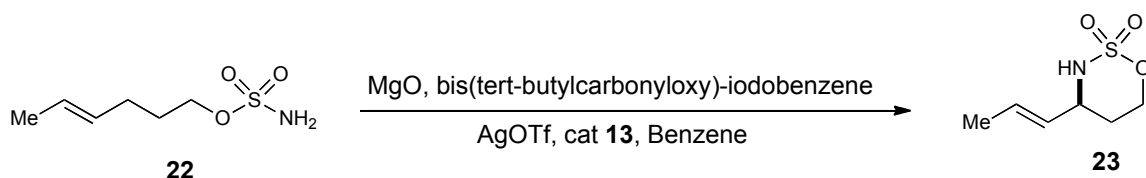
Procedure B. Purified by chromatography on silica gel (2:1 hexanes/EtOAc); white solid (71%); $^1\text{H NMR}$ (CDCl_3 , 400 MHz) δ 7.33 (td, 1H, $J = 7.8, 1.6$ Hz), 7.19 (dd, 1H, $J = 7.4, 1.6$ Hz), 6.99-6.94 (m, 2H), 5.47 (d, 2H, $J = 10.6$ Hz), 5.91-4.80 (m, 2H), 4.57 (ddd, 1H, $J = 11.3, 5.1, 1.2$ Hz), 3.89 (s, 3H), 2.48 (qd, 1H, $J = 12.8, 5.1$ Hz), 1.74 (dq, 1H, $J = 14.9, 2.7$ Hz) ppm; $^{13}\text{C NMR}$ (CDCl_3 , 100 MHz) δ 157.2, 130.2, 129.1, 125.7, 121.5, 111.5, 72.2, 59.3, 55.6, 29.1 ppm; **HRMS** calcd for $\text{C}_{11}\text{H}_{15}\text{NO}_3\text{S}$ 241.0774, found 242.04919; **IR** (thin film, cm^{-1}) ν 3281,

3252, 2970, 2938, 2840, 2353, 2067, 1605, 1585, 1491, 1373, 1250, 1185, 1062, 1009, 903, 776, 747, 723; **TLC** R_f = 0.9 (DCM).



***p*-Br-oxathiazinane (31)**

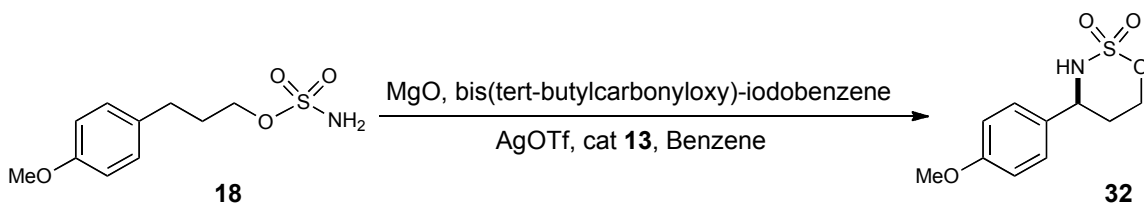
Procedure A. Purified by chromatography on silica gel (3:1 hexanes/EtOAc); white solid (60%); **¹H NMR** (DMSO, 400 MHz) δ 7.54 (d, 2H, J = 8.6 Hz), 7.24 (d, 2H, J = 8.6 Hz), 4.89-4.80 (m, 2H), 4.66 (ddd, 1H, J = 11.7, 5.1, 1.6 Hz), 4.34 (d, 1H, J = 9.4 Hz), 2.27-2.16 (m, 1H), 2.05-2.00 (dq, 1H, J = 14.5, 2.4 Hz) ppm; **¹³C NMR** (DMSO, 100 MHz) δ 138.6, 131.4, 128.9, 121.1, 72.0, 57.8, 29.7 ppm; **HRMS** calcd for $C_{10}H_{12}BrNO_2S$ 288.97726, found 291.94733; **IR** (thin film, cm^{-1}) ν 3260, 2958, 1430, 1418, 1348, 1189, 1074, 1001, 784; **TLC** R_f = 0.5 (2:1 hexane/EtOAc).



***Trans*-oxathiazinane (23)**

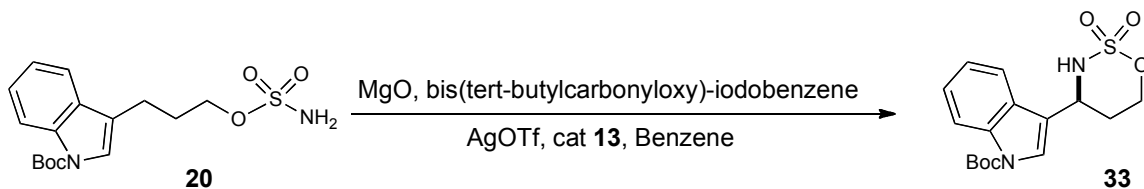
Procedure B. Purified by chromatography on silica gel (3:1 hexanes/EtOAc); colorless oil (60%); **¹H NMR** ($CDCl_3$, 400 MHz) δ 5.82-5.73 (m, 1H), 5.45-5.39 (ddd, 1H, J = 15.7, 5.9, 1.6 Hz), 4.74 (td, 1H, J = 12.1, 2.7 Hz), 4.55 (ddd, 1H, J = 11.7, 4.7, 2.0 Hz), 4.27 (br s, 1H), 4.06 (br d, 1H, J = 8.6 Hz), 1.92-1.76 (m, 3H),

1.73 (d, 3H, $J = 6.7$ Hz) ppm; ^{13}C NMR (CDCl₃, 100 MHz) δ 129.7, 128.2, 71.9, 57.0, 29.8, 18.0 ppm; HRMS calcd for C₆H₁₁NO₃S 177.0460, found 178.05083; IR (thin film, cm⁻¹) ν 3260, 3228, 2970, 2925, 2860, 2124, 1716, 1418, 1352, 1176, 1005, 858, 780, 727, 694, 551; TLC $R_f = 0.6$ (DCM).



p-OMe-oxathiazinane (**32**)

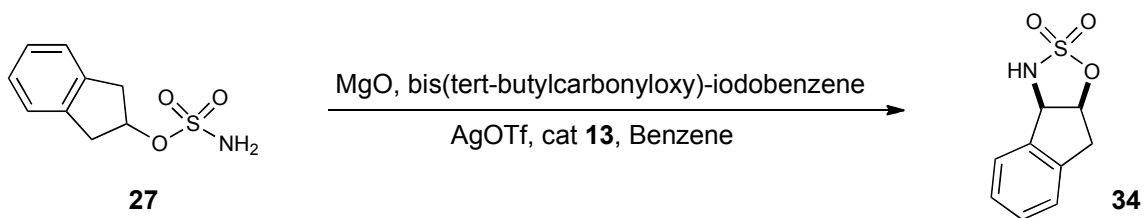
Procedure A. Purified by chromatography on silica gel (3:1 hexanes/EtOAc); white solid (68%); ^1H NMR (CDCl₃, 400 MHz) δ 7.29 (d, 2H, $J = 9.0$ Hz), 6.9 (d, 2H, $J = 8.6$ Hz), 4.87-4.79 (m, 2H), 4.67 (ddd, 1H, $J = 11.7, 5.1, 1.6$ Hz), 4.45 (br s, 1H), 3.81 (s, 3H), 2.30 (qd, 1H, $J = 12.5, 4.7$ Hz), 2.00 (dq, 1H, $J = 14.9, 2.0$ Hz) ppm; TLC $R_f = 0.7$ (3:2 DCM/diethyl ether).



Boc-indole-oxathiazinane (**33**)

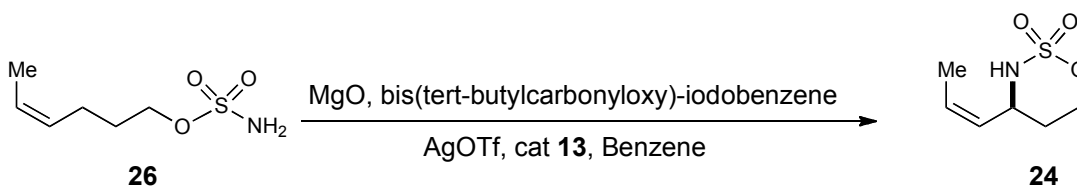
Procedure B. Purified by chromatography on silica gel (2:1 hexanes/EtOAc, column pretreated with TEA); white solid (57%); ^1H NMR (CDCl₃, 400 MHz) δ 8.12 (br d, 1H, $J = 7.4$ Hz), 7.73 (d, 1H, $J = 7.8$ Hz), 7.36 (t, 1H, $J = 7.0$ Hz), 7.28 (t, 1H, $J = 7.8$ Hz), 5.15 (td, 1H, $J = 12.1, 2.3$ Hz), 4.94 (td, 1H, $J = 12.1, 2.0$ Hz), 4.71 (dd, 1H, $J = 11.7, 4.7$ Hz), 4.36 (d, 1H, $J = 10.2$ Hz), 2.39 (qd, 1H, $J = 13.7,$

4.3 Hz), 2.17 (br d, 1H, $J = 14.1$ Hz), 1.67 (s, 9H) ppm; **TLC** $R_f = 0.3$ (2:1 hexanes/EtOAc).



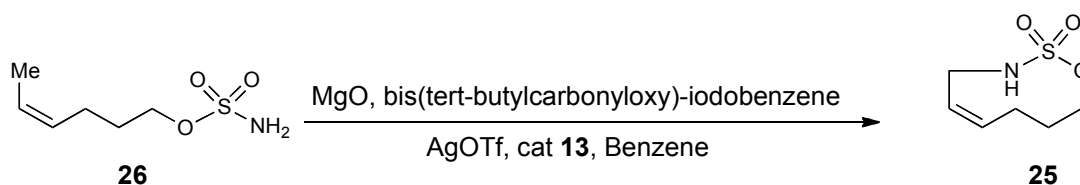
Indenyl-oxathiazinane (**34**)

Procedure B. Purified by chromatography on silica gel (DCM, column pretreated with TEA); white solid (42%); $^1\text{H NMR}$ (CDCl_3 , 400 MHz) δ 7.41-7.29 (m, 4H), 5.52 (td, 1H, $J = 6.3, 2.3$ Hz), 5.30 (br s, 1H), 4.59 (br s, 1H), 3.53-3.39 (m, 2H) ppm; **TLC** $R_f = 0.2$ (DCM).



Cis olefin 6 membered oxathiazinane (**24**)

Procedure B. Purified by passage through a silica gel pre-column (2:1 hexane/EtOAc) followed by chromatography on silica gel eluting with DCM; colorless oil (27%); $^1\text{H NMR}$ (CDCl_3 , 400 MHz) δ 5.79-5.71 (m, 1H), 5.24 (t, 1H, $J = 10.6$ Hz), 4.82-4.75 (m, 1H), 4.64-4.53 (m, 2H), 3.98 (d, 1H, $J = 8.2$ Hz), 1.93-1.70 (m, 2H), 1.74 (d, 3H, $J = 7.8$ Hz) ppm; $^{13}\text{C NMR}$ (CDCl_3 , 100 MHz) δ 131.1, 127.1, 72.0, 52.8, 30.2, 13.9 ppm; **HRMS** calcd for $\text{C}_6\text{H}_{11}\text{NO}_3\text{S}$ 177.0460, found 176.03857; **IR** (thin film, cm^{-1}) ν 3236, 3028, 2970, 2917, 2848, 1434, 1344, 1189, 1164, 1058, 997, 801, 792; **TLC** $R_f = 0.35$ (DCM).



Cis olefin 9 membered oxathiazinane (**25**)

Procedure B. Purified by passage through a silica gel pre-column (2:1 hexane/EtOAc) followed by chromatography on silica gel eluting with DCM; colorless oil (9%); **¹H NMR** (CDCl₃, 400 MHz) δ 5.83-5.72 (m, 2H), 4.59 (br s, 1H), 4.20 (t, 2H, *J* = 5.5 Hz), 3.73 (t, 2H, *J* = 6.3 Hz), 2.43 (q, 2H, *J* = 7.8 Hz), 1.83-1.78 (m, 2H) ppm; **¹³C NMR** (CDCl₃, 100 MHz) δ 133.9, 127.5, 68.1, 38.7, 26.5, 22.6 ppm; **HRMS** calcd for C₆H₁₁NO₃S 177.0460, found 176.03876; **IR** (thin film, cm⁻¹) ν 3277, 3019, 2958, 2929, 2852, 2619, 2366, 2182, 2047, 1426, 1336, 1160, 1042, 931, 894, 825, 727, 608; **TLC** R_f = 0.25 (DCM).

2.6 References

- Dick, A. R.; Sanford, M. S., Transition metal catalyzed oxidative functionalization of carbon-hydrogen bonds. *Tetrahedron* **2006**, 62, (11), 2439-2463.
- Davies, H. M. L.; Beckwith, R. E. J., Catalytic enantioselective C-H activation by means of metal-carbenoid-induced C-H insertion. *Chem. Rev.* **2003**, 103, (8), 2861-2903.
- Godula, K.; Sames, D., C-H bond functionalization in complex organic synthesis. *Science* **2006**, 312, (5770), 67-72.

4. Crabtree, R. H., Alkane C-H activation and functionalization with homogeneous transition metal catalysts; A century of progress - a new millennium in prospect. *J. Chem. Soc., Dalton Trans.* **2001**, (17), 2437-2450.
5. Breslow, R.; Gellman, S. H., Tolylsulfonylamidation of cyclohexane by a cytochrome P-450 model. *J. Chem. Soc., Chem. Comm.* **1982**, (24), 1400-1401.
6. Breslow, R.; Gellman, S. H., Intramolecular nitrene carbon-hydrogen insertions mediated by transition-metal complexes as nitrogen analogs of cytochrome P-450 reactions. *J. Am. Chem. Soc.* **1983**, 105, (22), 6728-6729.
7. Zhang, J.; Chan, P. W. H.; Che, C.-M., Enantioselective intramolecular amidation of sulfamate esters catalyzed by chiral manganese(III) Schiff-base complexes. *Tetrahedron Lett.* **2005**, 46, (32), 5403-5408.
8. He, L.; Chan, P. W. H.; Tsui, W.-M.; Yu, W.-Y.; Che, C.-M., Ruthenium(II) Porphyrin-Catalyzed Amidation of Aromatic Heterocycles. *Org. Lett.* **2004**, 6, (14), 2405-2408.
9. Liang, J.-L.; Yuan, S.-X.; Huang, J.-S.; Che, C.-M., Intramolecular C-N bond formation reactions catalyzed by ruthenium porphyrins: amidation of sulfamate esters and aziridination of unsaturated sulfonamides. *J. Org. Chem.* **2004**, 69, (11), 3610-3619.
10. Liang, J.-L.; Yuan, S.-X.; Chan, P. W. H.; Che, C.-M., Rhodium(II,II) dimer as an efficient catalyst for aziridination of sulfonamides and amidation of steroids. *Org. Lett.* **2002**, 4, (25), 4507-4510.
11. Liang, J.-L.; Yuan, S.-X.; Huang, J.-S.; Yu, W.-Y.; Che, C.-M., Highly diastereo- and enantioselective intramolecular amidation of saturated C-H bonds

catalyzed by ruthenium porphyrins. *Angew. Chem., Int. Ed.* **2002**, 41, (18), 3465-3468.

12. Au, S.-M.; Zhang, S.-B.; Fung, W.-H.; Yu, W.-Y.; Che, C.-M.; Cheung, K.-K., Ruthenium-mediated amidation of saturated C-H bonds and crystal structure of a bis(tosylamido)ruthenium(III) complex of 1,4,7-trimethyl-1,4,7-triazacyclononane. *Chem. Comm.* **1998**, (24), 2677-2678.

13. Liang, J.-L.; Huang, J.-S.; Yu, X.-Q.; Zhu, N.; Che, C.-M., Metalloporphyrin-mediated asymmetric nitrogen-atom transfer to hydrocarbons: aziridination of alkenes and amidation of saturated C-H bonds catalyzed by chiral ruthenium and manganese porphyrins. *Chemistry-- Eur. J.* **2002**, 8, (7), 1563-1572.

14. Yu, X.-Q.; Huang, J.-S.; Zhou, X.-G.; Che, C.-M., Amidation of saturated C-H bonds catalyzed by electron-deficient ruthenium and manganese porphyrins. A highly catalytic nitrogen atom transfer process. *Org. Lett.* **2000**, 2, (15), 2233-2236.

15. Zhou, X.-G.; Yu, X.-Q.; Huang, J.-S.; Che, C.-M., Asymmetric amidation of saturated C-H bonds catalyzed by chiral ruthenium and manganese porphyrins. *Chem. Comm.* **1999**, (23), 2377-2378.

16. Au, S.-M.; Huang, J.-S.; Yu, W.-Y.; Fung, W.-H.; Che, C.-M., Aziridination of alkenes and amidation of alkanes by bis(tosylimido)ruthenium(VI) porphyrins. A mechanistic study. *J. Am. Chem. Soc.* **1999**, 121, (39), 9120-9132.

17. Espino, C. G.; Du Bois, J., A Rh-catalyzed C-H insertion reaction for the oxidative conversion of carbamates to oxazolidinones. *Angew. Chem., Int. Ed.* **2001**, 40, (3), 598-600.
18. Nakamura, E.; Yoshikai, N.; Yamanaka, M., Mechanism of C-H bond activation/C-C bond formation reaction between diazo compound and alkane catalyzed by dirhodium tetracarboxylate. *J. Am. Chem. Soc.* **2002**, 124, (24), 7181-7192.
19. Lebel, H.; Huard, K.; Lectard, S., N-tosyloxycarbamates as a source of metal nitrenes: rhodium-catalyzed C-H insertion and aziridination reactions. *J. Am. Chem. Soc.* **2005**, 127, (41), 14198-14199.
20. Reddy Ravisekhara, P.; Davies Huw, M. L., Dirhodium tetracarboxylates derived from adamantylglycine as chiral catalysts for enantioselective C-H aminations. *Org. Lett.* **2006**, 8, (22), 5013-5016.
21. Fruit, C.; Mueller, P., Intramolecular asymmetric amidations of sulfonamides and sulfamates catalyzed by chiral dirhodium(II) complexes. *Helvetica Chimica Acta* **2004**, 87, (7), 1607-1615.
22. Redlich, M.; Hossain, M. M., Synthesis of asymmetric iron-pybox complexes and their application to aziridine forming reactions. *Tetrahedron Lett.* **2004**, 45, (49), 8987-8990.
23. Nishiyama, H.; Kondo, M.; Nakamura, T.; Itoh, K., Highly enantioselective hydrosilylation of ketones with chiral and C2-symmetrical bis(oxazoliny)pyridine-rhodium catalysts. *Organometallics* **1991**, 10, (2), 500-8.

24. Motoyama, Y.; Kurihara, O.; Murata, K.; Aoki, K.; Nishiyama, H., Chiral ruthenium-bis(oxazolinyl)pyridine complexes of α,β -unsaturated carbonyl compounds: enantioface-selective coordination of olefins. *Organometallics* **2000**, 19, (6), 1025-1034.
25. Espino, C. G.; Wehn, P. M.; Chow, J.; Du Bois, J., Synthesis of 1,3-difunctionalized amine derivatives through selective C-H bond oxidation. *J. Am. Chem. Soc.* **2001**, 123, (28), 6935-6936.
26. Nomura, K.; Sidokmai, W.; Imanishi, Y., Ethylene polymerization catalyzed by ruthenium and iron complexes containing 2,6-bis(2-oxazolin-2-yl)pyridine (pybox) ligand-cocatalyst system. *Bull. Chem. Soc. Jpn.* **2000**, 73, (3), 599-605.
27. Nishiyama, H.; Itoh, Y.; Sugawara, Y.; Matsumoto, H.; Aoki, K.; Itoh, K., Chiral ruthenium(II)-bis(2-oxazolin-2-yl)pyridine complexes. Asymmetric catalytic cyclopropanation of olefins and diazoacetates. *Bull. Chem. Soc. Jpn.* **1995**, 68, (5), 1247-1262.
28. Stambuli, J. P.; Stauffer, S. R.; Shaughnessy, K. H.; Hartwig, J. F., Screening of homogeneous catalysts by fluorescence resonance energy transfer. Identification of catalysts for room-temperature Heck reactions. *J. Am. Chem. Soc.* **2001**, 123, (11), 2677-2678.
29. Campos, K. R.; Woo, J. C. S.; Lee, S.; Tillyer, R. D., A general synthesis of substituted indoles from cyclic enol ethers and enol lactones. *Org. Lett.* **2004**, 6, (1), 79-82.

Chapter 3

Monoamine Oxidase: Laboratory to Clinical

The flavoenzyme monoamine oxidase (MAO) is a 60 kDa outer-mitochondrial membrane bound enzyme responsible for the oxidative deamination of biogenic amines and amine neurotransmitters like serotonin, dopamine, and epinephrine.¹ In mammals MAO exists in two isoforms, MAO A and MAO B, which are separate gene products located on the X-chromosome that correspond to amino acid sequences that are ~70% identical.² Because both MAO A and MAO B are comprised of 15 exons with identical intron-extron organization³, it has been proposed that genes encoding MAO A and MAO B evolved by a duplication event of a single ancestral MAO gene.⁴ This is further supported by the fact that lower invertebrates, like teleosts, express only one MAO.

On the other hand, both MAO A and MAO B are expressed in all mammals and are situated on the outer membrane of the mitochondria of most tissues; although, MAO A and MAO B demonstrate differential expression in these tissues.^{1, 5-10} MAO B is primarily responsible for the metabolism of dopamine, and it is predominantly expressed dopaminergic, serotonergic, and histaminergic neurons, as well as glial cells. Similarly, MAO A regulates the mood- and stress-related neurotransmitters such as norepinephrine, adrenaline and serotonin due to the high level of MAO A expression in catecholaminergic neurons.

Surprisingly, the distribution of MAO A versus MAO B is not always representative of their substrate specificity. For instance, while MAO A preferentially oxidizes serotonin it is not present in serotonergic neurons.

However, MAO B preferentially oxidizes phenylethylamine and dopamine, but has a strong presence in serotonergic neurons.¹¹ Instead, the role of MAO B appears to be for the protection of neurons from stimulation by exogenous amines which preventing their behaving as false neurotransmitters.

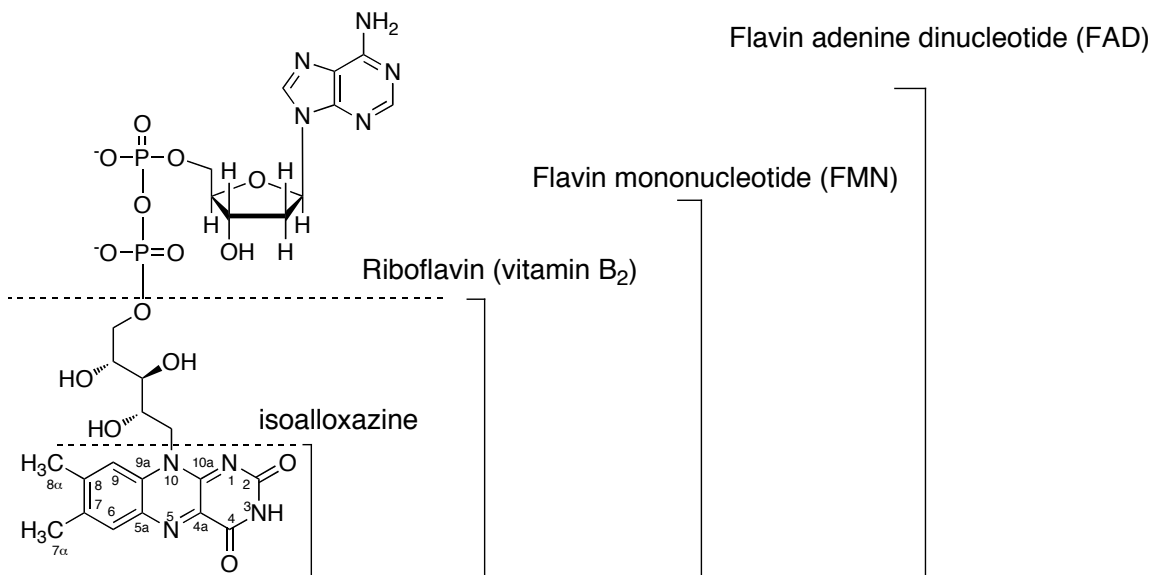
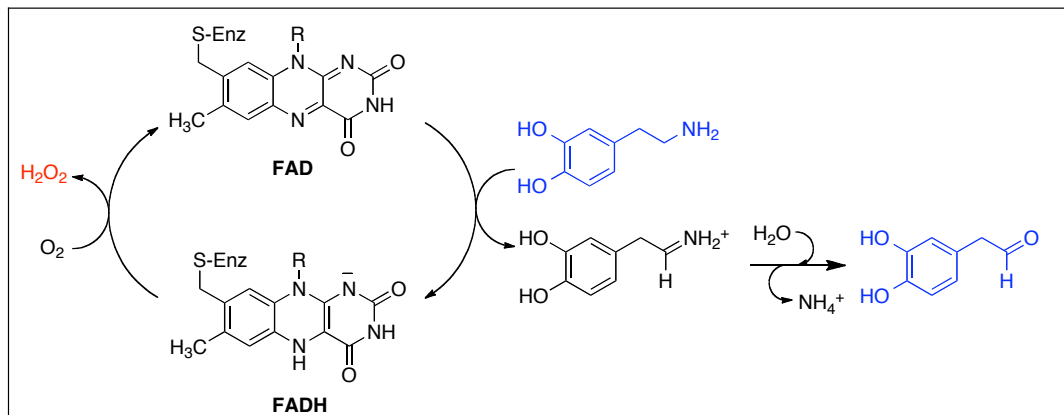


Figure 3.1. Structure of flavin-adenine-dinucleotide (FAD).

The active site of MAO contains an 8 α -S-cysteinyl covalently linked flavin-adenine-dinucleotide (FAD) cofactor (Figure 3.1), which is responsible for the oxidation of amines by conversion to their corresponding imines (Scheme 3.1). Scheme 3.1 illustrates that amine oxidation to the corresponding imine is concomitant with flavin reduction to the flavin-hydroquinone form. Molecular oxygen acts as an electron acceptor during the catalytic cycle regenerating oxidized FAD for oxidation of another substrate molecule, producing hydrogen peroxide as a byproduct of catalysis.



Scheme 3.1. MAO catalyzed oxidation of amine neurotransmitter, dopamine.

3.1 MAO as a Genetic Control for Behavior

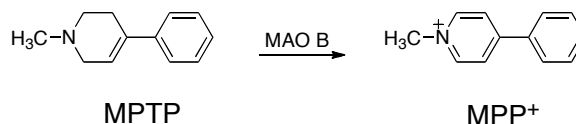
MAO plays a pivotal role in neural development during the early stages of embryogenesis. A recently published study identified two adolescent brothers lacking both MAO A and MAO B genes.¹² Both children exhibited severe mental retardation shortly after birth, and the lack of MAO resulted in the death of the one of the two siblings. While MAO plays an important role in neural development, several complimentary studies have shown that the MAO isozymes are also important in mood regulation. Specifically, MAO A deficiency in males has been shown to result in aggressive behavior under stress.^{13, 14} A Dutch family of eight males carried a point mutation in the MAO A gene which resulted in truncation of the isozyme rendering it inactive. This mutation was shown to result in abnormally aggressive behavior.^{14, 15}

Similar studies in rat and mice models have proven to be very useful in identifying the roles of MAO A and MAO B in neurotransmitter metabolism and

phenotype. MAO A knock-out (KO) mice exhibit aggressive behavior and hyper-reactivity to stress. These KO-mice have elevated levels of serotonin, norepinephrine, and dopamine. MAO B KO-mice do not exhibit aggressive behavior and demonstrate milder responses to stress.^{11, 16} Interestingly, only phenylethylamine levels are elevated in MAO B deficient mice. Double KO-mice lacking MAO activity show highly elevated reactivity to stress. These results illustrate that animals without any MAO do survive; although, they exhibit serious neurological problems.

3.2 Pharmacological Importance of MAO B: Potential Neuroprotectants

Early pharmacological interest in MAO stems from the pivotal discovery by Zeller that demonstrated that hydrazines are MAO inhibitors (MAOIs) that result in mood elevation.¹⁷ However, since the seminal findings of Zeller, MAO B activity has been linked to Parkinson's-like syndrome. One example is the MAO B bioactivation of MPTP to MPP⁺ (Scheme 3.2), which functions as a mitochondrial toxin through the inhibition of Complex I.¹⁸ Mice lacking MAO B activity through administration of MAO B specific inhibitors demonstrate resistance to MPTP.¹⁹⁻²¹



Scheme 3.2. MAO B bioactivation of MPTP

Correlations between high levels of monoamine oxidase and neurodegenerative disorders like Parkinson's disease (PD) and Alzheimer's disease have also been made.^{8, 22} Alzheimer's disease and Parkinson's disease are the two most prevalent neurodegenerative diseases in the western world.

The pathological hallmarks of these diseases are the loss of neurons in either the cortex and hippocampus (Alzheimer's disease) or the *substantia nigra* (PD).²³ The observation that expression of MAO B in human neuronal tissue increases ~4-5-fold with aging presents a rationale for the involvement of MAO B in age-related neurological disorders.²⁴ One explanation for the increase in MAO B levels with age stems from MAO B being predominately expressed in glial cells.^{25, 26} Therefore, the increase in MAO B activity can be attributed to the proliferation of these cells.

Increased expression of MAO B may explain the selective loss of dopaminergic neurons in PD patients. MAO B oxidation of dopamine results in the catalytic production of hydrogen peroxide as well as dopal. It has been well established that hydrogen peroxide formation can lead to the production of reactive oxygen species (ROS) resulting in cellular apoptosis and subsequent neurodegeneration. Furthermore, it has been demonstrated that the dopamine catabolite, dopal, is highly toxic to dopamine producing neurons.²⁷ Dopal has also been implicated in α -synuclein aggregation²⁸ which is involved in the etiology of PD as well as protein crosslinking²⁹ (Figure 3.2). It is within reason that the selective loss of dopaminergic neurons in the substantia nigra may be associated with the age-dependent increase in oxidation of dopamine by MAO B. Specific inhibitors of MAO B could function as neuroprotectants for an aging population.

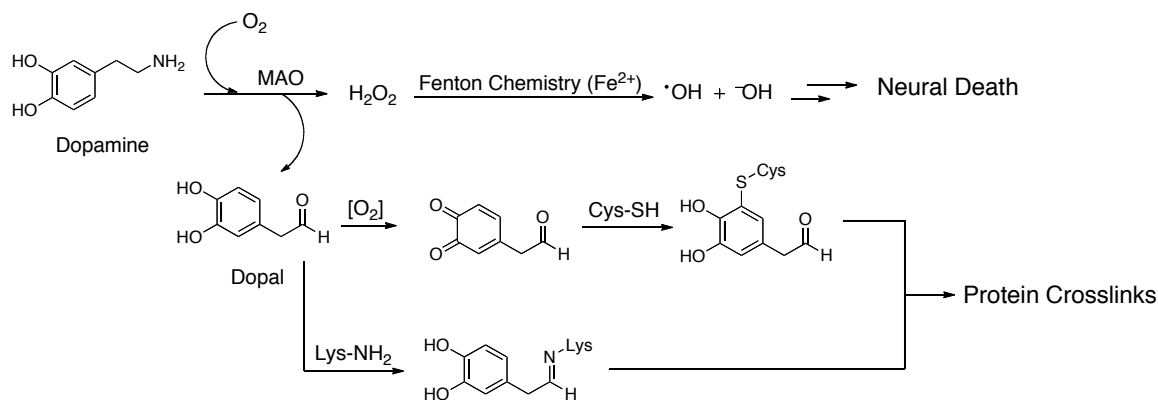


Figure 3.2. Pathway for MAO B generated oxidative damage within DA neurons, and pathway for protein crosslinking initiated by DOPAL.

3.3 Pharmacological Importance of MAO A: Potential Cardioprotectants

MAO A has also gained considerable interest in recent years as a pharmacological target. MAO A specifically oxidizes serotonin; although, MAO A effectively oxidizes dopamine as well.⁴ Genetic deletion of MAO A in mice (as well as human) results in aggressive behavior as well as serotonin-dependent ventricular hypertrophy.^{14, 30, 31} MAO A levels in rat cardiac tissue have been shown to increase ~9-fold with age resulting in increased levels of hydrogen peroxide³²; therefore, age-dependent increases in MAO A expression is likely to occur in humans as well. The increase in MAO A levels have been suggested to play a role in apoptosis and necrosis of cardiac cells. Parini and coworkers have shown that the MAOI, pargyline, effectively mediates cardiomyocyte apoptosis by reducing MAO A generated reactive oxygen species.³³ These studies have resulted in a revival of the development of MAO A specific inhibitors for clinical uses as cardioprotectants.³⁴ To design safe MAOIs that are potent, specific, and reversible is an ongoing challenge that can be addressed through an understanding of the structural and functional differences of MAO A and MAO B.

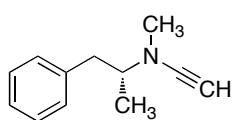
3.4 Clinical Use of MAOIs: Where We Stand Today

Immediately following the discovery of the therapeutic properties of MAO inhibition, aggressive development of MAOIs for the treatment of depression ensued. Currently there are six FDA approved MAOIs: rasagiline, selegiline (l-deprenyl), selegiline transdermal system, tranylcypromine, phenelzine, and isocarboxazid (Figure 3.3). Of these approved MAOI only selegiline and rasagiline are MAO B specific and presently used in Parkinson's therapy.³⁵ The drawback in using older generation FDA approved MAOIs (tranylcypromine, phenelzine, and isocarboxzid) in drug therapy is that they irreversibly inhibit both MAO A and MAO B.³⁶

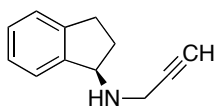
These nonselective, irreversible MAOIs have been shown to result in adverse pharmacological side effects like the well known "cheese effect." Foods rich in arylalkylamines, such as tyramine, are catabolized by MAO A after absorption into the gastrointestinal tract. Patients that consume foods rich in tyramine in combination with MAOI treatment are at risk of undergoing hypertensive crisis due to tyramine being a potent vasopressor.³⁵ Historically MAOIs have been developed for the treatment of depression, but these drugs lost favor with the clinical community due to side effects associated with global inhibition of MAO.³⁷ The advent of serotonin reuptake inhibitors resulted in a lack of interest in MAO A as a therapeutic target for the treatment of mood disorders.³⁵

Safinamide, currently in phase III clinical trials, has proven to be a promising candidate for PD treatment due to its high degree of selectivity for

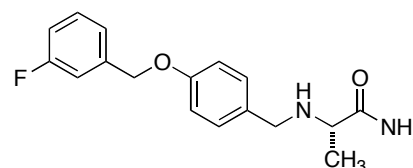
MAO B. Rasagiline, selegiline, and safinamide are promising therapeutic agents in that they selectively inhibited MAO B. These inhibitors, with the exception of Safinamide, are currently prescribed for the treatment of PD, and rasagiline is in clinical trials for the treatment of Alzheimer's disease. However, with the exception of safinamide, these FDA approved MAO B specific inhibitors irreversibly inactivated MAO B. In particular, selegiline metabolite, methamphetamine is highly toxic to cells and can result in adverse side effects. Therefore the development of highly specific, reversible MAOIs is important for the treatment of a vast number of age-related disorders.



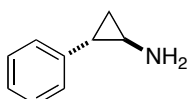
L-Deprenyl (Selegiline)
MAO B selective



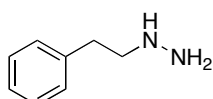
Rasagiline
MAO B selective



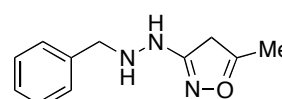
Safinamide*
MAO B selective



Tranylcypromine
nonselective



Phenelzine
nonselective



Isocarboxazid
nonselective

Figure 3.3. FDA approved MAOIs for the treatment of depression and Parkinson's Disease.
*Safinamide is currently in phase III clinical trials.

3.5 Understanding the Differences in MAO A and MAO B: A Molecular Look

Historically, the purification of the MAO A and MAO B isozymes presented a formidable challenge because both isozyme are present most mammalian tissues, and they are not readily separable from one another due to their

molecular similarities. Early sources of MAO A were isolated from placental tissue which required ~six placentas per enzyme purification.³⁸ The development of a yeast expression system from *Saccharomyces cerevisiae* allowed for the isolation of reagent quantities (~50-100 mg of protein per 20 L of culture).³⁹ Isolation of human MAO B was a greater challenge, and the most convenient source of MAO B was from bovine liver mitochondria.⁴⁰

Great advances in understanding the molecular differences through structural and mechanistic investigation of MAO A and MAO B were made after the development of high level expression systems for the production and isolation of both isozymes. Conditions for the overexpression of human liver MAO B⁴¹ and human liver MAO A⁴² in *Pichia pastoris* allowed for the purification of reagent quantities of protein (~100 mg per one liter of cell culture). MAO is localized to the outer mitochondrial membrane of the yeast cell and constitutes ~50% of the total protein associated with the outer mitochondrial fraction. This advance in protein expression and isolation allowed for facile genetic manipulation by site-directed mutagenesis as well as providing sufficiently high levels of protein for mechanistic and X-ray crystallography studies.

3.6 Crystallographic Studies of MAO

Crystal structures of human MAO B⁴³, human MAO A^{44, 45} and rat MAO A³⁶ have been determined to date (Figure 3.4). High resolution (up to 1.65 Å resolution) crystal structures of human MAO B in complex with a range of inhibitors have been determined. MAO A resolution is considerably lower at 2.2 Å resolution for human and 3.3 Å resolution for rat enzyme. All of the enzymes

demonstrate a high degree of similarity in their C_α coordinates and demonstrate similar folds. Membrane binding of these enzymes is located on the C-terminal 35-40 residues. The protein architecture around the FAD binding site as well as the position of the cofactor in the three structures is highly conserved. The flavin ring of the FAD is bent 30° from planarity about the N(5)-N(10) axis rather than the more common planar configuration. This bent structure may be due to strain in the FAD binding site, which may have catalytic relevance. This point requires further exploration.

The oligomeric state is the most notable difference in the overall structures of the three enzymes. Human MAO B and rat MAO A crystallize as dimers while human MAO A crystallizes in its monomeric form. Molecular modeling studies have resulted in the proposal that human MAO A's monomeric structure is due to a Glu151Lys substitution near the dimer interface. All other species of MAO A, as well as MAO B, have a Glu at the 151 position.⁴⁶ Membrane bound proteins are generally oligomeric in nature with dimerization being the most common form reported in the literature.⁴⁷

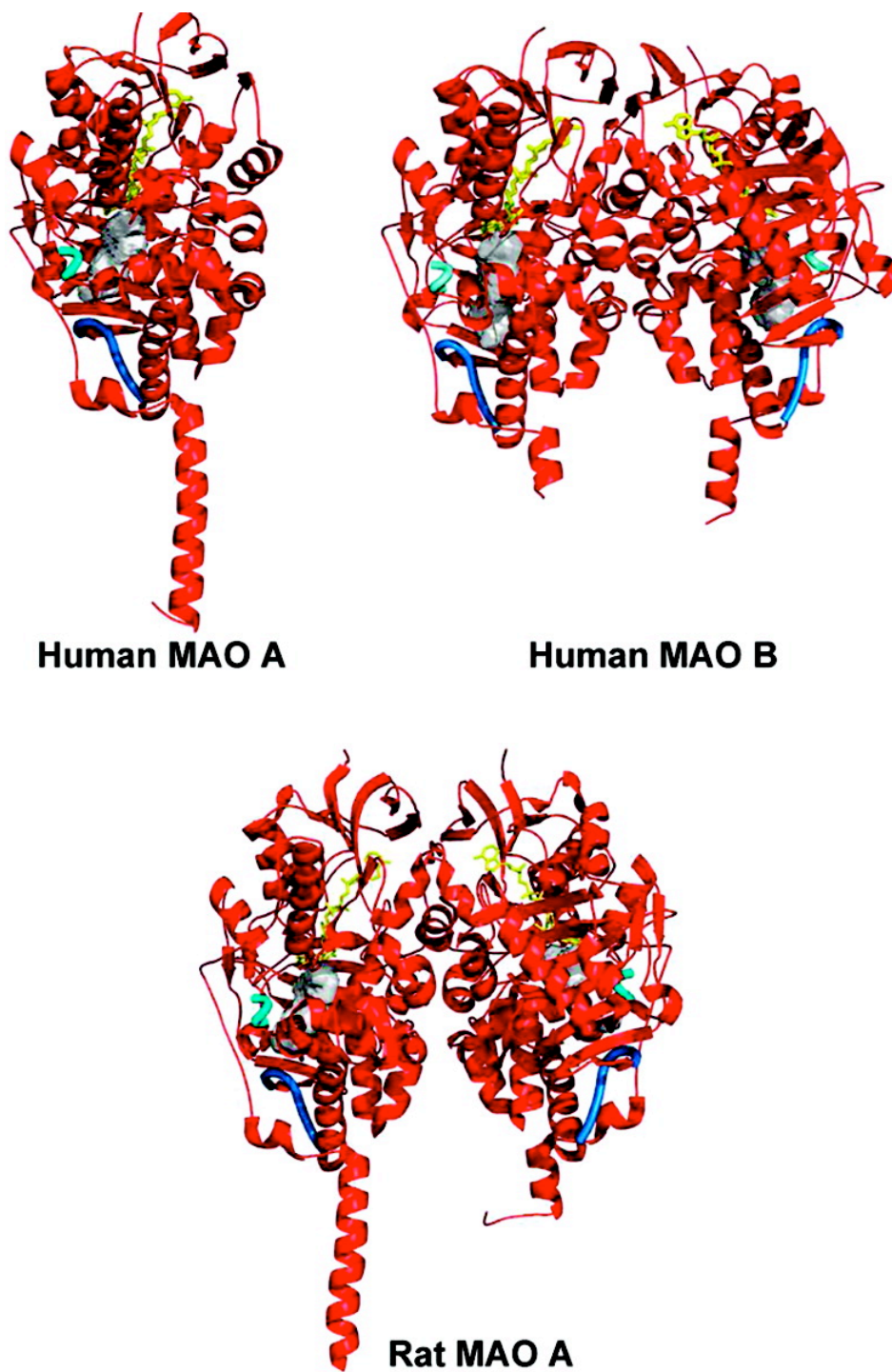


Figure 3.4. Ribbon diagram of X-ray crystal structures of human MAO A, human MAO B, and rat MAO A.⁴

3.7 *Probing the Oligomeric State of MAO*

To further probe the oligomeric state of membrane bound MAO, pulsed EPR (DEER) experiments were conducted by Upadhyay and colleagues using nitroxide spin-labeled pargyline analogues.⁴⁸ When exposed to MAO these analogues covalently bind to the FAD cofactor. This technique has been employed to probe distances up to 60 Å.⁴⁸ Furthermore, this technique is amenable to use with solubilized enzyme systems as well as membrane preparations. DEER experiments demonstrated that both human MAO A and MAO B are dimeric in their membrane bound forms and that the oligomeric state is independent of the residue (Glu or Lys) at the 151 position.⁴⁹ Detergent solubilized MAO, both rat and human MAO B, were found to be dimeric while human and rat MAO A is ~50% dimeric in solution. Although both the monomeric and dimeric states of human MAO A exist in solution, the monomeric state crystallizes more readily unlike human MAO B and rat MAO A which crystallize as dimers. Comparisons of the distances between the active sites of human MAO B and rat MAO A by x-ray crystallographic data measurements and DEER measurements suggest that the x-ray crystal structures are biologically significant (Figure 3.5)

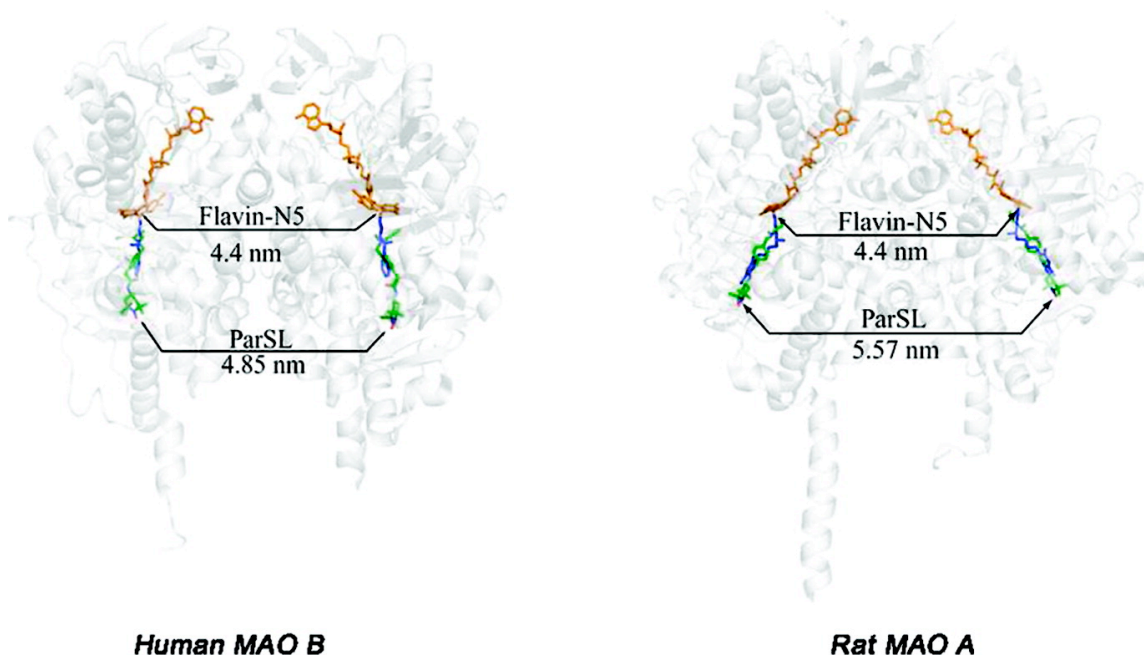


Figure 3.5. Comparison of the distances calculated from X-ray structures to DEER experiments. FAD is represented in orange, pargyline in blue and pargyline-spin labels are superimposed in green.⁵⁰

3.8 Comparison of MAO A and MAO B Active Site Cavities

Elucidation of rat and human MAOs reveals that substrate oxidation occurs within cavities that extend from the surface of the protein to the core of the protein where the FAD cofactor is bound. Both MAO A and MAO B active sites are mostly hydrophobic with the exception of hydrophilic residues immediately surrounding the re face of the flavin at FAD binding site. There are considerable differences in their architectures that result in differential substrate and inhibitor binding. Previous reports suggest that the major structural difference in MAO A and MAO B is that MAO A has a monopartite substrate cavity of 550 \AA^3 and MAO B is dipartite with a 290 \AA^3 entrance cavity and a 400 \AA^3 substrate cavity (Figure 6). Ile199 and Tyr326 function to separate the two cavities of MAO B creating either a large single cavity of $\sim 700 \text{ \AA}^3$ or two smaller cavities based on the rotational conformation of the Ile199 (Figure 3.6). The

Ile199 side chain is in a required “open” conformation when large inhibitors are bound and is “closed” with smaller inhibitors.

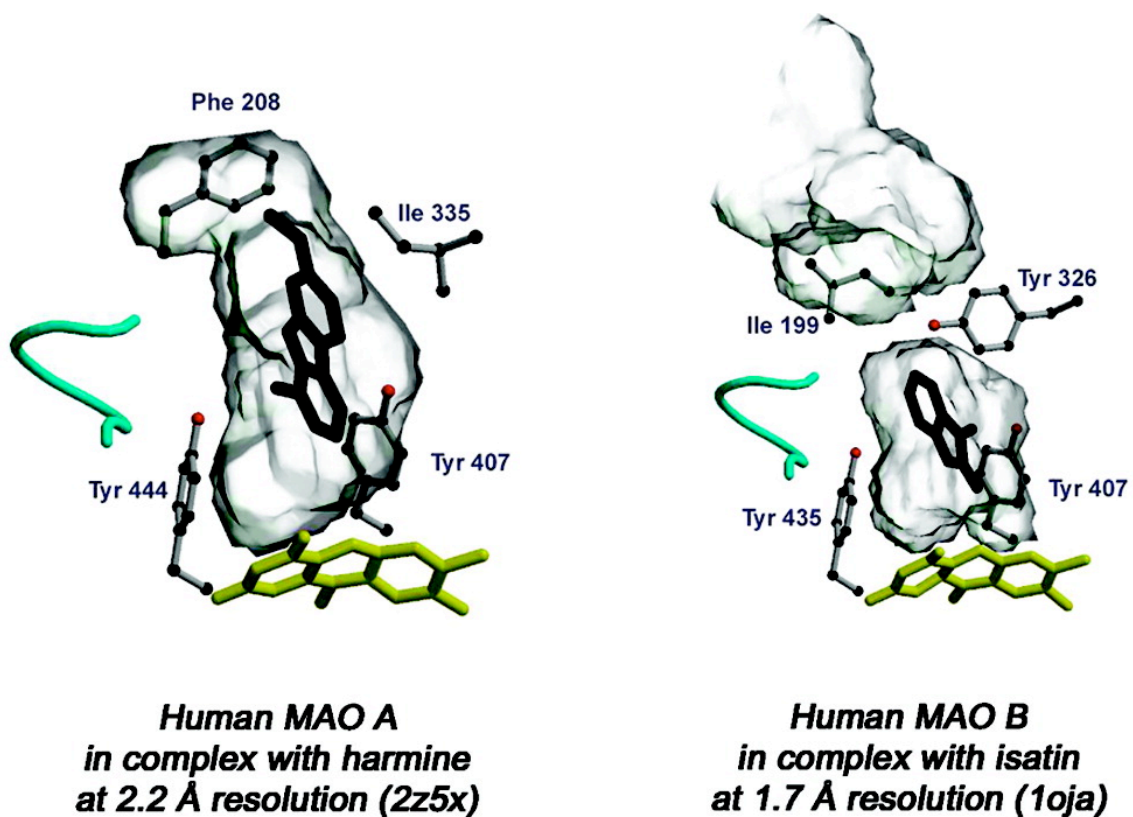


Figure 3.6. Comparisons of the human MAO A and MAO B active site cavities.⁴

The analogous residue in human and rat MAO A, Phe208, does not function as a gating residue. When the Ile199 of human MAO B is mutated to a Phe, the mutant no longer binds MAO B specific inhibitors.⁵¹ This is due to the mutation increasing the steric constriction due to the bulky side chain of the Phe in the active site. This substitution results in reduced flexibility and impedes the binding of large inhibitors. These results are analogous to reports on inhibitor binding to bovine MAO B, which also has a Phe substitution at position 199.

Caution should be taken in using different sources of enzyme for determining MAO B inhibition properties. Tyr326 of MAO B also represents a site of structural difference to MAO A. The bulky side chain of Tyr326 also cooperates in partitioning the two active site cavities of MAO B. The analogous residue in MAO A is an Ile335, which results in far less steric constrictions.

Other nonconserved residues within the active site include Cys172 and Leu171 in MAO B (Asn181 and Ile180 in MAO A, respectively). These residues do not significantly contribute to the overall shape of the active sites. The structural determinates for substrate and inhibitor specificities appear to be Ile199 and Tyr326 of MAO B (Phe208 and Ile335 of MAO A, respectively).

Both MAO A and MAO B have several conserved, catalytically relevant residues.⁵² Most notable of these are a pair of Tyr residues that comprise an aromatic cage within the active site. These residues are oriented perpendicular to the flavin ring of the enzyme and appear to have relevance in positioning the substrate within the active site to facilitate oxidation.⁵³ Furthermore, mutation of these residues results in decreased catalytic efficiency likely due the role of the aromatic cage in increasing the nucleophilicity of the amine substrate.⁵⁴ Similarly, a conserved Lys residue situated directly above the flavin ring both MAO isozymes has been proposed by molecular modeling studies to aid in the stabilization of the superoxide-FADH[•] radical pair as the initial intermediate on reoxidation of the FAD cofactor by molecular oxygen.⁵⁵ This Lys residue (Lys305 in MAO A and Lys296 in MAO B) engages in a H-bond through an ordered water molecule with the N(5) of the flavin. The catalytic importance of this residue has

been demonstrated in other flavoprotein like sarcosine oxidase where mutation of the Lys results in a dramatic decrease in catalytic efficiency *via* a 10^3 -fold decrease in O_2 reactivity.⁵⁶ Other flavoproteins containing Lys residues near the flavin binding site include: polyamine oxidase^{9,57} D-amino acid oxidase^{10,58} and L-amino acid oxidase.⁵⁹

3.9 Inhibitor Design and Inhibitor Binding to MAO

In general, MAO inhibitors contain an aromatic moiety (Figure 3.7), which is expected due to the aromatic nature of neurotransmitters. Although, there are examples of aliphatic ligands binding to the MAO B active site such as *trans,trans*-farnesol, oleamide, and di(2-hydroxyethyl)methyldodecylammonium (DiHEMDA) (Figure 3.8). While these inhibitors reversibly bind to the MAO B active site, there are a number of mechanism based inhibitors in the literature that inactivate MAO by covalent modification of the N(5) position of the flavin ring (Figure 3.9). There is one exception to this mode of irreversible inactivation is tranylcyromine (TCP). TCP is the only covalent inhibitor that has been identified to date that does not bind to the N(5) position of the flavin. Instead, TCP inactivates MAO through C4a adduct formation with the flavin.⁶⁰ Interestingly, structural data reported for the flavoprotein lysine-specific histone demethylase 1 (LSD-1) demonstrates that TCP inactivation results in both N(5) and C4a alkylation of the flavin ring.⁶¹ Therefore it has been suggested that inactivation of MAO results from an initial N(5) adduct which migrates to the C4a position. Isomerization of N(5) flavin adducts to the corresponding C4a adduct has been observed by Massey and Hemmerich in photoalkylation of

model flavins with phenylacetate.⁶²

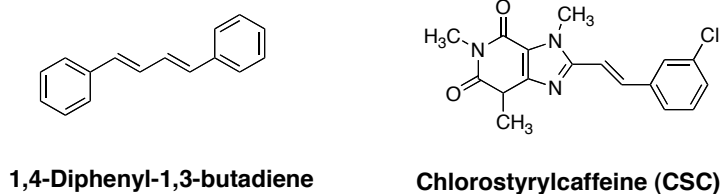


Figure 3.7. MAO B specific reversible inhibitors

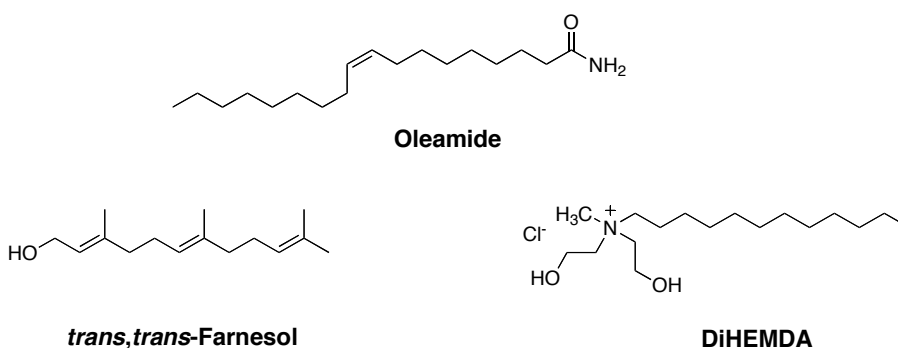


Figure 3.8. Reversible aliphatic MAO B inhibitors

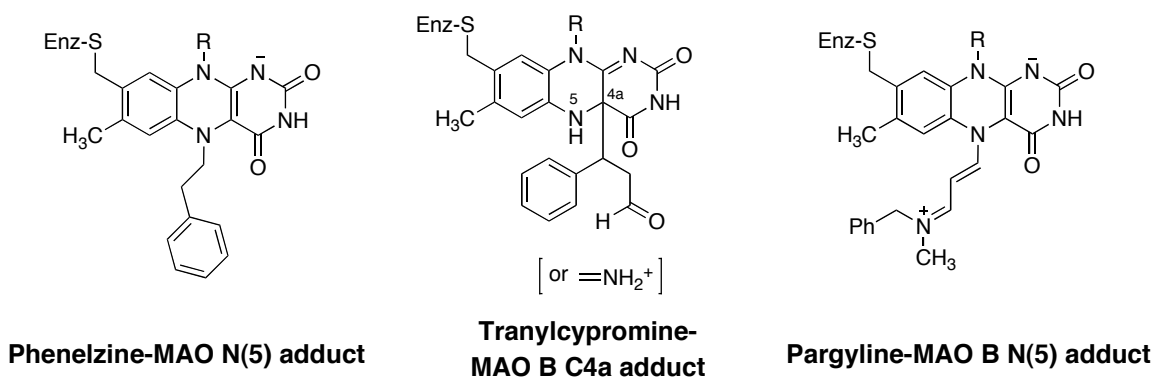


Figure 3.9. Common mechanism based inhibitor flavin adducts

While much is known about the inhibition properties of MAO B, specific inhibition of MAO A is still in its infancy. A revival of interest in the inhibition of MAO A stems from the MAO A being a potential target for cardioprotectants.⁶³ With the recent publication of a high resolution crystal structure⁴⁴, it is expected

that the MAO A field and MAO A specific inhibitor design will exhibit a similar level of growth as the MAO B field. To date it is known that MAO A preferentially binds bulky and more hydrophilic inhibitors (Figure 3.10).

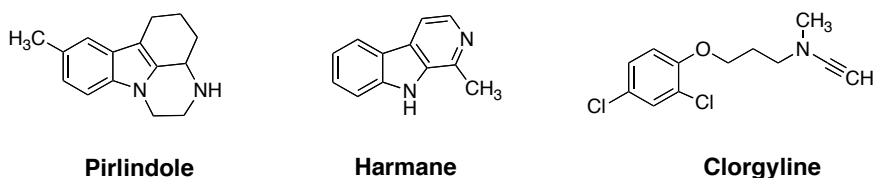
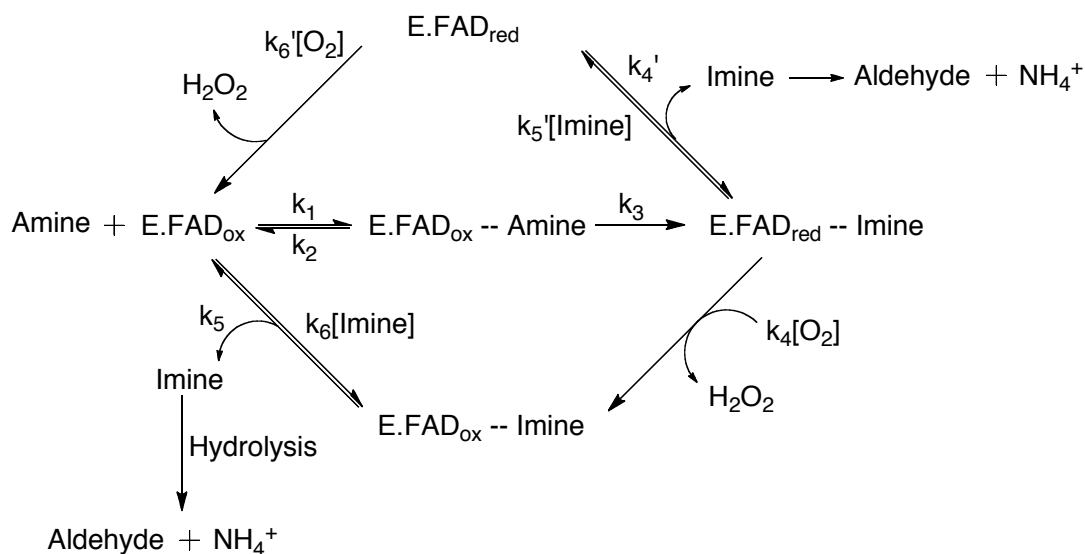


Figure 3.10. MAO A specific inhibitors

3.10 Reactions Catalyzed by MAO

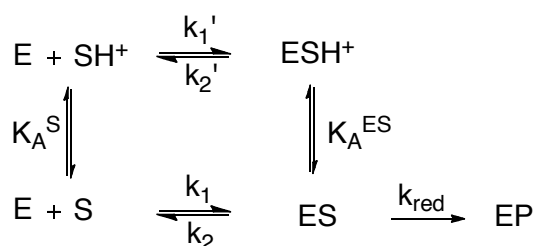
MAO catalyzes the oxidation of alkyl and aryl amine substrates *via* two half reactions: 1) oxidation of the amine with transfer of two reducing equivalents to the flavin; 2) oxidation of the flavin hydroquinone by molecular oxygen (Scheme 3.3).⁶⁴



Scheme 3.3. A schematic of the catalytic reaction pathway followed by MAO A and MAO B.

Reports have shown that only deprotonated amine substrates are oxidized by MAO, and the protonated imine is released from the enzyme.⁶⁵ Studies by

Dunn and coworkers have illustrated that upon binding to MAO A the pK_a of amine substrates are reduced by ~ 2 pK_a units further facilitating amine deprotonation prior to catalysis (Scheme 3.4).⁶⁶ A plot of k_{red}/K_s versus pH result in a bell-shape pH profile with a positive slope from pH 7.4 to 8.4, demonstrating a favorable deprotonation step which is optimal for catalysis. In the pH range 8.5 to 9.5, an unfavorable deprotonation of a site on the enzyme occurs which has deleterious effects on the rate of catalysis. Analogous experiments have not been conducted with MAO B.



Scheme 3.4. Reaction pathway presented by Dunn and colleagues.⁶⁶

The MAO B catalyzed oxidation of amines can proceed by either a ping-pong mechanism or by a ternary complex mechanism. The lower reaction pathway of Scheme 3.3 illustrates the ternary complex reaction pathway in which the amine substrate is oxidized to the imine and remains bound to the reduced enzyme. Molecular oxygen then binds to flavin-product complex and acts as an electron acceptor. Molecular oxygen undergoes a two electron reduction by the flavin hydroquinone ($FADH_2$) to form hydrogen peroxide resulting in reoxidation of the flavin cofactor (FAD). After reoxidation of flavin, the imine product dissociates where it is non-enzymatically hydrolyzed to the corresponding aldehyde liberating ammonia as a byproduct of catalysis. Most MAO substrates,

including benzylamine analogues, are oxidized *via* this ternary pathway.^{65, 67}

To date only three substrates have been reported to follow a ping-pong mechanism (upper loop reaction in Scheme 3.3). These include phenylethylamine, tyramine, and tryptamine.⁶⁸⁻⁷⁰ These oxidation reactions proceed by oxidation of amine substrate which is immediately followed by diffusion of the imine product from the active site. Diffusion of the imine from the active site is followed by O₂ binding to the free reduced enzyme, reoxidation of the flavin (FADH₂ to FAD), and diffusion of hydrogen peroxide.

In these reactions the rate of reoxidation of the reduced cofactor is generally much slower than those of the ternary complex pathway.⁷¹ The reoxidation pathway, ping-pong versus ternary complex formation, of the reduced flavin is governed by the rate of imine dissociation.⁶⁵ In the cases of phenylethylamine, tyramine, and tryptamine the rate of imine dissociation is much greater than the rate of flavin oxidation. In fact the rate of oxidation of the E_{red}-imine complex for phenylethylimine is five times faster than the free reduced enzyme; however, the facile dissociation of the imine product precludes oxidation of the ternary complex.⁷²

The reaction pathway of MAO A is dependent on substrate concentration.^{71, 73} The ternary complex pathway is preferred for enzyme reoxidation (lower loop of the reaction pathway in Scheme 3.3)⁷⁴; although, at low substrate concentration product release appears to be the rate limiting step suggesting a ping-pong mechanism is operating. In all cases the rate of reduction of MAO A is slower than the rate of reoxidation.⁷¹

MAO A and MAO B have differential affinities for O₂. The K_m value for the reaction of MAO A with O₂ is ~10 μM (using kynuramine as a substrate)⁷⁵ while MAO B has a K_m of ~330 μM (using benzylamine as a substrate).^{41, 67} The air saturation of O₂ in water at 25 °C is 240 μM. Therefore, MAO A is catalytically saturated at air-saturation while MAO B functions at approximately half V_{max}. This should be taken into consideration when analyzing steady state data.

3.11 Mechanism of Amine Oxidation

Limited sources of MAO A and MAO B prior to the early 1990s impeded the study of the molecular mechanism amine oxidation by MAO. Early preparations of MAO A and MAO B in *S. cerevisiae* allowed for preliminary mechanistic inquiries.^{39, 76} However, with development of the overexpression system in methotrophic yeast, *Pichia pastoris* provided reagent quantities (~100 mg per liter of cell culture) of protein allowing for the facile expression, purification and investigation of both human MAO A⁴² and MAO B.⁷⁷ This expression system also provided a route for the rapid development of mutant forms of MAO. Prior to the development the *Pichia* system, studies were performed using placental MAO A³⁸ and bovine liver MAO B, which were limited by low yielding preparations.⁷⁸

Investigation of C-H bond cleavage have unequivocally determined the stereochemistry of the H abstracted from the amine substrate is the pro-*R* hydrogen.⁷⁹ This is in contrast to copper-quinoprotein amine oxidases in which both pro-*R* and pro-*S* hydrogens are transferred to the catalytic center.⁸⁰ Large deuterium isotope effects of steady reactions illustrate that C-H bond cleavage is

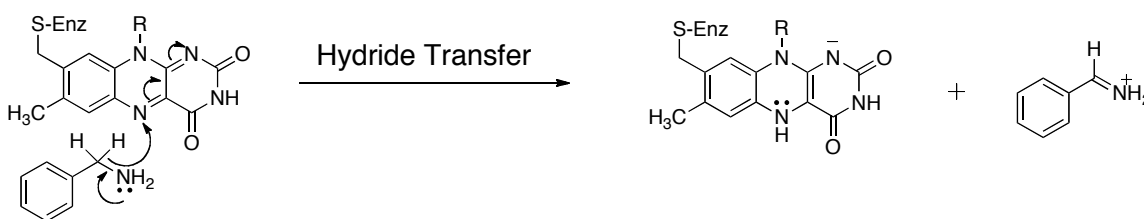
usually the rate limiting step in amine oxidation by MAO A and MAO B.^{74, 81, 82} Kinetic studies on bovine MAO B suggest that a hydrogen tunneling contribution is involved in the transfer of the hydrogen from the amine to the flavin.⁸³ While several investigations have been conducted to elucidate the exact mechanism of C-H bond cleavage, no definitive mechanism has been agreed upon by the MAO community.

Many mechanistic investigations of MAO and related flavoprotein oxidases have resulted in the proposal of three possible mechanisms for C-H bond cleavage during amine oxidation. Ongoing debate about the mechanism of C-H cleavage has resulted in a division of the scientific community between these three mechanisms. The prevailing mechanisms are: H⁻ transfer, H⁻ abstraction, and H⁺ abstraction. Both the amino acid oxidase and alcohol oxidase classes of flavoenzymes are believed to operate *via* hydride mechanism.^{4, 84, 85} Similarly, it is well documented that triplet flavin undergoes hydrogen atom abstraction⁸⁶; however, there is no evidence of ground state flavin undergoing a hydrogen atom abstraction mechanism. The proton abstraction mechanism was first proposed by Hamilton and coworkers⁸⁷ for flavin model system catalyzed dehydrogenation reaction. This mechanism was modified by Silverman and coworker where they proposed a SET-deprotonation hybrid mechanism.⁸⁸

3.11.1 Hydride Transfer Mechanism: H⁻

Scheme 3.5 illustrates the transfer of hydride from the α -C-H bond of the amine substrate to the N(5) of the flavin. Evidence supporting a hydride transfer mechanism originates from the observation that related flavoprotein oxidases^{89, 90}

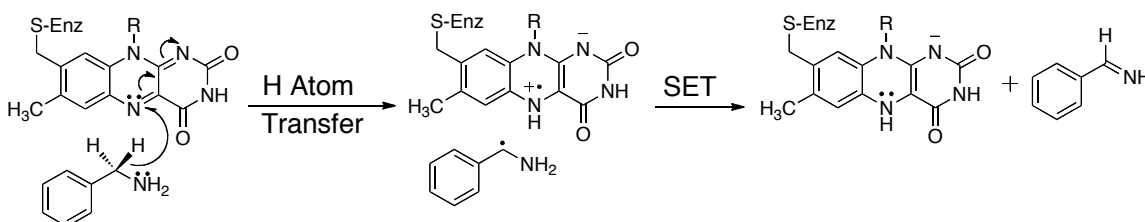
demonstrate an inverse kinetic isotope effect when competitive ^{15}N (V/K) values are measured. However, this data does not explain the MAO catalyzed oxidation of alkyl- and aryl-hydrazines to their corresponding diazenes. MAO A and MAO B readily oxidize substituted hydrazines to the corresponding diazene⁹¹ and hydrazine to N_2 gas.⁹² It is unlikely that a hydride is transferred from the nitrogen of hydrazine to the flavin N(5).⁹³ Indeed, amine oxidases are unique from other flavoproteins in their ability to catalyze the oxidation of hydrazine.



Scheme 3.5. Proposed hydride transfer mechanism for C-H bond cleavage

3.11.2 Radical Mechanisms: H^\bullet Transfer

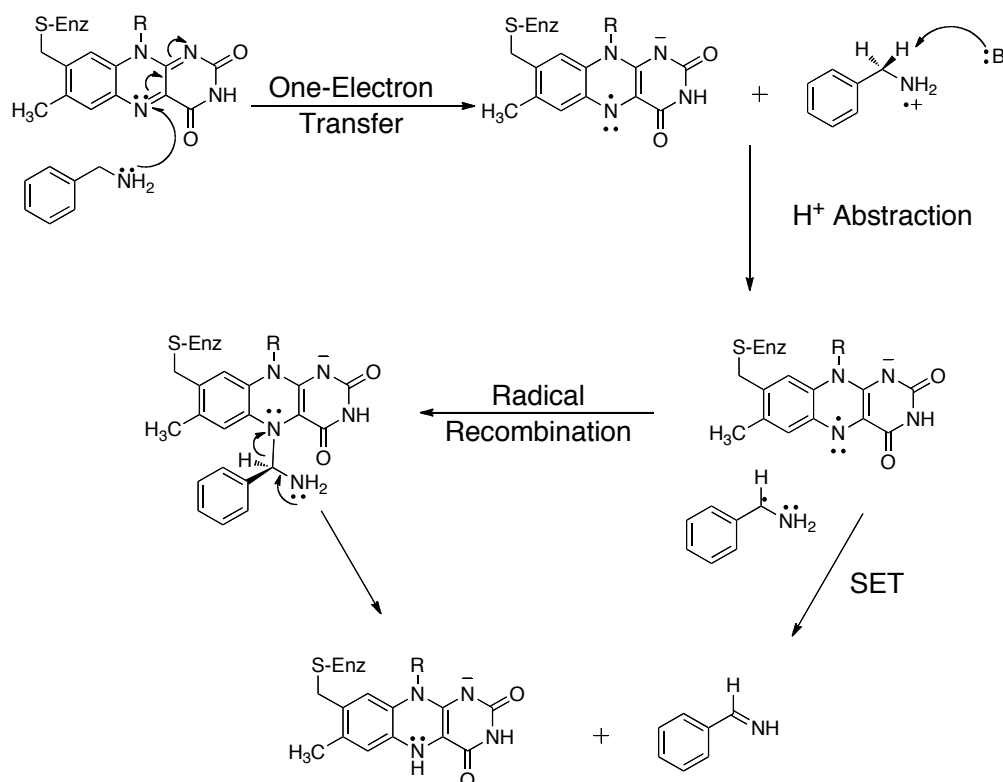
The hydrogen atom transfer mechanism involves hydrogen atom transfer from the α -C-H bond of the amine to the N(5) of the flavin followed by a single electron transfer to produce the flavin hydroquinone (Scheme 3.6). The lack of spectroscopic evidence for a flavin radical intermediate together with the lack of precedence for ground state flavin abstracting hydrogen atoms from organic molecules argues against a radical mechanism.



Scheme 3.6. Hydrogen atom abstraction

3.11.3.1 H^+ Abstraction Mechanisms: Aminium Cation Radical Mechanism

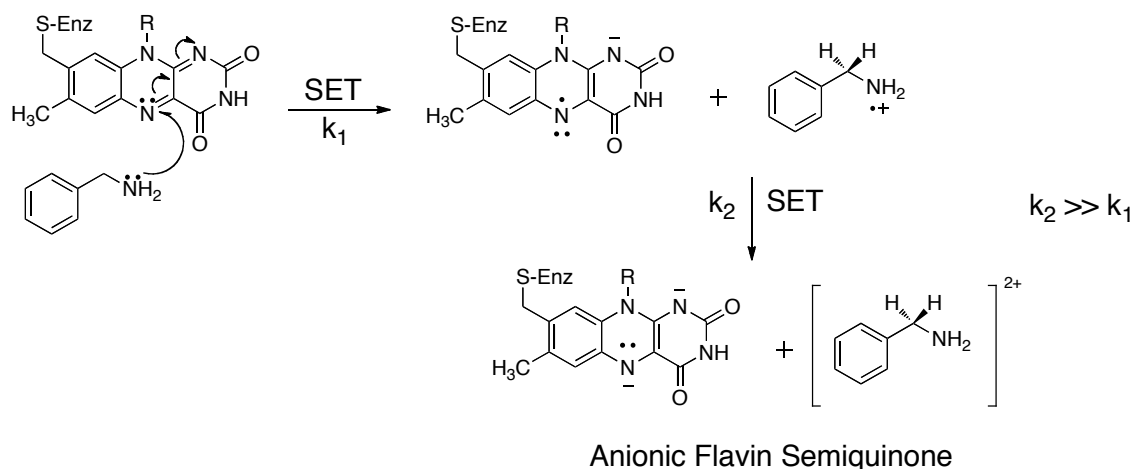
The aminium cation radical mechanism has received the most attention due to the extensive studies performed on 'radical clocks' by Silverman and coworkers (Scheme 3.7).⁸⁸ The mechanism is an adaptation between a strict deprotonation of the α -protons to the amine and a hydrogen atom abstraction. This mechanism originated from the observation that MAO B catalyzed oxidation of *N*-cyclopropylbenzylamine is predominately oxidized at the benzylic carbon (~70%) and only partially oxidized at the cyclopropyl carbon (30%). Because electrochemical oxidation produced a similar ratio of oxidation products, it was proposed that MAO follows a SET mechanism. The oxidation is initiated by delivering an electron to the flavin ring from the nitrogen of the amine. This mechanism was proposed to explain how the α -C-H bonds to the amine are deprotonated given their relatively high pK_a and in the absence of a strong base in the active site. Silverman proposed that a one electron oxidation of the amine nitrogen concomitant with a one electron reduction of the N(5) of the flavin would sufficiently lower the pK_a of the α -protons of the substrate for deprotonation.



Scheme 3.7. Silverman's proposed mechanism for C-H bond cleavage: aminium cation radical mechanism

The main flaw of this proposal is that the one electron oxidation-reduction potential of flavin is $\sim 40 \text{ mV}^{77}$ while the reduction potential of amines is $\sim 1.5 \text{ V}$. The reduction-potential of amine is too high to facilitate one electron transfer to the flavin. Furthermore, attempts to identify a radical intermediate during catalysis have not been fruitful. No effects are observed on the rate of reduction when a magnetic field is applied to the enzyme system unlike what would be expected for a SET mechanism involving a radical pair intermediate. Scrutton and coworkers propose a rapid electron transfer from the reduced flavin to a tyrosine residue within the active site. Evidence for the tyrosine radical is proposed from the interpretation of ENDOR experiments; although, mutation of the tyrosine residues does not provide significant changes in the hyperfine

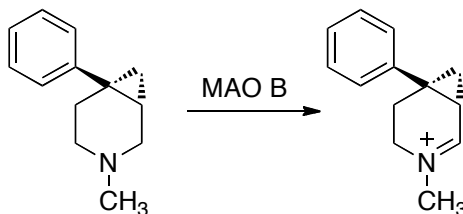
couple observed in the ENDOR spectra.^{94, 95} Ramsay and coworkers have attempted to explain the lack of evidence of a radical intermediate by suggesting that the rate a second electron transfer is much greater than the first electron transfer which results in an anionic flavin semiquinone.⁹⁶ The EPR spectra of the MAO A substrate reduction mirrors that of D-amino acid oxidase (DAAO) in which a hydride mechanism is generally accepted. Ramsay goes on to propose that this is evidence for a hydride transfer; although, the electron transfer occurs in two sequential steps rather than a concerted two electron transfer as is traditionally expected for a hydride transfer mechanism. Again, no evidence of a single electron transfer has been reported.



Scheme 3.8. Mechanism for C-H bond proposed by Ramsay and coworkers

To date, the only evidence to support a SET transfer mechanism is the observation that MAO catalyzed oxidation cyclopropylamines results in ring opening of the cyclopropyl-moiety followed by C4a flavin adduct formation (Figure 3.11). The SET probe Rimoldi's amine does not undergo ring opening when oxidized by MAO B (Scheme 3.9).⁹⁷ Oxidation of the tertiary amine proceeds smoothly in the absence of ring opening products or racemization of the

stereocenter.

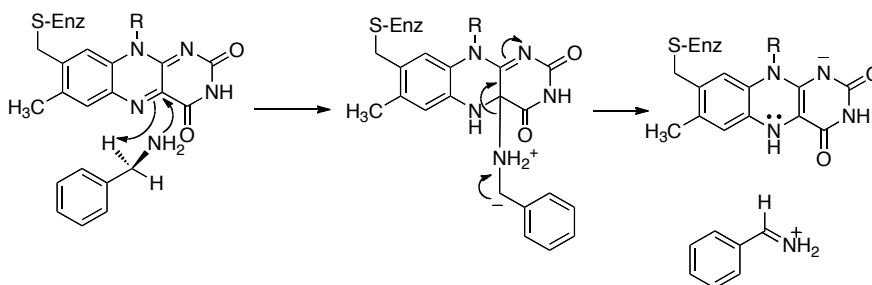


Scheme 3.9. Reaction of Rimoldi's amine with MAO B.

3.11.3.2 H^+ Abstraction Mechanisms: Polar Nucleophilic Mechanism

An alternative H^+ abstraction mechanism was proposed by Miller and Edmondson in which the electrophilic C4a position of the flavin undergoes a nucleophilic attack by the amine substrate (Scheme 3.10). This mechanism is an adaptation of the original mechanism proposed by Hamilton in which an active site base deprotonates the α -proton of the amine.⁸⁷ The absence of an active site base strong enough to facilitate deprotonation prevents this from being generally accepted as the mechanism of C-H bond cleavage. Miller and Edmondson proposed that the benzylic C-H ($pK_a \sim 25$)⁹⁸ is deprotonated by the transient active site base generated at the N(5) of flavin ($pK_a \sim 25$), immediately following the addition to the C4a position.⁹⁹ Support for this mechanism comes from Hammett plot analysis of steady state and rapid reaction kinetic data which shows a positive ρ value of ~ 2 for *para*-substituted benzylamine analogues. This behavior is consistent among human MAO A, mutant forms of human MAO A, rat MAO A, and zebrafish MAO (unpublished data).^{81, 100} Previous QSAR investigation of Cu-quinoprotein plasma amine oxidase also shows a ρ value of ~ 1.4 for C-H bond cleavage. The generally accepted mechanism for this related

amine oxidase is also a proton abstraction mechanism from a Schiff base intermediate. To date there is no evidence of a electronic contribution on the rate of catalysis when MAO B oxidizes a series of *para*-substituted benzylamine analogues.



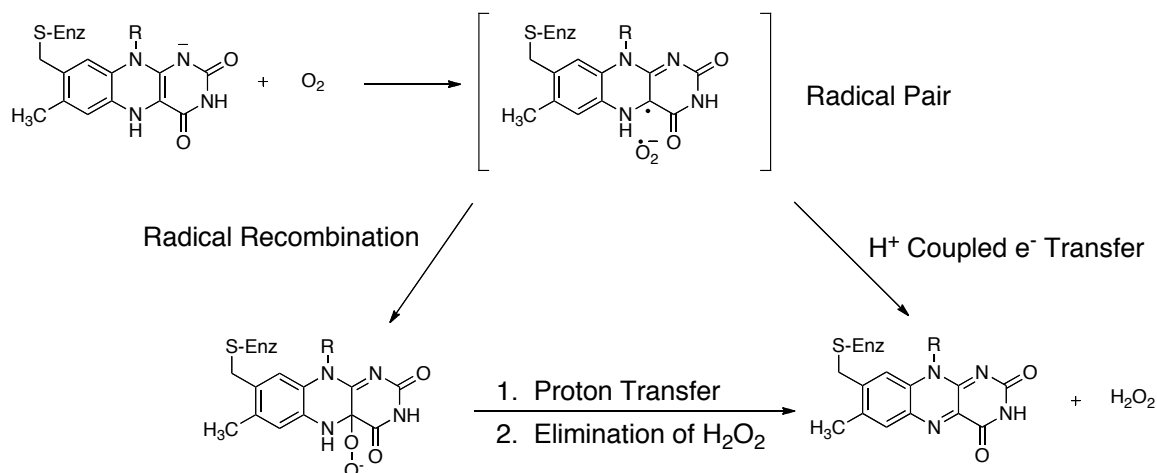
Scheme 3.10. Polar nucleophilic mechanism for C-H bond cleavage proposed by Miller and Edmondson

3.11.4 Generally Accepted Mechanism for Oxidation of Flavin by O_2

The generally accepted mechanism for the reaction of molecular oxygen with reduced MAO is a rate limiting single electron transfer step from the ground state reduced flavin to triplet oxygen to form the superoxide anion neutral flavin semiquinone pair (Scheme 3.11). The reaction can proceed by one of two possible pathways. The first pathway involves radical recombination to form the C4a-peroxyflavin adduct which is followed by protonation of the peroxyanion and elimination of hydrogen peroxide. The C4a peroxyflavin adduct has been well characterized using N(5)-alkylated lumiflavin analogues.¹⁰¹ The peroxyflavin intermediate have been observed in the flavoenzyme hydroxylase family¹⁰² as well as one flavoenzyme oxidase.^{103, 104}

The second pathway involves a proton coupled electron transfer in which no covalent intermediate is formed between the superoxide and flavin radical. Both theoretical calculations⁵⁵ and experimental studies on sarcosine oxidase¹⁰⁵

have been published in support of this pathway. Mutagenesis of the Lys residue that cooperated in a H-bond (through a water molecule) with the N(5) of the flavin results dramatic reduction of the rate of reoxidation of the flavin.



Scheme 3.11. Mechanism of reoxidation of reduced flavin by molecular oxygen

3.12 Dissertation Objectives

3.12.1 Elucidating the Role of Ile199 and Tyr326

The primary objective of this dissertation is to understand the functional characteristics that are unique to MAO B and to exploit these qualities for the selective inhibition of MAO B for the development of therapeutic agents. A major structural difference in human MAO A and MAO B is that MAO A has a monopartite substrate cavity of 550\AA^3 and MAO B is dipartite with a 290\AA^3 entrance cavity and a 400\AA^3 substrate cavity. Ile199 and Tyr326 function to separate these two cavities. The Ile199 side chain is in a required “open” conformation with large inhibitors and is “closed” with smaller inhibitors. These have been identified as structural deterrents for substrate and inhibitor recognition. To probe the function of these gating residues, Ile199Ala and Ile199Ala–Tyr326Ala mutant forms of MAO B were constructed, expressed in

Pichia pastoris, and purified.

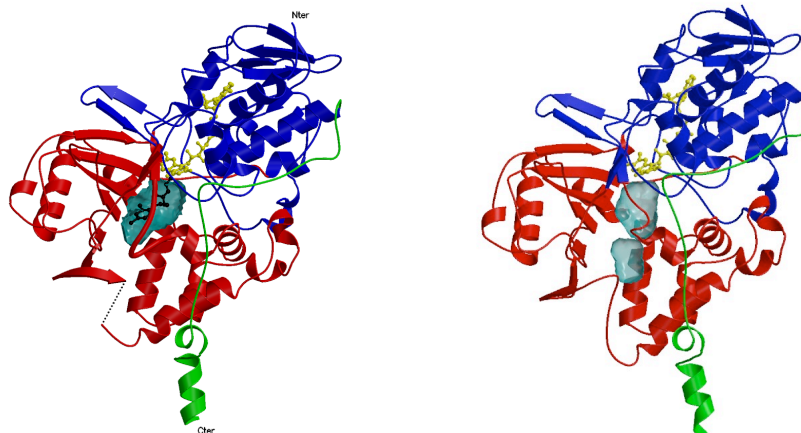


Figure 3.11. Comparison of the relative shapes of the MAO A and MAO B active sites.⁴⁵

3.12.2 Investigation of the Molecular Mechanisms of MAO B Specific Inhibitors

To design highly specific and potent MAO B inhibitors an understanding of the inhibitory properties of existing inhibitors is required. In this study three classes of inhibitors were investigated. These include mechanism-based inhibition, which exploits the substrate recognition of MAO B; reversible inhibition that promotes increased inhibitor-enzyme interactions through binding to the entrance and substrate cavities in concert; and the novel approach of targeting only the entrance cavity of MAO B.

3.12.2.1 Exploiting Substrate Reactivity unique to MAO B.

This investigation focuses on the selective, irreversible inhibition of MAO B with mofegiline. Mofegiline is the most potent inhibitor that has been studied to date. Mofegiline rapidly inhibits MAO B stoichiometrically within the first ms of exposure. The mofegiline-MAO B adduct exhibits spectral properties unlike

those of traditional flavin N(5) and C4a adducts, which is relevant for the study of related flavoproteins.

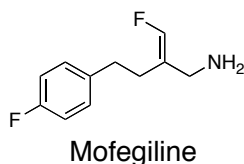


Figure 3.12. Structure of the MAO B specific inhibitor, mofegiline.

3.12.2.2 Rational Design of Inhibitors that Bind to Both the Entrance and Substrate Cavities.

Inhibitors that bridge the entrance cavity and substrate cavity together are thought to result in tighter binding and more selectivity for the B isozyme through promoting inhibitor-enzyme interactions. Caffeine is a weak ($K_i \sim 3$ mM), nonselective inhibitor of MAO A and MAO B. Upon functionalizing caffeine with a styryl moiety in the 8-position, chlorostyrylcaffeine no longer binds to MAO A while binding to MAO B is enhanced 15,000-fold. Using this as a platform for the design of novel MAO B inhibitors, a series of styrylisatin analogues were designed, synthesized, and their biological activity was assessed (Figure 3.5).

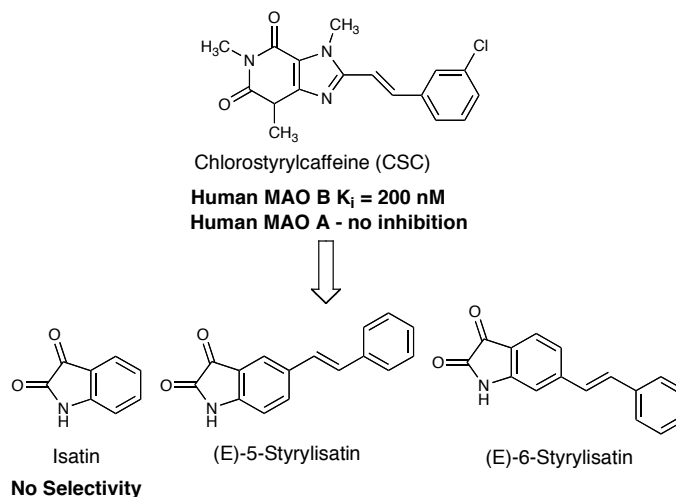
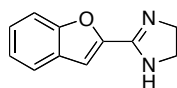


Figure 3.13. Development of styrylisatin analogus.

3.12.2.3 Novel Approach of Targeting the Entrance Cavity of MAO B.

Existing MAO B specific inhibitors are designed to promote binding to either the substrate cavity or the entrance and substrate cavities in unison. A novel approach to inhibitor binding is to target the entrance cavity alone through the use of imidazoline ligands such as 2-(2-benzofuranyl)-2-imidazoline (2-BFI). This is the first report of such binding to MAO B. The formation of the imidazoline binding site involves conformational changes of both the Ile199 'gating' residue as well as Tyr326, which is situated opposite to the Ile199.



2-(2-Benzofuranyl)-2-imidazoline (2-BFI)

Figure 3.14. Structure of 2-(2-benzofuranyl)-2-imidazoline (2-BFI).

3.13 References

1. Weyler, W.; Hsu, Y. P.; Breakefield, X. O., Biochemistry and genetics of monoamine oxidase. *Pharmacol. Ther.* **1990**, 47, (3), 391-417.
2. Bach, A. W.; Lan, N. C.; Johnson, D. L.; Abell, C. W.; Bembenek, M. E.; Kwan, S. W.; Seeburg, P. H.; Shih, J. C., cDNA cloning of human liver monoamine oxidase A and B: molecular basis of differences in enzymatic properties. *Proc. Natl. Acad. Sci. U S A* **1988**, 85, (13), 4934-4938.
3. Grimsby, J.; Chen, K.; Wang, L. J.; Lan, N. C.; Shih, J. C., Human monoamine oxidase A and B genes exhibit identical exon-intron organization. *Proc. Natl. Acad. Sci. U S A* **1991**, 88, (9), 3637-41.
4. Edmondson, D. E.; Binda, C.; Wang, J.; Upadhyay, A. K.; Mattevi, A., Molecular and mechanistic properties of the membrane-bound mitochondrial monoamine oxidases. *Biochemistry* **2009**, 48, (20), 4220-4230.
5. Rodriguez, M. J.; Saura, J.; Billett, E. E.; Finch, C. C.; Mahy, N., Cellular localization of monoamine oxidase A and B in human tissues outside of the central nervous system. *Cell Tissue Res.* **2001**, 304, (2), 215-20.
6. Willoughby, J.; Glover, V.; Sandler, M., Histochemical localisation of monoamine oxidase A and B in rat brain. *J. Neuro. Transm.* **1988**, 74, (1), 29-42.
7. Westlund, K. N.; Denney, R. M.; Rose, R. M.; Abell, C. W., Localization of distinct monoamine oxidase A and monoamine oxidase B cell populations in human brainstem. *Neuroscience* **1988**, 25, (2), 439-56.
8. Saura, J.; Luque, J. M.; Cesura, A. M.; Da Prada, M.; Chan-Palay, V.; Huber, G.; Loffler, J.; Richards, J. G., Increased monoamine oxidase B activity in

plaque-associated astrocytes of Alzheimer brains revealed by quantitative enzyme radioautography. *Neuroscience* **1994**, 62, (1), 15-30.

9. Luque, J. M.; Kwan, S.-W.; Abell, C. W.; Da Prada, M.; Richards, J. G., Cellular expression of mRNAs encoding monoamine oxidases A and B in the rat central nervous system. *J. Comp. Neurol.* **1995**, 363, (4), 665-80.

10. Jahng, J. W.; Houpt, T. A.; Wessel, T. C.; Chen, K.; Shih, J. C.; Joh, T. H., Localization of monoamine oxidase A and B mRNA in the rat brain by in situ hybridization. *Synapse (N. Y.)* **1997**, 25, (1), 30-36.

11. Shih, J. C.; Chen, K.; Ridd, M. J., Monoamine oxidase: from genes to behavior. *Annu. Rev. Neurosci.* **1999**, 22, 197-217.

12. Whibley, A.; Urquhart, J.; Dore, J.; Willatt, L.; Parkin, G.; Gaunt, L.; Black, G.; Donnai, D.; Raymond, F. L., Deletion of MAOA and MAOB in a male patient causes severe developmental delay, intermittent hypotonia and stereotypical hand movements. *Eur. J. Hum. Genet.*

13. Beaver, K. M.; Delisi, M.; Vaughn, M. G.; Barnes, J. C., Monoamine oxidase A genotype is associated with gang membership and weapon use. *Comprehensive Psychiatry* **2009**, 1-5.

14. Brunner, H. G.; Nelen, M. R.; van Zandvoort, P.; Abeling, N. G.; van Gennip, A. H.; Wolters, E. C.; Kuiper, M. A.; Ropers, H. H.; van Oost, B. A., X-linked borderline mental retardation with prominent behavioral disturbance: phenotype, genetic localization, and evidence for disturbed monoamine metabolism. *Am. J. Hum. Genet.* **1993**, 52, (6), 1032-9.

15. Brunner, H. G.; Nelen, M.; Breakefield, X. O.; Ropers, H. H.; van Oost, B. A., Abnormal behavior associated with a point mutation in the structural gene for monoamine oxidase A. *Science* **1993**, 262, (5133), 578-80.
16. Shih, J. C., Monoamine oxidases: from tissue homogenates to transgenic mice. *Neurochem. Res.* **2007**, 32, (10), 1757-61.
17. Zeller, E. A.; Barsky, J., In vivo inhibition of liver and brain monoamine oxidase by 1-isonicotinyl-2-isopropyl hydrazine. *Proc. Soc. Exper. Biology and Medicine* **1952**, 81, (2), 459-461.
18. Maret, G.; el Tayar, N.; Carrupt, P. A.; Testa, B.; Jenner, P.; Baird, M., Toxication of MPTP (1-methyl-4-phenyl-1,2,3,6-tetrahydropyridine) and analogs by monoamine oxidase. A structure-reactivity relationship study. *Biochem. Pharmacol.* **1990**, 40, (4), 783-92.
19. Langston, J. W.; Forno, L. S.; Rebert, C. S.; Irwin, I., Selective nigral toxicity after systemic administration of 1-methyl-4-phenyl-1,2,5,6-tetrahydropyridine (MPTP) in the squirrel monkey. *Brain Res.* **1984**, 292, (2), 390-4.
20. Heikkila, R. E.; Manzino, L.; Cabbat, F. S.; Duvoisin, R. C., Protection against the dopaminergic neurotoxicity of 1-methyl-4-phenyl-1,2,5,6-tetrahydropyridine by monoamine oxidase inhibitors. *Nature* **1984**, 311, (5985), 467-9.
21. Fuller, R. W.; Hemrick-Luecke, S. K., Deprenyl protection against striatal dopamine depletion by 1-methyl-4-phenyl-1,2,3,6-tetrahydropyridine in mice. *Res. Commun. Subst. Abuse* **1985**, 5, (4), 241-6.

22. Kumar, M. J.; Nicholls, D. G.; Andersen, J. K., Oxidative alpha-ketoglutarate dehydrogenase inhibition via subtle elevations in monoamine oxidase B levels results in loss of spare respiratory capacity: implications for Parkinson's disease. *J. Biol. Chem.* **2003**, *278*, (47), 46432-9.
23. Nussbaum, R. L.; Ellis, C. E., Alzheimer's disease and Parkinson's disease. *N. Engl. J. Med.* **2003**, *348*, (14), 1356-64.
24. Fowler, J. S.; Logan, J.; Volkow, N. D.; Wang, G.-J.; MacGregor, R. R.; Ding, Y.-S., Monoamine oxidase: radiotracer development and human studies. *Methods (San Diego, CA, U. S.)* **2002**, *27*, (3), 263-277.
25. Westlund, K. N.; Denney, R. M.; Kochersperger, L. M.; Rose, R. M., Distinct monoamine oxidase A and B populations in primate brain. *Science* **1985**, *230*, (4722), 181-3.
26. Levitt, P.; Pintar, J. E.; Breakefield, X. O., Immunocytochemical demonstration of monoamine oxidase B in brain astrocytes and serotonergic neurons. *Proc. Natl. Acad. Sci. U. S. A.* **1982**, *79*, (20), 6385-9.
27. Burke, W. J., 3,4-dihydroxyphenylacetaldehyde: A potential target for neuroprotective therapy in Parkinson's disease. *Curr. Drug Targets: CNS Neurol. Disord.* **2003**, *2*, (2), 143-148.
28. Burke, W. J.; Kumar, V. B.; Pandey, N.; Panneton, W. M.; Gan, Q.; Franko, M. W.; O'Dell, M.; Li, S. W.; Pan, Y.; Chung, H. D.; Galvin, J. E., Aggregation of $\alpha\pm$ -synuclein by DOPAL, the monoamine oxidase metabolite of dopamine. *Acta Neuropathol.* **2008**, *115*, (2), 193-203.

29. Rees, J. N.; Florang, V. R.; Eckert, L. L.; Doorn, J. A., Protein reactivity of 3,4-dihydroxyphenylacetaldehyde, a toxic dopamine metabolite, is dependent on both the aldehyde and the catechol. *Chem. Res. Toxicol.* **2009**, *22*, (7), 1256-63.
30. McDermott, R.; Tingley, D.; Cowden, J.; Frazzetto, G.; Johnson, D. D. P., Monoamine oxidase A gene (MAOA) predicts behavioral aggression following provocation. *Proc. Natl. Acad. Sci. U S A* **2009**, *106*, (7), 2118-2123.
31. Cases, O.; Seif, I.; Grimsby, J.; Gaspar, P.; Chen, K.; Pournin, S.; Mueller, U.; Aguet, M.; Babinet, C.; et al., Aggressive behavior and altered amounts of brain serotonin and norepinephrine in mice lacking MAOA. *Science* **1995**, *268*, (5218), 1763-6.
32. Maurel, A.; Hernandez, C.; Kunduzova, O.; Bompard, G.; Cambon, C.; Parini, A.; Frances, B., Age-dependent increase in hydrogen peroxide production by cardiac monoamine oxidase A in rats. *Am. J. Physiology-Heart and Circulatory Physiology* **2003**, *284*, (4), H1460-H1467.
33. Bianchi, P.; Kunduzova, O.; Masini, E.; Cambon, C.; Bani, D.; Raimondi, L.; Seguelas, M.-H.; Nistri, S.; Colucci, W.; Leducq, N.; Parini, A., Oxidative stress by monoamine oxidase mediates receptor-independent cardiomyocyte apoptosis by serotonin and postischemic myocardial injury. *Circulation* **2005**, *112*, (21), 3297-3305.
34. Gentili, F.; Pizzinat, N.; Ordener, C.; Marchal-Victorion, S.; Maurel, A.; Hofmann, R.; Renard, P.; Delagrance, P.; Pignini, M.; Parini, A.; Giannella, M., 3-[5-(4,5-dihydro-1H-imidazol-2-yl)-furan-2-yl]phenylamine (amifuraline), a

promising reversible and selective peripheral MAO-A Inhibitor. *J. Med. Chem.* **2006**, 49, (18), 5578-5586.

35. Stewart, J. W., Treating depression with atypical features. *J. Clin. Psychiatry* **2007**, 68 Suppl 3, 25-9.

36. Binda, C.; Wang, J.; Pisani, L.; Caccia, C.; Carotti, A.; Salvati, P.; Edmondson, D. E.; Mattevi, A., Structures of human monoamine oxidase B complexes with selective noncovalent inhibitors: Safinamide and coumarin analogs. *J. Med. Chem.* **2007**, 50, (23), 5848-5852.

37. Sweet, R. A.; Brown, E. J.; Heimberg, R. G.; Ciafre, L.; Scanga, D. M.; Cornelius, J. R.; Dube, S.; Forsyth, K. M.; Holt, C. S., Monoamine oxidase inhibitor dietary restrictions: what are we asking patients to give up? *J. Clin. Psychiatry* **1995**, 56, (5), 196-201.

38. Weyler, W.; Salach, J. I., Purification and properties of mitochondrial monoamine oxidase type A from human placenta. *J. Biol. Chem.* **1985**, 260, (24), 13199-13207.

39. Weyler, W.; Titlow, C. C.; Salach, J. I., Catalytically active monoamine oxidase type A from human liver expressed in *Saccharomyces cerevisiae* contains covalent FAD. *Biochem. Biophys. Res. Commun.* **1990**, 173, (3), 1205-1211.

40. Salach, J. I., Monoamine oxidase from beef liver mitochondria: simplified isolation procedure, properties, and determination of its cysteinyl flavin content. *Arch. Biochem. Biophys.* **1979**, 192, (1), 128-37.

41. Newton-Vinson, P.; Hubalek, F.; Edmondson, D. E., High-level expression of human liver monoamine oxidase B in *Pichia pastoris*. *Prot. Expr. Purif.* **2000**, 20, (2), 334-45.
42. Li, M.; Hubalek, F.; Newton-Vinson, P.; Edmondson, D. E., High-level expression of human liver monoamine oxidase A in *Pichia pastoris*: comparison with the enzyme expressed in *Saccharomyces cerevisiae*. *Prot. Expr. Purif.* **2002**, 24, (1), 152-62.
43. Binda, C.; Newton-Vinson, P.; Hubalek, F.; Edmondson, D. E.; Mattevi, A., Structure of human monoamine oxidase B, a drug target for the treatment of neurological disorders. *Nat. Struct. Biol.* **2002**, 9, (1), 22-26.
44. Son, S. Y.; Ma, J.; Kondou, Y.; Yoshimura, M.; Yamashita, E.; Tsukihara, T., Structure of human monoamine oxidase A at 2.2-angstrom resolution: the control of opening the entry for substrates/inhibitors. *Proc. Natl. Acad. Sci. U S A* **2008**, 105, (15), 5739-5744.
45. De Colibus, L.; Li, M.; Binda, C.; Lustig, A.; Edmondson, D. E.; Mattevi, A., Three-dimensional structure of human monoamine oxidase A (MAO A): relation to the structures of rat MAO A and human MAO B. *Proc. Natl. Acad. Sci. U S A* **2005**, 102, (36), 12684-12689.
46. Andres, A. M.; Soldevila, M.; Navarro, A.; Kidd, K. K.; Oliva, B.; Bertranpetit, J., Positive selection in MAOA gene is human exclusive: determination of the putative amino acid change selected in the human lineage. *Human Genetics* **2004**, 115, (5), 377-386.

47. Sachs, J. N.; Engelman, D. M., Introduction to the membrane protein reviews: The interplay of structure, dynamics, and environment in membrane protein function. *Ann. Rev. Biochemistry* **2006**, *75*, 707-712.
48. Fajer, P. G., Electron paramagnetic resonance (EPR) and spin-labelling. *Handb. Proteins* **2007**, *2*, 1001-1006.
49. Upadhyay, A. K.; Borbat, P. P.; Wang, J.; Freed, J. H.; Edmondson, D. E., Determination of the oligomeric states of human and rat monoamine oxidases in the outer mitochondrial membrane and octyl beta-D-glucopyranoside micelles using pulsed dipolar electron spin resonance spectroscopy. *Biochemistry* **2008**, *47*, (6), 1554-1566.
50. Upadhyay, A. K.; Borbat, P. P.; Wang, J.; Freed, J. H.; Edmondson, D. E., Determination of the oligomeric states of human and rat monoamine oxidases in the outer mitochondrial membrane and octyl β -D-glucopyranoside micelles using pulsed dipolar electron spin resonance spectroscopy. *Biochemistry* **2008**, *47*, (6), 1554-1566.
51. Hubalek, F.; Binda, C.; Khalil, A.; Li, M.; Mattevi, A.; Castagnoli, N.; Edmondson, D. E., Demonstration of isoleucine 199 as a structural determinant for the selective inhibition of human monoamine oxidase B by specific reversible inhibitors. *J. Biol. Chem.* **2005**, *280*, (16), 15761-15766.
52. Geha, R. M.; Chen, K.; Wouters, J.; Ooms, F.; Shih, J. C., Analysis of conserved active site residues in monoamine oxidase A and B and their three-dimensional molecular modeling. *J. Biol. Chem.* **2002**, *277*, (19), 17209-16.

53. Li, M.; Binda, C.; Mattevi, A.; Edmondson, D. E., Functional role of the "aromatic cage" in human monoamine oxidase B: structures and catalytic properties of Tyr435 mutant proteins. *Biochemistry* **2006**, 45, (15), 4775-4784.
54. Akyuez, M. A.; Erdem, S. S.; Edmondson, D. E., The aromatic cage in the active site of monoamine oxidase B: Effect on the structural and electronic properties of bound benzylamine and p-nitrobenzylamine. *J. Neural Transm.* **2007**, 114, (6), 693-698.
55. Prabhakar, R.; Li, M.; Musaev, D. G.; Morokuma, K.; Edmondson, D. E., A density functional theory (DFT) study of the spin forbidden dioxygen activation in monoamine oxidase B (MAO B). In *Flavins and Flavoproteins.*, Nishino, T.; Riura, R.; M., T.; K., F., Eds. ArchiTect, Inc.: Tokyo, 2005; pp 127–131.
56. Zhao, G. H.; Bruckner, R. C.; Jorns, M. S., Identification of the oxygen activation site in monomeric sarcosine oxidase: Role of Lys265 in catalysis. *Biochemistry* **2008**, 47, (35), 9124-9135.
57. Pollegioni, L.; Diederichs, K.; Molla, G.; Umhau, S.; Welte, W.; Ghisla, S.; Pilone, M. S., Yeast D-amino acid oxidase: Structural basis of its catalytic properties. *J. Mol. Biology* **2002**, 324, (3), 535-546.
58. Pawelek, P. D.; Cheah, J.; Coulombe, R.; Macheroux, P.; Ghisla, S.; Vrieling, A., The structure of L-amino acid oxidase reveals the substrate trajectory into an enantiomerically conserved active site. *EMBO J.* **2000**, 19, (16), 4204-4215.

59. Trickey, P.; Wagner, M. A.; Jorns, M. S.; Mathews, F. S., Monomeric sarcosine oxidase: structure of a covalently flavinylated amine oxidizing enzyme. *Structure with Folding & Design* **1999**, 7, (3), 331-345.
60. Binda, C.; Li, M.; Hubalek, F.; Restelli, N.; Edmondson, D. E.; Mattevi, A., Insights into the mode of inhibition of human mitochondrial monoamine oxidase B from high-resolution crystal structures. *Proc. Natl. Acad. Sci. U S A* **2003**, 100, (17), 9750-9755.
61. Yang, M.; Culhane, J. C.; Szewczuk, L. M.; Jalili, P.; Ball, H. L.; Machius, M.; Cole, P. A.; Yu, H., Structural Basis for the Inhibition of the LSD1 Histone Demethylase by the Antidepressant trans-2-Phenylcyclopropylamine. *Biochemistry* **2007**, 46, (27), 8058-8065.
62. Walker, W. H.; Hemmerich, P.; Massey, V., Reductive photoalkylation of flavin nucleus and flavin catalyzed photodecarboxylation of phenyl acetate. Studies in Flavin Series .15. *Helvetica Chimica Acta* **1967**, 50, (8), 2269-2279.
63. Lairez, O.; Calise, D.; Bianchi, P.; Ordener, C.; Spreux-Varoquaux, O.; Guilbeau-Frugier, C.; Escourrou, G.; Seif, I.; Roncalli, J.; Pizzinat, N.; Galinier, M.; Parini, A.; Mialet-Perez, J., Genetic deletion of MAO-A promotes serotonin-dependent ventricular hypertrophy by pressure overload. *J. Mol. Cellular Cardiology* **2009**, 46, (4), 587-595.
64. Edmondson, D. E.; Binda, C.; Mattevi, A., Structural insights into the mechanism of amine oxidation by monoamine oxidases A and B. *Arch. Biochemistry and Biophy.* **2007**, 464, (2), 269-276.

65. Edmondson, D. E.; Bhattacharyya, A. K.; Walker, M. C., Spectral and kinetic studies of imine product formation in the oxidation of p-(N,N-dimethylamino)benzylamine analogues by monoamine oxidase B. *Biochemistry* **1993**, 32, (19), 5196-202.
66. Dunn, R. V.; Marshall, K. R.; Munro, A. W.; Scrutton, N. S., The pH dependence of kinetic isotope effects in monoamine oxidase A indicates stabilization of the neutral amine in the enzyme-substrate complex. *FEBS J.* **2008**, 275, (15), 3850-8.
67. Walker, M. C.; Edmondson, D. E., Structure-activity relationships in the oxidation of benzylamine analogues by bovine liver mitochondrial monoamine oxidase B. *Biochemistry* **1994**, 33, (23), 7088-7098.
68. Edmondson, D. E.; Bhattacharyya, A. K.; Walker, M. C., Spectral and kinetic studies of imine product formation in the oxidation of p-(N,N-dimethylamino)benzylamine analogs by monoamine oxidase B. *Biochemistry* **1993**, 32, (19), 5196-202.
69. Ragan, C. I.; Galante, Y. M.; Hatefi, Y.; Ohnishi, T., Resolution of mitochondrial NADH dehydrogenase and isolation of two iron-sulfur proteins. *Biochemistry* **1982**, 21, (3), 590-4.
70. Pearce, L. B.; Roth, J. A., Human brain monoamine oxidase type B: mechanism of deamination as probed by steady-state methods. *Biochemistry* **1985**, 24, (8), 1821-6.

71. Tan, A. K.; Ramsay, R. R., Substrate-specific enhancement of the oxidative half-reaction of monoamine oxidase. *Biochemistry* **1993**, 32, (9), 2137-43.
72. Husain, M.; Edmondson, D. E.; Singer, T. P., Kinetic studies on the catalytic mechanism of liver monoamine oxidase. *Biochemistry* **1982**, 21, (3), 595-600.
73. Ramsay, R. R., Kinetic Mechanism of Monoamine Oxidase-A. *Biochemistry* **1991**, 30, (18), 4624-4629.
74. Nandigama, R. K.; Edmondson, D. E., Structure-activity relations in the oxidation of phenethylamine analogues by recombinant human liver monoamine oxidase A. *Biochemistry* **2000**, 39, (49), 15258-65.
75. Ramsay, R. R., Kinetic mechanism of monoamine oxidase A. *Biochemistry* **1991**, 30, (18), 4624-9.
76. Urban, P.; Andersen, J. K.; Hsu, H. P.; Pompon, D., Comparative membrane locations and activities of human monoamine oxidases expressed in yeast. *FEBS Lett.* **1991**, 286, (1-2), 142-6.
77. Newton-Vinson, P.; Edmondson, D. E., High-Level Expression, Structural, Kinetic, and Redox Characterization of Recombinant Human Liver Monoamine Oxidase B. In *Flavins and Flavoproteins*, Ghisla, S.; Kroneck, P.; Macheroux, P.; H., S., Eds. Agency for Scientific Publications: Berlin, 1999; pp 431-434.
78. Salach, J. I., Mono-Amine Oxidase from Beef-Liver Mitochondria - Simplified Isolation Procedure, Properties, and Determination of Its Cysteinyl Flavin Content. *Arch. Biochemistry and Biophys.* **1979**, 192, (1), 128-137.

79. Yu, P. H.; Bailey, B. A.; Durden, D. A.; Boulton, A. A., Stereospecific deuterium substitution at the alpha-carbon position of dopamine and its effect on oxidative deamination catalyzed by MAO-a and MAO-B from different tissues. *Biochemical Pharmacology* **1986**, 35, (6), 1027-1036.
80. Farnum, M. F.; Klinman, J. P., Stereochemical Probes of Bovine Plasma Amine Oxidase - Evidence for Mirror-Image Processing and a Syn Abstraction of Hydrogens from C-1 and C-2 of Dopamine. *Biochemistry* **1986**, 25, (20), 6028-6036.
81. Miller, J. R.; Edmondson, D. E., Structure-activity relationships in the oxidation of para-substituted benzylamine analogues by recombinant human liver monoamine oxidase A. *Biochemistry* **1999**, 38, (41), 13670-13683.
82. Walker, M. C.; Edmondson, D. E., Structure-Activity Relationships in the Oxidation of Benzylamine Analogs by Bovine Liver Mitochondrial Monoamine Oxidase B. *Biochemistry* **1994**, 33, (23), 7088-98.
83. Jonsson, T.; Edmondson, D. E.; Klinman, J. P., Hydrogen tunneling in the flavoenzyme monoamine oxidase B. *Biochemistry* **1994**, 33, (49), 14871-14878.
84. Binda, C.; Mattevi, A.; Edmondson, D. E., Structure-function relationships in flavoenzyme-dependent amine oxidations: a comparison of polyamine oxidase and monoamine oxidase. *J. Biol. Chem.* **2002**, 277, (27), 23973-23976.
85. Harris, C. M.; Pollegioni, L.; Ghisla, S., pH and kinetic isotope effects in D-amino acid oxidase catalysis - Evidence for a concerted mechanism in substrate dehydrogenation via hydride transfer. *Eur. J. Biochemistry* **2001**, 268, (21), 5504-5520.

86. Fukuzumi, S.; Kojima, T., Control of redox reactivity of flavin and pterin coenzymes by metal ion coordination and hydrogen bonding. *JBIC, J. Biol. Inorg. Chem.* **2008**, 13, (3), 321-333.
87. Brown, L. E.; Hamilton, G. A., Some model reactions and a general mechanism for flavoenzyme-catalyzed dehydrogenations. *J. Am. Chem. Soc.* **1970**, 92, (24), 7225-7.
88. Yamasaki, R. B.; Silverman, R. B., Mechanism for reactivation of N-cyclopropylbenzylamine-inactivated monoamine oxidase by amines. *Biochemistry* **1985**, 24, (23), 6543-6550.
89. Kurtz, K. A.; Rishavy, M. A.; Cleland, W. W.; Fitzpatrick, P. F., Nitrogen isotope effects as probes of the mechanism of D-amino acid oxidase. *J. Am. Chem. Soc.* **2000**, 122, (51), 12896-12897.
90. Ralph, E. C.; Hirschi, J. S.; Anderson, M. A.; Cleland, W. W.; Singleton, D. A.; Fitzpatrick, P. F., Insights into the mechanism of flavoprotein-catalyzed amine oxidation from nitrogen isotope effects on the reaction of N-methyltryptophan oxidase. *Biochemistry* **2007**, 46, (25), 7655-7664.
91. Binda, C.; Wang, J.; Li, M.; Hubalek, F.; Mattevi, A.; Edmondson, D. E., Structural and mechanistic studies of arylalkylhydrazine inhibition of human monoamine oxidases A and B. *Biochemistry* **2008**, 47, (20), 5616-5625.
92. Imada, Y.; Iida, H.; Naota, T., Flavin-catalyzed generation of diimide: An environmentally friendly method for the aerobic hydrogenation of olefins. *J. Am. Chem. Soc.* **2005**, 127, (42), 14544-14545.

93. Pasto, D. J.; Taylor, R. T., Reduction with diimide. *Org. React.* **1991**, 40, 91-155.
94. Dunn, R. V.; Munro, A. W.; Turner, N. J.; Rigby, S. E.; Scrutton, N. S., Tyrosyl radical formation and propagation in flavin dependent monoamine oxidases. *Chembiochem* 11, (9), 1228-31.
95. Rigby, S. E. J.; Hynson, R. M. G.; Ramsay, R. R.; Munro, A. W.; Scrutton, N. S., A stable tyrosyl radical in monoamine oxidase A. *J. Biol. Chem.* **2005**, 280, (6), 4627-4631.
96. Kay, C. W. M.; El Mkami, H.; Molla, G.; Pollegioni, L.; Ramsay, R. R., Characterization of the covalently bound anionic flavin radical in monoamine oxidase a by electron paramagnetic resonance. *J. Am. Chem. Soc.* **2007**, 129, (51), 16091-16097.
97. Bissel, P.; Khalil, A.; Rimoldi, J. M.; Igarashi, K.; Edmondson, D.; Miller, A.; Castagnoli, N., Stereochemical studies on the novel monoamine oxidase B substrates (1R, 6S)- and (1S, 6R)-3-methyl-6-phenyl-3-azabicyclo[4.1.0]heptane. *Bioorg. Med. Chem.* **2008**, 16, (7), 3557-3564.
98. Bordwell, F. G.; Cheng, J. P.; Satish, A. V.; Twyman, C. L., Acidities and homolytic bond-dissociation energies (Bdes) of benzyl-type C-H bonds in sterically congested substrates. *J. Org. Chem.* **1992**, 57, (24), 6542-6546.
99. Macheroux, P.; Ghisla, S.; Sanner, C.; Ruterjans, H.; Muller, F., Reduced flavin: NMR investigation of N5-H exchange mechanism, estimation of ionisation constants and assessment of properties as biological catalyst. *BMC Biochem.* **2005**, 6, 26.

100. Wang, J.; Edmondson, D. E., Do monomeric vs dimeric forms of MAO-A make a difference? A direct comparison of the catalytic properties of rat and human MAO-A's. *J. Neural Trans.* **2007**, 114, (6), 721-724.
101. Bruce, T. C., 4a-Peroxyflavins. *Oxidases Relat. Redox Syst., Proc. Int. Symp., 3rd* **1982**, 423-46.
102. Massey, V., Activation of molecular-oxygen by flavins and flavoproteins. *J. Biol. Chem.* **1994**, 269, (36), 22459-22462.
103. Orville, A. M.; Lountos, G. T.; Finnegan, S.; Gadda, G.; Prabhakar, R., Crystallographic, Spectroscopic, and Computational Analysis of a Flavin C4a-Oxygen Adduct in Choline Oxidase. *Biochemistry* **2009**, 48, (4), 720-728.
104. Sucharitakul, J.; Prongjit, M.; Haltrich, D.; Chaiyen, P., Detection of a C4a-hydroperoxyflavin intermediate in the reaction of a flavoprotein oxidase. *Biochemistry* **2008**, 47, (33), 8485-8490.
105. Zhao, G.; Bruckner, R. C.; Schuman Jorns, M., Identification of the Oxygen Activation Site in Monomeric Sarcosine Oxidase: Role of Lys265 in Catalysis. *Biochemistry* **2008**, 47, (35), 9124-9135.

Chapter 4

Development of MAO B Specific Inhibitors: From Investigation to Design

It is known that the age-related increase in MAO B levels in neuronal tissue together with the catalytic production of H₂O₂ (leading to reactive oxygen species) contributes to cellular apoptosis and subsequent neurodegeneration. Therefore, specific inhibitors of MAO B could function as neuroprotectants. This chapter focused on three approaches for the design of inhibitors specific to MAO B: 1. exploiting the substrate recognition of MAO B through mechanism based inhibition (section 4.1); 2. designing inhibitors that bridge both the entrance cavity and the substrate to increase enzyme-ligand interactions (section 4.2); 3. exploring the novel approach of targeting only the entrance cavity of MAO B (section 4.3).

4.1 Mechanistic Studies of the Mechanism Based inhibitor Mofegiline

4.1.1 Development of Mofegiline as an Inhibitor of MAO B.

Mofegiline (Figure 4.1.1) belongs to a class of mechanism-based inhibitors that are characterized by their halo-allylamine functionality. It was proposed that this compound acts as a mechanism-based inhibitor of MAO B in line with the earlier observations by Rando and Eigner¹ who demonstrated that chloroallylamine was a time-dependent, irreversible inhibitor of MAO. Their studies suggested that inhibition of rat liver MAO by allylamine occurs *via* oxidation of the amine moiety followed by covalent adduct formation with the N(5) position of the flavin (Scheme 4.1.1A). This proposal was supported by the

observation that the absorption spectrum of the enzyme-bound flavin is “bleached” after inhibition and remains in this form after removal of excess reagent either by gel filtration or by dialysis.

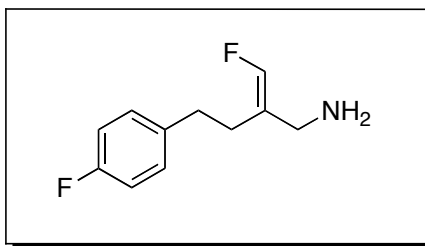
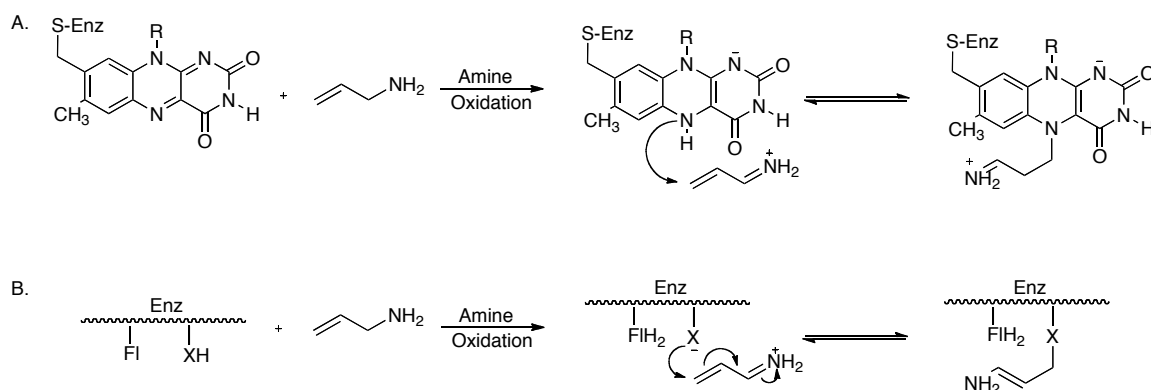


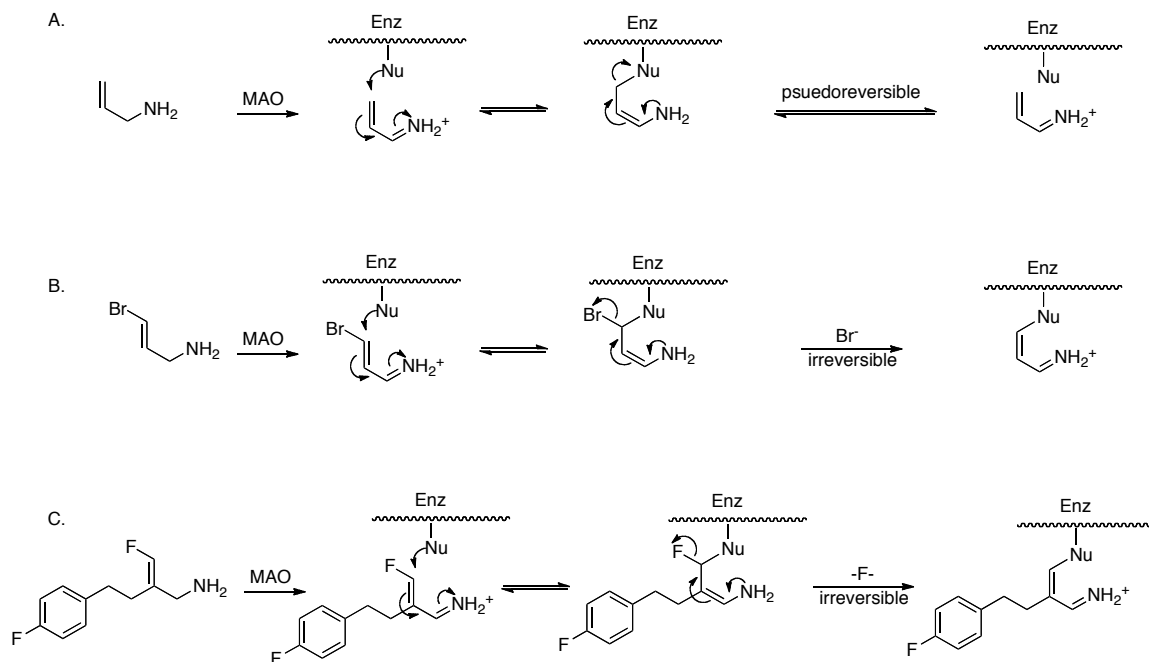
Figure 4.1.1. Structure of mofegiline

This suggestion was later challenged by Silverman and coworkers² when they showed that tritium labeled allylamine remains attached to the protein after denaturation and demonstrated the flavin is reoxidized on denaturation. These observations led to the proposal that inhibition is achieved by catalytic oxidation of allylamine to its imine followed by Michael addition of an active site nucleophilic amino acid residue to the unsaturated imine (Scheme 4.1.1B). This proposed mechanism has prevailed in subsequent discussions describing the mode of MAO inhibition of allylamine inhibitor analogues, like Mofegiline, during the last 20 years.³⁻⁵



Scheme 4.1.1. A. The mechanism for allylamine inhibition of MAO proposed by Rando and Eigner. B. The mechanism of allylamine inhibition of MAO proposed by Silverman.

These findings inspired the production of a class of mechanism-based inhibitors referred to as allylamines.^{4, 6} The potency, specificity, and reversibility of these inhibitors can be tuned by the level of substitution on the olefin as well as the functionality present on the aromatic ring (Scheme 4.1.2A-C).³ Incorporation of a leaving group on the vinyl-carbon on allylamine affords irreversible inhibition of the enzyme (Scheme 4.1.2B). Extraordinary progress was made in the Merrell Dow Research Institute by McDonald and coworkers with the design of the nanomolar MAO B inhibitor Mofegiline.⁶ The incorporation of the less bulky vinyl fluorine moiety allows for increased potency through decreased steric perturbation (Scheme 4.1.2C).⁴



Scheme 4.1.2. Development of allylamine analogues for the inhibition of MAO. A. Inhibition of MAO by allylamine provides pseudoreversible inhibition. B. Installation of a bromide leaving group in the 3-position provide irreversible inhibition of MAO. C. Development of 3-fluoroallylamine, Mofegiline, provide potent irreversible inhibition of MAO by means of reducing steric constraints associated with the larger halogens like Br⁻.

This specific compound demonstrated nanomolar inhibitory properties for the inhibition of rat brain mitochondrial MAO B and was shown to be highly

specific for rat MAO B with a 190-fold higher affinity for the MAO B isoform.⁴ Additional pharmacological interest in Mofegiline stems from its anti-inflammatory properties *via* the inactivation of the copper-dependent amine oxidase, semicarbazide-sensitive amine oxidase (SSAO/VAP-1).⁷ While information on the potency of Mofegiline has been known for some time, the molecular mechanism of inhibition as well as the molecular basis for its high level of specificity remains unknown. The human studies are limited to platelet MAO B or secretion of metabolites in urine.^{4, 8} Therefore, a great deal of information could be learned from studies with purified human MAO A and MAO B, which permit studies to establish molecular insights into the mode of inhibition and identification of the residue responsible for MAO inhibition.

MAO A and MAO B are known from a large number studies in various laboratories to be thiol sensitive enzymes.⁹ Both MAO A and MAO B contain nine cysteine residues with seven of them in highly conserved positions.¹⁰ A non-conserved cysteine residue (Cys172) located near the active site, might be responsible for the selective inhibition of MAO B by Mofegiline. Surveying the 34 x-ray crystal structures of monoamine oxidase deposited in the RCSB protein database, there are no examples of inhibitors that modify an amino acid residue on MAO, which prompted additional interest in this inhibitor.

With access to purified recombinant human MAO A¹¹ and MAO B¹² as well as conditions for the crystallization of inhibitor-bound MAO B,¹³ we initiated a collaborative study to further define the molecular details for the inhibition of human MAO B with Mofegiline. A combination of solution and crystallographic

studies demonstrate that Mofegiline inhibits human MAO B *via* covalent flavin modification in a rapid and highly specific reaction.

4.1.2 Results and Discussion

4.1.2.1 Inhibition of Human MAO B with Mofegiline.

Incubation of purified human MAO B with Mofegiline leads to rapid and irreversible stoichiometric inhibition of catalytic activity. Reversible binding of Mofegiline to the catalytic site of MAO B prior to irreversible inactivation is shown from competitive inhibition experiments which show an apparent K_i of 28 nM (Figure 4.1.2); a value similar in magnitude to the IC_{50} value (3.6 nM) determined for membrane bound rat MAO B.⁴

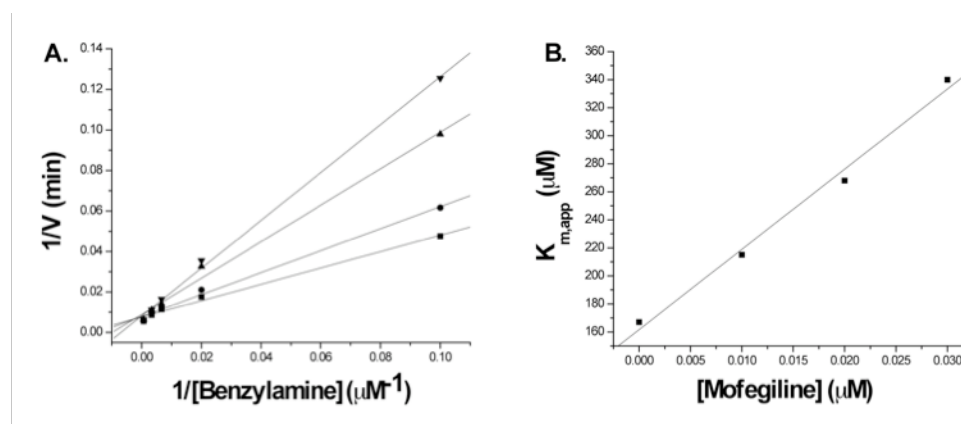


Figure 4.1.2. Mofegiline is a competitive inhibitor of human MAO-B. A. The activity of MAO-B was assayed at varied concentrations of benzylamine with a constant inhibitor concentration. B. The inhibitor concentration was plotted as a function of apparent K_m for the determination of the inhibition constant.

The data in Figure 4.1.3A show a linear loss of activity on titration of MAO B with sub-stoichiometric amounts of Mofegiline with complete inhibition observed at a stoichiometry of 1.0 mole Mofegiline/mole E-FAD. Inhibition occurs rapidly and is complete by the time an enzyme sample can be withdrawn and

assayed. Titration of enzyme samples with inactive protein in solution results in lower stoichiometries for complete inhibition demonstrating the requirement for functional enzyme involvement in the reaction.

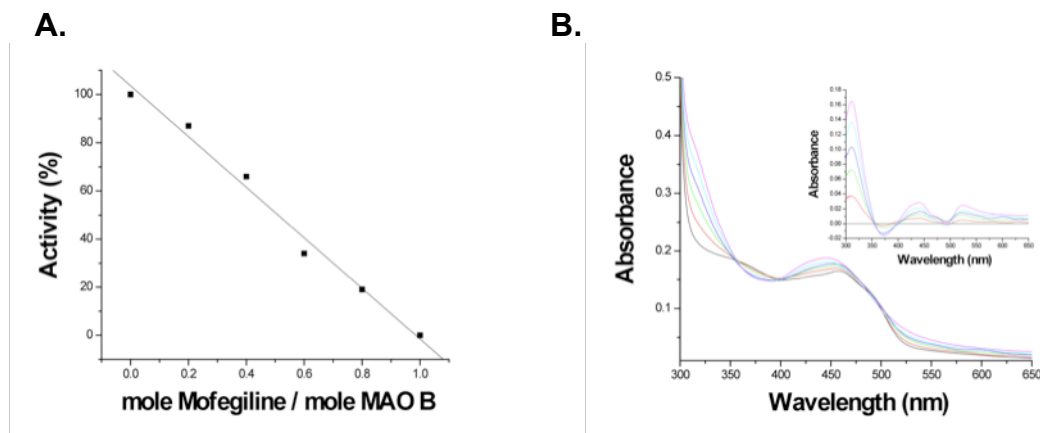


Figure 4.1.3. Titration of MAO B with substoichiometric levels of Mofegiline. A. The quantitative loss of activity of human MAO B with stoichiometric levels of Mofegiline. B. Effect of Mofegiline inhibition of MAO-B on the absorption spectra in the visible and near UV region due to the flavin: (—) 0.0, (—) 0.2, (—) 0.4, (—) 0.6, (—) 0.8, (—) 1.0 (mol Mofegiline/mol MAO-B). Inset. The difference absorption spectra observed on subtraction of the spectrum of uninhibited MAO-B from those observed during the titration: (—) 0.0, (—) 0.2, (—) 0.4, (—) 0.6, (—) 0.8, (—) 1.0 (mol Mofegiline/mol MAO-B).

Ion-selective electrode experiments show the release of one mole of fluoride ion per mole of MAO B inhibited which confirms that fluoride is eliminated during the inhibition reaction. When the visible absorption spectrum of the enzyme (due to the covalent FAD) is monitored during the titration, spectral perturbations are observed (Figure 4.1.3B); however, no “bleaching” of the oxidized flavin absorbance at 450 nm is observed as expected if either flavin N(5) or C(4a) adducts were formed. For comparison, the spectral data in Figure 4.1. 3 show spectral changes observed for phenethylhydrazine-inhibited MAO B (N(5) adduct, Figure 4.1.4A)¹⁴ and for tranylcypromine-inhibited MAO B (C(4a) adduct, Figure 4.1.4B).¹³ The flavin absorbance shifts in λ_{\max} from 455 nm to 445 nm on

mofegiline inhibition of MAO B along with a small increase in the molar extinction coefficient from $12,000 \text{ M}^{-1}\text{-cm}^{-1}$ to $12,900 \text{ M}^{-1}\text{-cm}^{-1}$ (Figure 4.1.3B). Difference spectral data (inset, Figure 4.1.3B) show maximal spectral changes on inhibition occur in the near UV region with a minimum at 370 nm, a maximum at 320 nm, and isosbestic points at 350 nm and 395 nm.

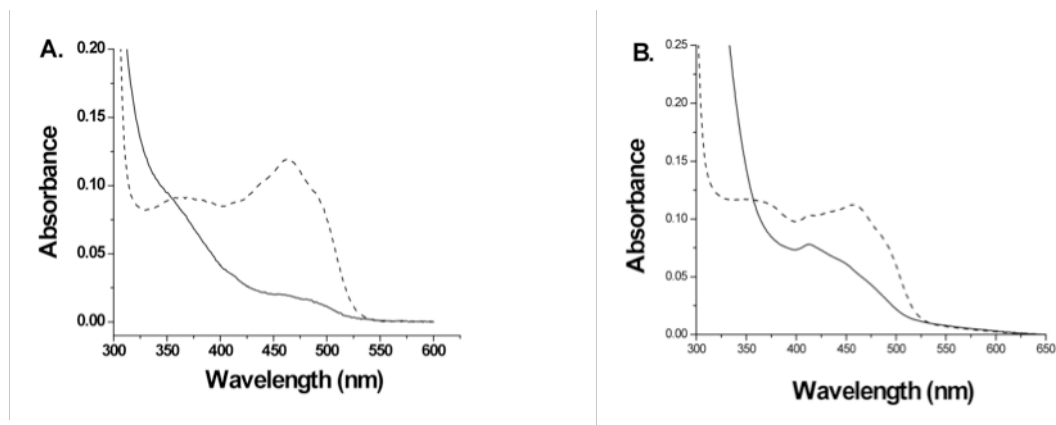


Figure 4.1.4. The visible and near UV absorption spectra of flavin N(5) and of flavin C(4a) adducts of MAO B. A. Oxidized MAO-B (---), After phenylethylhydrazine inhibition (N(5) flavin adduct) (—). B. Oxidized MAO-B (---), After tranylcypromine inhibition (C(4a) adduct) (—).

These spectral data suggest the inhibitor binds in the vicinity of the covalent FAD but do not suggest a covalent modification of the coenzyme. If that scenario were true, the FAD cofactor should be reactive to chemical reduction by sodium dithionite. The addition of excess dithionite to a sample of Mofegiline-inhibited MAO B shows no reduction of the flavin since no observable bleaching at 450 nm occurs. When dithionite is added to a sample of Mofegiline-inhibited MAO B complex in the presence of non-functional enzyme, only a partial bleaching of the 450 nm absorption occurs. These experiments show that the flavin coenzyme in Mofegiline-inhibited MAO B is resistant to chemical reduction

and that non-functional MAO B is unreactive with Mofegiline which further supports the conclusion that this compound is a mechanism-based inhibitor.

The visible CD spectrum of the Mofegiline-MAO B complex (Figure 4.1.5) differs from that of free enzyme with an intense negative dichroic band at 340 nm which is similar in both position and intensity with those CD spectra of MAO B inhibited by compounds forming covalent flavin N(5) adducts (Figure 4.1.5).

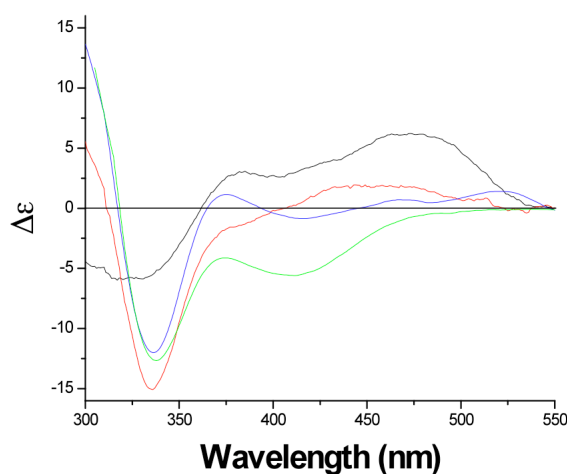


Figure 4.1.5. Circular dichroism spectra of oxidized human MAO-B, Mofegiline inhibited MAO-B, and of known MAO-B flavin N(5) adducts. Oxidized MAO-B (—), After inhibition by Mofegiline (—), the MAO-B N(5) flavin adduct formed after inhibition by pargyline (—), and the MAO-B N(5) flavin adduct formed after inhibition by phenylethyldiazine (—).

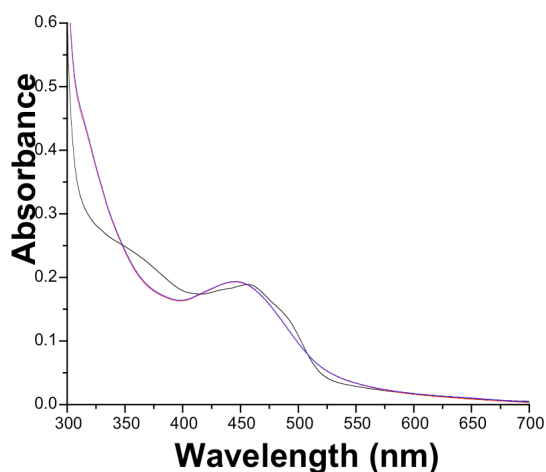


Figure 4.1.6. The visible and near UV absorption spectra observed after anaerobic inhibition of MAO B by Mofegiline. Oxidized MAO B (—), Mofegiline-MAO B adduct under argon (—), Mofegiline-MAO B adduct formed aerobically (—).

To determine whether catalytic turnover is involved in the inhibition reaction, the influence of oxygen in the inhibition process was examined. Inhibition reactions carried out in the presence of a coupled enzyme system that detects any H_2O_2 production (Amplex Red/Horseradish Peroxidase)¹⁵ show no detectable levels of H_2O_2 . The addition of Mofegiline to oxidized MAO B under anaerobic conditions results in complete inhibition of the enzyme with spectral properties (Figure 4.1.6) identical to that of found during aerobic inhibition of the enzyme. Assay of anaerobically-withdrawn samples show complete inhibition. Furthermore, no spectral changes are detected on exposure of anaerobic Mofegiline-inhibited MAO B to air. These experiments demonstrate that no catalytic turnover occurs during the inhibition. If Mofegiline is a mechanism-based inhibitor, inhibition occurs during a single turnover.

To probe whether reduced MAO B is subject to inhibition by Mofegiline, a sample of enzyme was reduced anaerobically with a stoichiometric amount of benzylamine. Mofegiline was then anaerobically added and the visible absorbance spectral properties of the enzyme followed. The data in Figure 4.1.7 show that the absorbance of the reduced enzyme increases on addition of Mofegiline to level only ~50 % of that observed with Mofegiline-inhibited MAO B formed under aerobic conditions. The anaerobic removal and assay of an aliquot of enzyme from this experiment exhibits no activity. Upon exposure to oxygen, the spectrum exhibits properties identical to aerobically inhibited MAO B. Attempts to determine the rate of MAO B flavin reduction by Mofegiline by

stopped flow experiments show the rate is too fast to measure and occurs within the 1-2 ms dead time of the instrument.

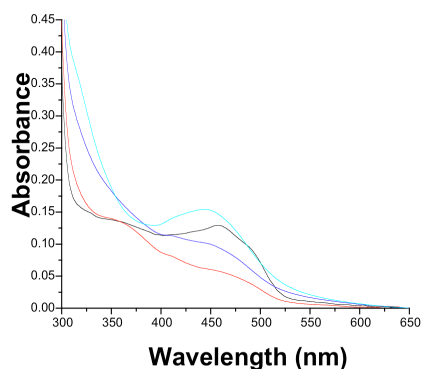


Figure 4.1.7. Absorption spectral changes in MAO B after anaerobic reduction with a stoichiometric amount of benzylamine followed by the anaerobic addition of 1.5 molar equivalents of Mofegiline. Exposure of the sample to oxygen results in additional spectral changes in the flavin absorption region to a spectrum that is identical to that observed with aerobically inhibited MAO B with Mofegiline. Absorption spectra of: Oxidized MAO B (—), Reduced MAO B (—), After the anaerobic addition of Mofegiline (—), Sample after exposure to air (—).

4.1.2.2 Structure of Mofegiline-Inhibited MAO B.

To provide conclusive evidence for suggested covalent modification of MAO B on inhibition by Mofegiline, the inhibited enzyme was crystallized and its

structure determined by x-ray crystallography. Crystals of Mofegiline-

inhibited MAO B diffract to 2.3 Å resolution.

The structure of the complex about the flavin active site is shown in Figure 4.1.8.

These structural data provide direct evidence that the inhibitor is bound to the enzyme as a flavin N(5) adduct.

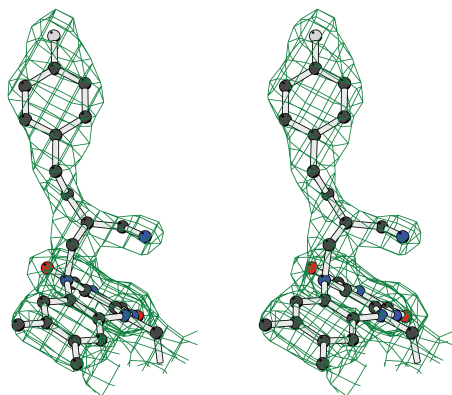


Figure 4.1.8. Structure of human MAO B in complex with the Mofegiline. Stereoview of the final 2Fo-Fc electron density map (contoured at 1.3 σ level). Carbons are in black, oxygen in red, nitrogen in blue, sulfurs in yellow, and fluorine in grey.

The inhibitor adopts an extended conformation spanning from the flavin ring to the entrance of the substrate cavity. The aromatic ring is located in the rear of the cavity and it is oriented perpendicular to the flavin ring as typically

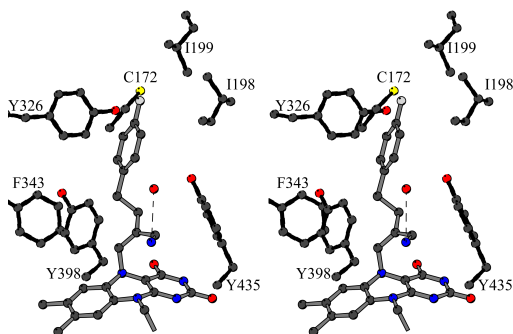


Figure 4.1.9. The binding mode of Mofegiline to the human MAO B active site. Atom colors are as in Figure 8A. The inhibitor covalent bonds are depicted in grey. The H-bond between the inhibitor nitrogen atom and a water molecule is outlined by a dashed line.

observed for most other MAO B-inhibitor complexes.¹³ Ile199 adopts a conformation in which its side chain is positioned in the “open” conformation resulting in the fusion of the entrance and substrate cavities (Figure 4.1.9). This

“open” conformation has been previously observed with other bulky inhibitors such as N-(2-aminoethyl)-4-chlorobenzamide and 1,4-diphenyl-2-butene, which also force the opening of the Ile199 gate.¹³ The bound Mofegiline participates in numerous hydrophobic and van der Waals interactions with active site side chains (Cys172, Ile198, Ile199, Phe343, Tyr326, Tyr398, and Tyr 435). The electron density clearly defines the positions of several ordered water molecules, one of which forms a H-bond interaction with the Mofegiline nitrogen atom. No extra electron density is found close to the covalent bond of the flavin N(5), which proves that the fluorine atom has been eliminated and supports the argument that the carbon (from Mofegiline) is sp^2 hybridized. The Mofegiline nitrogen atom, which we interpret as an imine group, lies in front of the flavin ring between side chains of Tyr398 and Tyr435 that form the catalytically important aromatic cage¹⁶ (Figure 4.1.9). These structural data support the idea that the aromatic cage can function as a recognition site for the substrate amine group.¹⁷

4.1.2.3 Mofegiline Interactions with Purified Human MAO A.

A similar series of experiments were performed using recombinant human MAO A to compare inhibition properties that might help explain why Mofegiline exhibits a marked specificity for MAO B. Mofegiline functions as a competitive inhibitor with MAO A with a measured K_i value ($1.1 \mu\text{M}$) ~40-fold weaker than that observed with MAO B (Figure 4.1.10). Dilution of the MAO A-inhibitor mixture shows return of catalytic activity demonstrating that no irreversible inhibition occurs. Like MAO B, inhibition reactions carried out in the presence of the Amplex Red/Horseradish Peroxidase coupled assay show no detectable levels of H_2O_2 produced; therefore, no catalytic oxidation of the amine moiety is observed for MAO A.

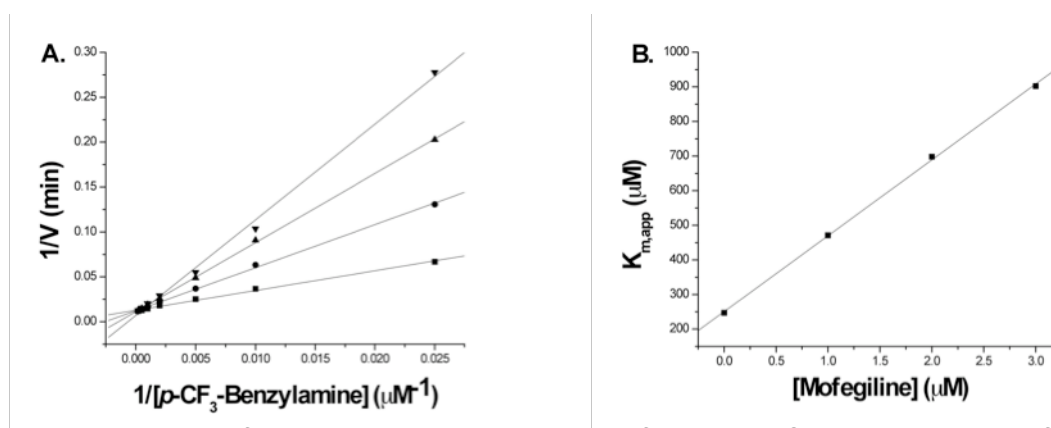


Figure 4.1.10. Mofegiline is a competitive inhibitor of human MAO A. A. The activity of MAO A was assayed at varied concentrations of *p*-CF₃-benzylamine with a constant inhibitor concentration. B. The inhibitor concentration was plotted as a function of apparent K_m for the determination of the inhibition constant.

Similarly, the anaerobic addition of Mofegiline to MAO A shows no evidence for enzyme flavin reduction even at high concentrations of inhibitor (Figure 4.1.11A). These experiments suggest the failure of MAO A to oxidize the amine moiety of Mofegiline may account for its resistance to inhibition. Anaerobic substrate reduction of MAO A followed by the addition of Mofegiline

does not result in any irreversible inhibition but does show modest spectral changes from 300-350 nm in the UV/Visible spectrum (Figure 4.1.11B). The CD spectrum of the Mofegiline-MAO A complex exhibits a mild perturbation of the flavin spectrum; however, the spectrum does not resemble those of MAO A flavin-N(5) adducts. These experiments demonstrate Mofegiline is a weaker, reversible MAO A inhibitor that is much more potent for MAO B. The structural basis for this difference in behavior of Mofegiline for the two isozymes for will be addressed in the discussion section.

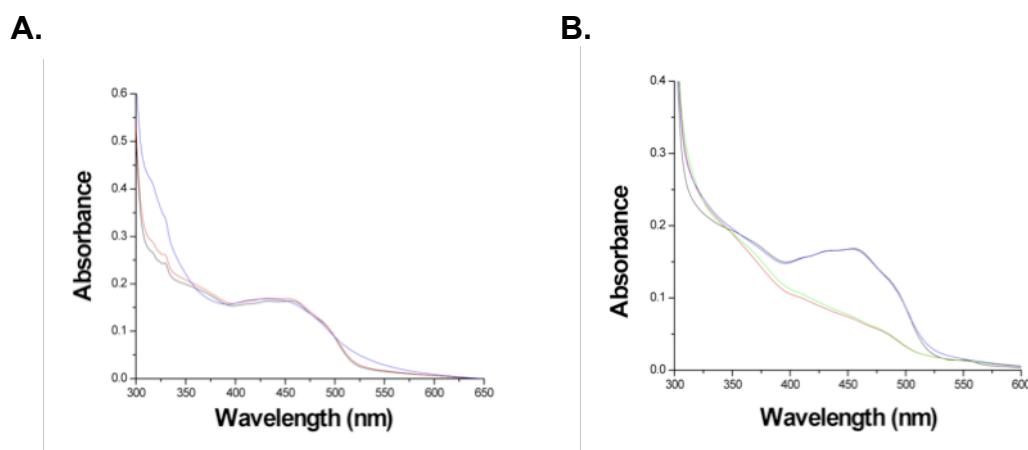
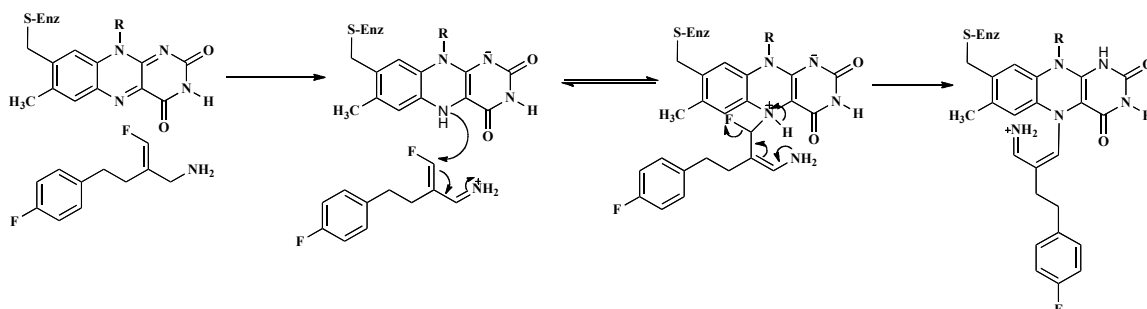


Figure 4.1.11. A. Spectral changes in the UV/Vis spectrum of human MAO A on anaerobic addition of a 10-fold molar excess of Mofegiline. Only small spectral changes in the flavin chromophore occur after incubation times of greater than 30 minutes. Absorption spectra of: Oxidized MAO A (—), After the anaerobic addition of Mofegiline (—), Mofegiline and MAO A incubated aerobically at 25 °C for 30 minutes (—). B. Absorption spectral changes on the anaerobic reduction of MAO A with a stoichiometric amount of *p*-trifluoromethylbenzylamine followed by the anaerobic addition of 10-fold excess Mofegiline (which does not result in any observed spectral changes). Exposure of the sample to oxygen shows re-oxidation of the flavin with minor changes in 300-350 nm region of the spectrum. Absorption spectra of: Oxidized MAO A (—), Reduced MAO A (—), After the anaerobic addition of Mofegiline (—), After exposure of the sample to O₂ (—).

4.1.2.4 Differential Inhibition Motifs of Mofegiline with MAO A and MAO B.

Model system studies have shown that reduced flavins are known to react with alkyl halides to form flavin N(5) adducts.¹⁸ Recent studies of the flavin

dependent isopentenyl pyrophosphate isomerase¹⁹ have shown that fluorinated substrate analogues react with the reduced flavin coenzyme to form flavin N(5) alkyl adducts with elimination of the fluorine atom as F⁻. With the knowledge of the behavior of these flavin alkylating systems, we suggest the initial step of the inhibition of MAO B by Mofegiline involves flavin reduction concurrent with amine oxidation to the imine. The imine intermediate then undergoes a Michael addition of the sp³ N(5) of the flavin hydroquinone. The instability of the enamine intermediate results in elimination of F⁻ to form the highly conjugated flavin N(5) adduct. (Scheme 4.1.3). This inhibition reaction is very rapid and occurs in a single catalytic turnover since no O₂ uptake or H₂O₂ production is observed during inhibition.



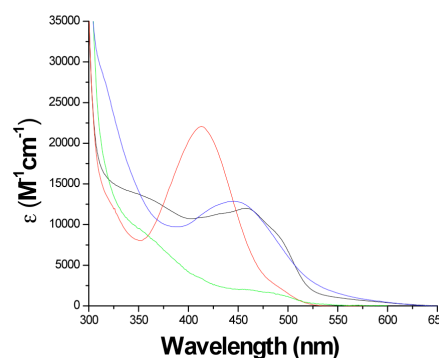
Scheme 4.1.3. Revised mechanism for the irreversible inhibition of MAO B by Mofegiline with N(5) flavin alkylation to produce a highly conjugated flavocyanine adduct.

Preliminary interpretations of the UV/Vis profile of the Mofegiline-MAO B complex suggest that the flavin absorption bands are perturbed on Mofegiline inhibition but that no covalent addition to the flavin moiety occurs. However, the x-ray crystal structure of the Mofegiline-MAO B complex with supporting CD data demonstrate that the flavin is indeed modified on Mofegiline inhibition but in a manner with both differences and similarities with flavin adducts involving alkylation at N(5) or C(4a). The data collected from the reaction of reduced MAO

B with Mofegiline (Figure 4.1.7) show that the initial adduct, while inactive, is not identical with the Mofegiline adduct formed on aerobic inhibition. The incomplete spectral changes may be indicative of flavin re-oxidation by reduction of the vinyl group of Mofegiline. The reduction of olefins by flavin containing enzymes has long been known.^{20, 21} The observed increase in the absorption spectrum upon exposure to oxygen reflects full oxidation of the enzyme followed by Mofegiline-adduct formation signaling the requirement for amine reduction to attain Mofegiline-MAO B adduct formation. These data provide additional support for the hypothesis that Mofegiline inhibition of MAO B involves flavin reduction as an initial chemical step.

One interesting aspect that deserves further study is the description of factors that give the N(5) alkylated flavin its absorption spectral properties that differ marginally from those of the oxidized form of the flavin and differ extensively from those exhibited by other N(5) or C(4a) flavin adducts. The most reasonable explanation is that the extensive conjugation of the N(5) alkyl group (including the vinyl double bond and the imine double bond) with the flavin ring is sufficient to permit the spectral transitions found in the 450 nm region. Addition of acetylenic inhibitors to the MAO B or MAO A flavins result in N(5) flavocyanine adducts with maximal absorption at 415 nm and an ϵ_M of 21, 000 $M^{-1}cm^{-1}$ reflecting their extended conjugation (Figure 4.1.12).²² Geometric differences between these two types of MAO B flavin N(5) adducts likely contribute to their observed spectral differences.

Unlike MAO B, Mofegiline is a reversible competitive inhibitor of MAO A and does not form a covalent adduct with the flavin. Addition of high concentrations of Mofegiline to MAO A results in only modest spectral changes in the 300-400 nm region of the flavin UV/Vis spectrum



and no reduction of the flavin upon extended incubation (Figure 4.1.11A). The CD spectral data do not support the formation of a flavin-N(5) adduct with MAO

Figure 4.1.12. Comparison of absorption spectral properties of MAO B and the flavin adducts of MAO B adducts with various inhibitors. Oxidized MAO B (—), Pargyline-inhibited MAO B (—), Phenylethylhydrazine-inhibited MAO B (—), and Mofegiline-inhibited MAO B (—).

A. An explanation for this differential behavior between MAO A and MAO B is found on comparison of their respective substrate specificities. Previous and current data show that 4-phenylbutylamine is a competitive inhibitor of human MAO A ($K_i = 31 \mu\text{M}$)²³ but is a substrate for human MAO B ($k_{\text{cat}} = 109 \pm 5 \text{ min}^{-1}$ and $K_m = 19 \pm 3 \mu\text{M}$; $k_{\text{cat}}/K_m = 5.8 \text{ min}^{-1}\mu\text{M}^{-1}$) (Figure 4.1.13). Mofegiline is a close structural analogue of 4-phenylbutylamine, and thus is poorly suited to function as a substrate for MAO A but does so for MAO B. These considerations further support the notion that amine oxidation is a requirement for irreversible inhibition of MAO B by Mofegiline. The Michael addition of nucleophiles to a conjugated Michael acceptor occurs much more rapidly than addition to an unconjugated vinyl group, supporting the requirement for amine oxidation to an imine for inactivation to occur. In addition, steric factors are likely involved in the non-reactivity of the amine moiety of Mofegiline for MAO A.

However, pre-reducing the flavin of MAO A with a stoichiometric amount of substrate does not influence its reactivity toward Mofegiline (Figure 4.1.11B).

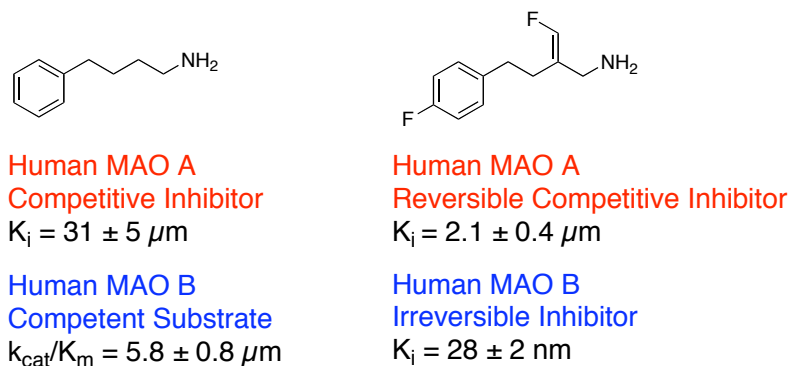


Figure 4.1.13. Comparison of the inhibitory properties of Mofegiline and 4-phenylbutylamine with human MAO A versus human MAO B.

4.1.3 Conclusions

Mofegiline is a highly selective, stoichiometric inhibitor of MAO B that forms an N(5) adduct with the covalent flavin coenzyme in a single catalytic turnover. X-ray structural data of the inhibited enzyme provide definitive evidence for the structure of the inhibited form. The conjugated iminium group is the site for nucleophilic attack by the N(5) of the reduced flavin which is followed by irreversible fluoride elimination. The resulting N(5) adduct is highly conjugated (Scheme 4.1.3) with spectral properties more like those of resting oxidized flavin or to N(5) flavocyanine adducts than to other N(5) or C(4a) alkyl flavins. The high level of Mofegiline selectivity towards MAO B is suggested to result from the nature of its alkyl side chain which is a feature that should be taken into consideration for the design of future MAO A or MAO B specific inhibitors.

4.1.4 Materials and Methods

Recombinant human liver MAO B and MAO A were expressed in *Pichia pastoris* and purified by published protocol.^{11, 12} Mofegiline was synthesized according to a published procedure.^{24, 25} Standard MAO A and MAO B activity assays were performed spectrophotometrically using *p*-trifluoromethylbenzylamine and benzylamine, respectively at 25 °C in a 50 mM phosphate buffer (pH 7.5) and 0.5% (w/v) RTX-100.

Competitive Inhibition Assays. K_i values for Mofegiline inhibition of MAO A and MAO B were determined by measuring the initial rates of substrate oxidation (six different concentrations) in the presence of varying concentrations of inhibitor (four different concentrations). All samples were incubated for 5 minutes at 25 °C prior to the addition of enzyme. K_i values were calculated by plotting the apparent K_m values for each Mofegiline concentration as a function of Mofegiline concentration.

Fluoride Electrode Experiment. A sample of human MAO B (10 μ M, 10 nmol) was desalted by gel filtration over a G-25 Sephadex column in 50 mM potassium phosphate buffer (pH 7.5), 0.8 % n-octyl- β -D-glucopyranoside, and 20% glycerol. The enzyme sample was inhibited with one equivalent of Mofegiline (2.3 μ g, 10 nmol), immediately filtered over a PM-10 filter, and subsequently adjusted with total ion strength adjustment buffer (TISAB III with CDTA) to balance the ion concentration. The filtrate was analyzed by an Accumet combination fluoride specific electrode. The released fluoride concentration was verified by the addition of an internal fluoride standard. A control sample of human MAO B in

the absence of Mofegiline was prepared by following the same experimental protocol.

Circular Dichroism Spectroscopy. An Aviv model 62DS circular dichroism spectrophotometer was utilized for the collection of the spectra reported. All spectra were collected from 550 nm to 300 nm with a 1 s dwell time in a 1 cm path length cell. Samples were analyzed in 3 mL quartz cells with concentrations ranging from 25 μ M to 40 μ M. A total of 5 repetitive scans were averaged, and the spectra were smoothed using an adjacent-point averaging function. All spectral data were acquired in 50 mM potassium phosphate, pH 7.5 containing 0.8% (w/v) β -D-octylglucoside.

Anaerobic UV/Vis Experiments. A Cary50 UV/Vis spectrophotometer was utilized for the collection of the spectra reported. All spectra were collected from 650 nm to 300 nm with a 1 cm path length quartz cuvette fitted to Schlenk glassware designed for anaerobic experiments with syringe injection ports for the addition of deoxygenated substrates (benzylamine and *p*-trifluoromethylbenzylamine for MAO B and MAO A, respectively).

Briefly, all solutions (enzyme, inhibitor, and substrate) were degassed six times and purged with argon gas. The enzyme solution was held under positive argon pressure while stoichiometric substrate was added for the reduction of the flavin. The spectral properties were recorded. Mofegiline was then added while the changes in absorption properties were noted. All spectral data were acquired in 50 mM potassium phosphate, pH 7.5 containing 0.8% (w/v) β -D-octylglucoside with MAO concentrations ranging from 10 μ M to 20 μ M.

Crystallographic methods. Crystallographic studies were performed as described by the Mattevi laboratory.¹³ Briefly, inhibited human MAO B in 50 mM potassium phosphate pH 7.5, 8.5 mM Zwittergent 3-12 was crystallized by mixing equal volumes of protein sample and reservoir solution (12% PEG4000, 100 mM ADA buffer pH 6.5, 70 mM Li₂SO₄). X-ray diffraction data were collected at 100 K at the beam-line ID14-EH2 of European Synchrotron Radiation Facility in Grenoble. Data processing and scaling were carried out using MOSFLM²⁶ and programs of the CCP4 package.²⁷ The coordinates of the MAO B-isatin complex¹³ were used as initial model after removal of all water and inhibitor atoms. Crystallographic refinements were performed with the programs REFMAC5²⁸ and Coot.²⁹

4.1.5 References

1. Rando, R. R.; Eigner, A., Pseudo-Irreversible Inhibition of Monoamine-Oxidase by Allylamine. *Mol. Pharma.* **1977**, 13, (6), 1005-1013.
2. Silverman, R. B.; Hiebert, C. K.; Vazquez, M. L., Inactivation of monoamine oxidase by allylamine does not result in flavin attachment. *J. Biol. Chem.* **1985**, 260, (27), 14648-52.
3. Palfreyman, M. G.; McDonald, I. A.; Bey, P.; Schechter, P. J.; Sjoerdsma, A., Design and early clinical evaluation of selective inhibitors of monoamine oxidase. *Prog. Neuropsychopharmacol Biol. Psychiatry* **1988**, 12, (6), 967-87.
4. Palfreyman, M. G.; Mcdonald, I. A.; Zreika, M.; Cremer, G.; Haegele, K. D.; Bey, P., Mdl-72,974a - a Selective Mao-B Inhibitor with Potential for Treatment of Parkinsons-Disease. *J. Neural Transm.-Gen. Sec.* **1993**, 101-111.

5. McDonald, I. A.; Lacoste, J. M.; Bey, P.; Wagner, J.; Zreika, M.; Palfreyman, M. G., Dual Enzyme-Activated Irreversible Inhibition of Monoamine-Oxidase. *Bioorg. Chem.* **1986**, 14, (2), 103-118.
6. McDonald, I. A.; Lacoste, J. M.; Bey, P.; Palfreyman, M. G.; Zreika, M., Enzyme-activated irreversible inhibitors of monoamine oxidase: phenylallylamine structure-activity relationships. *J. Med. Chem.* **1985**, 28, (2), 186-93.
7. Palfreyman, M. G.; McDonald, I. A.; Bey, P.; Danzin, C.; Zreika, M.; Cremer, G., Haloallylamine Inhibitors of Mao and Ssao and Their Therapeutic Potential. *J. Neural Transm.-Suppl.* **1994**, (41), 407-414.
8. Dow, J.; Piriou, F.; Wolf, E.; Dulery, B. D.; Haegele, K. D., Novel carbamate metabolites of mofegiline, a primary amine monoamine oxidase B inhibitor, in dogs and humans. *Drug Metab. Dispos.* **1994**, 22, (5), 738-49.
9. Van Houten, K. A.; Kim, J. M.; Bogdan, M. A.; Ferri, D. C.; Mariano, P. S., A new strategy for the design of monoamine oxidase inactivators. Exploratory studies with tertiary allylic and propargylic amino alcohols. *J. Am. Chem. Soc.* **1998**, 120, (24), 5864-5872.
10. Bach, A. W.; Lan, N. C.; Johnson, D. L.; Abell, C. W.; Bembenek, M. E.; Kwan, S. W.; Seeburg, P. H.; Shih, J. C., cDNA cloning of human liver monoamine oxidase A and B: molecular basis of differences in enzymatic properties. *Proc. Natl. Acad. Sci. U S A* **1988**, 85, (13), 4934-4938.
11. Li, M.; Hubalek, F.; Newton-Vinson, P.; Edmondson, D. E., High-level expression of human liver monoamine oxidase A in *Pichia pastoris*: comparison

with the enzyme expressed in *Saccharomyces cerevisiae*. *Prot. Expr. Purif.* **2002**, 24, (1), 152-62.

12. Newton-Vinson, P.; Hubalek, F.; Edmondson, D. E., High-level expression of human liver monoamine oxidase B in *Pichia pastoris*. *Prot. Expr. Purif.* **2000**, 20, (2), 334-45.

13. Binda, C.; Li, M.; Hubalek, F.; Restelli, N.; Edmondson, D. E.; Mattevi, A., Insights into the mode of inhibition of human mitochondrial monoamine oxidase B from high-resolution crystal structures. *Proc. Natl. Acad. Sci. U S A* **2003**, 100, (17), 9750-9755.

14. Binda, C.; Wang, J.; Li, M.; Hubalek, F.; Mattevi, A.; Edmondson, D. E., Structural and mechanistic studies of arylalkylhydrazine inhibition of human monoamine oxidases A and B. *Biochemistry* **2008**, 47, (20), 5616-5625.

15. Zhou, M.; Panchuk-Voloshina, N., A one-step fluorometric method for the continuous measurement of monoamine oxidase activity. *Anal. Biochemistry* **1997**, 253, (2), 169-74.

16. Li, M.; Binda, C.; Mattevi, A.; Edmondson, D. E., Functional role of the "aromatic cage" in human monoamine oxidase B: Structures and catalytic properties of Tyr435 mutant proteins. *Biochemistry* **2006**, 45, (15), 4775-4784.

17. Binda, C.; Newton-Vinson, P.; Hubalek, F.; Edmondson, D. E.; Mattevi, A., Structure of human monoamine oxidase B, a drug target for the treatment of neurological disorders. *Nat. Struct. Biol.* **2002**, 9, (1), 22-26.

18. Muller, F.; Hemmerich, P.; Ehrenberger, A.; Palmer, G.; Massey, V., Chemical and Electronic Structure of Neutral Flavin Radical as Revealed by Electron Spin

Resonance Spectroscopy of Chemically and Isotopically Substituted Derivatives. *Eur.J. Biochemistry* **1970**, 14, (1), 185-&.

19. Rothman, S. C.; Johnston, J. B.; Lee, S.; Walker, J. R.; Poulter, C. D., Type II isopentenyl diphosphate isomerase: Irreversible inactivation by covalent modification of flavin. *J. Am. Chem. Soc.* **2008**, 130, (14), 4906-4913.

20. Benson, T. E.; Marquardt, J. L.; Marquardt, A. C.; Etzkorn, F. A.; Walsh, C. T., Overexpression, Purification, and Mechanistic Study of Udp-N-Acetylenolpyruvylglucosamine Reductase. *Biochemistry* **1993**, 32, (8), 2024-2030.

21. Benson, T. E.; Walsh, C. T.; Massey, V., Kinetic characterization of wild-type and S229A mutant MurB: Evidence for the role of ser 229 as a general acid. *Biochemistry* **1997**, 36, (4), 796-805.

22. Hubalek, F.; Binda, C.; Li, M.; Herzig, Y.; Sterling, J.; Youdim, M. B.; Mattevi, A.; Edmondson, D. E., Inactivation of purified human recombinant monoamine oxidases A and B by rasagiline and its analogues. *J. Med. Chem.* **2004**, 47, (7), 1760-1766.

23. Nandigama, R. K.; Edmondson, D. E., Structure-activity relations in the oxidation of phenethylamine analogues by recombinant human liver monoamine oxidase A. *Biochemistry* **2000**, 39, (49), 15258-15265.

24. Evans, J. C.; Goralski, C. T.; Rand, C. L.; Vosejka, P. C. Preparation of (E)-1-amino-2-(fluoromethylene)-4-(p-fluorophenyl)butane. 94-315041 5488188, 19940929., 1996.

25. McDonald, I. A.; Bey, P.; Zreika, M.; Palfreyman, M. G., MDL 72,974A Monoamine Oxidase Type B inhibitor. *Drugs of the Future* **1991**, 16, (5), 428-431.
26. Leslie, A. G. W., Integration of macromolecular diffraction data. *Acta Crystallographica Sect. D-Biol. Crystall.* **1999**, 55, 1696-1702.
27. Bailey, S., The Ccp4 Suite - Programs for Protein Crystallography. *Acta Crystallographica Sect. D-Biol. Crystall.* **1994**, 50, 760-763.
28. Murshudov, G. N.; Vagin, A. A.; Dodson, E. J., Refinement of macromolecular structures by the maximum-likelihood method. *Acta Crystallographica Sect. D-Biol. Crystall.* **1997**, 53, 240-255.
29. Emsley, P.; Cowtan, K., Coot: model-building tools for molecular graphics. *Acta Crystallographica Sect. D-Biol. Crystall.* **2004**, 60, 2126-2132.

Chapter 4.2 Development of Inhibitors that Bridge Both Active Site Cavities

4.2.1 Inhibitors that Bridge Both Cavities of MAO B: Styrylisatin Analogues

Elucidation of the high resolution crystal structure of MAO B revealed inhibitor selectivity of the MAO B isozyme is enhanced by increasing enzyme-inhibitor interactions through the design of ligands that bridge both the entrance and substrate cavity.¹⁻³ There are a number of examples of MAO inhibitors in the literature which demonstrate increased affinity upon binding to MAO versus MAO A based on the inhibitor bridging both the entrance cavity and the substrate cavity. Figure 4.2.1 shows examples of the dual cavity binding motif of 1,4-diphenyl-2-butene,⁴ farnesol,² and safinamide⁵ which bind only to MAO B and not to MAO A.

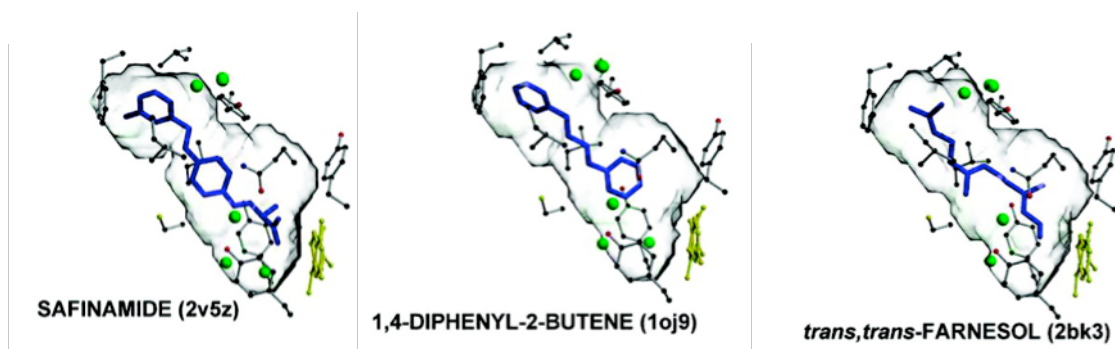


Figure 4.2.1. X-ray crystal structures of MAO B in complex with inhibitors that bridge both the entrance and substrate cavities. The pdb codes are listed in parenthesis.

Another example of such a phenomenon is observed in the case of 8-(3-chlorostyryl)caffeine (CSC). Caffeine is a very poor, reversible inhibitor of MAO A and MAO B ($K_i \sim 4$ mM), which shows no preference for either isozyme. Functionalization of caffeine with the styryl moiety in the 8-position to form CSC results in a loss of binding to MAO A (Figure 4.2.2) and very tight binding to the MAO B isoform (K_i of CSC = 200 nM).²

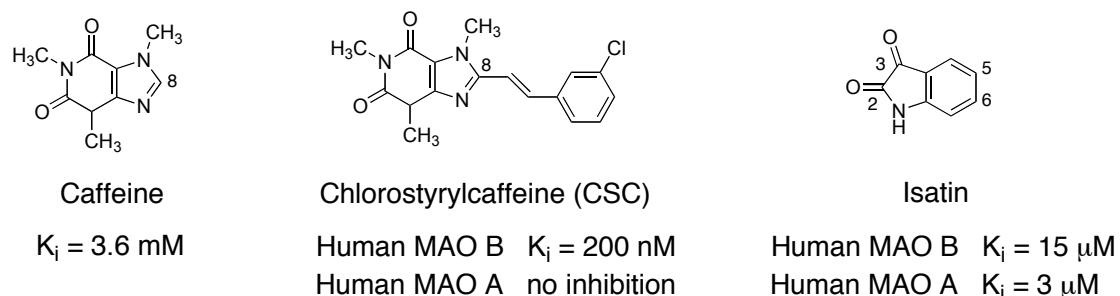
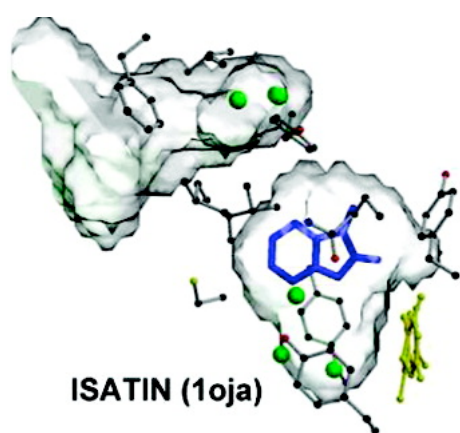


Figure 4.2.2. Structures and numbering system for MAO inhibitors, caffeine, CSC, and isatin.

Isatin is a small reversible, non-specific inhibitor of MAO, which was chosen for this study due to the tighter binding of isatin to MAO versus caffeine ($K_i = 3 \text{ }\mu\text{M}$, MAO B and $K_i = 15 \text{ }\mu\text{M}$, MAO A).² Isatin binds only in the substrate cavity of MAO B leaving the entrance cavity unoccupied (Figure 4.2.3). X-ray crystallographic characterization of MAO B in complex with isatin confirms that isatin binds to the substrate cavity of MAO B with the dioxindolyl carbonyls in the 2- and 3-positions facing the flavin cofactor while the C-5 is directed toward the entrance cavity. Therefore, it is reasonable to assume that functionalization of the 5- and even the 6-position would allow the styryl group to occupy that entrance cavity. Since the inhibitor potency of caffeine to MAO B is increased



45,000-fold upon functionalizing with a styryl moiety, four styrylisatin analogue were designed and synthesized in collaboration with the Petzer laboratory and their inhibitory properties were studied.⁶

Figure 4.2.3. X-ray crystal structure of human MAO B in complex with the small molecule inhibitor, isatin. The pdb code for this structure is listed in parenthesis.

4.2.2 Results and Discussion

4.2.2.1 Design of inhibitor compounds.

Adding the styryl moiety to isatin was hypothesized to promote binding affinity by forcing the ligand to bind to both the entrance cavity and the substrate cavity thereby increasing the number of interactions between the inhibitor and the enzyme active site. It was also thought that this functionalization would provide an inhibitor that is MAO B specific as is CSC. With a platform for the design of styryl-substituted isatin analogues, a series of molecular model experiments were performed to predict the binding affinity of the proposed inhibitors. These studies were carried out using the crystallographic structure of Safinamide in complex with MAO B (2V5Z.pdb) as a model. Safinamide is a reversible MAO B specific inhibitor that occupies both the entrance cavity and the substrate cavity of the enzyme where the side chain of the Ile199 residue rotates into an open conformation to allow for fusion of both cavities to accommodate the Safinamide molecule.⁵ The Autodocking experiments were performed using the LigandFit application of Discovery Studio 1.7 as previously outlined.⁷ These calculations suggest that 5-styrylisatin analogues would be favored by the MAO B active site due to the shape of the active site in accommodating the aromatic ring of the styryl-moiety (Figure 4.2.4).

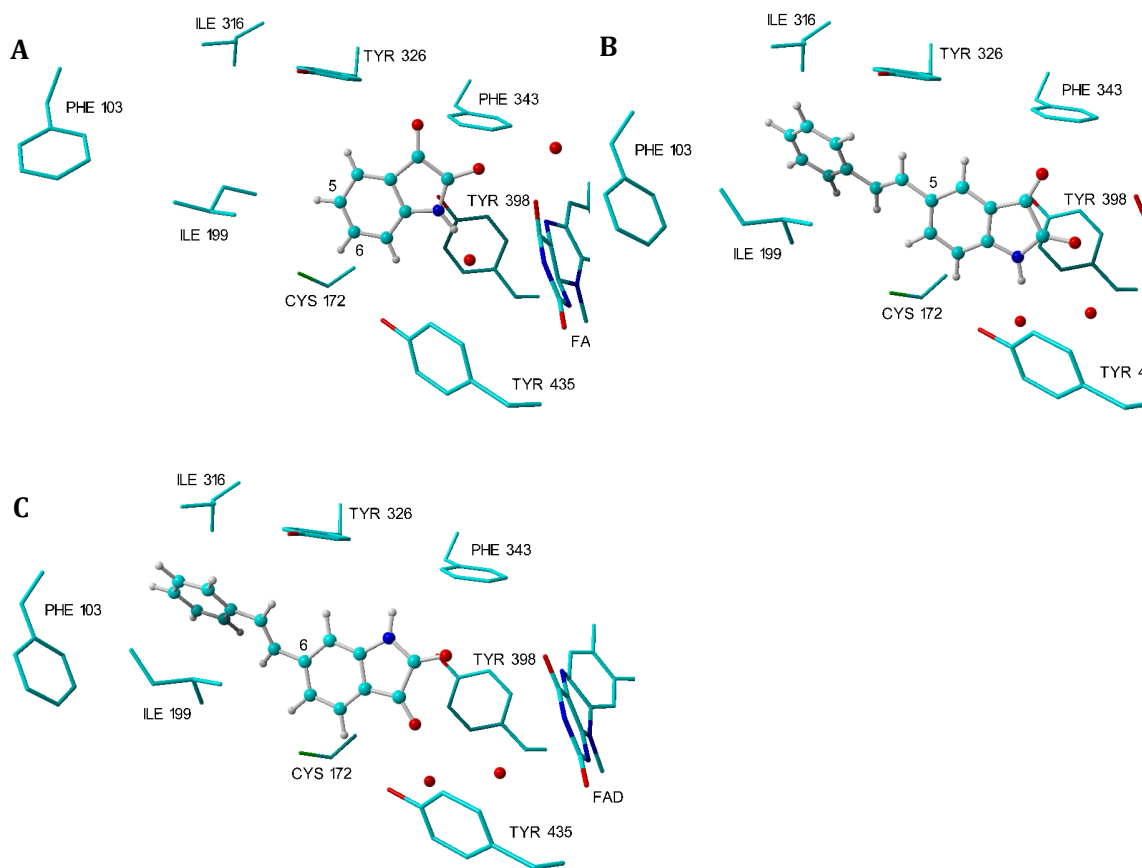


Figure 4.2.4. Binding modes determined by Autodocking calculations of isatin and isatin-functionalized with a styryl side chain in the MAO B active site. The coordinates of MAO B in complex with Safinamide (2V5Z.pdb) was selected for this cadre of experiments. A. Binding mode of isatin. B. Binding mode of 5-styrylisatin. C. Binding mode of 6-styrylisatin.

The docking experiments show that the binding mode of the dioxindolyl ring is oriented in a similar fashion to the isatin x-ray crystal structure with the amide nitrogen H-bonded to a water molecule in the active site (Compare Figure 4.2.3 and 4.2.4A-C). In the case of 6-styrylisatin, the dioxindolyl is rotated $\sim 180^\circ$ to allow the C-6 styryl-side chain to extend into the entrance cavity (Figure 4.2.4C). In both the C-5 and C-6 substituted isatins, the styryl-moiety is oriented into the entrance cavity with the Ile199 side chain rotated into an open conformation.

To provide insights into the anticipated selectivity of the styrylisatin analogues, a series of docking experiments were performed with MAO A as well. Given that CSC does not bind to MAO A, we expected the styrylisatins would not bind to the MAO A isozyme. Using the crystallographic structure of MAO A in complex with the reversible inhibitor harmine (2Z5X.pdb)⁸ molecular docking of 5-styrylisatin and 6-styrylisatin to MAO A was carried out using the protocol described previously.⁷ The top-ranked docking solutions reveal that 5-styrylisatin is accommodated best by the MAO A isozyme with the dioxindolyl ring positioned close to the FAD cofactor (Figure 4.2.5). Interestingly, these docking results mirror those of MAO B with the dioxindolyl ring rotated 180° from that of the free isatin structure when functionalized by the styryl side chain at the C-6 position.

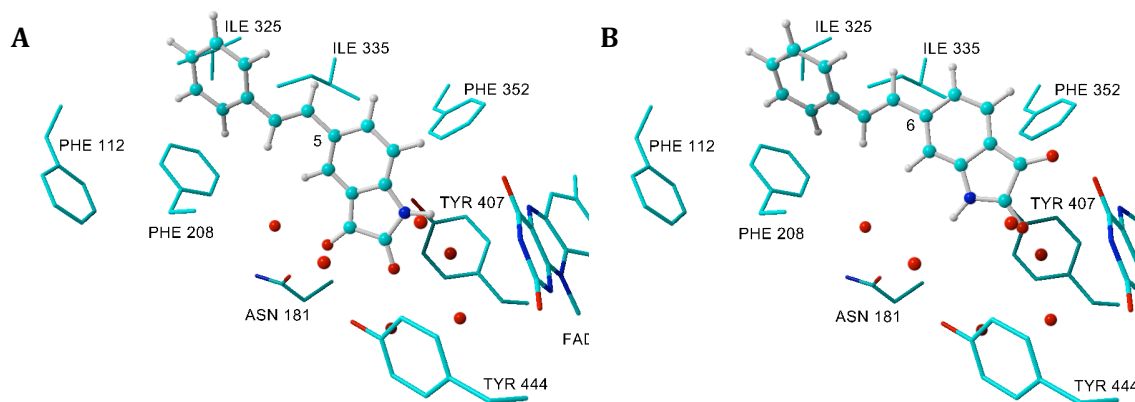


Figure 4.2.5. The docking solutions obtained with LigandFit for the binding of: A. 5-styrylisatin, and B. 6-styrylisatin in the active site of MAO-A (2Z5X.pdb).

4.2.2.2 Biological Evaluation of Styrylisatin Analogues.

With the molecular modeling studies in mind, a series of four styrylisatin analogues were synthesized by the Petzer laboratory and subjected to biological

testing (Figure 4.2.6). These compounds showed low stability in both organic solvent and water due to the dioxindolyl ring being susceptible to hydrolysis. To prevent erroneous results due to degradation of the compounds, all of the compounds were tested in the same day that they were taken into solution (Table 4.2.1).

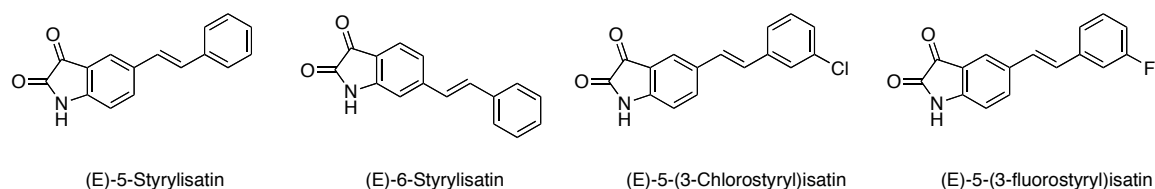
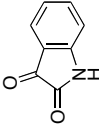
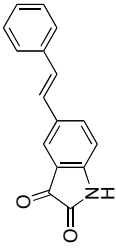
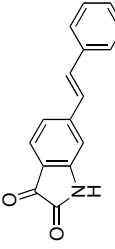
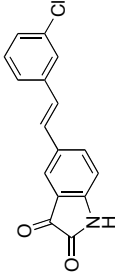
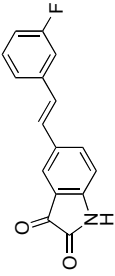


Figure 4.2.6. Structures of the styrylisatin analogues selected for the inhibition study.

To determine the mode of inhibition, time dependent inactivation studies were performed using MAO A, MAO B, and MAO B Ile199Ala. Upon dilution of the inhibitor-enzyme complex, full activity of the enzyme was observed confirming that these are reversible inhibitors. Furthermore, the absorption properties of the FAD cofactor of MAO were unchanged ($\lambda_{450\text{nm}}$) upon addition of the styrylisatin analogues, which suggests no covalent modification of the flavin.

Competition experiments were carried out to determine the K_i values of the styrylisatin analogues with MAO A and MAO B. All of the compounds in Figure 4.2.6 are competitive reversible inhibitors of MAO with varying binding affinities based on the enzyme surveyed. Lineweaver-Burk plots of the styrylisatin analogues are consistent with competitive inhibition (Figure 4.2.7-4.2.10).

Table 4.2.1. Inhibitory properties of isatin and styrylisatin analogues with MAO.

Entry	Inhibitor	Hwt MAO A (μM) ^a	Hwt MAO B (μM) ^b	MAO B 1199A (μM) ^a	Selectivity
1	 Isatin	15 ^c	3 ^c	12 \pm 2	No selectivity for either isozyme
2	 (E)-5-Styrylisatin	1.07 \pm 0.05	0.305 \pm 0.03	3.4 \pm 0.7	4 fold selective for MAO B
3	 (E)-6-Styrylisatin	35 \pm 4	0.78 \pm 0.06	3.4 \pm 0.6	45 fold selective for MAO B
4	 (E)-5-(3-Chlorostyryl)isatin	7.1 \pm 0.5	2.0 \pm 0.2	13 \pm 2	4 fold selective for MAO B
5	 (E)-5-(3-fluorostyryl)isatin	2.6 \pm 0.1	0.6 \pm 0.1	7 \pm 1	4 fold selective for MAO B

^a The K_i values were determined spectrophotometrically using *p*-trifluoromethylbenzylamine as a substrate.

^b The K_i values were determined spectrophotometrically using benzylamine as a substrate.

^c Values were obtained from published study on the inhibitor properties of isatin with purified recombinant human MAO A and MAO B.²

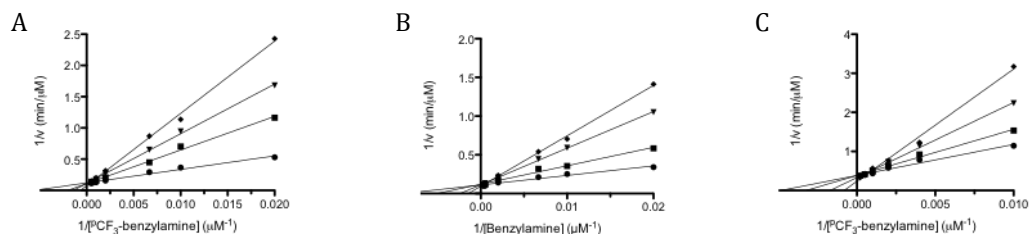


Figure 4.2.7. Lineweaver-Burk plots of: A. Hwt MAO A, B. Hwt MAO B, C. MAO B Ile199Ala with varied concentrations of (E)-5-styrlisatin in competition with substrate.

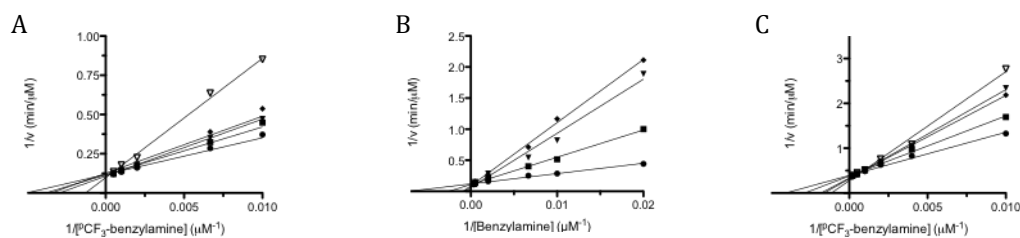


Figure 4.2.8. Lineweaver-Burk plots of: A. Hwt MAO A, B. Hwt MAO B, C. MAO B Ile199Ala with varied concentrations of (E)-5-(3-chlorostyryl)isatin in competition with substrate.

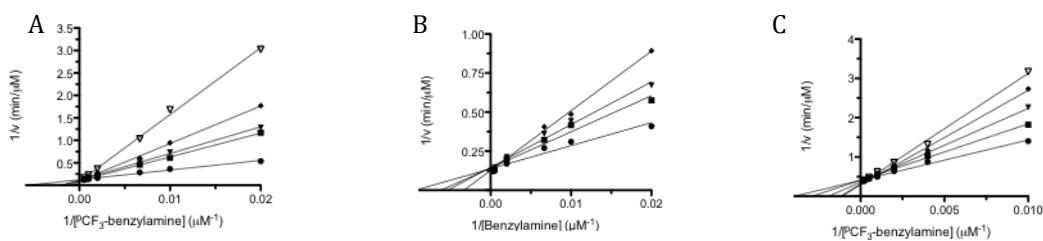


Figure 4.2.9. Lineweaver-Burk plots of: A. Hwt MAO A, B. Hwt MAO B, C. MAO B Ile199Ala with varied concentrations of (E)-5-(3-fluorostyryl)isatin in competition with substrate.

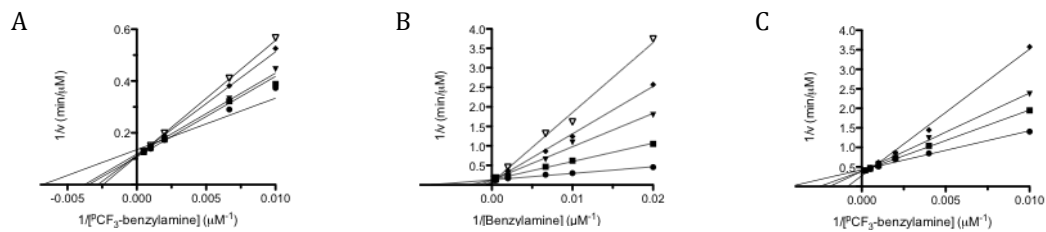


Figure 4.2.10. Lineweaver-Burk plots of: A. Hwt MAO A, B. Hwt MAO B, C. MAO B Ile199Ala with varied concentrations of (E)-6-Styrlisatin in competition with substrate.

Styrylisatin analogues substituted at the C-5 position of the dioxoindolyl ring bind to MAO with high nanomolar to low micromolar affinities (Table 4.2.1, entries 2, 4, and 5). (*E*)-5-Styrylisatin exhibits the highest affinity for MAO B ($K_i = 305 \pm 30$ nM) but exhibits poor selectivity for MAO B versus MAO A. The C-5 substituted styrylisatin analogues bind to MAO A with only 4-fold lower selectivity with respect to the MAO B isozyme. Substitution at the C-6 position of the dioxoindolyl ring results in marked selectivity for MAO B. Surprisingly, (*E*)-6-styrylisatin (Table 4.2.1, entry 3) binds to MAO B with nanomolar affinity ($K_i = 780 \pm 60$ nM) while exhibiting poor affinity for MAO A. The differential affinity of this inhibitor for either isozyme lends to 45-fold selectivity of (*E*)-6-styrylisatin for MAO B.

The Ile199 side chain is in a required “open” conformation with large inhibitors and is “closed” with smaller inhibitors. To probe the function of this gating residue, the Ile199Ala mutant form of MAO B was constructed, expressed in *Pichia pastoris*, and purified. The Ile199Ala mutant exhibits increased K_i values (4 to 12-fold increase in K_i , Table 4.2.1) with assayed with the styrylisatin analogues listed in Figure 4.2.6. This observation further illustrates the importance of the Ile199 “gate” in inhibitor recognition.

4.2.2.3 Importance of Planarity in Designing MAO B Specific Inhibitors.

To our surprise the styrylisatin analogues exhibit only modest selectivity for the MAO B isoform (4 to 45-fold selectivity for MAO B) unlike the inhibitor, CSC which shows no observable binding to MAO A. To better understand this

difference, the structures of (E)-5-styrylisatin, (E)-6-styrylisatin, and CSC were compared after energy minimization in Chem3-D (Figure 4.2.11). The most striking difference in this analysis is that the caffeine ring and the styryl side chain are coplanar in the case of CSC while the styrylisatin analogues show the isatin ring rotated at a 90° angle to the styryl-moiety. The narrow active site of MAO B favors planar aryl-inhibitors unlike MAO A due to the larger side of the active site. Therefore, geometric considerations are as vital as chemical functionality when designing novel, selective MAO inhibitors.

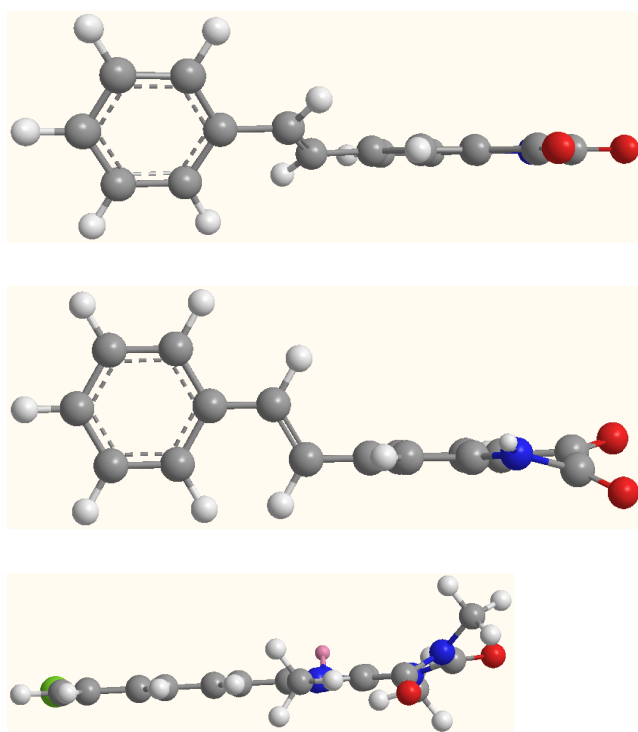


Figure 4.2.11. Energy-minimized structures of 5-styrylisatin (top), 6-styrylisatin (middle), and CSC (bottom). The energy-minimized conformations were constructed using Chem-3D (CambridgeSoft). Oxygen atoms are in red, nitrogen atoms in blue, and chlorine atoms in green. The isatin or caffeine rings are perpendicular to the plane of the page.

4.2.3 Conclusions

The (E)-5-styrylisatin and (E)-6-styrylisatin analogues are a promising new class of ligands for MAO B and of MAO A. The findings of this study support the hypothesis that the inhibition potencies of small molecule inhibitors may be improved by substitution with side chains that promote binding to both the entrance and substrate cavities of MAO B. The surprising finding that (E)-styrylisatins are also competitive inhibitors of MAO A, in contrast to results with CSC, show that consideration of the relative geometries are important factors in the design of MAO inhibitors.

4.2.4 Materials and Methods

Recombinant human liver MAO B and MAO A were expressed in *Pichia pastoris* and purified by published protocols.^{9, 10} The construction, expression and purification of MAO B Ile199Ala is discussed in detail in Chapter 5. Synthesis of the styrylisatin analogues in Figure 4.2.6 was carried out by the Petzer laboratory at North-west University in South Africa. Modeling studies of the binding of the styrylisatin analogues was also carried out by the Petzer laboratory. Energy minimization of the styrylisatins and CSC was performed using Chem3-D version 12.0 (CambridgeSoft).

Competitive Inhibition Assays. K_i values for styrylisatin analogue inhibition of MAO A, MAO B, and MAO B Ile199Ala were determined by measuring the initial rates of substrate oxidation (six different concentrations) in the presence of varying concentrations of inhibitor (four different concentrations). All samples were incubated for 5 minutes at 25 °C prior to the addition of enzyme. Binding

constants were determined using global fit analysis of the hyperbolic fit of enzyme activity upon varied concentrations of inhibitor using the Graphpad Prism data analysis software. Standard MAO A and MAO B activity assays were performed spectrophotometrically using *p*-trifluoromethylbenzylamine and benzylamine, respectively at 25 °C in a 50 mM phosphate buffer (pH 7.5) and 0.5% (w/v) RTX-100. The Ile199Ala mutant form was assayed using *p*-trifluoromethylbenzylamine as a substrate in the buffer conditions described above.

4.2.5 References

1. Vlok, N.; Malan, S. F.; Castagnoli, N., Jr.; Bergh, J. J.; Petzer, J. P., Inhibition of monoamine oxidase B by analogues of the adenosine A2A receptor antagonist (E)-8-(3-chlorostyryl)caffeine (CSC). *Bioorg. Med. Chem.* **2006**, 14, (10), 3512-21.
2. Hubalek, F.; Binda, C.; Khalil, A.; Li, M.; Mattevi, A.; Castagnoli, N.; Edmondson, D. E., Demonstration of isoleucine 199 as a structural determinant for the selective inhibition of human monoamine oxidase B by specific reversible inhibitors. *J. Biol. Chem.* **2005**, 280, (16), 15761-15766.
3. van den Berg, D.; Zoellner, K. R.; Ogunrombi, M. O.; Malan, S. F.; Terre'Blanche, G.; Castagnoli, N., Jr.; Bergh, J. J.; Petzer, J. P., Inhibition of monoamine oxidase B by selected benzimidazole and caffeine analogues. *Bioorg. Med. Chem.* **2007**, 15, (11), 3692-702.
4. Binda, C.; Li, M.; Hubalek, F.; Restelli, N.; Edmondson, D. E.; Mattevi, A., Insights into the mode of inhibition of human mitochondrial monoamine oxidase B

from high-resolution crystal structures. *Proc. Natl. Acad. Sci. U S A* **2003**, 100, (17), 9750-9755.

5. Binda, C.; Wang, J.; Pisani, L.; Caccia, C.; Carotti, A.; Salvati, P.; Edmondson, D. E.; Mattevi, A., Structures of human monoamine oxidase B complexes with selective noncovalent inhibitors: Safinamide and coumarin analogs. *J. Med. Chem.* **2007**, 50, (23), 5848-5852.

6. Van der Walt, E. M.; Milczek, E. M.; Malan, S. F.; Edmondson, D. E.; Castagnoli, N., Jr.; Bergh, J. J.; Petzer, J. P., Inhibition of monoamine oxidase by (E)-styrylisatin analogues. *Bioorg. Med. Chem. Lett.* **2009**, 19, (9), 2509-2513.

7. Ogunrombi, M. O.; Malan, S. F.; Terre'blanche, G.; Castagnoli, N., Jr.; Bergh, J. J.; Petzer, J. P., Structure-activity relationships in the inhibition of monoamine oxidase B by 1-methyl-3-phenylpyrroles. *Bioorg. Med. Chem.* **2008**, 16, (5), 2463-72.

8. Son, S. Y.; Ma, J.; Kondou, Y.; Yoshimura, M.; Yamashita, E.; Tsukihara, T., Structure of human monoamine oxidase A at 2.2-angstrom resolution: the control of opening the entry for substrates/inhibitors. *Proc. Natl. Acad. Sci. U S A* **2008**, 105, (15), 5739-5744.

9. Newton-Vinson, P.; Hubalek, F.; Edmondson, D. E., High-level expression of human liver monoamine oxidase B in *Pichia pastoris*. *Prot. Expr. Purif.* **2000**, 20, (2), 334-45.

10. Li, M.; Hubalek, F.; Newton-Vinson, P.; Edmondson, D. E., High-level expression of human liver monoamine oxidase A in *Pichia pastoris*: comparison

with the enzyme expressed in *Saccharomyces cerevisiae*. *Prot. Expr. Purif.* **2002**, 24, (1), 152-62.

4.3 Targeting the Entrance cavity of MAO B as a Novel Site for Inhibition: Elucidation of the Imidazoline Binding Site.

4.3.1 History of Imidazoline Ligands and MAO.

Imidazoline ligands are antihypertensive agents that are prescribed for the treatment of high blood pressure. This class of ligands is characterized by their imidazole ring, which is functionalized in the 2-position to produce a large library of biologically active analogues (Figure 4.3.1). Additional ligands that can bind to imidazoline binding sites (IBS) have the guanidine functionality. One of the most well known and prescribed of these compounds is clonidine which has been shown to bind to α_2 -adrenoreceptors (α -AR). Prior to Bousquet's discovery of multiple IBS¹, the α -AR were given sole credit for the antihypertensive effects of the imidazoline ligands; however the receptor(s) responsible for the antihypertensive properties of imidazolines is a point under much debate due to the lack of information available the IBS. To date three IBS (I₁, I₂, and I₃) have been observed; although, their identities remain a point of controversy.²

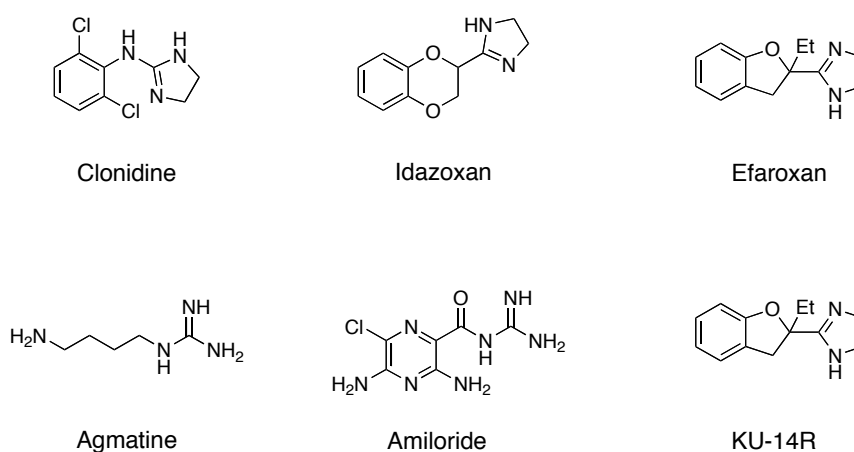


Figure 4.3.1. The structures of common imidazoline ligands

4.3.1.1 Classification of IBS: I_1 -, I_2 - and I_3 -Sites.

The distinctions for the 3 subtypes of IBS are based on their relative affinities to imidazoline ligands. I_1 sites are characterized by their preference for 2-aminoimidazolines, like clonidine, and are found in the brain stem.¹ It is generally accepted that I_1 -IBS is a G-protein coupled receptor which is ~43 kDa in size.³ Although additional IBS have been identified, the I_1 -IBS is the most widely attributed to the control of systemic blood pressure. Far less is known about I_3 -IBS which are located in pancreatic β -cells and modulate insulin secretion⁴. These sites preferentially bind efaroxan (agonist)⁵ and KU14R (antagonist)⁶ (Figure 4.3.1).

4.3.1.2 Elucidation of the I_2 -IBS.

Considerable literature has been published surrounding the I_2 -IBS. This receptor has puzzled the imidazoline community for some time due to conflicting reports on their properties in the literature. The I_2 -IBS preferentially bind idazoxan and interact with 2-aminoimidazolines with lower affinity. These sites are located in the brain as well as the liver and has been shown to modulate amine turnover.⁷ More detailed studies have shown that I_2 -IBS are localize to the outer membrane of the mitochondria of peripheral and central tissues.^{8, 9} The I_2 -IBS can be subcategorized by its affinity for the guanidine diuretic, amiloride. These subtypes are referred to as I_{2a} (amiloride sensitive) and I_{2b} (amiloride insensitive). While the pharmacological role of the I_2 -IBS has not been identified, a number of behavioral alteration and clinical disorders have been associated

with changes in available I₂-IBS. These disorders include tolerance or dependence on opioids;¹⁰ neurodegenerative disorders;^{11, 12} major depression;¹³ and alterations in eating behavior in rats.¹⁴ Based on available data regarding the pharmacological profiles and tissue distribution of I₂-IBS, it is widely accepted that monoamine oxidase (MAO) possesses an I₂ site.

Discrepancies in both tissue distribution¹⁵ and quantification of sites¹⁶ with regard to MAO possessing an I₂ sites has resulted in proposal that more than one protein could possess an I₂ binding site. Some sources have identified MAO as the sole I₂ site,^{17, 18} while others have suggested that creatine kinase may possess an I₂ site.¹⁹ There are several reports that suggest that not all of the I₂ sites can be attributed to MAO alone.^{2,18-20} There are a number of reviews published describing the location of IBS receptors,²⁰⁻²² the pharmacology of these sites,^{23, 24} and medicinal chemistry of imidazoline ligands;² however, to date there is no structural evidence available for the I₂-IBS.

Because no structural data are available for I₂-IBS (the receptors have not been cloned), a number of highly specific I₂-IBS ligands have been developed to further probe and characterize the I₂-site (Figure 4.3.2). The most notable of these ligands are ¹²⁵I-iodoazidophenoxymethylimidazoline (¹²⁵I-AZIPI, photoaffinity label), 2-(4,5-dihydroimidazol-2-yl)-quinoline (BU224), 4-chloro-2-(imidazoline-2-yl)isoindoline (RS45041), and 2-(2-benzofuranyl)-2-imidazoline (2-BFI).²⁵⁻²⁷ These ligands exhibit little or no binding to I₁-IBS or α₂-ARs. Additionally I₂-specific IBS ligands can be categorized into four chemical families: 2-imidazolines, guanidines, 2-aminoimidazolines and carbolines.² By far the

most studied of these ligands is 2-BFI. The frequency of 2-BFI studies is due to the availability of the radiolabeled form ($[^3\text{H}]2\text{-BFI}$) and its high level of selectivity for I_2 -IBS (both I_{2a} - and I_{2b} -IBS) over I_1 -IBS.²⁸

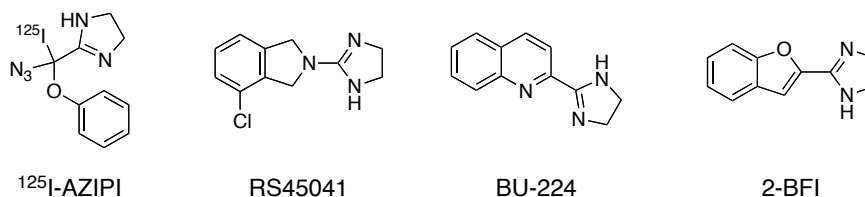


Figure 4.3.2. Structures of I_2 specific ligands.

4.3.1.3 Evidence for MAO B as I_2 -IBS.

Compelling evidence supports the suggestion that MAO is the I_2 -IBS. In particular, I_2 -IBS have a molecular weight of ~60 kDa and these sites co-express with MAO in MAO transfected yeast.²⁰ Furthermore, purified, photoaffinity labeled I_2 receptors from human placenta and liver tissue demonstrate molecular weights and amino acid sequencing consistent with both isoforms of MAO.¹⁷ Autoradiographical labeling of I_2 -IBS in rat brain is consistent with the distribution of both MAO A and MAO B further giving credence to the assertion that I_2 -IBS is a site on MAO.²⁹ Interestingly, MAO inhibitors clorgyline and deprenyl disrupt the binding of I_2 ligands *in vivo* when administered to rats,³⁰ although, *in vitro* studies showed that MAO inhibitor, phenylzine, does not prevent the binding of imidazolines to I_2 sites.³¹

The inhibition properties of imidazolines with mitochondrial preparations of human, rat, and rabbit MAO B have been described as competitive, mixed and noncompetitive, which lead to the proposal that MAO B has an allosteric site.

Further evidence of the location of this site was provided when Raddatz and coworkers used ^{125}I -AZIPI to photoaffinity label the site of modification on MAO B. The I_2 site was found to reside between residues Lys149-Met222 (Figure 4.3.3).¹⁷

While there is compelling evidence to suggest MAO has an I_2 site, it has been shown that imidazoline ligands inhibit MAO weakly ($K_i \sim$ micromolar range). This is inconsistent with *in vivo* I_2 -IBS binding studies where imidazoline ligands like 2-BFI have been shown to bind to I_2 -IBS with K_d values in the nanomolar range.³² These conflicting data lead to the proposal that a subpopulation of MAO contains an I_2 site.³³

4.3.1.4 *Tranlycypromine Potentiation of 2-BFI Binding.*

Great advances in understanding anomalies in the literature regarding MAO and I_2 -IBS were made when a group of researchers at Eli Lilly demonstrated that MAO inhibitor, tranlycypromine (TCP), potentiates the binding of 2-BFI to human MAO B.³⁴⁻³⁶ Inhibition of membrane fractions of MAO B isolated from human brain, human platelets, and rat brain were investigated in this study. Incubation of membrane fractions isolated from human platelets and human brain tissues with TCP increased the available I_2 -IBS by ~14-fold (determined by an increase in B_{max}) when comparing to untreated membrane fractions.³⁶ This corresponds to ~90% of the available TCP-inhibited MAO in the preparation possessing an I_2 site versus only ~10% of untreated MAO having an I_2 site.

Interestingly, incubation of rat tissues with TCP did not result in enhanced binding of 2-BFI. Incubation of recombinant human MAO A membrane fractions also did not result in an increase of I₂-IBS. Membrane preparations of recombinant human and rat MAO B from MAO transfected Sf-9 insect cells were studied in parallel for comparison and produced similar results. When surveying other known I₂-IBS specific ligands, the potentiation of TCP was not observed.³⁷

These data suggest that inhibition of human MAO B with TCP results in a high affinity site. All studies described in the literature to date have been performed using crude membrane particles, which precludes the crystallographic, spectroscopic, and thermodynamic study of the interactions of 2-BFI to human MAO B.

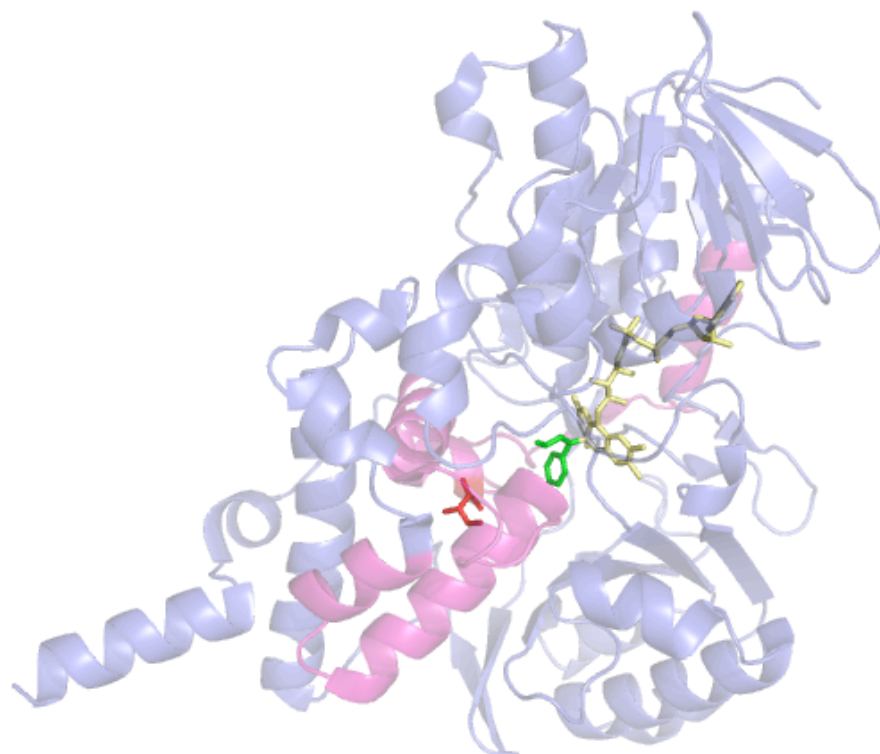


Figure 4.3.3. Xray structure for TCP-inhibited human WT MAO B (PDB code 2XFU). Raddatz identified the residues Lys129-Met222 as the I2 site of MAO B,¹⁷ which are highlighted here in magenta. The Ile199 gate residue is featured in red and marks the division of the entrance cavity from the substrate cavity. The flavin cofactor is highlighted in yellow with the TCP shown in green.

Given that the structure of TCP-inhibited MAO B has been elucidated by Binda and coworkers (PDB code 2XFU),³⁸ we set out to understand the enhanced binding observed with TCP-inhibited MAO B by reviewing the labeling studies of Raddatz and coworkers (which is depicted in Figure 4.3.3 by highlighting residues 149-222 in magenta in the crystal structure of TCP-inhibited MAO B). Noteworthy, the Ile199 “gate” residue is rotated to the closed position when TCP is bound to the enzyme (depicted in red in Figure 4.3.3) allowing for separation of the entrance cavity and substrate cavity of human MAO B, which lead to the proposal that this site would form a strong binding pocket for the imidazoline within the entrance cavity of human MAO B. This bipartite nature of

human MAO B is not conserved in the MAO A isoform which has a monopartite active site.

Having access to purified rat and human MAO as well as Ile199Ala and Ile199Ala-Tyr326Ala mutant forms of MAO B, we set out to further understand the mechanism of enhanced binding of 2-BFI to TCP-inhibited MAO B. We were particularly interested in this phenomenon because of its relevance to drug-drug interactions as well as presenting a novel mechanism for the selective inhibition of MAO B. Further, we wanted to develop a systematic method for studying the I₂-IBS so that we could identify endogenous ligands that may elicit the same response.

4.3.2 Results

4.3.2.1 Crystallization of MAO with 2-BFI.

In collaboration with Mattevi laboratory at the University of Pavia, four crystal structures of MAO in complex with 2-BFI were determined. To elucidate the high affinity binding site on human MAO B, TCP-inhibited MAO B was co-crystallized with 2-BFI to provide a 1.9 Å X-ray structure (PDB code 2XFU). The crystal structure showed that 2-BFI binds to the entrance cavity of MAO B while TCP forms a C(4a) adduct with the flavin cofactor within the substrate cavity (Figure 4.3.4).

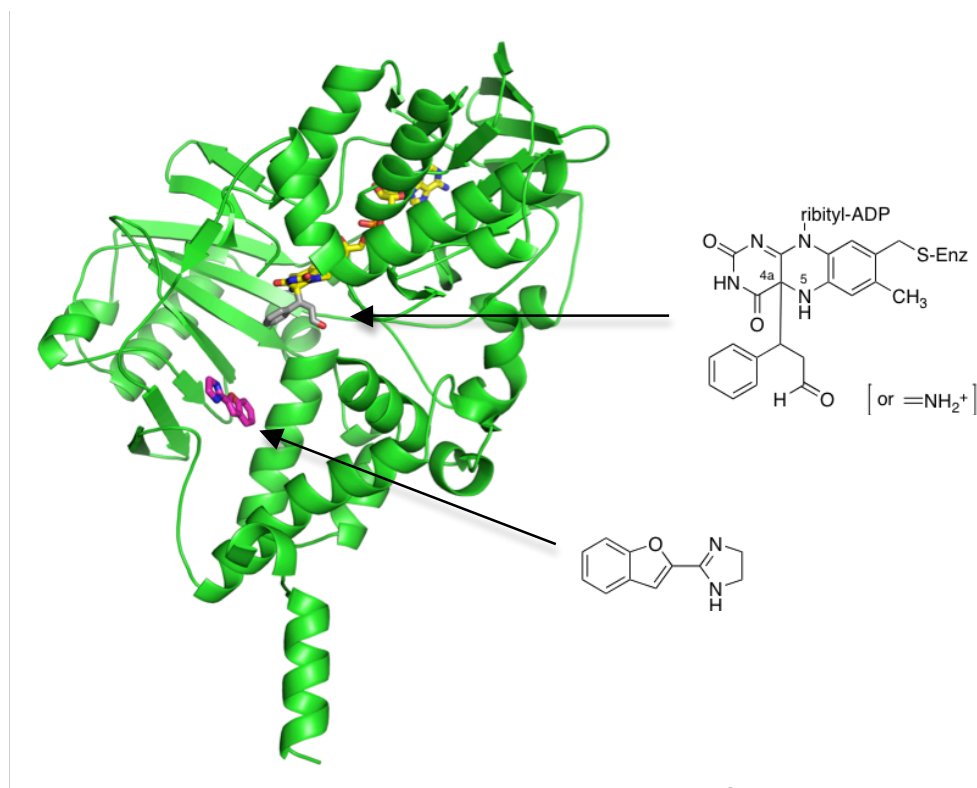


Figure 4.3.4. Tranilcypromine inhibited human WT MAO B in complex with 2-BFI.

Within the entrance cavity, the imidazoline ring of 2-BFI forms H-bonds with the Pro102 and Tyr326 (Figure 4.3.5A). Due to H-bonding between the Pro102 and 2-BFI, the loop spanning the residues from 100-103 moves toward the interior of the protein. H-bonding between Glu206 and Tyr326 is also observed upon 2-BFI binding to TCP-inhibited MAO B. This phenomenon is unique to this structure as this conformation of Gln206 is not observed in any other known MAO B complex.³⁹ The Ile199 residue is rotated into a closed conformation which, together with the Ile316, creates a hydrophobic cleft where the benzofuran ring of 2-BFI is situated.

To understand the differential binding observed between native MAO B and TCP-inhibited MAO B, human MAO B was co-crystallized with 2-BFI in the

absence of TCP. Interestingly, 2-BFI only binds to the entrance cavity of the enzyme, leaving the substrate cavity vacant (Figure 4.3.5B). The Ile199 gating residue is now found in the open conformation, which disrupts the hydrophobic pocket observed in the TCP-inhibited MAO B structure. While H-bonding is still observed from the Pro102 and Tyr326, Gln206 is no longer in a conformation that facilitates interactions with the Tyr326.

To probe the fidelity of the 2-BFI site, we co-crystallized 2-BFI with rasagiline-inhibited MAO B (Figure 4.3.5C) as well as MAO B in complex with isatin (Figure 4.3.5D). Rasagiline is an irreversible inhibitor of MAO B that forms an N(5) adduct with the flavin cofactor, while isatin is a small reversible MAO B inhibitor. Consistent with the other structures determined, 2-BFI binds to the entrance of rasagiline-inhibited MAO B. Neither the Ile199 or Gln206 are in conformational states that facilitate high affinity binding (compare Figure 4.3.5A with 5C-D). Interestingly in the case of isatin, the Ile199 is in a closed conformation, yet the Gln206 does not engage in H-bonding interactions with Tyr326.

These data show that the imidazoline binding site in human MAO B is a discrete binding site within the entrance cavity, and that this site exists in the presence and absence of ligands bound to the substrate cavity. Although experiments were attempted to determine if this site exists while substrate is bound to the active site (phenylethylamine), we were unsuccessful collecting quality data. Competition experiments were designed to aid in addressing this concern and will be described in detail in the next section.

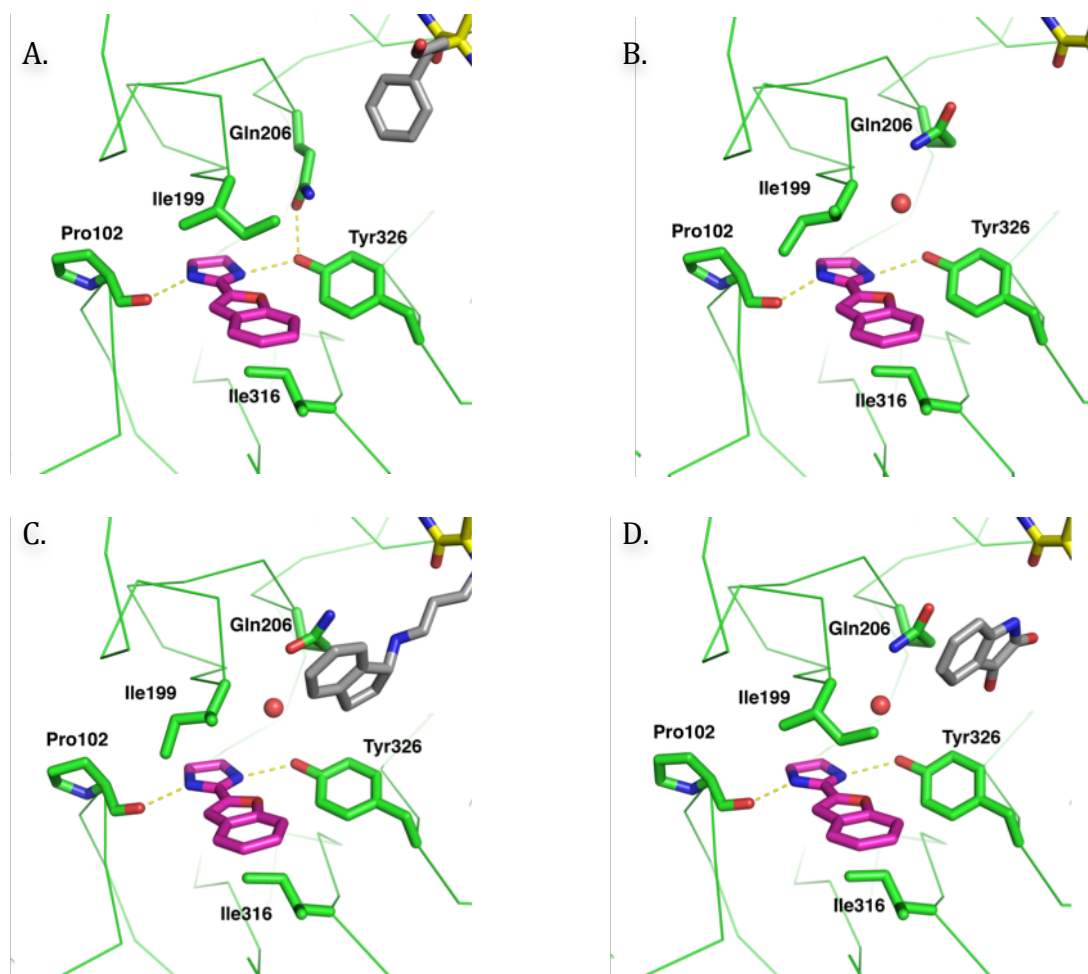


Figure 4.3.5. Close up of the entrance cavity of MAO B when 2-BFI is bound. A TCP-MAO B, B. Native MAO B, C. Rasagiline, D. Isatin.

Site directed mutagenesis studies were carried to further understand the roles of the Ile199 gating residue as well as Tyr326. Ile199Ala and Ile199Ala-Tyr326Ala mutant forms of human MAO B were constructed, purified, and investigated. The TCP-Ile199Ala mutant was co-crystallized with 2-BFI and exhibited the same binding motif as WT MAO B (Figure 4.3.6). The conformation of the Gln206 is consistent with that of WT (compare Figure 4.3.5A with Figure 4.3.6).

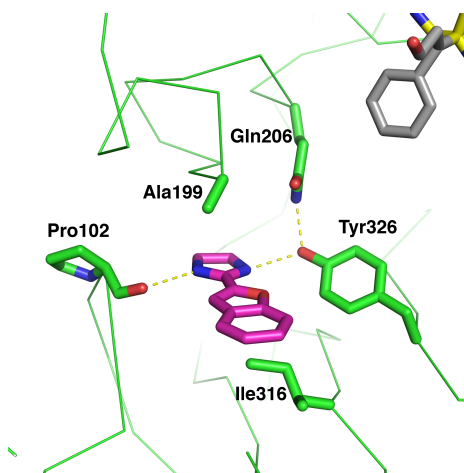
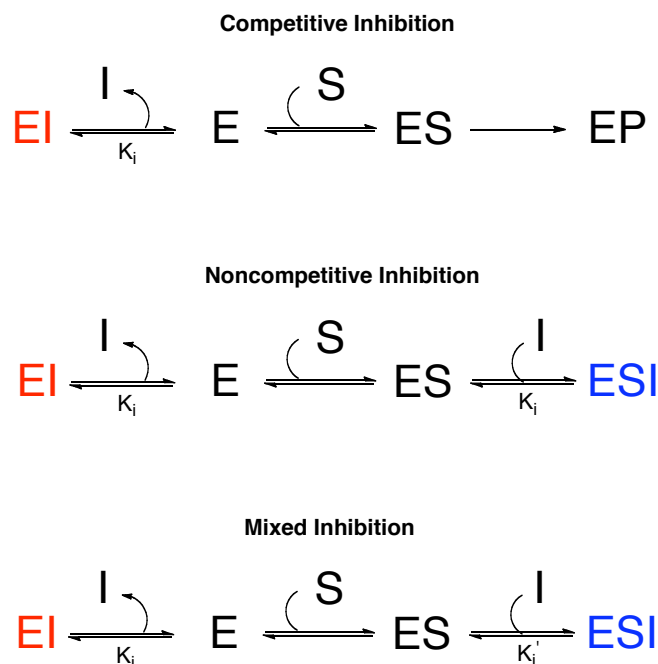


Figure 4.3.6. TCP-inhibited Ile199Ala MAO B co-crystallized with 2-BFI.

4.3.2.2 Competition Experiments with 2-BFI.

Because 2-BFI reversibly binds to MAO, competition experiments were conducted to establish the effect of 2-BFI on the activity on the enzymes. Global fit analysis was performed to determine the mode of inhibition as well as inhibition constants (Table 1). In this study, human MAO A, both human and rat MAO B, Ile199Ala MAO B and Ile199Ala-Tyr326Ala MAO B were examined. This investigation demonstrates that 2-BFI has differential effects on each of the enzymes evaluated in this study. In some cases, 2-BFI competitively inhibits MAO (2-BFI only binds to free enzyme), while in other cases MAO is noncompetitively inhibited by 2-BFI (2-BFI binds equally to the substrate-enzyme complex and free enzyme). Competitive, noncompetitive, and mixed inhibition are reviewed in Scheme 1 to provide clarity for the reader.



Scheme 4.3.1. Review of possible modes of inhibition for 2-BFI inhibition of MAO. Competitive inhibition defined by the ability of the inhibitor to bind only to the free enzyme. Noncompetitive inhibitors can bind with equal affinity to the enzyme-substrate (or product) complex and free enzyme. Mixed inhibitor have differential binding affinities for the free enzyme versus enzyme-substrate (or product) complex which are described as K_i and K_i' .

Surprisingly, 2-BFI acts as a competitive inhibitor of both human MAO A and MAO B with K_i of $17 \pm 1 \mu\text{M}$ and $20 \pm 2 \mu\text{M}$, respectively. Competitive inhibition seemed unlikely for MAO B given that 2-BFI does not bind to the substrate cavity like traditional MAO B inhibitors. For this reason a number of replots of the data were constructed to verify the mode of inhibition. Lineweaver-Burk, Dixon, and Cornish-Bowden plots confirm that 2-BFI is a competitive inhibitor of human MAO B (Figure 4.3.7 and 4.3.8). Deuterated-benzylamine was used as a substrate for MAO B to ascertain the effects of varying the relative concentrations of E_{ox} versus E_{red} on the binding mode of the inhibitor. Specifically, using deuterated benzylamine as a substrate increases the steady state concentration of E_{ox} in the assay. No effect is observed between the

deutero- and proteo-benzylamine, further confirming the assignment of the mode of inhibition as competitive. Contrary to the human enzyme, 2-BFI inhibits rat MAO B in a noncompetitive fashion as determined by global fit analysis (K_i of $257 \pm 45 \mu\text{M}$) (Figure 4.3.9).

Interestingly, mutations to the gating residues of human MAO B has dramatic effects on the mode of inhibition and the inhibition constant of 2-BFI with the enzymes. Unlike human WT MAO B, the MAO B Ile199Ala mutant is noncompetitively inhibited by 2-BFI with an increased K_i of $58 \pm 6 \mu\text{M}$ (~3-fold increase in K_i). The mode of inhibition of 2-BFI appears to switch from mixed inhibition, at low concentrations of 2-BFI, to noncompetitive inhibition, at high concentrations of 2-BFI (see Figure 4.3.10). Incidentally, the MAO B Ile199Ala-Tyr326Ala double mutant is competitively inhibited by 2-BFI exhibiting a large increase the K_i in comparison to WT MAO B. ($K_i = 181 \pm 34 \mu\text{M}$, ~9-fold increase). Evidence suggests that the imidazoline binding site is fully disrupted in the Ile199Ala-Tyr326Ala mutant form. No crystallographic data is available for the double mutant due to the reduced binding affinity of 2-BFI to the mutant.

Table 4.3.1. Competition experiments to determine the mode of inhibition of 2-BFI with MAO.

Entry	Enzyme	K_i (μM)	Mode of Inhibition
1	^a hMAO B	20 ± 2	Competitive
2	^b hMAO B	25 ± 4	Competitive
3	^c hMAO A	17 ± 1	Competitive
4	^c hMAO B Ile199Ala	58 ± 6	Noncompetitive
5	^c hMAO B Ile199Ala-Tyr326Ala	181 ± 34	Competitive
6	^d rMAO B	257 ± 45	Noncompetitive

The K_i values were determined spectrophotometrically using a horseradish peroxidase-ampex red coupled assay with: ^abenzylamine, ^b α,α -²H₂-benzylamine, ^c*p*-CF₃-benzylamine, or ^dphenylethylamine as a substrate.

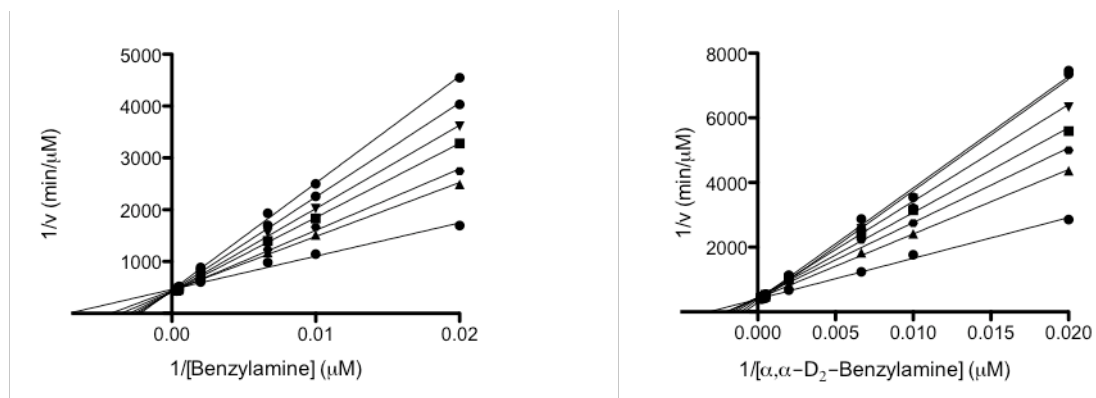


Figure 4.3.7. Lineweaver-Burk of human MAO B using benzylamine as a substrate (left) and α,α - $^2\text{H}_2$ -benzylamine as a substrate (right).

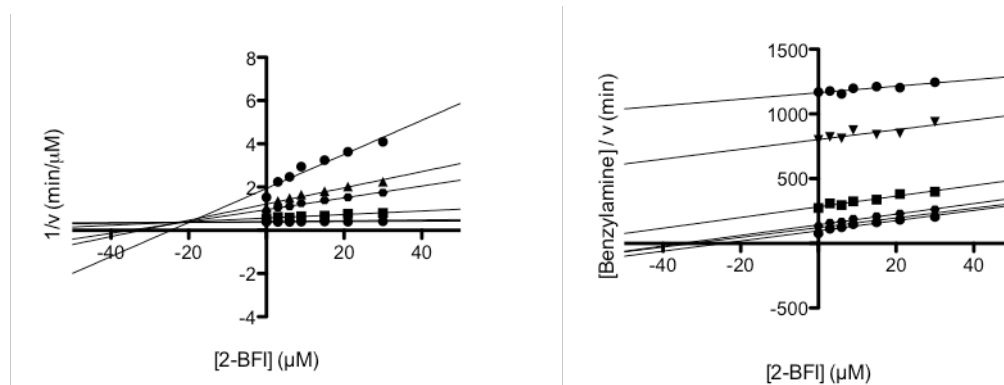


Figure 4.3.8. Replots of 2-BFI inhibition of human MAO B using benzylamine as a substrate. Left panel is Dixon plot and right panel is the Cornish-Bowden plot.

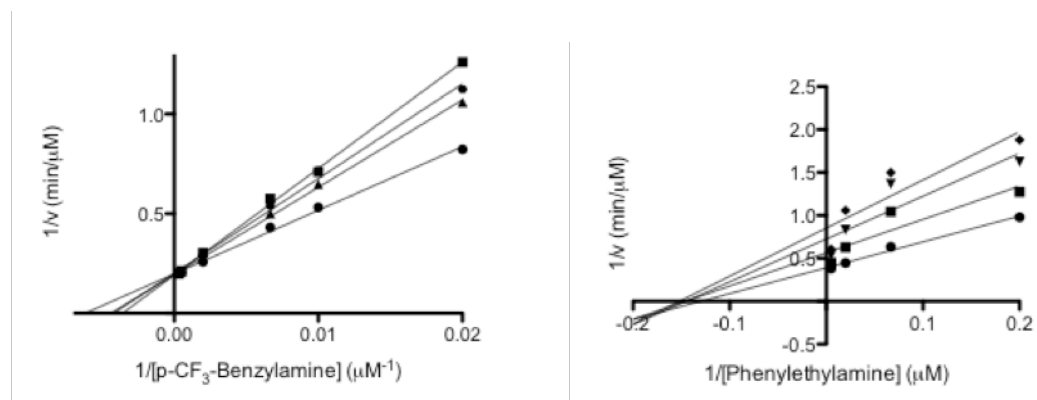


Figure 4.3.9. Lineweaver-Burk plots of human MAO A (left) and rat MAO B (right) with 2-BFI. Competition experiments using $p\text{-CF}_3$ -benzylamine (MAO A) and phenylethylamine (rat MAO B) as a substrate and 2-BFI as an inhibitor.

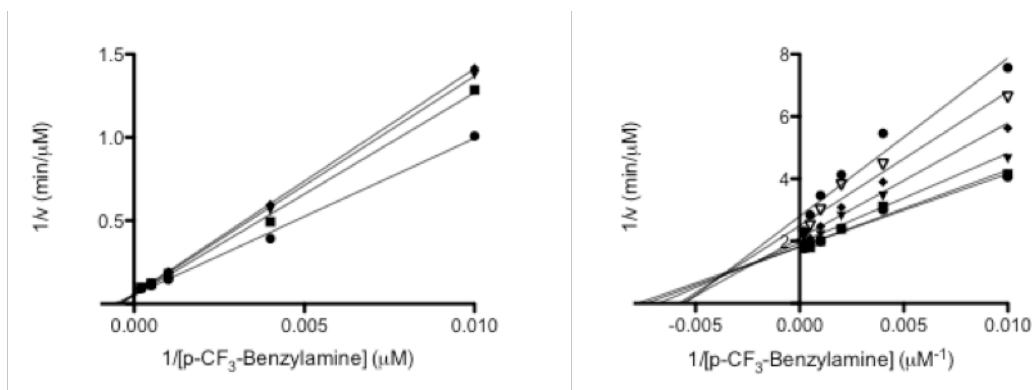


Figure 4.3.10. Lineweaver-Burk plots of Ile199Ala-Tyr326Ala (left) and Ile199Ala (left) mutant forms of MAO B with 2-BFI. Competition experiments using *p*-CF₃-benzylamine as a substrate and 2-BFI as an inhibitor.

4.3.2.3 Competition Experiments using Farnesylamine as a Substrate.

Not having access to crystallization conditions for the structure elucidation of rat MAO B, we set out to design an experiment that would provide insights into the location of the 2-BFI binding site. Given that the mode of inhibition is noncompetitive and that the amino acid sequences of rat and human MAO are ~90% identical, we hypothesized that 2-BFI binds to the entrance cavity of rat MAO B much like the human enzyme. To test this hypothesis, we used a substrate that would extend the length of the active site, bridging both the

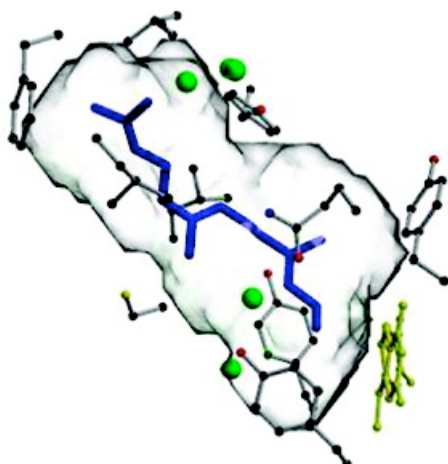


Figure 4.3.11. X-ray crystal structure of the human MAO B-farnesol complex (PDB code 2BK3).

entrance and substrate cavities. It is well known that farnesol, a reversible MAO B specific inhibitor, binds to MAO by traversing both the substrate and entrance cavity of human MAO B (Figure 4.3.11). Although the X-ray crystal structure

of rat MAO B in complex with farnesol has not been determined, it can be assumed that the binding mode will be similar to that of human MAO B.

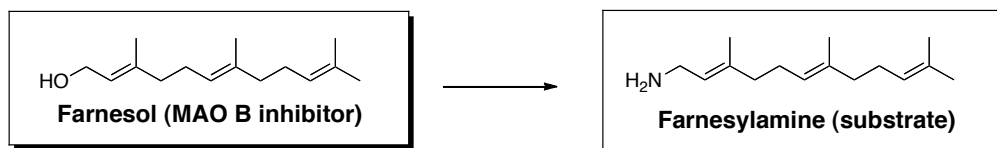


Figure 4.3.12. The structures of farnesol and farnesylamine.

Farnesylamine is the substrate analogue to this inhibitor (Figure 4.3.12). Using farnesylamine as a substrate for rat MAO B the mode of inhibition of 2-BFI shifted from noncompetitive inhibition ($K_i = K_i' = 257 \pm 45 \mu\text{M}$, $R^2 = 0.9551$) to competitive inhibition ($K_i = 67 \pm 5 \mu\text{M}$, $R^2 = 0.9943$), meaning that 2-BFI only binds to free enzyme and not to the enzyme-substrate complex. As a control, human MAO B was investigated and also shows competitive inhibition ($K_i = 8.3 \pm 0.6 \mu\text{M}$).

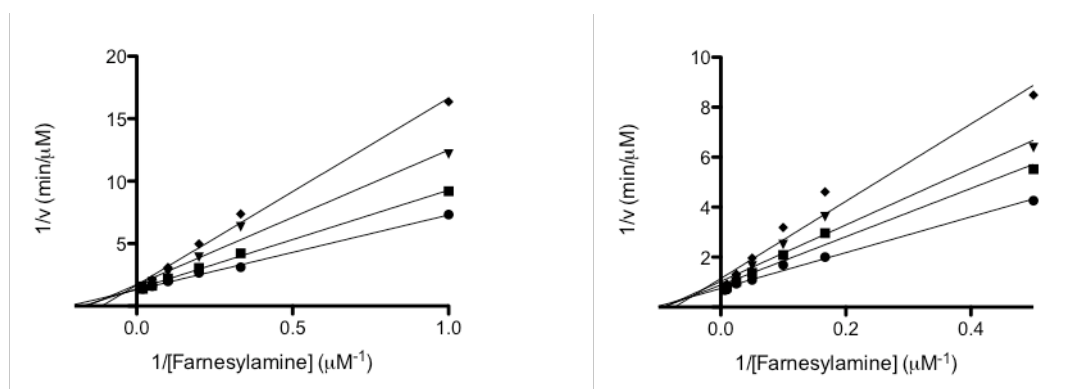


Figure 4.3.13. Lineweaver-Burk plots of human MAO B (left) and rat MAO B (left). Competition experiments using farnesylamine as a substrate and 2-BFI as an inhibitor.

4.3.2.4 Development of a Fluorescence Binding Assay for 2-BFI.

While competition experiment can provide a wealth of information about the mode of inhibition of 2-BFI, these experiments cannot be employed with inhibited enzyme and therefore cannot be used to understand the effect of TCP on the binding of 2-BFI. Equipped with the knowledge that 2-BFI is fluorescent, we set out to develop a fluorescence binding assay to observe the binding properties of 2-BFI with MAO. Free enzyme preparations were compared to TCP-inhibited MAO, and the results of these experiments are summarized in Table 2.

Table 4.3.2. Binding of 2-BFI to MAO B determined by fluorescence quenching assay.

Entry	Enzyme	K_d (μM)
1	hMAO B	15 ± 4
2	TCP-hMAO B	0.012 ± 0.002
3	Benzylhydrazine-MAO B	No observable binding
4	Propargylamine-MAO B	No observable binding
5	TCP-hMAO B Ile199Ala	No observable binding
6	TCP-rMAO B	No observable binding
7	TCP-hMAO A	No observable binding

By observing the quenching of fluorescence of 2-BFI upon binding to MAO B, the K_d values for native MAO B and TCP-inhibited MAO B were determined. Consistent with published data, 2-BFI binds to TCP-inhibited enzyme in the low nanomolar range ($K_d = 12 \pm 2$ nM). 2-BFI binds to native MAO B at low micromolar concentrations ($K_d \sim 15 \pm 4$ μM). The quenching of 2-BFI is shown in Figure 4.3.11. When rat MAO B and the mutant forms of human MAO B were investigated, the poor binding affinities of 2-BFI for these enzymes prevented accurate determinations of their K_d values due to the limitation of the

fluorescence assay at higher concentrations of MAO. TCP-inhibited samples of MAO A, rat MAO B, and Ile199Ala do not result in nanomolar binding. Further, inhibition of MAO B with benzylhydrazine and propargylamine, small irreversible MAO inhibitors which presumably do not disrupt the 2-BFI binding site, does not potentiate the binding of 2-BFI.

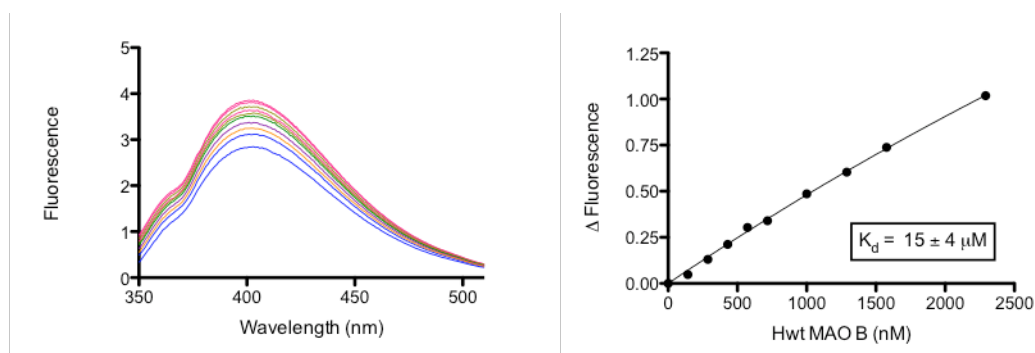


Figure 4.3.14. Fluorescence quenching assay of native MAO B and 2-BFI.

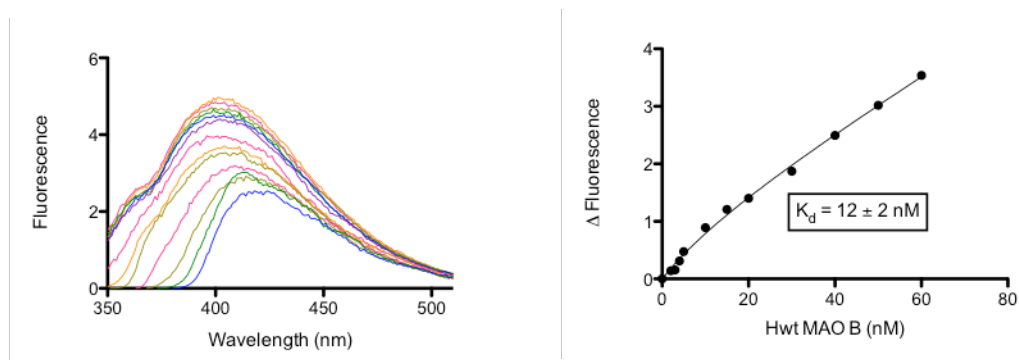


Figure 4.3.15. Fluorescence quenching assay of TCP-MAO B adduct and 2-BFI.

4.3.2.5 Development of Thermal Denaturation Experiments for Screening Purposes.

To have access to a wider range of K_d values, several methods were explored during the course of this study; however, most failed to provide useful

date. Isothermal titration calorimetry (ITC) and differential scanning calorimetry (DSC) were explored for the purpose of determining binding constants by measuring the heat of binding. However because MAO is a membrane bound protein, solubilizing MAO requires working with a detergent system, which caused difficulties in acquiring accurate thermodynamic data.

The Mattevi group has shown that inhibitor binding to MAO results in increased stability of the enzyme leading to an increase in the T_m for thermal denaturation of the protein.⁴⁰ Other groups have shown that circular dichroism (CD) can be employed to observe the effects of binding interactions on the unfolding of a protein.⁴¹ By observing changes in the optical rotation of l_{220} , the loss of α -helix was monitored as a function of temperature.

Table 4.3.3. Thermal denaturation experiments determined by optical rotation at $\lambda_{220\text{nm}}$.

Entry	Enzyme Sample	Melting Temperature (°C)
1	Human MAO B	50.58 ± 0.04
2	hMAO B + 2-BFI	53.40 ± 0.06
3	TCP-hMAO B	57.86 ± 0.06
4	TCP-hMAO B + 2-BFI	61.53 ± 0.07
5	Deprenyl-hMAO B	65.77 ± 0.05
6	Deprenyl-hMAO B + 2-BFI	65.86 ± 0.06
7	hMAO B + Safinamide	55.71 ± 0.07
8	hMAO B + Isatin	52.67 ± 0.04
9	hMAO B + Isatin + 2-BFI	53.30 ± 0.05
10	hMAO B + R-MAI ^b	56.08 ± 0.04 ^a
11	hMAO B + R-MAI ^b + 2-BFI	54.89 ± 0.07 ^a

^a When native human MAO B from this experiment was resubmitted for melting studies, it was found to melt at 51.01 ± 0.1 °C and human MAO B in complex with 2-BFI was shown to melt at 54.32 ± 0.05 °C. ^b (R)-N-methyl aminoindan (R-MAI).

Addition of an inhibitor to MAO B results in mild to significant increasing in T_m . For example, native MAO B has a T_m of ~50 °C (Table 3, entry 1) while having reversible inhibitors bound to the active site increases the T_m by 3 to 5 °C

(entries 2 and 7-11). Covalently bound inhibitors, like TCP and deprenyl, increase the T_m of MAO B more dramatically, ~7 to 15 °C (entries 3 and 5). Using this approach, we looked for increases in T_m as an indication of 2-BFI binding. Using the TCP-human MAO B complex, the T_m was increased by ~3.7 °C when 2-BFI is added to the complex while 2-BFI added to native MAO B increases the T_m by ~2.8 °C (compare 1-5). When 2-BFI is added to the MAO B-deprenyl complex, the melting temperature is unchanged (entries 5 and 6). Interestingly, the 2-BFI-isatin-MAO B complex does not exhibit a dramatic increase in stability with respect to the isatin-MAO B complex alone (entries 8 and 9). The MAO B-(R)-N-methyl aminoindan (R-MAI) complex appears to decrease in stability when 2-BFI is introduced to the system suggesting that there is some competition between the R-MAI and 2-BFI for the active site.

4.3.3 Discussion

X-ray crystallography unambiguously shows that 2-BFI binds to the entrance cavity of human MAO B in the presence or absence of ligands occupying the substrate cavity. These data are consistent with previous studies using membrane particle of MAO B. More specifically, the X-ray crystal structure demonstrates that 2-BFI binds to a location on the protein previously identified by photoaffinity labeling studies identifying Lys149-Met222¹⁷ (Figure 4.3.16). The assignment of imidazoline ligands as noncompetitive and mixed inhibitors of MAO B is also consistent with the X-ray structure which illustrates that 2-BFI does not bind to the substrate cavity of MAO B.⁴² There is no evidence of 2-BFI binding in the substrate cavity of human or rat MAO B which is confirmed by

competition experiments using farnesylamine and X-ray crystallography of native human WT MAO B; although, 2-BFI likely binds to human MAO A within the monopartite active site with a similar binding motif to other MAO inhibitors. Fluorescence quenching experiments show that TCP-inhibition of human MAO A does not result in an enhancement of 2-BFI binding.



Figure 4.3.16. X-ray crystal structure of TCP-inhibited human MAO B with 2-BFI bound to the I₂ site. Residues Lys129-Met222 identified as the I₂ site of MAO B by photoaffinity labeling studies¹⁷ are highlighted here in magenta. The flavin cofactor is highlighted in yellow with the TCP shown in green.

4.3.3.1 Understanding the Potentiation of 2-BFI Binding to TCP-human B.

The enhancement in binding of 2-BFI upon TCP-inhibition of human MAO B (~1000-fold increase) is due to the cooperative interactions of the binding site which result in a $\Delta(\Delta G) \sim -4.2$ kcal/mol. One source of favorable energy is

through the alterations to the active site shaping loop of MAO B. Pro102 on the active site shaping loop forms a H-bond with the imidazoline ring increasing the rigidity to the 2-BFI binding pocket. Similarly, when 2-BFI is bound to MAO B Ile199 and Ile316 form a hydrophobic “sandwich” around the benzofuran ring of 2-BFI. Inhibition of MAO B with TCP results structural changes where cooperative hydrophobic interactions strengthen the H-bonding interactions of the Gln206 with the Tyr326 which also engages in H-bonding interactions with the imidazoline ring of 2-BFI. The conformational changes associated with TCP-inhibition of MAO B results in the loss of an ordered water molecule within the active site, which provides further evidence of the increased hydrophobicity of the active site when TCP is bound. The cooperative nature of increasing hydrophobicity of a binding pocket on increase in H-bond energetics has also been extensively investigated and demonstrated by Muley and coworkers for binding affinities of thrombin inhibitors.⁴³ The Muley study demonstrated the limitations associated with molecular modeling techniques which treat intermolecular interactions as additive effects and neglect to address the cooperative nature of these effects that are observed experimentally.

With a sequence identity of ~90% between rat and human MAO B, it is unusual that TCP does not potentiate the binding of 2-BFI to the rat enzyme as observed with human MAO B. One possible explanation for the lack of enhanced binding is that rat MAO B has a Val side chain rather than a Ile in the 316 position. This modest substitution probably results in considerable alterations in the hydrophobic environment present in human MAO B. This is not

the first example of such a phenomenon in an enzyme system. Both tRNA synthetase⁴⁴ and the PXP domain of the potassium ion channel⁴⁵ demonstrate alterations in hydrophobic contributions to function on substitution of a Val for an Ile. Such an observation demonstrates a limitation in using rat MAO as a model system for inhibition studies, and this consideration should be kept in mind when designing and testing new imidazoline compounds for MAO B with rat versus human enzyme. Likewise, the Ile199Ala mutant form of human MAO B substitutes an Ala for the Ile in the 199 position. This substitution disrupts the hydrophobic sandwich of the Ile199 and Ile316 precluding enhanced binding of 2-BFI to the TCP-inhibited Ile199Ala mutant form of MAO B.

4.3.4 Conclusions

These studies explain the differential behavior of the I₂-IBS reported in the literature by showing the mode of inhibition is dependent on the mammalian source of MAO (results vary from rat to human enzyme). Caution should be taken in using rat, mouse and other model organisms for the development and study of MAOs as these organisms may display differential affinities and binding modes. This investigation also provides insights for understanding the inconsistency of *in vivo* studies on the I₂-IBS and *in vitro* studies of MAO with imidazoline ligands. Herein we report that TCP facilitates nanomolar binding of 2-BFI through locking the Ile199 and Gln206 into conformations that strengthen the binding pocket of 2-BFI through cooperative interaction. The high affinity binding I₂ site is likely induced by endogenous ligand-bound form of human MAO B, which is similar in nature to the TCP-inhibited form of MAO B. The

phenomenon of ligand-induced conformational changes that result in the formation of a high affinity binding site provides a novel platform for the development of highly specific MAO B inhibitor as no such phenomenon is observed in MAO A.

4.3.5 Materials and Methods

Crystallographic Conditions. Crystals of MAO B and the Ile199A mutant were grown using established protocols;³⁸ the enzyme was incubated with the covalent inhibitor (either tranylcypromine or rasagiline), gel filtered to remove the inhibitor excess and then incubated with 2-BFI prior to crystallization. Data collections were performed at the ESRF (Grenoble, France), and high-resolution structural analysis was performed as previously described.³⁸

Protein Isolation. Recombinant human liver MAO B⁴⁶ and MAO A⁴⁷ as well as recombinant rat MAO B⁴⁸ were expressed in *Pichia pastoris* and purified by published protocols. The construction, expression and purification of MAO B Ile199Ala and Ile199Ala-Tyr326Ala is discussed in detail in Chapter 5.

Competition Assays. K_i values for 2-BFI inhibition of human MAO A, rat and human MAO B, MAO B Ile199Ala, and MAO B Ile199Ala-Tyr326Ala were determined by measuring the initial rates of substrate oxidation (six to eight different concentrations) in the presence of varying concentrations of inhibitor (four to eight different concentrations). All samples were incubated for 5 minutes at 25 °C prior to the addition of enzyme. All assays were performed using a

horseradish peroxidase-amplex red coupled assay to provide consistency with all of the enzymes in this study. Standard MAO A and MAO B activity assays were performed using *p*-trifluoromethylbenzylamine and benzylamine, respectively at 25 °C in a 50 mM phosphate buffer (pH 7.5) and 0.5% (w/v) RTX-100. Rat MAO B was assayed using phenylethylamine as a substrate in the buffer conditions described above. The Ile199Ala and Ile199Ala-Tyr326Ala mutant forms were assayed using *p*-trifluoromethylbenzylamine as a substrate. MAO B Ile199Ala was assayed using the buffer conditions described above; however, MAO B Ile199Ala-Tyr326Ala shows low activity at neutral pH therefore the buffer conditions were changed to 50 mM CHES buffer at pH 9.3 and 0.5% (w/v) RTX-100.

Binding constants were determined using global fit analysis of the hyperbolic fit of enzyme activity upon varied concentrations of inhibitor using the Graphpad Prism data analysis software. The mode of inhibition was determined also using global fit analysis of the activity curves in the presence and absence of 2-BFI to fit equations for competitive, mixed, noncompetitive and uncompetitive inhibition; the fit lending to the highest R^2 value was selected for determining the binding constants. Linear re-plots of the data were used for visualization, and no kinetic values were calculated from these re-plots.

Fluorescence Binding Assays. Binding of 2-BFI was measured by monitoring the fluorescence emission intensities in the 350 – 600 nm spectral range on an Aminco Bowman Series 2 luminescence spectrophotometer using a 1 cm

pathlength quartz cuvette. Data was collected as a loss in 2-BFI fluorescence emission on binding to the enzyme. This data were then re-plotted as a change in fluorescence versus concentration of MAO and fit to a single site binding curve for determination of the K_d .

For the high affinity site (nanomolar K_d), 10 nM 2-BFI was dissolved in a buffer solution of 50 mM potassium phosphate at pH 7.4 which had been filtered through a 0.2 micron filter to remove any particulates that could result in light scattering. This solution was titrated with 1-10 μ M TCP-inhibited MAO in μ L portions. A control was set-up by titrating MAO B into the buffer listed above in the absence of 2-BFI. The spectra were then subtracted from the 2-BFI binding titration to remove the background fluorescence of MAO. Bind was determined by calculating the $\Delta_{\text{fluorescence}}$ at λ_{399} , after the control titration had been subtracted, and these data were fit to a one site binding curving using the Dunn and Raftery method to account for ligand depletion at the low concentration of inhibitor.⁴⁹

The TCP-inhibited MAO samples were prepared by titrating a solution of MAO in 50 mM potassium phosphate at pH 7.2 in 50% glycerol (v/v) with minimal TCP (in an aqueous solution) until a full loss of activity was observed. These buffer conditions are the only conditions that prevent precipitation of the protein in the presence of TCP. The samples were then allowed to incubate overnight at 4 °C (no change in efficiency was observed when incubating overnight at -20 °C), and were then centrifuge for 5 minutes at 13.2 rpm (no pellet was observed when using a 50% glycerol solution). TCP-inhibited MAO samples that were not

allowed to incubate overnight did not demonstrate high affinity binding. Likewise, samples that incubated over several days were shown to have slightly lower K_d values ($\sim 6.3 \pm 2.5$ nM), but this came with significant light scattering due to rapid precipitation of the protein upon addition to the 2-BFI solution. A 24 hour incubation period at 4 °C was ideal for error minimization and protein conformational changes that were required for the formation of the high affinity site.

$$Y = 0.5 * F_0 [(X + K_d + B_{max}) - \sqrt{(X + K_d + B_{max})^2 - (4 * X * B_{max})}]; \quad (1)$$

where $F_0 = 1$ (maximum fluorescence enhancement), $X = [\text{MAO}]$ and $Y = B_{max}$ at full occupancy
(measured by $\Delta\text{Fluorescence}$)

To probe the low affinity site binding (micromolar K_d), slightly different conditions were employed. Using a 1 cm pathlength quartz cuvette, 20 μM 2-BFI was dissolved in a buffer solution of 50 mM potassium phosphate at pH 7.4, 20% glycerol (v/v), and 0.8% OGP (w/v). This solution was titrated with 40 μM MAO in 10-100 μL portions. A control was set-up by titrating native MAO into the buffer listed above in the absence of 2-BFI. The spectra were then subtracted from the 2-BFI binding titration to remove the background fluorescence of MAO. Binding was determined by calculating the $\Delta_{\text{fluorescence}}$ at λ_{399} , after the control titration had been subtracted, and these data were fit to a one site binding curving using the Graphpad prism.

$$Y = B_{max} * X / (K_d + X); \quad (2)$$

where $X = [\text{MAO}]$ and $Y = \Delta_{\text{Fluorescence}}$

Due to the low quantum yield of 2-BFI, the conditions of the fluorescence binding assay varied from the studies of the high to the low affinity site. Note that no detergent is using in the buffer for the high affinity site due to detergent quenching the 2-BFI fluorescence at low concentrations of 2-BFI. The low affinity site was investigated in a detergent system due to the poor solubility of MAO in the absence of detergent. The assay was also limited by not having access to the high concentrations of MAO in solution. The assay could not exceed 2.5 μM MAO due to precipitation of the protein in the presence of 2-BFI and the light scatter that resulted.

Thermal Denaturation Studies. All experiments were conducted in a 1 mm pathlength quartz cuvette using a Jasco J-810 spectropolarimeter to determine the circular dichroism reading. Samples were prepared in 50 mM potassium phosphate at pH 7.4, 0.8% (w/v) OGP, and 20% glycerol. All samples of MAO was diluted to 0.5 g/L (8 μM) in the buffer described above. Prior to variable temperature experiments, the CD absorption spectra of all samples were collect at 20 °C from 190 nm to 260 nm to insure the quality and consistence of the enzyme. Variable temperature experiments were performed at $\lambda_{222\text{nm}}$ heating from 20 °C to 90 °C in 0.5 °C increments with a ramp speed of 1 °C/min and a 30 s dwell time. Melting curves were fit using Origin data analysis software (Fits are shown in Figure 4.3.17-4.3.22).

TCP-inhibited enzyme samples were prepared by titrating MAO with TCP until full inhibition was observed (determined using the activity assay describe above) and A_{450} was bleached. Deprenyl inhibited MAO B was prepared having a final

concentration 50 μM deprenyl (no activity was observed). Safinamide and isatin experiments were both performed using 15 μM final concentration of ligand. Because the K_i of R-MAI is ~ 17 μM , the final concentration of this ligand was increased to 45 μM . Inhibited and native enzyme samples were tested with and without 2-BFI ($[2\text{-BFI}]_{\text{final}} = 15$ μM).

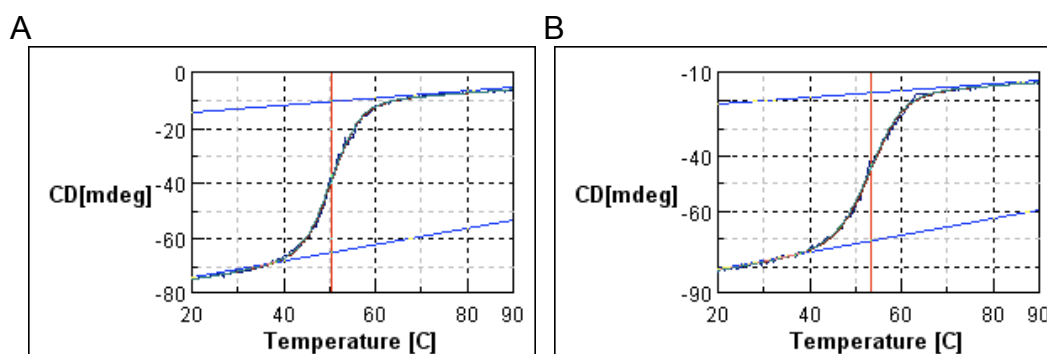


Figure 4.3.17. A. Melting temperature curves for A. WT MAO B, B. WT MAO B and 2-BFI.

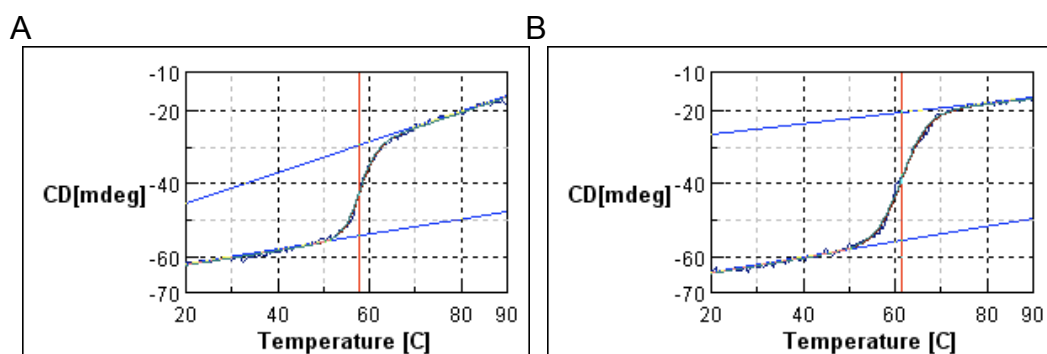


Figure 4.3.18. A. Melting temperature curves for A. TCP-inhibited WT MAO B, B. TCP-inhibited WT MAO B and 2-BFI.

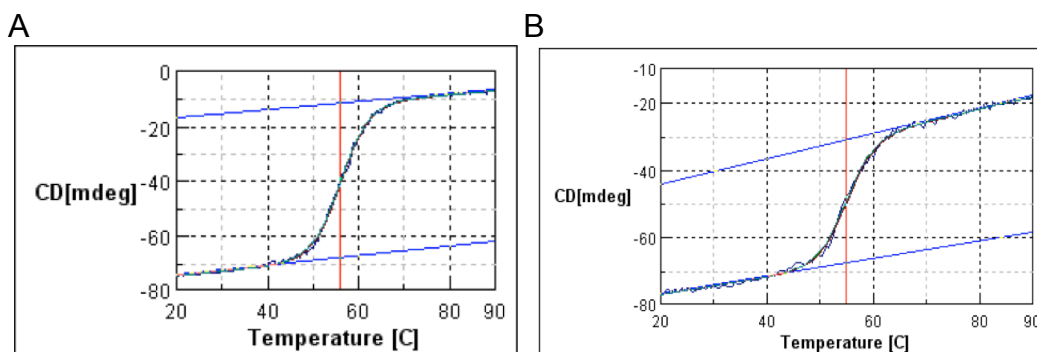


Figure 4.3.19. A. Melting temperature curves for A. WT MAO B and R-MAI, B. WT MAO B, R-MAI, and 2-BFI.

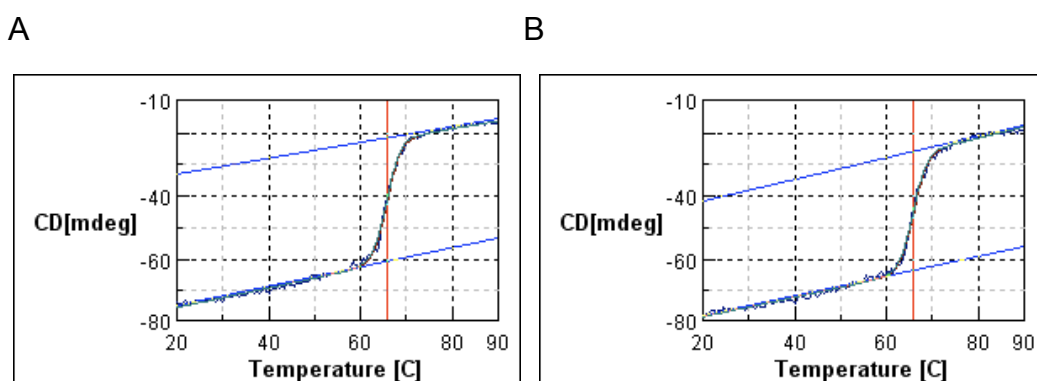


Figure 4.3.20. A. Melting temperature curves for A. Deprenyl-inhibited WT MAO B, B. Deprenyl-inhibited WT MAO B and 2-BFI.

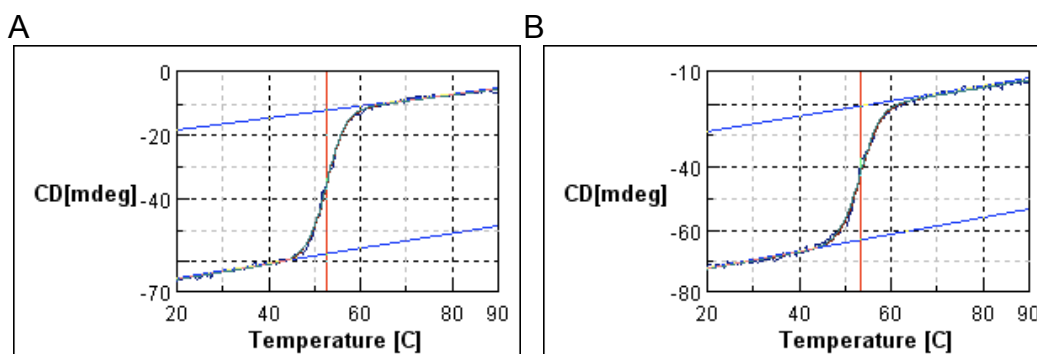


Figure 4.3.21. A. Melting temperature curves for A. WT MAO B and isatin, B. WT MAO B, isatin, and 2-BFI.

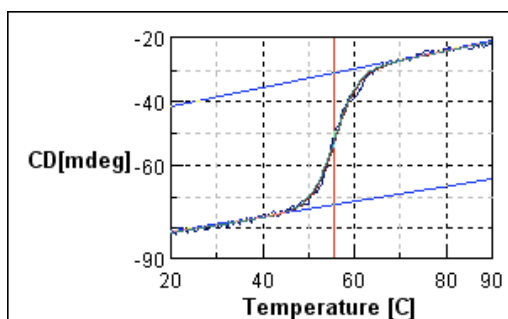


Figure 4.3.22. A. Melting temperature curve for WT MAO B and safinamide.

4.3.6 References

1. Bousquet, P.; Feldman, J.; Schwartz, J., Central cardiovascular effects of alpha adrenergic drugs: differences between catecholamines and imidazolines. *J. Pharmacol. Exp. Ther.* **1984**, 230, (1), 232-6.
2. Dardonville, C.; Rozas, I., Imidazoline binding sites and their ligands: an overview of the different chemical structures. *Med. Res. Rev.* **2004**, 24, (5), 639-61.
3. Dontenwill, M.; Vonthron, C.; Greney, H.; Magnier, C.; Heemskerk, F.; Bousquet, P., Identification of human I1 receptors and their relationship to $\alpha\pm 2$ -adrenoceptors. *Ann. N. Y. Acad. Sci.* **1999**, 881, (Imidazoline Receptors and Their Endogenous Ligands), 123-134.
4. Chan, S. L.; Brown, C. A.; Scarpello, K. E.; Morgan, N. G., The imidazoline site involved in control of insulin secretion: characteristics that distinguish it from I1- and I2-sites. *Br. J. Pharmacol.* **1994**, 112, (4), 1065-70.

5. Morgan, N. G.; Chan, S. L. F.; Mourtada, M.; Monks, L. K.; Ramsden, C. A., Imidazolines and pancreatic hormone secretion. *Ann. N. Y. Acad. Sci.* **1999**, 881, (Imidazoline Receptors and Their Endogenous Ligands), 217-228.
6. Clews, J.; Morgan, N. G.; Ramsden, C. A., Preparation of the I-3 imidazoline receptor antagonist KU14R and related 2,3-dihydrobenzo[b]furan derivatives. *Synthesis-Stuttgart* **2001**, (10), 1546-1550.
7. Alemany, R.; Olmos, G.; Garcia-Sevilla, J. A., Labelling of I2B-imidazoline receptors by [3H]2-(2-benzofuranyl)-2-imidazoline (2-BFI) in rat brain and liver: characterization, regulation and relation to monoamine oxidase enzymes. *Naunyn Schmiedebergs Arch. Pharmacol.* **1997**, 356, (1), 39-47.
8. Tesson, F.; Parini, A., Identification of an imidazoline-guanidinium receptive site in mitochondria from rabbit cerebral cortex. *Eur. J. Pharmacol., Mol. Pharmacol. Sect.* **1991**, 208, (1), 81-3.
9. Tesson, F.; Limon, I.; Parini, A., Tissue-specific localization of mitochondrial imidazoline-guanidinium receptive sites. *Eur. J. Pharmacol.* **1992**, 219, (2), 335-8.
10. Boronat, M. A.; Olmos, G.; Garcia-Sevilla, J. A., Attenuation of tolerance to opioid-induced antinociception by idazoxan and other I2-ligands. *Ann. N. Y. Acad. Sci.* **1999**, 881, (Imidazoline Receptors and Their Endogenous Ligands), 359-363.
11. Heemskerk, F. M. J.; Dontenwill, M.; Greney, H.; Vonthron, C.; Bousquet, P., Evidence for the existence of imidazoline-specific binding sites in

synaptosomal plasma membranes of the bovine brainstem. *J. Neurochem.* **1998**, 71, (5), 2193-2202.

12. Garcia-Sevilla, J. A.; Escriba, P. V.; Guimon, J., Imidazoline receptors and human brain disorders. *Ann. N. Y. Acad. Sci.* **1999**, 881, (Imidazoline Receptors and Their Endogenous Ligands), 392-409.

13. Meana, J. J.; Barturen, F.; Martin, I.; Garcia-Sevilla, J. A., Evidence of increased non-adrenoceptor [³H]idazoxan binding sites in the frontal cortex of depressed suicide victims. *Biol. Psychiatry* **1993**, 34, (7), 498-501.

14. Polidori, C.; Gentili, F.; Pigini, M.; Quaglia, W.; Panocka, I.; Massi, M., Hyperphagic effect of novel compounds with high affinity for imidazoline I(2) binding sites. *Eur. J. Pharmacol.* **2000**, 392, (1-2), 41-9.

15. Raddatz, R.; Lanier, S. M., Relationship between imidazoline/guanidinium receptive sites and monoamine oxidase A and B. *Neurochem. Int.* **1997**, 30, (1), 109-17.

16. Sastre, M.; Garcia-Sevilla, J. A., Densities of I2-imidazoline receptors, alpha 2-adrenoceptors and monoamine oxidase B in brains of suicide victims. *Neurochem. Int.* **1997**, 30, (1), 63-72.

17. Raddatz, R.; Parini, A.; Lanier, S. M., Localization of the imidazoline binding domain on monoamine oxidase B. *Mol. Pharmacol.* **1997**, 52, (4), 549-53.

18. Tesson, F.; Limon-Boulez, I.; Urban, P.; Puype, M.; Vandekerckhove, J.; Coupry, I.; Pompon, D.; Parini, A., Localization of I2-imidazoline binding sites on monoamine oxidases. *J. Biol. Chem.* **1995**, 270, (17), 9856-61.

19. Kimura, A.; Tyacke, R. J.; Robinson, J. J.; Husbands, S. M.; Minchin, M. C.; Nutt, D. J.; Hudson, A. L., Identification of an imidazoline binding protein: creatine kinase and an imidazoline-2 binding site. *Brain Res.* **2009**, 1279, 21-8.
20. Parini, A.; Gargalidis Moudanos, C.; Pizzinat, N.; Lanier, S. M., The elusive family of imidazoline binding sites. *Trends Pharmacol. Sci.* **1996**, 17, (1), 13-16.
21. Molderings, G. J., Imidazoline receptors: basic knowledge, recent advances and future prospects for therapy and diagnosis. *Drugs Future* **1997**, 22, (7), 757-772.
22. Regunathan, S.; Reis, D. J., Imidazoline receptors and their endogenous ligands. *Annu. Rev. Pharmacol. Toxicol.* **1996**, 36, 511-44.
23. Eglen, R. M.; Hudson, A. L.; Kendall, D. A.; Nutt, D. J.; Morgan, N. G.; Wilson, V. G.; Dillon, M. P., 'Seeing through a glass darkly': casting light on imidazoline 'I' sites. *Trends Pharmacol. Sci.* **1998**, 19, (9), 381-390.
24. Olmos, G.; Alemany, R.; Boronat, M. A.; Garcia-Sevilla, J. A., Pharmacologic and molecular discrimination of I2-imidazoline receptor subtypes. *Ann. N. Y. Acad. Sci.* **1999**, 881, (Imidazoline Receptors and Their Endogenous Ligands), 144-160.
25. Lanier, S. M.; Ivkovic, B.; Singh, I.; Neumeyer, J. L.; Bakthavachalam, V., Visualization of multiple imidazoline/guanidinium-receptive sites. *J. Biol. Chem.* **1993**, 268, (21), 16047-51.

26. MacKinnon, A. C.; Redfern, W. S.; Brown, C. M., [3H]-RS-45041-190: a selective high-affinity radioligand for I2 imidazoline receptors. *Br. J. Pharmacol.* **1995**, 116, (2), 1729-36.
27. Hudson, A. L.; Chapleo, C. B.; Lewis, J. W.; Husbands, S.; Grivas, K.; Mallard, N. J.; Nutt, D. J., Identification of ligands selective for central I2-imidazoline binding sites. *Neurochem. Int.* **1997**, 30, (1), 47-53.
28. Hosseini, A. R.; King, P. R.; Louis, W. J.; Gundlach, A. L., [3H]2-(2-benzofuranyl)-2-imidazoline, a highly selective radioligand for I2-imidazoline receptor binding sites. Studies in rabbit kidney membranes. *Naunyn-Schmiedeberg's Arch. Pharmacol.* **1997**, 355, (1), 131-138.
29. MacInnes, N.; Handley, S. L., Autoradiographic localisation of [3H]2-BFI imidazoline I2 binding sites in mouse brain. *Eur. J. Pharmacol.* **2005**, 516, (2), 139-44.
30. Olmos, G.; Gabilondo, A. M.; Miralles, A.; Escriba, P. V.; Garcia-Sevilla, J. A., Chronic treatment with the monoamine oxidase inhibitors clorgyline and pargyline down-regulates non-adrenoceptor [3H]-idazoxan binding sites in the rat brain. *Br. J. Pharmacol.* **1993**, 108, (3), 597-603.
31. Alemany, R.; Olmos, G.; Garcia-Sevilla, J. A., The effects of phenelzine and other monoamine oxidase inhibitor antidepressants on brain and liver I2 imidazoline-preferring receptors. *Br. J. Pharmacol.* **1995**, 114, (4), 837-45.
32. Carpene, C.; Collon, P.; Remaury, A.; Cordi, A.; Hudson, A.; Nutt, D.; Lafontan, M., Inhibition of amine oxidase activity by derivatives that recognize imidazoline I2 sites. *J. Pharmacol. Exp. Ther.* **1995**, 272, (2), 681-8.

33. Gargalidis-Moudanos, C.; Remaury, A.; Pizzinat, N.; Parini, A., Predominant expression of monoamine oxidase B isoform in rabbit renal proximal tubule: regulation by I2 imidazoline ligands in intact cells. *Mol. Pharmacol.* **1997**, 51, (4), 637-643.
34. Wiest, S. A.; Steinberg, M. I., Binding of [3H]2-(2-benzofuranyl)-2-imidazoline (BFI) to human brain: potentiation by tranylcypromine. *Life Sci.* **1997**, 60, (9), 605-615.
35. Steinberg, M. I.; Wiest, S. A. Potentiation of 2-(2-benzofuranyl)-2-imidazoline binding sites. 97-US181369816828, 19971006., 1998.
36. Steinberg, M. I.; Wiest, S. A.; Pickard, R. T.; Chen, K.; Shih, J. C., Binding of the imidazoline ligand 3H-2-benzofuranyl-2-imidazoline (BFI) to human brain and platelets. Potentiation by tranylcypromine and role of MAO isoforms. *Ann. N. Y. Acad. Sci.* **1999**, 881, (Imidazoline Receptors and Their Endogenous Ligands), 193-198.
37. Wiest, S. A.; Steinberg, M. I., 3H[2-(2-benzofuranyl)-2-imidazoline] (BFI) binding in human platelets: modulation by tranylcypromine. *Naunyn-Schmiedeberg's Arch. Pharmacol.* **1999**, 360, (2), 209-216.
38. Binda, C.; Li, M.; Hubalek, F.; Restelli, N.; Edmondson, D. E.; Mattevi, A., Insights into the mode of inhibition of human mitochondrial monoamine oxidase B from high-resolution crystal structures. *Proc. Natl. Acad. Sci. U S A* **2003**, 100, (17), 9750-9755.

39. Edmondson, D. E.; Binda, C.; Wang, J.; Upadhyay, A. K.; Mattevi, A., Molecular and mechanistic properties of the membrane-bound mitochondrial monoamine oxidases. *Biochemistry* **2009**, 48, (20), 4220-4230.
40. Forneris, F.; Orru, R.; Bonivento, D.; Chiarelli, L. R.; Mattevi, A., ThermoFAD, a Thermofluor-adapted flavin ad hoc detection system for protein folding and ligand binding. *FEBS J.* **2009**, 276, (10), 2833-40.
41. Greenfield, N. J., Using circular dichroism collected as a function of temperature to determine the thermodynamics of protein unfolding and binding interactions. *Nat. Protoc.* **2006**, 1, (6), 2527-35.
42. Ozaita, A.; Olmos, G.; Boronat, M. A.; Lizcano, J. M.; Unzeta, M.; Garcia-Sevilla, J. A., Inhibition of monoamine oxidase A and B activities by imidazol(ine)/guanidine drugs, nature of the interaction and distinction from I2-imidazoline receptors in rat liver. *Br. J. Pharmacol.* **1997**, 121, (5), 901-912.
43. Muley, L.; Baum, B.; Smolinski, M.; Freindorf, M.; Heine, A.; Klebe, G.; Hangauer, D. G., Enhancement of hydrophobic interactions and hydrogen bond strength by cooperativity: synthesis, modeling, and molecular dynamics simulations of a congeneric series of thrombin inhibitors. *J. Med. Chem.* 53, (5), 2126-35.
44. Silvian, L. F.; Wang, J.; Steitz, T. A., Insights into editing from an ile-tRNA synthetase structure with tRNA^{ile} and mupirocin. *Science* **1999**, 285, (5430), 1074-7.
45. Imbrici, P.; Grottesi, A.; D'Adamo, M. C.; Mannucci, R.; Tucker, S. J.; Pessia, M., Contribution of the central hydrophobic residue in the PXP motif of

voltage-dependent K⁺ channels to S6 flexibility and gating properties. *Channels (Austin)* **2009**, 3, (1), 39-45.

46. Newton-Vinson, P.; Hubalek, F.; Edmondson, D. E., High-level expression of human liver monoamine oxidase B in *Pichia pastoris*. *Prot. Expr. Purif.* **2000**, 20, (2), 334-45.

47. Li, M.; Hubalek, F.; Newton-Vinson, P.; Edmondson, D. E., High-level expression of human liver monoamine oxidase A in *Pichia pastoris*: comparison with the enzyme expressed in *Saccharomyces cerevisiae*. *Prot. Expr. Purif.* **2002**, 24, (1), 152-62.

48. Upadhyay, A. K.; Wang, J.; Edmondson, D. E., Comparison of the structural properties of the active site cavities of human and rat monoamine oxidase a and B in their soluble and membrane-bound forms. *Biochemistry* **2008**, 47, (2), 526-536.

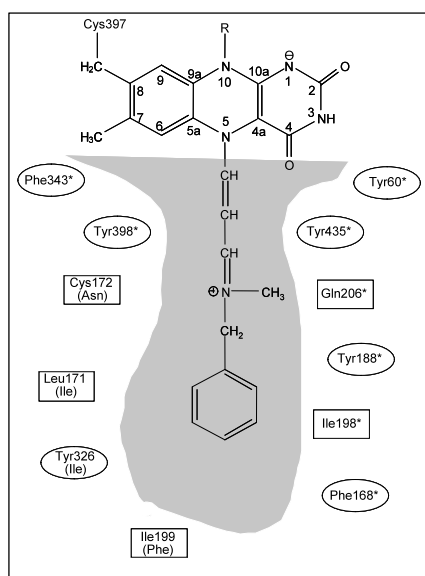
49. Dunn, S. M.; Raftery, M. A., Cholinergic binding sites on the pentameric acetylcholine receptor of *Torpedo californica*. *Biochemistry* **1993**, 32, (33), 8608-15.

Chapter 5.

Elucidating the Role of the 'Gating' Residues of Human MAO B

5.1 Background and Significance

Reports in the literature have shown that long, planar compounds with extended π -conjugation, like 8-(3-chlorostyryl)caffeine (CSC)¹ and *trans,trans*-farnesol², are potent and highly specific inhibitors of human MAO B. However, many of these compounds do not bind to either human MAO A or bovine MAO B. This prompted an investigation into the structural difference between human MAO B and bovine MAO B as well as human MAO A to explain the differential binding of these human MAO B specific inhibitors. Sequence alignment of the human MAO A and human MAO B revealed several nonconserved residues within the active site which include Cys172 and Leu171 in MAO B (Asn181 and Ile180 in MAO A, respectively). These residues do not result in major structural



changes within the active site. However, Ile199 of human MAO B appears to have considerable influence on the shape of the active site (Phe208 in MAO A). With the elucidation of a high-resolution crystal structure of human MAO B, it was observed that the Ile199 varies between two distinct rotational conformations when human MAO B is in complex with inhibitors of varied size.³

Figure 5.1. Cartoon of the pargyline inhibited human MAO B active site. All conserved amino acid residues in both MAO B and MAO A are denoted by an asterisk. The amino acid substitution in MAO A for the nonconserved residues are given in parenthesis.⁴

5.1.1 Identification of the 'Gating' Functions of Ile199.

When smaller inhibitors are bound to the substrate cavity of the active site, the side chain of Ile199 rotates into a closed conformation, which creates a bipartite active site composed of an entrance cavity of $\sim 300 \text{ \AA}^3$ and a substrate cavity of $\sim 400 \text{ \AA}^3$. Conversely with larger inhibitors bound to the active site, the side chain of Ile199 rotates into an open conformation allowing for fusion of the entrance and substrate cavities which results in one large active site cavity $\sim 700 \text{ \AA}^3$ in volume. With the Ile199 rotated into an open conformation the two cavities are fused which allows the enzyme to accommodate larger inhibitors like CSC and farnesol (Figure 5.2).

It was then proposed that the Ile199 amino acid residue acts as a gate between two cavities within the active site. It has also been proposed that this residue serves as a structural determinant for substrate and inhibitor recognition. In contrast, a 'gating' mechanism has not been observed in MAO A; instead, the amino acid residue in the analogous position is Phe208 which is observed in a permanently open state. Figure 5.2 presents eight x-ray crystal structures of human MAO B in complex with both reversible and covalent inhibitors of varying size. Note, that rotation of the Ile199 allows for either fusion or separation of the two cavities of the active site regardless of the inhibition mechanism. The position of the Ile199 is solely dependent on the size of the inhibitor bound.

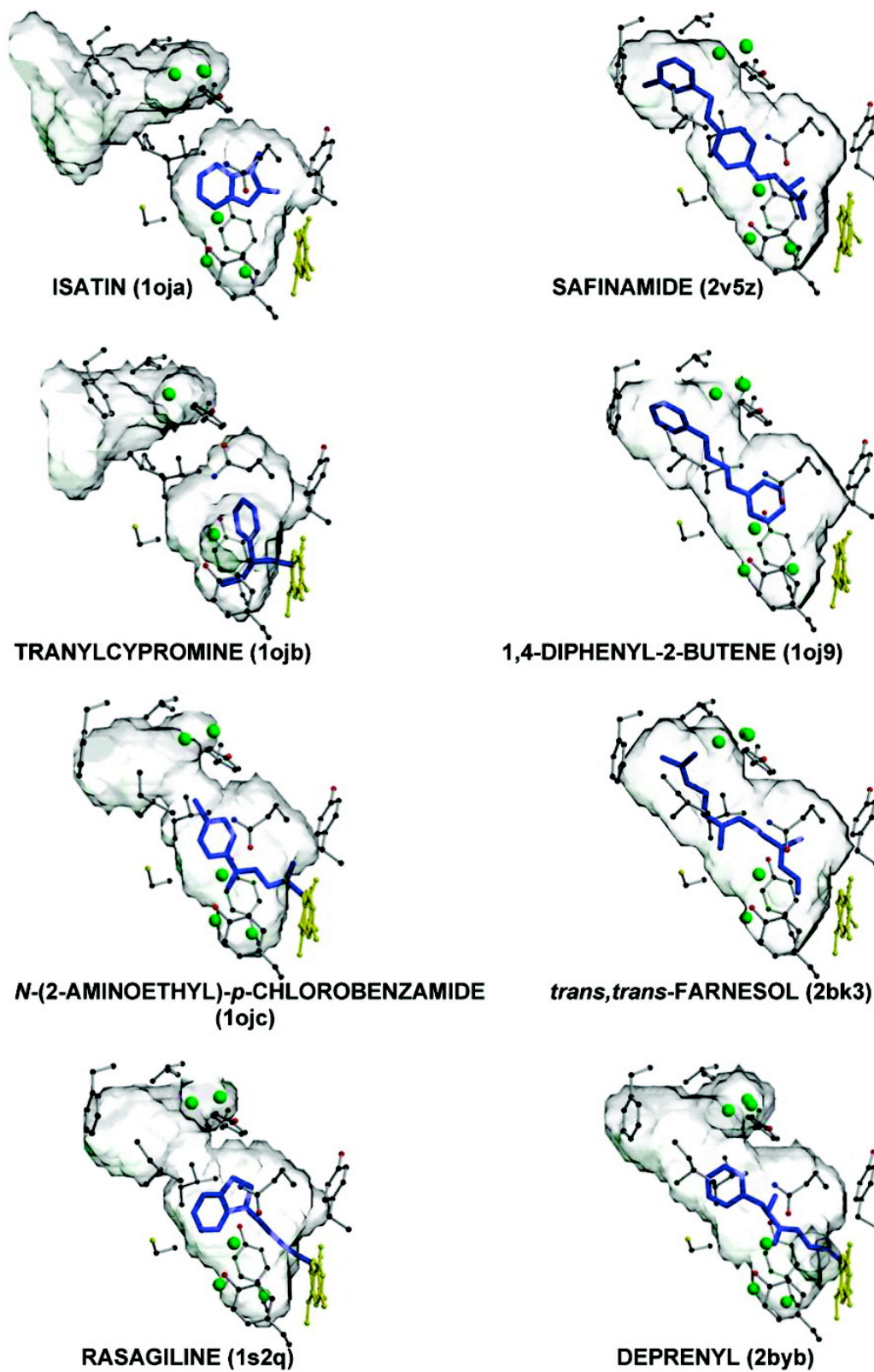


Figure 5.2. Demonstration of the gating mechanism of human MAO B. PDB codes are list in parenthesis.⁵

5.1.2 The Role of Tyr326.

Opposite to the Ile199 “gating” residue is Tyr326 which also displays modest conformational changes based when inhibitors are bound to the active site of human MAO B (Figure 5.3).⁶ The Tyr326 together with the Ile199 serve to separate the entrance cavity and substrate cavity. The entrance cavity is the first site that an inhibitor (or substrate) must pass through to enter the substrate cavity. The substrate cavity houses the covalent flavin cofactor, which is responsible for the oxidative degradation of amines and is the site of covalent modification when mechanism based inhibitors are employed.⁵ These gating residues give human MAO B a bipartite active site.

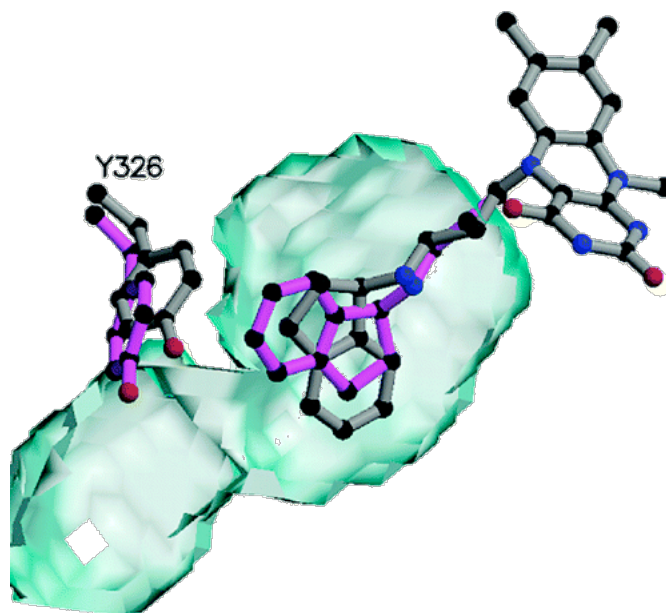


Figure 5.3. Human MAO B in complex with rasagiline.⁶ Comparison of the binding modes of rasagiline and *N*-pargyl-1(S)-aminoindan (S-PAI). The flavin ring, the inhibitor, and the Tyr326 side chain of the rasagiline structure are illustrated in gray. The inhibitor and the Tyr326 side chain of the S-PAI complex are in magenta.

The sequence alignment of human MAO A, bovine MAO B and human MAO B revealed that these enzyme are highly similar (>70%) although they have differences within their respective active sites. Most notably the Ile199 is

substituted for a Phe in bovine MAO B (Phe199). Sequence comparisons of human MAO B and human MAO A show that the analogous position in MAO A is Phe208 (Figure 5.1). While less is known about the structural characteristics of

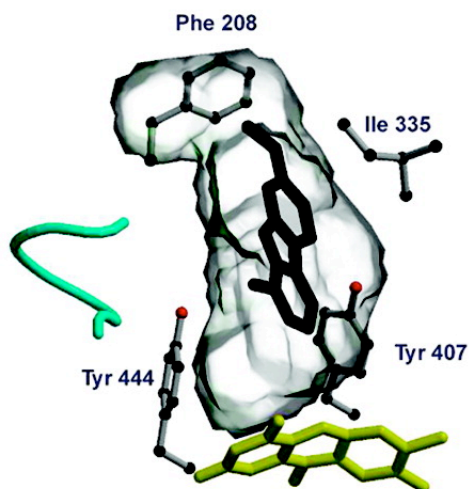


Figure 5.4. Human MAO A co-crystallized with harmine (PDB code 2Z5X).

human MAO A compared to MAO B, some generalizations can be made from the 2.2 Å crystal structure^{7, 8} in combination with SAR studies⁵ of the enzyme. Human MAO A has a monopartite active site of approximately 550 Å³ and preferentially binds bulky-tricyclic fuse-ring system inhibitors like

harmine (Figure 5.4).

5.1.3 Point Mutation of the Ile199 to a Phe.

Equipped with the knowledge that both bovine MAO B and human MAO A have a Phe substituted for an Ile in the 199-position, a series of experiment were conducted by Hubálek and coworkers to elucidate the role of the Ile199 gate.⁹ Point mutation of the Ile199 with a Phe results in a loss in the binding of large reversible MAO B specific inhibitors like 1,4-diphenyl-2-butene, CSC, and farnesol. This mirrored the results with human MAO A and bovine MAO B where there is no observable binding of these inhibitors. X-Ray crystallographic studies illustrate that there is no movement of the Phe199 in the Ile199Phe MAO B mutant, and that this residue is fixed in the open conformation. Smaller

inhibitors, like isatin, bind to the Ile199Phe mutant with similar affinity when compared to WT MAO B. It was determined that the Phe substitution results in increased steric interactions when inhibitors are bound to the active site, and these steric interactions result in abolished binding of larger inhibitors. The results of this study are summarized in Figure 5.5.

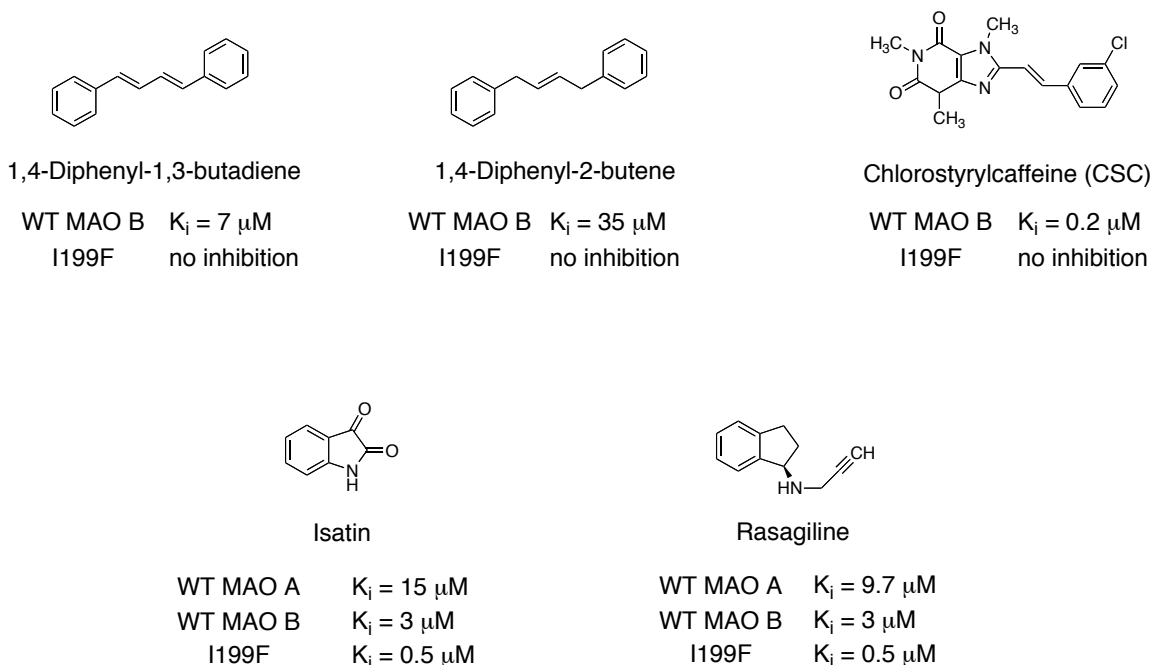


Figure 5.5. Summary of the findings of Hubalek.⁹ Top panel are human MAO B specific inhibitors that do not bind to human MAO A or bovine MAO B. The low panel represents inhibitors that nonspecific, small MAO inhibitors that bind to human MAO A and B as well as bovine MAO B.

5.1.4 Abolishing the Gating Mechanism of Human MAO B.

With the proposal that the Ile199 is a structural determinant of human MAO B, we set out to better understand the role of this gating function in inhibitor and substrate specificity as well as catalytic function. Given substitution of a larger amino acid, like Phe, for the Ile199 creates a more sterically constricted active site, we decided to install an Ala. We postulated that an Ile199Ala point mutation would permanently “open” the gate and allow for tighter binding of MAO

B specific inhibitors that traverse both the entrance cavity and the substrate cavity. With this in mind we constructed, expressed, and purified the Ile199Ala mutant form of MAO B.

5.1.5 Creating a Monopartite Active Site in Human MAO B.

Ile199 together with Tyr326 are involved in creation of a bipartite cavity (Figure 5.6). This bipartite character is proposed to result in the unique inhibition properties of MAO B. To create a more MAO A-like active site we mutated both the Ile199 and Tyr326 to Ala residues thereby further opening the active site of human MAO B to have monopartite character. With this we constructed, expressed, and purified the Ile199Ala-Tyr326Ala double mutant form of MAO B.

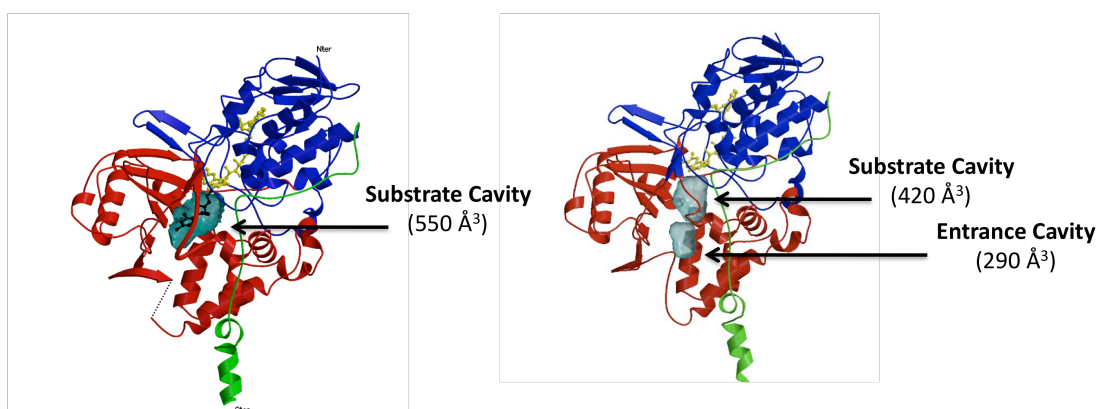


Figure 5.6. Comparison of the active site structures of human MAO A and human MAO B.⁸

5.2 Inhibitions Studies.

To probe the structural properties of both mutants forms we set out to investigate the inhibition properties using: 1. Nonspecific inhibitors; 2. MAO B specific inhibitors; 3. MAO A specific inhibitors; 4. Mechanism based inhibitors. These studies provide a clearer picture of the binding properties of both mutants and provided insights into the shape characteristics of both enzyme cavities.

5.2.1. Investigation of Nonspecific Inhibitors.

There are a number of inhibitors that bind to both MAO A and MAO B. When bound to MAO B these inhibitors competitively bind to the entrance cavity solely (Figure 5.7). Tranylcypromine (TCP) is an irreversible MAOI that binds to MAO A and MAO B in the low micromolar range ($K_i = 34$ and $3 \mu\text{M}$, respectively). This inhibitor competitively inhibits both mutant forms with weaker affinity. In the case of the Ile199Ala-Tyr326A mutant form ($K_i = 17 \pm 3 \mu\text{M}$), TCP binds with the same affinity as WT MAO A while the Ile199Ala mutant ($K_i = 11 \pm 3 \mu\text{M}$) has intermediate properties. Isatin, on the other hand, is a small, reversible, nonspecific MAOI. Isatin competitively binds to the Ile199Ala single mutant ($K_i = 12 \pm 2 \mu\text{M}$) with similar affinity to that of MAO A ($K_i = 15 \mu\text{M}$).³ Isatin binding to the Ile199Ala-Tyr326Ala double mutant ($K_i = 360 \pm 40 \mu\text{M}$) is almost abolished by the double mutation. In contrast, bulky MAOIs like tetrindole favor the double ala mutation ($K_i = 14 \pm 1 \mu\text{M}$) over the single ala mutation ($K_i = 52 \pm 3 \mu\text{M}$).

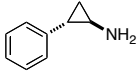
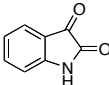
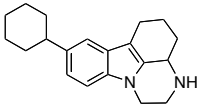
		
Tranylcypromine (TCP)	Isatin	Tetrindole
WT MAO A $K_i = 34 \pm 1 \mu\text{M}$	WT MAO A $K_i = 15 \mu\text{M}^a$	WT MAO A $K_i = 5.3 \pm 0.2 \mu\text{M}^b$
WT MAO B $K_i = 3.0 \pm 0.3 \mu\text{M}$	WT MAO B $K_i = 3 \mu\text{M}^a$	WT MAO B $K_i = 20 \pm 2 \mu\text{M}$
I199A $K_i = 11 \pm 3 \mu\text{M}$	I199A $K_i = 12 \pm 2 \mu\text{M}$	I199A $K_i = 52 \pm 3 \mu\text{M}$
I199A-Y326A $K_i = 17 \pm 3 \mu\text{M}$	I199A-Y326A $K_i = 360 \pm 40 \mu\text{M}$	I199A-Y326A $K_i = 14 \pm 1 \mu\text{M}$

Figure 5.7. Kinetic studies of nonspecific MAO inhibitors. ^adata quoted from reference 9, ^bdata provided by Dr. Jin Wang.

5.2.2 MAO B Specific inhibitors.

Most MAO B specific inhibitors bind to the active site of the enzyme by traversing both the entrance cavity and the substrate cavity which force the

(Figure 5.2). These inhibitors do not bind to WT MAO A. All of the inhibitors investigated in this study bind to WT MAO B and the two mutant forms in a competitive fashion. In the case of the Ile199Ala mutant form, these inhibitors bind with ~4 to 24-fold higher affinity (Figure 5.8). Safinamide ($K_i = 4 \pm 0.6 \mu\text{M}$), CSC ($K_i = 1.7 \pm 0.3 \mu\text{M}$), and farnesol ($K_i = 18 \pm 3 \mu\text{M}$) bind to the Ile199Ala-Tyr326Ala double mutant with ~10-fold weaker affinity. The Ile199Ala-Tyr326Ala double mutant is no longer inhibited by Zonisamide, 1,4-diphenyl-1,3-butadiene, and 1,4-diphenyl-2-butene.

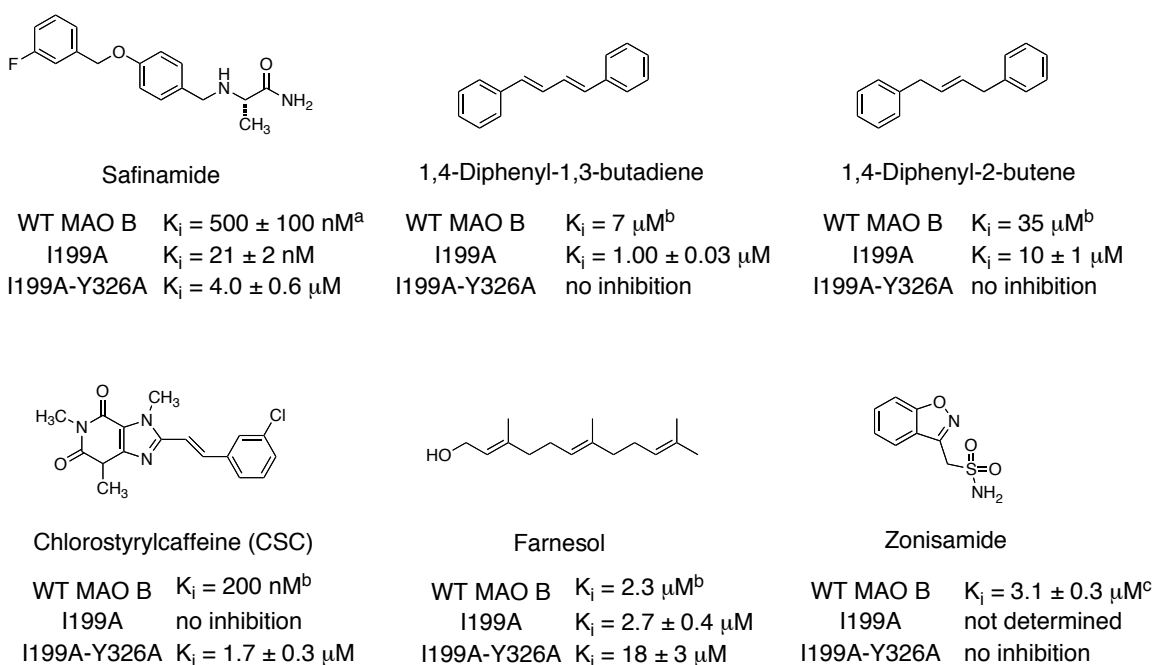


Figure 5.8. Kinetic studies of MAO B specific inhibitors. ^adata quoted from reference 10, ^bdata quoted from reference 9, ^cdata collected by Mrs. Milagros Aldeco.

5.2.3 MAO A Specific Inhibitors.

MAO A specific inhibitors are generally bulkier fused ring systems which can make more interactions with the open monopartite active site of MAO A. While pirlindole, harmine, and methylene blue bind to MAO A with nanomolar affinity, these inhibitors demonstrate very weak binding to WT MAO B. The

affinity, these inhibitors demonstrate very weak binding to WT MAO B. The Ile199Ala mutant shows almost no affinity for these MAO A-specific inhibitors (Figure 5.9). On the other hand, the Ile199Ala-Tyr326Ala double mutant demonstrate properties closer to MAO A. In the case of pirlindole, neither MAO B or the Ile199Ala single mutant are inhibited, while the Ile199Ala-Tyr326Ala double mutant is competitively inhibited by pirlindole in the low nanomolar range ($K_i = 4.1 \pm 0.2 \mu\text{M}$). Harmane binds to both MAO B ($K_i = 140 \pm 47 \mu\text{M}$) and Ile199Ala ($K_i = 165 \pm 17 \mu\text{M}$) with similar affinities while the inhibitory properties of Harmane to the Ile199Ala mutant is much weaker ($K_i = 550 \pm 50 \mu\text{M}$). Methylene blue competitively binds to MAO A ($K_i = 25 \text{ nM}$) and the Ile199Ala-Tyr326Ala mutant ($K_i = 143 \pm 14 \text{ nM}$) in the nanomolar range while the inhibition constant for MAO B in the low micromolar range ($K_i = 1 \mu\text{M}$).

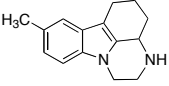
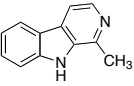
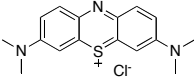
					
Pirlindole		Harmane		Methylene Blue	
WT MAO A	$K_i = 0.92 \pm 0.04 \mu\text{M}^a$	WT MAO A	$K_i = 0.58 \pm 0.02 \mu\text{M}^a$	WT MAO A	$K_i = 0.025 \pm 0.001 \mu\text{M}^a$
WT MAO B	no inhibition	WT MAO B	$K_i = 140 \pm 47 \mu\text{M}$	WT MAO B	$K_i = 1.01 \pm 0.05 \mu\text{M}$
I199A	no inhibition	I199A	$K_i = 550 \pm 50 \mu\text{M}$	I199A	not determined
I199A-Y326A	$K_i = 4.1 \pm 0.2 \mu\text{M}$	I199A-Y326A	$K_i = 165 \pm 17 \mu\text{M}$	I199A-Y326A	$K_i = 0.143 \pm 14 \mu\text{M}$

Figure 5.9. Kinetic studies of MAO A specific inhibitors. ^adata collected by Dr. Jin Wang.

5.2.4 Mechanism Based Inhibitors.

Mechanism based inhibitors exploit the general reactivity of the enzyme by mimicking a substrate. Three examples of such inhibitors are identified in this section. L-Deprenyl⁴, rasagiline⁶, and mofegiline¹¹ are MAO B specific mechanism based inhibitors that have been investigated for the treatment of Parkinson's disease. These inhibitors demonstrate low micromolar or nanomolar

affinity for MAO B. While the Ile199Ala mutant form of MAO B binds to L-deprenyl ($K_i = 8 \pm 1 \mu\text{M}$), rasagiline ($K_i = 1.6 \pm 0.1 \mu\text{M}$), and Mofegiline ($K_i = 129 \pm 2 \text{ nM}$) with similar affinity as WT MAO B, the Ile199Ala-Tyr326Ala MAO B double mutant has considerably weaker affinity for these inhibitors. The Ile199Ala-Tyr326Ala mutant binds these inhibitors in the mid-micromolar range (Figure 5.10).

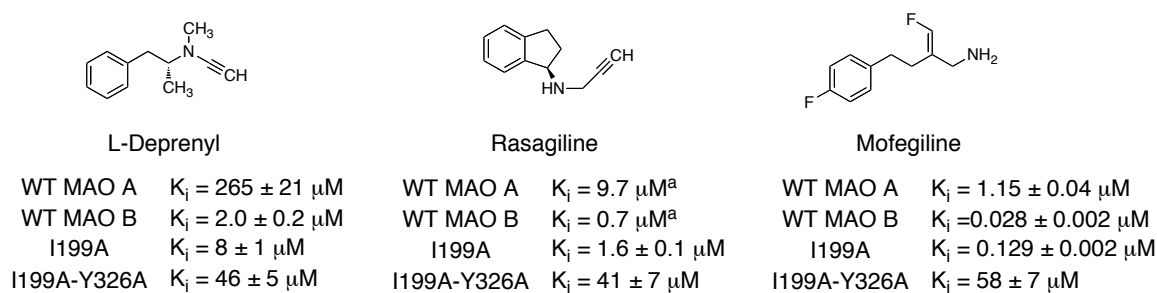


Figure 5.10. Kinetic studies of mechanism based inhibitors. ^adata quoted from reference 12.

5.2.5 Aminoindans: Small reversible Inhibitors.

Rasagiline metabolites, N-methyl-1(R)-aminoindan (R-MAI) and (R)-aminoindan (R-AI), act as weak inhibitors of MAO A and MAO B (Figure 5.11). The Ile199Ala mutant is weakly inhibited by R-MAI ($K_i = 44 \pm 7 \mu\text{M}$) and R-AI ($K_i = 99 \pm 3 \mu\text{M}$) competitively. The Ile199Ala-Tyr326Ala double mutation results in a dramatic loss in binding of R-MAI ($K_i = 360 \pm 30 \mu\text{M}$) and R-AI ($K_i = 591 \pm 76 \mu\text{M}$).

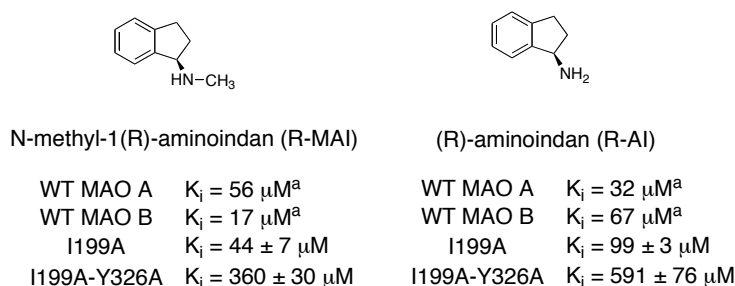


Figure 5.11. Kinetic studies of rasagiline metabolites. ^adata quoted from reference 13.

5.3 Discussion

5.3.1 Binding Properties of the Ile199Ala MAO B Mutant.

When small inhibitors like, isatin and TCP, are bound to WT MAO B, the Ile199 gate rotates to a closed conformation (Figure 5.2).⁹ Permanently opening the 'gate' through point mutation of the Ile199 to an Ala results in 3-4-fold reduced binding of smaller inhibitors that bind to only the entrance cavity. MAO B specific inhibitors that traverse both the entrance cavity and the substrate cavity force the Ile199 'gate' to rotate into an open conformation which allows for fusion of the two cavities (Figure 5.2). As expected, the Ile199Ala mutation has a positive effect on the binding of this class of inhibitors. These compounds inhibit the mutant form of MAO B up to 24-fold better than WT. To our surprise, CSC does not bind to the Ile199Ala mutant. This may be due to the Tyr326 occupying a different conformation when the Ile199 is absent due to less restriction on the space of the active site. Clearly the increased freedom of the Tyr326 residue has deleterious effects on CSC binding. MAO A specific inhibitors do not bind to the MAO B single mutant with increased affinity. This is not surprising given that these inhibitors are designed to bind to a monopartite active site. There is little affect on the binding properties of mechanism based inhibitors to the Ile199Ala mutant. These inhibitors bind to the enzyme with similar affinity to that of WT MAO B. Interestingly, R-MAI and R-AI bind to the single mutant with much lower affinity. Like isatin and TCP, these inhibitors bind exclusively to substrate cavity WT MAO B, and the Ile199 'gating' residue is found in a closed conformation by X-ray crystallography.¹⁴ These data suggest that point mutation of the Ile199

results in enhance binding of MAO B specific inhibitors that bind to both the substrate and entrance cavities, while destabilizing the binding of smaller inhibitors that bind exclusively to the substrate cavity.

5.3.2 Binding Properties of the Ile199Ala-Tyr329Ala MAO B Mutant.

Investigations of inhibitor-binding to the double mutant reveals that this mutant form of MAO B has more monopartite character than WT MAO B. MAO A has a monopartite active site and as such analysis of MAO A specific inhibitors can provide insights into the character of the Ile199Ala-Tyr326Ala active site. MAO A specific inhibitors bind to the double mutant with increased affinity relative to WT MAO B. Interestingly, smaller inhibitors like TCP, isatin, R-AI, and R-MAI bind to the double mutant considerably weaker (up to 120-fold weaker binding). MAO B specific inhibitors which favor a bipartite active site bind to the double mutant with ~10-fold weaker affinity or not at all. This phenomenon may be due to altered hydration compared to of the Ile199Ala-Tyr326Ala active site as nonpolar inhibitors like 1,4-diphenyl-1,3-butadiene and 1,4-diphenyl-2-butene do not bind to the double mutant while inhibitors that are decorated with heteroatoms retain binding to the double mutant.

5.4 Structural Studies.

To empirically assess the effect that these two mutations have on the shape of the active site, both mutants were co-crystallized with inhibitors bound to the active site. Crystallization of the mutant forms was accomplished using the published protocol for WT MAO B.⁴

5.4.1 Ile199Ala MAO B Structural Studies.

The Ile199Ala mutant form of MAO B was co-crystallized with nanomolar inhibitor, safinamide, to a 2.2 Å resolution. The crystal structure clearly shows that there are no alterations to the active site geometries other than the Ile side chain of the Ile199 is replaced with a methyl group. Figure 5.12 illustrates safinamide adopting the same binding mode whether bound to the single mutant or WT enzyme. Safinamide occupies both the entrance and substrate cavity with the Tyr326 demonstrating no conformational changes. The TCP-inhibited Ile199Ala mutant was co-crystallized in the presence of 2-BFI and diffracts to 2.1 Å resolution. The details of 2-BFI binding to the Ile199Ala mutant are discussed extensively in chapter 5.4.

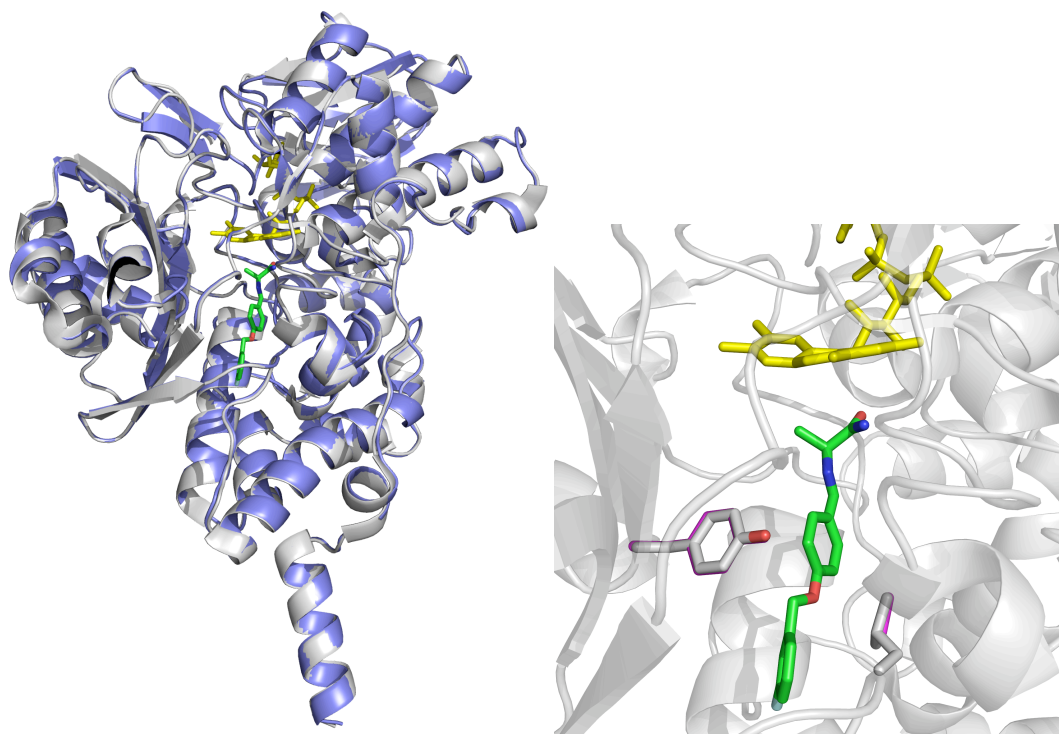


Figure 5.12. X-ray crystal structure of human MAO B (grey) overlapped with MAO B Ile199Ala mutant (lavender). Ile199, and Tyr326 of WT MAO B are represented in grey; safinamide in green; Ala199 and Try326 of the MAO B Ile199Ala mutant are depicted in magenta. The flavin cofactor shown in yellow.

5.4.2 Ile199Ala-Tyr326Ala MAO B Structural Studies.

The 2.2 Å resolution x-ray crystal structure of the Ile199Ala-Tyr326Ala MAO B mutant in complex with the nanomolar inhibitor, methylene blue, has been determined (Figure 5.13). The active site is no longer divided by the side chains of Ile199 or Tyr326 allowing for one large monopartite active site cavity. Methylene blue binds near the flavin ring of the FAD cofactor and extends into the entrance cavity.

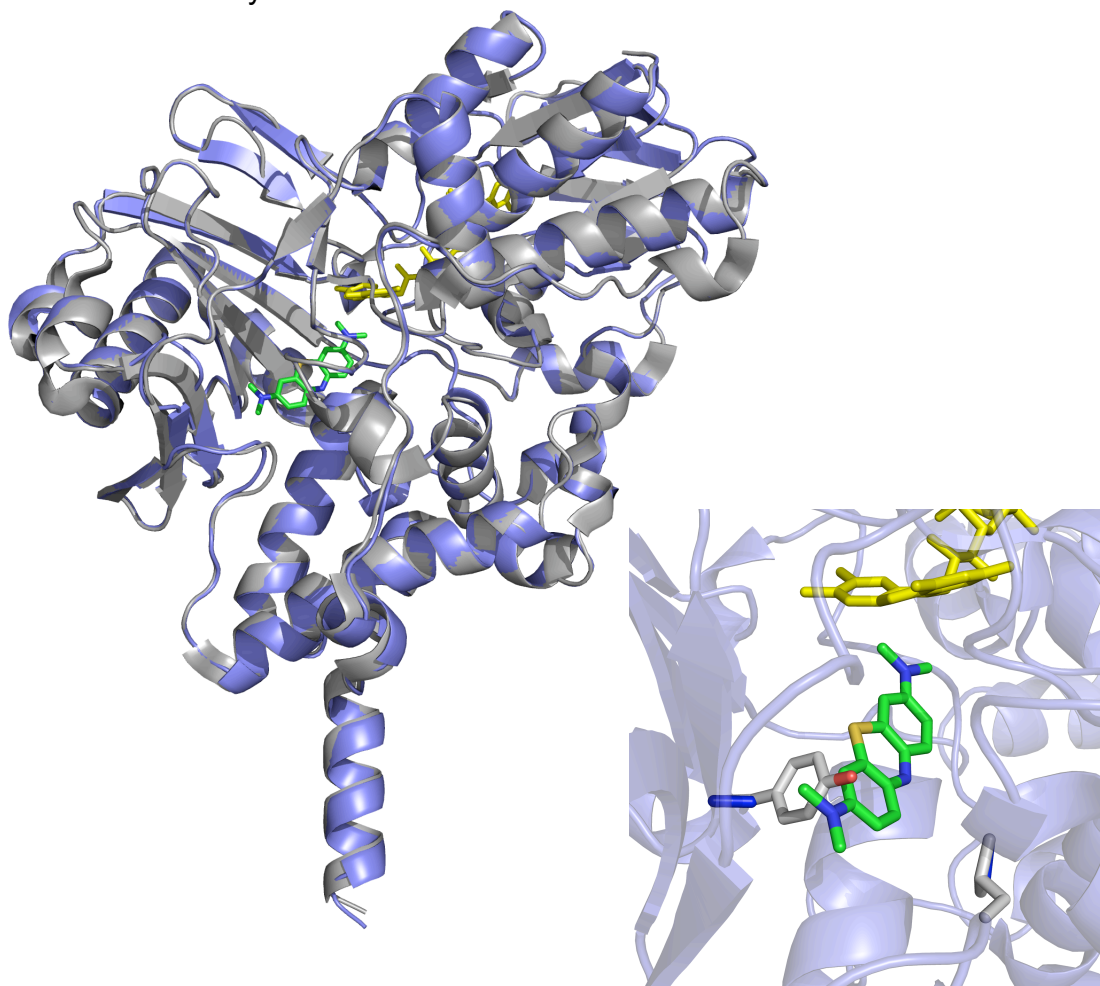


Figure 5.13. X-ray crystal structure of human MAO B (grey) overlapped with MAO B Ile199Ala-Tyr326Ala mutant (lavender). Methylene blue is shown in green; Ala199, and Ala326 of MAO B Ile199Ala-Tyr326Ala mutant are represented in blue; and Ile199 and Try326 of WT MAO B are depicted in grey. The flavin cofactor shown in yellow.

5.5 Activity Studies of the Ile199Ala MAO B Mutant.

Table 5.1. Substrate specificity of the Ile199Ala mutant form of MAO B and comparison with WT MAO A and WT MAO B

Substrate	Enzyme	k_{cat}	K_m (μM^{-1})	k_{cat}/K_m ($\text{min}^{-1}\mu\text{M}^{-1}$)
<i>p</i> -(CO ₂ H)-Benzylamine ^a	H MAO B	No reactivity	-	-
	H MAO A	0.84 ± 0.03	64 ± 3	0.013 ± 0.0008
	Ile199Ala	No reactivity	-	-
Kynuramine ^b	H MAO B	96 ± 1	27 ± 2	3.55 ± 0.27
	H MAO A	146 ± 1	118 ± 4	1.24 ± 0.04
	Ile199Ala	88 ± 2	94 ± 8	0.936 ± 0.082
Dopamine ^c	H MAO B	65 ± 2	128 ± 15	0.51 ± 0.06
	H MAO A	71 ± 4	240 ± 42	0.30 ± 0.06
	Ile199Ala	208 ± 5	10,300 ± 1,300	0.0201 ± .0025
Serotonin ^c	H MAO B	33 ± 2	2,270 ± 310	0.015 ± 0.002
	H MAO A	182 ± 8	295 ± 46	0.62 ± 0.10
	Ile199Ala	No reactivity	-	-

^aDetermined spectrophotometrically using Amplex Red/horseradish peroxidase couple assay.

^bDetermined spectrophotometrically at $\lambda_{316\text{nm}}$.

^cDetermined by monitoring oxygen consumption using oxygen probe.

To examine the effects of the Ile199Ala point mutation on the catalytic properties of the enzyme several substrates were tested using a 50 mM potassium phosphate buffer system at pH 7.5 with 0.5% (w/v) reduced triton. *p*-CO₂H-benzylamine is a MAO A specific substrate which does not react with MAO B. This substrate is also unreactive with the Ile199Ala mutant. The Ile199Ala mutant oxidizes kynuramine, although it displays poorer binding (the K_m values is increased 3.5-fold in comparison to WT MAO B). Interesting, dopamine is

oxidized 3x faster by the mutant compared to WT; however, the K_m is increased 80-fold which results in overall decrease in catalytic efficiency. The Ile199Ala mutant does not oxidize serotonin.

To survey the effects of substrate size on substrate binding, a series of benzylic amines were investigated. While the rate of the reaction is relatively unchanged upon increasing the methylene linker, the K_m decreases (binding to the mutant increases) as the length of the linker increases. Binding is favorable with extended substrates leading to an overall increase in catalytic efficiency. A similar trend is not observed with WT MAO B or WT MAO A.

Table 5.2. SAR study of increasing the length of the methylene linker in benzylic amines.

Substrate	Enzyme	k_{cat}	K_m (μM^{-1})	k_{cat}/K_m ($min^{-1}\mu M^{-1}$)
Benzylamine ^a	H MAO B	300 ± 8	150 ± 27	2.0 ± 0.4
	H MAO A	2.50 ± 0.15	1080 ± 50	0.0025 ± 0.0002
	Ile199Ala	228 ± 13	2133 ± 409	0.107 ± 0.021
Phenylethylamine ^b	H MAO B	172 ± 3	9.4 ± 0.9	18 ± 2
	H MAO A	54 ± 1	1481 ± 80	0.36 ± 0.02
	Ile199Ala	123 ± 2	40 ± 2	3.1 ± 0.2
4-Phenylbutylamine ^b	H MAO B	110 ± 5	19 ± 3	5.8 ± 0.8
	H MAO A	-	-	$K_i = 31 ± 5$
	Ile199Ala	135 ± 3	8.9 ± 0.7	15 ± 1

^aDetermined spectrophotometrically at λ_{250nm} .

^bDetermined spectrophotometrically using Amplex Red/horseradish peroxidase couple assay.

While the Ile199Ala MAO B mutant retains catalytic activity similar to that of WT MAO B, the substrate recognition of the mutant is severely affected. These data further illustrate that the Ile199 'gating' residue acts as a structural

determinate for substrate and inhibitor recognition. Interestingly, this residue does not appear to have any catalytical function rather it is vital to substrate recognition and binding.

5.6 Activity Studies of the Ile199Ala-Tyr326Ala MAO B Mutant.

To examine the effects of the Ile199Ala-Tyr326Ala point mutations on the catalytic properties of the enzyme, the oxidation of several substrates was investigated using a 50 mM potassium phosphate buffered system at pH 7.5 with 0.5% (w/v) reduced triton. Phenylethylamine ($K_m = 703 \mu\text{M}$), 3-phenylpropylamine ($K_m = 355 \mu\text{M}$), and 4-phenylbutylamine ($K_m = 55 \mu\text{M}$) demonstrate decreasing K_m values when increasing the linker distance between the amine and the benzene ring, similar to the observed trend for the Ile199Ala single mutant. Oxidation of kynuramine also displays weaker catalytic efficiency ($k_{\text{cat}}/K_m = 0.22 \pm 0.02 \text{ min}^{-1}\mu\text{M}^{-1}$) compared to WT MAO B ($k_{\text{cat}}/K_m = 3.55 \pm 0.27 \text{ min}^{-1}\mu\text{M}^{-1}$). Benzylamine is a poor substrate for the double mutant with a K_m value that exceeded the solubility of the substrate in water (estimated at 69 mM by fitting to the Michaelis-Menten equation). The second order rate constant was determined to be 0.00158 hr^{-1} . Interestingly, *para*-trifluoromethylbenzylamine is a competent substrate for the double mutant unlike benzylamine. This was suspected to be due to the lower pK_a of the amine of *para*-trifluoromethylbenzylamine ($\text{pK}_a \sim 8.8$) relative to benzylamine ($\text{pK}_a \sim 9.3$). This prompted an investigation of the effects of pH on the rate of catalysis by WT MAO B and the two mutant forms.

Table 5.3. Substrate investigation

Substrate	k_{cat}	K_m (μM^{-1})	k_{cat}/K_m ($\text{min}^{-1}\mu\text{M}^{-1}$)
Benzylamine ^a	2nd order rate constant determined to be $0.00158 \pm 0.00006 \text{ hr}^{-1}$		
Phenylethylamine ^b	110 ± 2	703 ± 58	0.16 ± 0.01
3-Phenylpropylamine ^b	141 ± 1	355 ± 9	0.40 ± 0.01
4-Phenylbutylamine ^b	142 ± 1	55 ± 2	2.6 ± 0.1
Kynuramine ^c	64 ± 2	289 ± 23	0.22 ± 0.02
<i>p</i> -CF ₃ -Benzylamine ^d	265 ± 9	836 ± 89	0.32 ± 0.04

^aDetermined spectrophotometrically at $\lambda_{250\text{nm}}$. Enzyme saturates $\sim 69 \text{ mM}$, which exceeds the limits of the solubility of benzylamine in water. Second order rate constant was determined to be $2.63 \times 10^{-5} \pm 9.9 \times 10^{-7} \text{ min}^{-1}$. ^bDetermined spectrophotometrically using Amplex Red/horseradish peroxidase couple assay. ^cDetermined spectrophotometrically at $\lambda_{316\text{nm}}$. ^dDetermined spectrophotometrically at $\lambda_{243\text{nm}}$.

5.7 pH Studies

It is well established that only deprotonated amines are oxidized by MAO.¹⁵ Studies on the pH dependence of MAO A catalysis have demonstrated that the pK_a of amine substrates are reduced by $\sim 2 \text{ pK}_a$ units on binding to the active site.¹⁶ Steady-state analysis and reductive half reactions monitored by stopped-flow were in excellent agreement illustrating the reduction of the amine pK_a during catalysis. Plots of k_{red}/K_s (and k_{cat}/K_m) versus pH exhibit a bell-shape pH profile at pH 6.5 to 9.5 demonstrating a favorable deprotonation step in the pH range 7.4 to 8.4, which is optimal for catalysis. An unfavorable deprotonation step occurs at higher pH (pH of ~ 8.5 to 9.5), which the authors attribute to the deprotonation of a site on the enzyme.

Because analogous studies have not been conducted describing the pH dependence of MAO B catalysis, an investigation of the pH profile of the WT,

Ile199Ala, and Ile199Ala-Tyr326Ala MAO B enzymes were carried out. Steady-state investigations of the pH dependence of benzylamine (pK_a 9.33) and *p*-CF₃-benzylamine (pK_a 8.75) oxidation was explored from pH 7.0-9.5. Benzylamine and *p*-CF₃-benzylamine were chosen because of their differential pK_a values (~ 0.58 pK_a units) and relatively similar structure.

The pH dependence of k_{cat} is illustrated in Figure 5.13. WT MAO B shows a strong pH dependence with a calculated pK_a of 7.3 ± 0.2 . The pH dependence of benzylamine oxidation by WT MAO B is in excellent agreement with the reported values for WT MAO A (pH profile of k_{cat} results in a calculated pK_a values of 7.9 ± 0.1).¹⁶ This value is ~ 2 pK_a units lower than the pK_a of benzylamine (pK_a of benzylamine·HCl is ~ 9.33). To our surprise, the Ile199Ala MAO B mutant demonstrates a similar pH dependence (see the overlap of the black and blue curves in Figure 5.14) and results in a pK_a of 7.6 ± 0.1 . Due to the high saturation values for benzylamine at low pH for the Ile199Ala-Tyr326Ala MAO B mutant, accurate fits to the data for pK_a calculations could not be extrapolated.

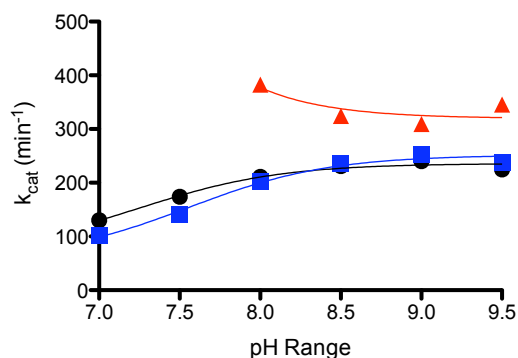


Figure 5.14. pH dependence of k_{cat} using benzylamine as a substrate for: MAO B (\bullet , black), MAO B Ile199Ala (\blacksquare , blue), MAO B Ile199Ala-Tyr326Ala (\blacktriangle , red).

The pH dependence of V/K is illustrated in Figure 5.15. The V/K term describes all of the catalytic step up to and including C-H bond cleavage. This is a very useful description of the role of pH on the binding (K_m) of the substrate. Interestingly, the catalytic efficiency of WT MAO B exhibits a strong sigmoidal pH dependence with a calculated pK_a of 8.72 ± 0.04 indicating that only one deprotonation step occurs in this pH range. The pH profile of V/K of WT MAO B is unlike that of WT MAO A which exhibits a bell-shaped curve suggesting an unfavorable deprotonation step at high pH. Comparison of the calculated pK_a of the first deprotonation step of WT MAO A (pK_a of 8.5 ± 0.1) and the pK_a of the deprotonation step of WT MAO B (pK_a of 8.72 ± 0.04) show excellent agreement.

To our surprise, the Ile199Ala MAO B and the Ile199Ala-Tyr326Ala MAO B mutants demonstrate a similar pH dependence of V/K and result in pK_a values of 9.1 ± 0.1 and 8.2 ± 0.7 , respectively. To aid in comparison of the pH profiles of the three enzymes, the $\text{Log}(V/K)$ pH dependence is shown in Figure 5.15B. Note that the Ile199Ala-Tyr326Ala MAO B mutant appears to reduce the pK_a of benzylamine more efficiently than the Ile199Ala MAO B mutant. These data together illustrate that the poorer catalytic activity of the Ile199Ala and Ile199Ala-Tyr326Ala mutants are not a result of inability of the enzyme to deprotonate benzylamine. Instead the increase in catalytic efficiency appears to be K_m dependent.

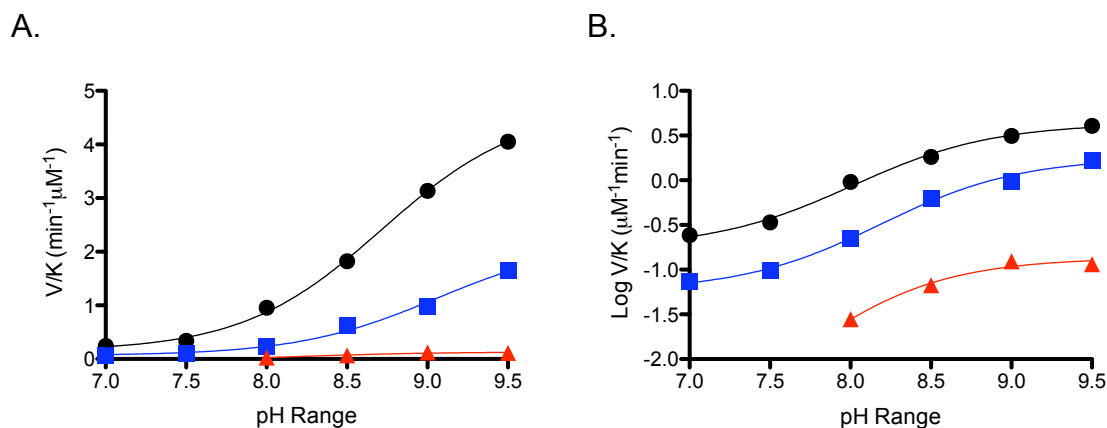


Figure 5.15. pH dependence of V/K using benzylamine as a substrate for: MAO B (●, black), MAO B Ile199Ala (■, blue), MAO B Ile199Ala-Tyr326Ala (▲, red). A. pH profile for V/K . B. pH profile for $\text{Log}(V/K)$.

While these results are compelling, the uses of steady-state measurements may raise questions about the interpretation of these results. The K_m for O_2 for WT MAO B is $\sim 330 \mu\text{M}$ when using benzylamine as a substrate. Because the air saturation of water at 25°C is $\sim 240 \mu\text{M}$, the reaction of WT MAO B with benzylamine is about half velocity. Using *p*-CF₃-benzylamine as a substrate, the K_m for O_2 is decrease to $12 \pm 1 \mu\text{M}$ for both WT MAO B and the Ile199Ala MAO B mutant (the K_m for O_2 has not been determined for the Ile199Ala-Tyr326Ala mutant form of MAO B). Furthermore, the $\text{p}K_a$ of *p*-CF₃-benzylamine is 8.75, which is $\sim 0.6 \text{ p}K_a$ units lower than benzylamine. With this in mind, the pH dependence of *p*-CF₃-benzylamine oxidation was explored using the three enzymes described above.

The effects of binding of the substrate to the active site have modest effects on the $\text{p}K_a$ of *p*-CF₃-benzylamine (Figure 5.16). When calculating the $\text{p}K_a$ from the pH dependence of V/K , the calculated $\text{p}K_a$ for WT MAO ($\text{p}K_a$ of 8.6 ± 0.1) and Ile199Ala MAO B mutant ($\text{p}K_a$ of 8.5 ± 0.3) are very similar.

Surprisingly, the Ile199Ala-Tyr326Ala MAO B mutant (pK_a of 8.1 ± 0.3) reduced the pK_a of the amine more efficiently.

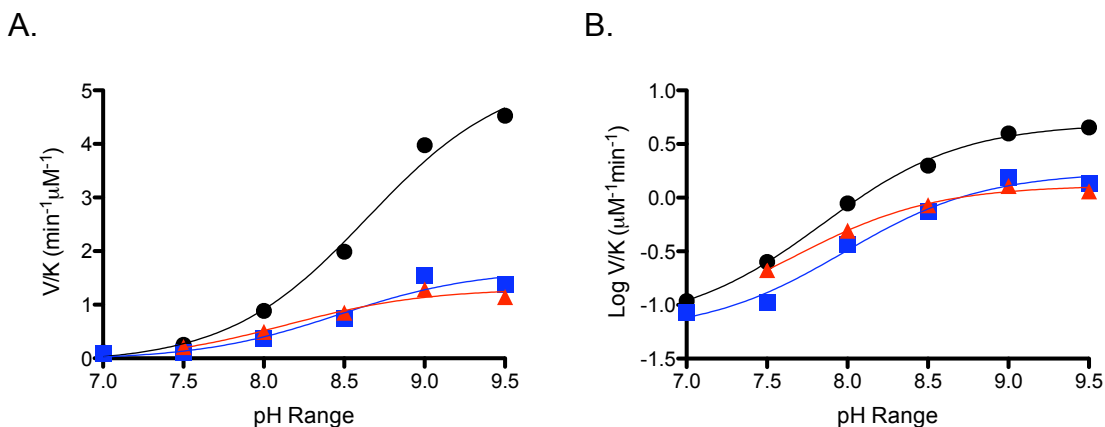


Figure 5.16. pH dependence of V/K using pCF_3 -benzylamine as a substrate for: MAO B (●, black), MAO B Ile199Ala (■, blue), MAO B Ile199Ala-Tyr326Ala (▲, red). A. pH profile for V/K . B. pH profile for $\text{Log}(V/K)$.

Figure 5.17 illustrates the pH dependence of k_{cat} for the three enzyme. The double mutant form of MAO B displays the most dramatic pH dependence on enzyme turnover. A 2.2-fold increase in k_{cat} is observed from pH 7.5 to pH 9.5 which results in a calculated pK_a value of 7.9 ± 0.1 . The pK_a value calculate from WT MAO B data is one pK_a unit higher at 8.9 ± 0.4 . Data obtained from investigation of the Ile199Ala MAO B mutant is comparable to WT MAO B (pK_a 8.17 ± 0.09).

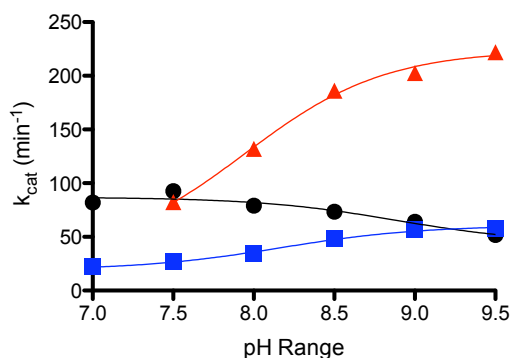


Figure 5.17. pH dependence of k_{cat} using pCF_3 -benzylamine as a substrate for: MAO B (●, black), MAO B Ile199Ala (■, blue), MAO B Ile199Ala-Tyr326Ala (▲, red).

5.8 Mechanistic studies:

Quantitative structure-activity relationships (QSAR) are used to describe how changes in structure elicit analogous changes in reactivity. Hammett identified a relationship between the ionization energies of benzoic acids and electronic effects of the substituents.^{17, 18} Hansch produced a compilation of experimentally derived parameters which have become widely used in comparisons of structure and reactivity.¹⁹ Derived from earlier studies by Hammett, Hansch derived an equation (1) to relate the binding or rates of reaction of substrates to an enzyme.

$$\log k \text{ (or } K_d) = \rho (\sigma) + A (\pi) + B (V_w) \text{ (or } E_s) + C \quad (1)$$

In this equation, k is the rate of product formation of enzyme turnover. K_d is the dissociation constant and describes the binding of the ligand to the active site. The value of ρ is the calculated reaction constant that is determined by the slope of the line produced from plots of the data. The parameter σ is the Hammett constant, which describe the electronic character. A positive value denotes electron-withdrawing properties while a negative value is characteristic

of electron-donation. The effects of the σ may be interpreted as an effect on the ionization energy of the compound or can describe intermolecular forces between the ligand and the receptor such as H-bonding, charge-charge, or charge-dipole interactions. The hydrophobic constant, π , is defined as $\log P_x - \log P_H$ where P_x is the partition coefficient of the substituent and P_H is the unsubstituted reference compound (ie. hydrogen). To account for the size of the substituent the term V_w is employed. V_w describes the van der Waals volume of the substituent which is calculated from the atomic radius. Use of E_s can also be employed for determining the steric contribution of the substituent. E_s is the Taft steric constant which is derived from the steric hinderance that is associated with the acid catalyzed hydrolysis of α -substituted acetates. Both E_s and V_w are complimentary tools when relating the steric contributions of a substituent to reaction rate or ligand bind.

In the 1990s the Edmondson laboratory set out to determine if the rate of MAO catalysis was dependent on the electronic character of the substrate. Using Hammett plots would provide additional evidence in support of a hydride mechanism (electron-donating group enhanced) or a H⁺ abstraction mechanism (electron-withdrawing group enhanced) by either decreasing the nucleophilic character of the hydride or increasing the acidity of the proton of the substrate, respectively (Figure 5.18). Upon comparison of α,α -dideuterobenzylamine analogues, all substrates demonstrated a primary kinetic isotope effect confirming that C-H bond cleavage is the rate-limiting step during catalysis. The pK_a of the amine substrates are corrected from the final data analysis.

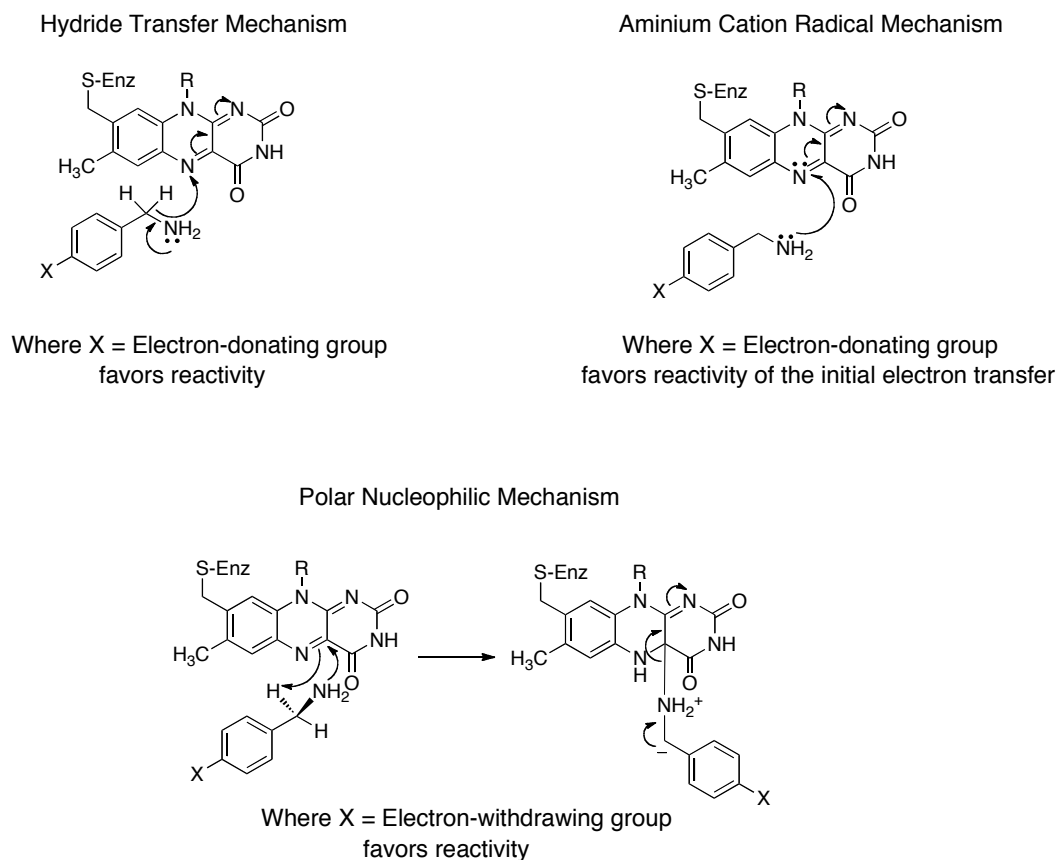


Figure 5.18. Comparison of effects of *para*-substitutions on the rates of reaction expected for the three proposed mechanisms of MAO oxidation of benzylamine

When probing for a Hammett relationship for the oxidation of *para*-substituted benzylamine analogues, human liver MAO A and bovine liver MAO B provide differential results (Figure 5.19). This is a surprising result given that MAO A and MAO B are thought to demonstrate similar catalytic function. Human liver MAO A shows a strong positive correlation (ρ value of ~ 2) between the electron-withdrawing character of the substituent and the rate of catalysis. Conversely, MAO B does not show a QSAR relationship.

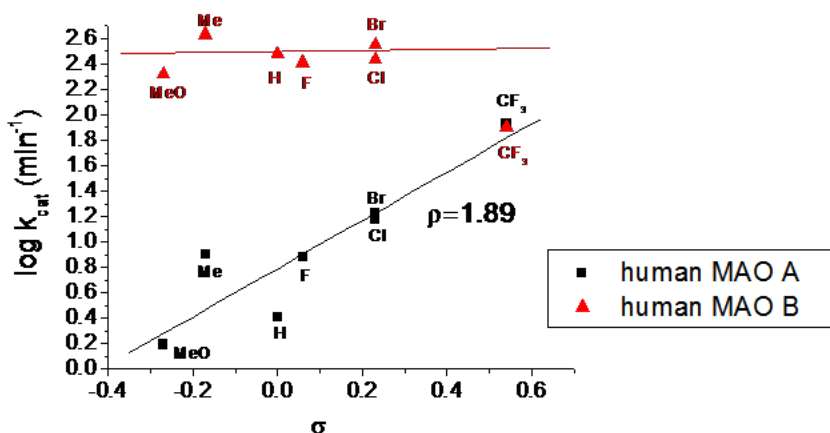
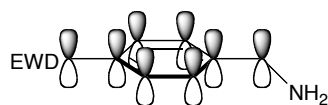


Figure 5.19. Effects of *para*-substituent on the rate of oxidation of the substrate. The QSAR relationship of bovine WT MAO B is illustrated in red while human WT MAO A is illustrated in black.

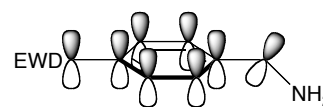
The lack of QSAR effect for MAO B was suspected to be due to the bipartite nature of the active site. This prevents full π -orbital overlap and does not allow for induction of the electronic effect to be transferred to the α -protons of the amine. The monopartite nature of the WT MAO A active site facilitates full electronic induction of the electron-withdrawing group (Figure 5.20).

α -protons are coplanar with aromatic ring



π overlap in the MAO A active site binding pocket

no π overlap due to the α -protons being out of plane



π overlap in the MAO B active site binding pocket

Figure 5.20. Out of plane interactions of *para*-substituted benzylamine analogues.

Using the Ile199Ala and Ile199Ala-Tyr326Ala mutant forms of MAO B as mechanistic probes, the effects of electron-withdrawing substituents in the *para*-position were explored. Abolishing the gating function of MAO B was proposed to

aid in the overlap of the π -orbitals allowing for full transmission of electronic character. Similarly, the Ile199Ala-Tyr326Ala double mutant was investigated due to its monopartite character, which parallels that of MAO A. Because MAO A exhibits strong dependence on electronic properties of the substrate, it was proposed that the Ile199Ala-Tyr326Ala would demonstrate a similar dependence.

5.8.1 QSAR Effects: Ile199Ala MAO B Mutant

Table 5.4 summarizes the catalytic properties for the Ile199Ala MAO B mutant with *para*-substituted benzylamine analogues. Assays were collected in 50 mM potassium phosphate buffer at pH 7.5 with 0.5% (w/v) reduced triton. The Ile199Ala MAO B mutant exhibits a primary kinetic isotope effect (KIE) when comparing both the $^Dk_{\text{cat}}$ (KIE of 2 to 7) and $^D(V/K)$ (KIE of 4 to 10).

Table 5.4. Kinetic properties of the Ile199Ala mutant using *para*-substituted benzylamine analogues.

<i>Para</i>- Substituent	α,α-Proteo		α,α-Deuteuro	
	$k_{\text{cat (H)}} \text{ (min}^{-1}\text{)}$	$K_{\text{m (H)}} \text{ (}\mu\text{M)}$	$k_{\text{cat (D)}} \text{ (min}^{-1}\text{)}$	$K_{\text{m (D)}} \text{ (}\mu\text{M)}$
H	176	2133	60	2603
CF ₃	34	123	4.9	173
Br	183	189	52	186
Cl	222	237	95	350
F	272	1821	134	3254
Me	149	787	31	573
OMe	175	1144	41	1300

Table 5.5. Kinetic isotope effects for the oxidation benzylamine analogous with the Ile199Ala mutant.

Para-Substituent	$^D k_{cat}$	$^D(V/K)$
	$^D k_{cat} = k_{cat(H)}/k_{cat(D)}$	$^D(V/K) = [k_{cat(H)} / K_m(H)] / [k_{cat(D)} / K_m(D)]$
H	3	4
CF ₃	7	10
Br	4	3
Cl	2	3
F	2	4
Me	5	4
OMe	4	5

Table 5.6. Calculated K_d of the substrate for the Ile199Ala mutant

Para-Substituent	Parameter		K_d (corrected) (μM)
	pK_a	K_d (corrected) = K_d (observed) / 1+ antilog (pK _a - pH)	
H	9.33	41	
CF ₃	8.75	9.7	
Br	9.08	4.7	
Cl	9.08	11.1	
F	9.27	78	
Me	9.52	4.9	
OMe	9.63	9.9	

The binding constants (K_d) of the benzylamine analogues to the Ile199Ala mutant were calculated and corrected for pK_a. The calculated K_d ranged from ~5 μ M to 80 μ M (Table 5.6). Larger *para*-substituents, like a CF₃-group, have a positive effect on binding exhibiting the lowest K_d values, while smaller

substituents like hydrogen and fluorine demonstrated the highest K_d values ($K_d = 41 \mu\text{M}$ and $78 \mu\text{M}$, respectively).

Linear regression analysis of the relationship between turnover (k_{cat}) and the electronic parameter (σ) revealed a modest negative relationship with a ρ value of -0.7 ± 0.4 (Figure 5.21). The small F value of 3.5 suggests that this relationship is statistically insignificant. The catalytic properties (K_d and k_{cat}) of the Ile199Ala mutant do not exhibit an observable dependence on electronic, hydrophobic, or steric properties of the *para*-substituent. Multiple regression analysis of the data does not reveal any additional insights into the dependence of the *para*-substituent on catalysis.

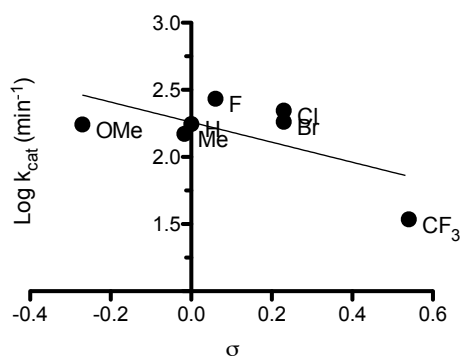


Figure 5.21. Dependence of k_{cat} on the electronic properties of the *para*-substituent.

5.8.2 QSAR Effects: Ile199Ala-Tyr326Ala MAO B Mutant

The catalytic properties of the Ile199Ala-Tyr326Ala mutant was explored in 50 mM CHES buffer at pH 9.3 with 0.5% (w/v) reduced triton (Table 5.7). Slightly different assay conditions were necessary for the study due to an increase in the K_m of the substrates at lower pH. All of the substrates in this

study demonstrate primary KIE demonstrating that C-H bond cleavage is the rate limiting step (Table 5.8).

Table 5.7. Kinetic properties of the Ile199Ala-Tyr326Ala mutant using *para*-substituted benzylamine analogues.

<i>Para</i>- Substituent	α,α-Proteo		α,α-Deuteuro	
	$k_{\text{cat (H)}} \text{ (min}^{-1}\text{)}$	$K_{\text{m (H)}} \text{ (}\mu\text{M)}$	$k_{\text{cat (D)}} \text{ (min}^{-1}\text{)}$	$K_{\text{m (D)}} \text{ (}\mu\text{M)}$
H	283	866	63	1817
CF ₃	171	74	49	111
Br	162	36	71	69
Cl	226	80	91	160
F	283	471	66	787
Me	190	84	44	159
OMe	162	134	31	253

Table 5.8. Kinetic isotope effects for the oxidation benzylamine analogues with the Ile199Ala-Tyr326Ala mutant.

<i>Para</i>- Substituent	$^{\text{D}}k_{\text{cat}}$	$^{\text{D}}(V/K)$
	$^{\text{D}}k_{\text{cat}} = k_{\text{cat(H)}}/k_{\text{cat(D)}}$	$^{\text{D}}(V/K) = [k_{\text{cat (H)}} / K_{\text{m (H)}}] / [k_{\text{cat (D)}} / K_{\text{m (D)}}]$
H	5	9
CF ₃	3	5
Br	2	4
Cl	2	5
F	4	7
Me	4	8
OMe	5	10

The K_d values are considerably higher for the double mutant than the single mutant (Table 5.9). K_d values range from ~60 μM to 1 mM with binding favoring larger substituents much like the observed trend for the Ile199Ala mutant. The weakest binding in this study was observed using benzylamine as a substrate; however, it did demonstrate the highest turnover (Table 5.7).

Table 5.9. Calculated K_d of the substrate for the Ile199Ala-Tyr326Ala mutant

Parameter		K_d (corrected) (μM)
Para Substituent	$\text{p}K_a$	K_d (corrected) = K_d (observed) / $1 + \text{antilog}(\text{p}K_a - \text{pH})$
H	9.33	1009
CF_3	8.75	98
Br	9.08	59
Cl	9.08	133
F	9.27	457
Me	9.52	68
OMe	9.63	90

Figure 5.22 illustrates that analysis of $\text{Log } k_{\text{cat}}$ versus electronic parameter does not reveal any correlations (the error for the slope is greater than the value of the slope). Multiple regression analysis do, however, revealed strong correlations between both the electronic parameter (σ) and hydrophobic effects (π) on the catalytic efficiency ($\text{Log } V/K$). This results in an overall equation of

$$\text{Log } V/K = 1.3 \pm 0.2 \pi - 0.8 \pm 0.3 \sigma - 0.4 \pm 0.1$$

with an R^2 value of 0.91, $P = 0.08$, and $F = 20$. It should be stated that the correlations are modest and exhibit relatively high error, particularly in reference to the ρ value of -0.8 ± 0.3 (~38% error) for the electronic dependence.

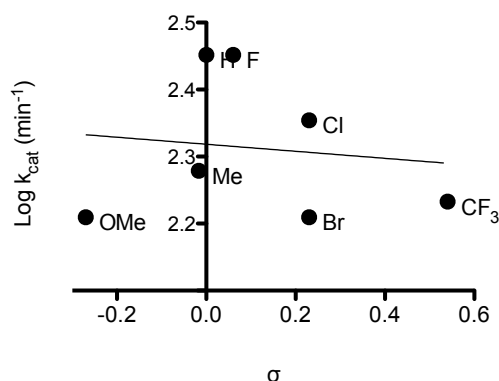


Figure 5.22. Dependence of k_{cat} on the electronic properties of the *para*-substituent.

5.6.3 Interpretation of the QSAR Effects of the MAO B Mutant Enzymes

While the studies of the QSAR effect of *para*-substituted benzylamine analogues have provide considerable insights into the catalytic mechanism of amine oxidation, this technique has proven to be less informative with MAO B. These data demonstrate that the catalytic mechanism is considerably more complex and several factors drive turnover. While the V/K for benzylamine oxidation by the double mutant does appear to be influenced by electronic contributions, these contributions are mild and should not be over interpreted due to the high level of error with respect to the correlation (~38% error).

5.9 Conclusions

The Ile199Ala and Ile199Ala–Tyr326Ala mutant forms of MAO B proved to be excellent models for the investigation of the roles of the Ile199 and Tyr326 ‘gating’ residues. Both mutants exhibit catalytic activities that are only mildly

altered with dramatic increases in K_m values. Kinetic studies show no alteration in the pH dependence of these enzymes versus WT MAO B. This further illustrates that the catalytic properties remain unchanged; however, the substrate recognition of these mutant enzymes is severely altered demonstrating the roles of these residues in substrate recognition. On increasing the pH of the assay, a dramatic increase is observed in the binding affinities of amine substrates for the Ile199Ala-Tyr326Ala mutant form (and a less dramatic but similar affect is observed for the Ile199Ala single mutant). This is likely due to the reduced water solubility of the unprotonated amine resulting in a greater thermodynamic push to occupy the hydrophobic active site of the enzyme. Support for these claims also arises from the observation that both mutant forms of MAO B exhibit reduced binding affinity for MAO B specific inhibitors as well as small reversible inhibitors. These mutant enzymes exhibit lowered binding affinities relative to wild-type enzyme for small inhibitors further demonstrating the requirement for a “closed” substrate cavity for inhibition. Structural data on the Ile199Ala MAO B mutant and the Ile199Ala-Tyr326Ala MAO B mutant shows no alterations in active site geometry. These data together demonstrate that Ile199 and Tyr326 are structural determinants for MAO B, and these residues play a crucial role in both substrate and inhibitor recognition.

5.10 Materials and Methods

Recombinant human liver MAO B and MAO A were expressed in *Pichia pastoris* and purified by published protocols.^{20, 21} Ile199Ala MAO B and Ile199Ala-Tyr326Ala mutant enzymes were prepared by gene mutations using the

Stratagene Quik-Change XL Site-Directed Mutagenesis kit and confirmed by gene sequence analysis. Standard MAO A and MAO B activity assays were performed spectrophotometrically using *p*-trifluoromethylbenzylamine ($\lambda = 243$ nm) and benzylamine ($\lambda = 250$ nm), respectively at 25 °C in a 50 mM phosphate buffer (pH 7.5) and 0.5% (w/v) RTX-100. MAO B Ile199Ala assays were performed spectrophotometrically using *p*-trifluoromethylbenzylamine ($\lambda = 243$ nm) as a substrate at 25 °C in a 50 mM phosphate buffer (pH 7.5) and 0.5% (w/v) RTX-100. MAO B Ile199Ala-Tyr326Ala assays were performed spectrophotometrically using *p*-bromobenzylamine ($\lambda = 243$ nm) at 25 °C in a 50 mM CHES (pH 9.3) and 0.5% (w/v) RTX-100.

Competitive Inhibition Assays. K_i values for the inhibition of MAO A, MAO B, MAO B Ile199Ala, and MAO B Ile199Ala-Tyr326Ala were determined by measuring the initial rates of substrate oxidation (six different concentrations) in the presence of varying concentrations of inhibitor (a minimum of four different concentrations). Binding constants were determined using global fit analysis of the hyperbolic fit of enzyme activity upon varied concentrations of inhibitor using the Graphpad Prism data analysis software.

Crystallographic methods. Crystallographic studies were performed as described by the Mattevi laboratory.³ Briefly, inhibited enzyme in 50 mM potassium phosphate pH 7.5, 8.5 mM Zwittergent 3-12 was crystallized by mixing equal volumes of protein sample and reservoir solution (12% PEG4000, 100 mM ADA buffer pH 6.5, 70 mM Li₂SO₄). X-ray diffraction data were collected at 100 K at the beam-line ID14-EH2 of European Synchrotron Radiation Facility in Grenoble.

Data processing and scaling were carried out using MOSFLM²² and programs of the CCP4 package.²³ Crystallographic refinements were performed with the programs REFMAC5²⁴ and Coot.²⁵

Activity Studies of The Ile199Ala MAO B Mutant. All activity assay were carried out at 25 °C in a 50 mM phosphate buffer (pH 7.5) and 0.5% (w/v) RTX-100. Kinetic constants for dopamine and serotonin were determined by monitoring oxygen consumption using an oxygen electrode. Kinetic constants for *p*(CO₂H)-benzylamine, phenylethylamine, and 4-phenylbutylamine were determined spectrophotometrically ($\lambda = 560$ nm) using a horseradish peroxidase/amplex red couple assay for the detection hydrogen peroxide production. Kinetic constants for kynuramine and benzylamine were determined spectrophotometrically at 316 nm and 250 nm, respectively.

Activity Studies of The Ile199Ala-Tyr326Ala MAO B Mutant. All activity assay were carried out at 25 °C in a 50 mM CHES (pH 9.3) and 0.5% (w/v) RTX-100. Kinetic constants for *p*(CO₂H)-benzylamine, phenylethylamine, 3-phenylpropylamine and 4-phenylbutylamine were determined spectrophotometrically ($\lambda = 560$ nm) using a horseradish peroxidase/amplex red couple assay for the detection hydrogen peroxide production. Kinetic constants for kynuramine ($\lambda = 316$ nm), benzylamine ($\lambda = 250$ nm) and *p*CF₃-benzylamine ($\lambda = 243$ nm) were determined spectrophotometrically.

Qualitative Structure Activity Relationship Assays. All kinetic constants were determined spectrophotometrically by observing reactions in the steady-state. Extinction coefficients as well as wavelength of the aldehyde products have been

previously reported by Walker and Edmondson.²⁶ All activity assay using the MAO B Ile199Ala mutant were carried out at 25 °C in a 50 mM phosphate buffer (pH 7.5) and 0.5% (w/v) RTX-100. All activity assay using the MAO B Ile199Ala-Tyr326Ala mutant were carried out at 25 °C in a 50 mM CHES (pH 9.3) and 0.5% (w/v) RTX-100.

pH studies. All activity assays were performed spectrophotometrically using *p*-trifluoromethylbenzylamine ($\lambda = 243$ nm) and benzylamine ($\lambda = 250$ nm) as a substrate at 25 °C in a buffer containing 50 mM potassium phosphate, 50 mM sodium pyrophosphate phosphate, and 50 mM CHES with 0.5% (w/v) RTX-100. The pH was adjusted to 7.5, 8.0, 8.5, 9.0, or 9.5 depending on the assay.

5.11 References

1. Chen, J. F.; Steyn, S.; Staal, R.; Petzer, J. P.; Xu, K.; Van Der Schyf, C. J.; Castagnoli, K.; Sonsalla, P. K.; Castagnoli, N., Jr.; Schwarzschild, M. A., 8-(3-Chlorostyryl)caffeine may attenuate MPTP neurotoxicity through dual actions of monoamine oxidase inhibition and A2A receptor antagonism. *J. Biol. Chem.* **2002**, 277, (39), 36040-4.
2. Fowler, J. S.; Logan, J.; Wang, G. J.; Volkow, N. D.; Telang, F.; Zhu, W.; Franceschi, D.; Pappas, N.; Ferrieri, R.; Shea, C.; Garza, V.; Xu, Y.; Schlyer, D.; Gatley, S. J.; Ding, Y. S.; Alexoff, D.; Warner, D.; Netusil, N.; Carter, P.; Jayne, M.; King, P.; Vaska, P., Low monoamine oxidase B in peripheral organs in smokers. *Proc Natl Acad Sci U S A* **2003**, 100, (20), 11600-5.

3. Binda, C.; Li, M.; Hubalek, F.; Restelli, N.; Edmondson, D. E.; Mattevi, A., Insights into the mode of inhibition of human mitochondrial monoamine oxidase B from high-resolution crystal structures. *Proc. Natl. Acad. Sci. U S A* **2003**, 100, (17), 9750-9755.
4. Binda, C.; Newton-Vinson, P.; Hubalek, F.; Edmondson, D. E.; Mattevi, A., Structure of human monoamine oxidase B, a drug target for the treatment of neurological disorders. *Nat. Struct. Biol.* **2002**, 9, (1), 22-26.
5. Edmondson, D. E.; Binda, C.; Wang, J.; Upadhyay, A. K.; Mattevi, A., Molecular and mechanistic properties of the membrane-bound mitochondrial monoamine oxidases. *Biochemistry* **2009**, 48, (20), 4220-4230.
6. Binda, C.; Hubalek, F.; Li, M.; Herzig, Y.; Sterling, J.; Edmondson, D. E.; Mattevi, A., Crystal structures of monoamine oxidase B in complex with four inhibitors of the N-propargylaminoindan class. *J. Med. Chem.* **2004**, 47, (7), 1767-1774.
7. Son, S. Y.; Ma, J.; Kondou, Y.; Yoshimura, M.; Yamashita, E.; Tsukihara, T., Structure of human monoamine oxidase A at 2.2-angstrom resolution: the control of opening the entry for substrates/inhibitors. *Proc. Natl. Acad. Sci. U S A* **2008**, 105, (15), 5739-5744.
8. De Colibus, L.; Li, M.; Binda, C.; Lustig, A.; Edmondson, D. E.; Mattevi, A., Three-dimensional structure of human monoamine oxidase A (MAO A): relation to the structures of rat MAO A and human MAO B. *Proc. Natl. Acad. Sci. U S A* **2005**, 102, (36), 12684-12689.

9. Hubalek, F.; Binda, C.; Khalil, A.; Li, M.; Mattevi, A.; Castagnoli, N.; Edmondson, D. E., Demonstration of isoleucine 199 as a structural determinant for the selective inhibition of human monoamine oxidase B by specific reversible inhibitors. *J. Biol. Chem.* **2005**, 280, (16), 15761-15766.
10. Binda, C.; Wang, J.; Pisani, L.; Caccia, C.; Carotti, A.; Salvati, P.; Edmondson, D. E.; Mattevi, A., Structures of human monoamine oxidase B complexes with selective noncovalent inhibitors: Safinamide and coumarin analogs. *J. Med. Chem.* **2007**, 50, (23), 5848-5852.
11. Dow, J.; Piriou, F.; Wolf, E.; Dulery, B. D.; Haegele, K. D., Novel carbamate metabolites of mofegiline, a primary amine monoamine oxidase B inhibitor, in dogs and humans. *Drug Metab. Dispos.* **1994**, 22, (5), 738-49.
12. Hubalek, F.; Binda, C.; Li, M.; Herzig, Y.; Sterling, J.; Youdim, M. B. H.; Mattevi, A.; Edmondson, D. E., Inactivation of purified human recombinant monoamine oxidases A and B by rasagiline and its analogues. *J. Med. Chem.* **2004**, 47, (7), 1760-1766.
13. Sterling, J.; Veinberg, A.; Lerner, D.; Goldenberg, W.; Levy, R.; Youdim, M.; Finberg, J., (R)(+)-N-propargyl-1-aminoindan (rasagiline) and derivatives: highly selective and potent inhibitors of monoamine oxidase B. *J. Neural. Transm. Suppl.* **1998**, 52, 301-5.
14. Binda, C.; Hubalek, F.; Li, M.; Herzig, Y.; Sterling, J.; Edmondson, D. E.; Mattevi, A., Binding of rasagiline-related inhibitors to human monoamine oxidases. a kinetic and crystallographic analysis. *J. Med. Chem.* **2005**, 48, (26), 8148-8154.

15. Edmondson, D. E.; Bhattacharyya, A. K.; Walker, M. C., Spectral and kinetic studies of imine product formation in the oxidation of p-(N,N-dimethylamino)benzylamine analogues by monoamine oxidase B. *Biochemistry* **1993**, 32, (19), 5196-202.
16. Dunn, R. V.; Marshall, K. R.; Munro, A. W.; Scrutton, N. S., The pH dependence of kinetic isotope effects in monoamine oxidase A indicates stabilization of the neutral amine in the enzyme-substrate complex. *FEBS J.* **2008**, 275, (15), 3850-8.
17. Hammett, L. P., Some relations between reaction rates and equilibrium constants. *Chem. Rev.* **1935**, 17, 125-36.
18. Hammett, L. P., Reaction rates and indicator acidities. *Chem. Rev.* **1935**, 16, 67-79.
19. Hansch, C.; Leo, A.; Hoekman, D., In *Exploring QSAR: hydrophobic, electronic, and steric constants*, American Chemical Society: Washington, DC, 1995.
20. Newton-Vinson, P.; Hubalek, F.; Edmondson, D. E., High-level expression of human liver monoamine oxidase B in *Pichia pastoris*. *Protein Expr. Purif.* **2000**, 20, (2), 334-45.
21. Li, M.; Hubalek, F.; Newton-Vinson, P.; Edmondson, D. E., High-level expression of human liver monoamine oxidase A in *Pichia pastoris*: comparison with the enzyme expressed in *Saccharomyces cerevisiae*. *Protein Expr. Purif.* **2002**, 24, (1), 152-62.

22. Leslie, A. G. W., Integration of macromolecular diffraction data. *Acta Crystallographica Sect. D-Biol. Crystallography* **1999**, 55, 1696-1702.
23. Bailey, S., The Ccp4 Suite - Programs for Protein Crystallography. *Acta Crystallographica Sect. D-Biol. Crystallography* **1994**, 50, 760-763.
24. Murshudov, G. N.; Vagin, A. A.; Dodson, E. J., Refinement of macromolecular structures by the maximum-likelihood method. *Acta Crystallographica Sect. D-Biol. Crystallography* **1997**, 53, 240-255.
25. Emsley, P.; Cowtan, K., Coot: model-building tools for molecular graphics. *Acta Crystallographica Sect. D-Biol. Crystallography* **2004**, 60, 2126-2132.
26. Walker, M. C.; Edmondson, D. E., Structure-Activity Relationships in the Oxidation of Benzylamine Analogs by Bovine Liver Mitochondrial Monoamine Oxidase B. *Biochemistry* **1994**, 33, (23), 7088-98.